

---

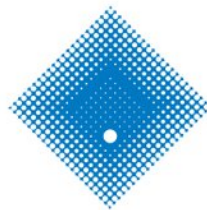
# Automatic Detection of Neurological Disorders using Brain Signal Data

---

Md Nurul Ahad Tawhid

*Thesis submitted for the fulfilment of the requirements for the degree of  
**Doctor of Philosophy***

Victoria University, Melbourne, Australia  
Institute for Sustainable Industries and Liveable Cities (ISILC)



**VICTORIA  
UNIVERSITY**

---

October, 2023

## *Abstract*

Managing neurological disorders is a major challenge for public health and health care systems in Australia and around the world. Currently, there is no reliable way of identifying disorders from brain signal data automatically, quickly, and accurately. Electroencephalography (EEG) is a powerful and popular technique to capture brain signal data for neurological disorder diagnosis through visual inspection. But this process is time-consuming, subjective, exhaustive, and error-prone. EEG records the electrical activities of the brain and provides important information about changes in electrophysiological brain dynamics for neurological diseases including autism spectrum disorder (ASD), schizophrenia (SZ), epilepsy, and Alzheimer’s disease.

While EEG signals provide substantial insight into brain activity, there is a limited body of research dedicated to the automated detection and assessment of various neurological diseases and disorders. Even today, experts frequently evaluate the EEG signal manually. Therefore, it is necessary to develop a computer-aided diagnostic (CAD) system for the precise and automatic diagnosis of neurological disorders as early as possible. Classification methods play a crucial role in distinguishing EEG segments and assessing an individual’s health status. The effective utilisation of appropriate classification algorithms to accurately and efficiently identify distinct EEG signals associated with various disorders poses a significant challenge in designing a reliable and efficient CAD system.

This study intends to work towards the detection of two neurological disorders, named ASD and SZ. Existing research works related to these two diseases have some limitations, such as:

**Research problem 1:** Those are still insufficient and have scope to improve in terms of accuracy and performance.

**Research problem 2:** Very few studies have considered developing a system for classification of multiple neurological disorders in a single framework.

**Research problem 3:** Most of the studies are related to a particular disease and verified using a specific dataset, which left questions about their effectiveness on other datasets of the same disease as well as their efficacy on other diseases.

**Research problem 4:** Lack of CAD systems for assisting clinicians in diagnosis of those diseases.

The key aim of this project is to address the issues mentioned above by developing several innovative frameworks that will use EEG data to automatically and efficiently identify ASD and SZ. We have used several publicly available datasets for validation of the proposed methods.

To address research problem 1, we have proposed a time-frequency spectrogram image-based framework for ASD classification using both machine learning (ML) and deep learning (DL)-based classification techniques (**Chapter 3**). In this technique, EEG signals are first converted into spectrogram images using the short-time Fourier transform (STFT),

and then those images are used as input for different ML and DL-based classifiers. Experimental results show that both ML and DL methods performed well in the EEG signal classification between ASD and healthy control (HC) subjects, but DL performed better than the ML-based classifiers. The research finding also indicates that the proposed method can be used for developing a CAD system for the identification of ASD from HC subjects.

Similarly, for SZ detection, we have developed a framework using an entropy topographic image with a DL-based convolutional neural network (CNN) model (**Chapter 4**). We used Shannon entropy to extract entropy values from each channel of the EEG signal and then plotted them on the brain scalp to produce the topographic image. Then those images are trained and classified using our proposed CNN model. The obtained results indicate that the proposed method can be used for brain signal data mining purposes.

The second research problem motivates us to propose our third research work: developing a multi-class classifier for multiple neurological disorders using spectrogram images of EEG signal data (**Chapter 5**). In this technique, we have extended our proposed method of ASD classification to a five-class classification framework. In this method, we have classified four neurological disorders, namely ASD, SZ, epilepsy, and Parkinson's disease, from HC subjects. We have used two histogram-based feature extractors and four ML-based classifiers to categorise those extracted features. We have also used DL-based models for the classification of those images, and the obtained result shows a promising outcome.

To solve the third research problem, we have developed a generic CNN model for the classification of EEG data for different neurological disorders (**Chapter 6**). Most of the previous frameworks worked for a particular disease and a particular EEG dataset, which motivated us to create a generic CNN model that can work with different neurological disease classifications. The experimental results show promising outcomes on different datasets from various neurological diseases.

Finally, to resolve the first and fourth research problem, we have proposed a framework for subject-independent SZ detection using a DL-based Convolutional Long Short-Term Memory (ConvLSTM) model (**Chapter 7**). The proposed model is designed to perform classification independently of training and testing subjects so that it can perform classification in real-life situations where new testing EEG data is unknown to the trained model. Finally, we have developed a web-based CAD system for SZ detection using the proposed ConvLSTM-based framework.

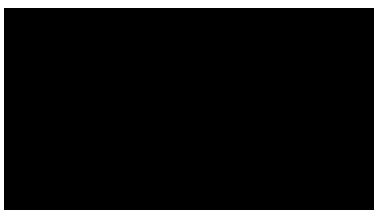
As of now, the outcome of this PhD work is four journal articles and two conference papers related to the proposed methods that have been published in reputed journals and conferences. One more article is currently under review. Also, the developed web-platform-based CAD system will be a helpful tool for the clinical diagnosis of different neurological disorders.

## Declaration of Authenticity

I, **Md Nurul Ahad Tawhid**, declare that the **Doctor of Philosophy** thesis entitled “**Automatic Detection of Neurological Disorders using Brain Signal Data**” is no more than 80,000 words in length including quotes and exclusive of tables, figures, appendices, bibliography, references and footnotes. This thesis contains no material that has been submitted previously, in whole or in part, for the award of any other academic degree or diploma. Except where otherwise indicated, this thesis is my own work.

I have conducted my research in alignment with the [Australian Code for the Responsible Conduct of Research](#) and [Victoria University’s Higher Degree by Research Policy and Procedures](#).

Signed



---

Date: October 11, 2023

---

## Ethics Declaration

I, **Md Nurul Ahad Tawhid**, declare that the **Doctor of Philosophy** thesis entitled “**Automatic Detection of Neurological Disorders using Brain Signal Data**” has used seven different EEG datasets of six different neurological disorders: Autism Spectrum Disorder, Schizophrenia, Epilepsy, Parkinson’s Disease, Mild Cognitive Impairment, and Attention Deficit Hyperactivity Disorder. All of these datasets are collected from online repositories that are publicly available for research purposes, and no personal identification of the subjects is shared with those datasets. There is no use of animals or humans in this research, which is why there was no ethical approval required for this project.

Signed: 

---

Date: October 11, 2023

---

## *Acknowledgements*

I want to start by thanking Allah, the Almighty, for His strength and guidance.

I have had the privilege of working with amazing individuals during my PhD journey and have tremendously benefited from their assistance. I would want to use this opportunity to offer my heartfelt thanks to everyone who has assisted me and contributed in various capacities.

My supervisor, Prof Hua Wang, for his unwavering guidance, expertise, and invaluable mentorship throughout this research journey. Your support has been instrumental in shaping the direction and quality of this dissertation. My associate supervisor, Dr Siuly Siuly, for her ongoing inspiration, direction, support, encouragement, counsel, advise, patience, and tailored remarks during my PhD study. She was an approachable supervisor who motivated me to achieve my goals. I would also like to express my sincere gratitude and appreciation to my associate supervisor, Dr Kate Wang, for her continuous encouragement, support, valuable advice, and suggestions. I consider myself really fortunate and grateful to have worked with such a fantastic supervision team. Without their ongoing assistance and support, I am not sure how I would be able to complete my research.

I would like to take this opportunity to express my profound gratitude to the esteemed faculty members of Victoria University. Their unwavering commitment to academic excellence, insightful feedback, and tireless efforts to nurture a vibrant research atmosphere have had an enduring and transformative impact on my academic journey. In addition, I would like to thank and appreciate my postgraduate colleagues in our research group for the discussions, suggestions, and guidance they provided, particularly during our group talks. I also want to express my gratitude to all of my friends for their support and encouragement.

I would like to extend my sincere appreciation to the open data sources that have made this project possible. In an era of information sharing and collaboration, the availability of open data has been instrumental in shaping the outcomes of this endeavour. The generosity of organisations and individuals who have made their data freely accessible to the public is a testament to the spirit of transparency and collective progress. Without the wealth of data provided by these open sources, the scope and depth of this project would have been significantly constrained. The open data sources utilised in this project have not only enriched the quality of our research but have also played a crucial role in fostering innovation, driving evidence-based decision-making, and advancing our understanding in various domains.

I acknowledge the efforts of the data providers, curators, and maintainers who have dedicated their time and resources to ensure the reliability and accessibility of these invaluable datasets. Your commitment to open data principles has had a significant impact on the broader community of researchers, analysts, and policymakers.

I am also grateful for the financial support provided by the Australian Research Council Linkage Project, offered by Victoria University, which enabled me to carry out this research. This financial support is gratefully acknowledged. I want to express my gratitude

to the Research Funding Team for their constant support and proper guidance.

I am deeply grateful to express my heartfelt appreciation to the Institute for Sustainable Industries and Liveable Cities (ISILC) for their generosity in extending my scholarship by an additional six months. This extension holds great significance in my academic journey and research pursuits.

I would like to extend my sincere gratitude and recognition to all the esteemed individuals whose work has served as the bedrock of this dissertation. Your invaluable contributions to the field have been nothing short of indispensable in shaping and informing the entirety of this research.

Lastly, my family, for their unwavering love, encouragement, and patience during this challenging academic pursuit. Your belief in me has been a constant source of motivation. My deepest and sincerest thanks go to my parents for their everlasting support throughout my life. My loving brothers and sisters for their support. Last but most importantly, I would like to thank my wife, Sanjida Akhter, for all her support and help. This work would not have been possible without her caring and support. Of course, I am also thankful to our adorable sons, Md Shahzaib Aman and Mohammad Shahzain Ayaan, for bringing a lot of joy, happiness, and enduring love to our lives. I would like to dedicate this dissertation to my family, without whom I am absolutely nothing.

This dissertation would not have been possible without the collective support, encouragement, and contributions of these individuals and institutions. Thank you for being a part of this academic journey.

Md Nurul Ahad TAWHID  
Melbourne, Australia  
October, 2023

## List of Publications

1. Md. Nurul Ahad Tawhid, Siuly Siuly, and Hua Wang. Diagnosis of autism spectrum disorder from EEG using a time–frequency spectrogram image-based approach. *Electronics Letters*, 56(25), pp.1372-1375, 2020. **(Published)**
2. Md. Nurul Ahad Tawhid, Siuly Siuly, Hua Wang, Frank Whittaker, Kate Wang and Yanchun Zhang. A spectrogram image based intelligent technique for automatic detection of autism spectrum disorder from EEG. *Plos one*, 16(6), p.e0253094, 2021. **(Published)**
3. Md. Nurul Ahad Tawhid, Siuly Siuly, Kate Wang, and Hua Wang. Data Mining Based Artificial Intelligent Technique for Identifying Abnormalities from Brain Signal Data. In *International Conference on Web Information Systems Engineering*, pp. 198-206. Springer, Cham, 2021. **(Published)**
4. Md. Nurul Ahad Tawhid, Siuly Siuly, Kate Wang, and Hua Wang. Brain data mining framework involving entropy topography and deep learning. In *Databases Theory and Applications: 33rd Australasian Database Conference, ADC 2022*, pp. 161-168. Cham: Springer International Publishing, 2022. **(Published)**
5. Md. Nurul Ahad Tawhid, Siuly Siuly, Kate Wang, Hua Wang. Textural feature based intelligent approach for abnormality detection from brain signal data. *Plos one*, 17(11), p.e0277555, 2022.**(Published)**
6. Md. Nurul Ahad Tawhid, Siuly Siuly, Kate Wang, and Hua Wang. Automatic and Efficient Framework for Identifying Multiple Neurological Disorders from EEG Signals. *IEEE Transactions on Technology and Society*, vol. 4, no. 1, pp. 76-86, March 2023. **(Published)**
7. Md. Nurul Ahad Tawhid, Siuly Siuly, Kate Wang, Hua Wang. GENet: A Generic Neural Network for Detecting Various Neurological Disorders from EEG. *(Under review in IEEE Transactions on Cognitive and Developmental Systems, Date of submission: May 10, 2023)*
8. Md. Nurul Ahad Tawhid, Siuly Siuly, Kate Wang, Hua Wang. SISDNet: A Subject Independent Schizophrenia Detection Neural Network Using EEG Data. *(Manuscript ready for submission)*

# List of Abbreviations

<b>2D</b>	<b>2-Dimensional</b>
<b>3s</b>	<b>Three Seconds</b>
<b>AB</b>	<b>AdaBoost</b>
<b>Acc</b>	<b>Accuracy</b>
<b>AD</b>	<b>Alzheimer’s Disease</b>
<b>ADC</b>	<b>Analog-to-Digital Converter</b>
<b>ADHD</b>	<b>Attention Deficit Hyperactivity Disorder</b>
<b>ADT</b>	<b>Automated Diagnostic Tool</b>
<b>AI</b>	<b>Artificial Intelligence</b>
<b>AM–FM</b>	<b>Amplitude Modulation–Frequency Modulation</b>
<b>ANN</b>	<b>Artificial Neural Network</b>
<b>AOD</b>	<b>Auditory Odd-Ball</b>
<b>AP</b>	<b>Action Potential</b>
<b>ApEn</b>	<b>Approximate Entropy</b>
<b>ASD</b>	<b>Autism Spectrum Disorder</b>
<b>AUC</b>	<b>Area Under the ROC Curve</b>
<b>BCI</b>	<b>Brain Computer Interface</b>
<b>BiS</b>	<b>BiSpectrum</b>
<b>CAD</b>	<b>Computer-Aided Diagnosis</b>
<b>CAR</b>	<b>Common Average Referencing</b>
<b>cCENTRIST</b>	<b>completed CENsus TRanform hISTogram</b>
<b>CCR</b>	<b>Correct Classification Rate</b>
<b>CDC</b>	<b>Centers for Disease Control and Prevention</b>
<b>CENTRIST</b>	<b>CENsus TRanform hISTogram</b>
<b>CFS</b>	<b>Correlation-based Feature Selection</b>
<b>CGP17Pat</b>	<b>Cyclic Group of Prime order Pattern</b>
<b>CNN</b>	<b>Convolutional Neural Network</b>
<b>ConV</b>	<b>ConVolution</b>
<b>ConvLSTM</b>	<b>Convolutional Long Short-Term Memory</b>
<b>CT</b>	<b>Computerized Tomography</b>
<b>CTM</b>	<b>Central Tendency Measure</b>
<b>CV</b>	<b>Cross Validation</b>
<b>CWT</b>	<b>Continues Wavelet Transform</b>
<b>DA</b>	<b>Discriminant Analysis</b>
<b>DBSCAN</b>	<b>Density-Based Spatial Clustering of Applications with Noise</b>

<b>DFT</b>	<b>D</b> iscrete <b>F</b> ourier <b>T</b> ransform
<b>DL</b>	<b>D</b> eep <b>L</b> earning
<b>DNNs</b>	<b>D</b> eep <b>N</b> eural <b>N</b> etworks
<b>DP</b>	<b>D</b> ouglas- <b>P</b> eucker
<b>DSM-5</b>	<b>D</b> iagnostic and <b>S</b> tatistical <b>M</b> anual of <b>M</b> ental <b>D</b> isorders
<b>DSS</b>	<b>D</b> ecision <b>S</b> upport <b>S</b> ystem
<b>DT</b>	<b>D</b> ecision <b>T</b> ree
<b>DWT</b>	<b>D</b> iscrete <b>W</b> avelet <b>T</b> ransform
<b>EBT</b>	<b>E</b> nsemble <b>B</b> agged <b>T</b> ree
<b>ECG</b>	<b>E</b> lectro <b>C</b> ardio <b>G</b> raphy
<b>ECoG</b>	<b>E</b> lectro <b>C</b> ortico <b>G</b> raphy
<b>EEG</b>	<b>E</b> lectro <b>E</b> ncephalo <b>G</b> raphy
<b>EFE</b>	$\mu$ <b>V</b> otional <b>F</b> acial <b>E</b> xpression
<b>EM</b>	<b>E</b> xpectation- <b>M</b> aximisation
<b>EMD</b>	<b>E</b> mpirical <b>M</b> ode <b>D</b> ecomposition
<b>EP</b>	<b>E</b> pilepsy
<b>EPNN</b>	<b>E</b> nhanced <b>P</b> robabilistic <b>N</b> eural <b>N</b> etwork
<b>EPSP</b>	<b>E</b> xcitatory <b>P</b> ost <b>S</b> ynaptic <b>P</b> otential
<b>ERP</b>	<b>E</b> vent- <b>R</b> elated <b>P</b> otential
<b>ERT</b>	<b>E</b> xtremely <b>R</b> andomised <b>T</b> rees
<b>EWT</b>	<b>E</b> mpirical <b>W</b> avelet <b>T</b> ransformation
<b>F1</b>	<b>F</b> 1 score
<b>FAWT</b>	<b>F</b> lexible <b>A</b> lytic <b>W</b> avelet <b>T</b> ransform
<b>FC</b>	<b>F</b> ully <b>C</b> onnected
<b>FDs</b>	<b>F</b> ractal <b>D</b> imensions
<b>FE</b>	<b>F</b> eature <b>E</b> xtraction
<b>FFT</b>	<b>F</b> ast <b>F</b> ourier <b>T</b> ransform
<b>FLDA</b>	<b>F</b> isher <b>L</b> inear <b>D</b> iscriminant <b>A</b> nalysis
<b>FLSSVM</b>	<b>F</b> lexible <b>L</b> east <b>S</b> quare <b>S</b> VM
<b>fMRI</b>	<b>f</b> unctional <b>M</b> agnetic <b>R</b> esonance <b>I</b> maging
<b>FN</b>	<b>F</b> alse <b>N</b> egative
<b>FP</b>	<b>F</b> alse <b>P</b> ositive
<b>FPR</b>	<b>F</b> alse <b>P</b> ositive <b>R</b> ate
<b>FSA</b>	<b>F</b> orward <b>S</b> election <b>A</b> lgorithm
<b>FT</b>	<b>F</b> ourier <b>T</b> ransform
<b>FTQWT</b>	<b>F</b> lexible <b>T</b> unable <b>Q</b> <b>W</b> avelet <b>T</b> ransform
<b>FuzzyEn</b>	<b>F</b> uzzy <b>E</b> ntropy
<b>GENet</b>	<b>G</b> eneric <b>E</b> EG neural <b>N</b> etwork
<b>GRNN</b>	<b>G</b> eneralised <b>R</b> egression <b>N</b> eural <b>N</b> etwork
<b>GRU</b>	<b>G</b> ated <b>R</b> ecurrent <b>U</b> nit
<b>HC</b>	<b>H</b> ealthy <b>C</b> ontrols
<b>HFD</b>	<b>H</b> iguchi <b>F</b> ractal <b>D</b> imension

<b>HLV</b>	<b>Histogram of Local Variance</b>
<b>HRA</b>	<b>High Risk for Autism</b>
<b>Hz</b>	<b>Hertz</b>
<b>ICA</b>	<b>Independent Component Analysis</b>
<b>ICD-11</b>	<b>International Classification of Diseases 11th Revision</b>
<b>iEEG</b>	<b>intracranial EEG</b>
<b>IIR</b>	<b>Infinite Impulse Response</b>
<b>ILSVRC</b>	<b>ImageNet Large Scale Visual Recognition Challenge</b>
<b>IMFs</b>	<b>Intrinsic Mode Functions</b>
<b>INCA</b>	<b>Iterative Neighbourhood Component Analysis</b>
<b>IPSP</b>	<b>Inhibitory PostSynaptic Potential</b>
<b>KAU</b>	<b>King Abdulaziz University</b>
<b>K-CM</b>	<b>K-Contractive Map</b>
<b><i>k</i>NN</b>	<b><i>k</i>-Nearest Neighbors</b>
<b>LBP</b>	<b>Linear Binary Pattern</b>
<b>LDA</b>	<b>Linear Discriminant Analysis</b>
<b>LgBP</b>	<b>Logarithmic Band Power</b>
<b>LOOCV</b>	<b>Leave-One-Out-Cross Validation</b>
<b>LOSO</b>	<b>Leave One Subject Out</b>
<b>LR</b>	<b>Logistic Regression</b>
<b>LRC</b>	<b>Low-Risk Controls</b>
<b>LSFE</b>	<b>Least Square Feature Extraction</b>
<b>LSTM</b>	<b>Long Short-Term Memory</b>
<b>LSVM</b>	<b>Linear Support Vector Machine</b>
<b>LTP</b>	<b>Local Ternary Pattern</b>
<b>LZC</b>	<b>Lempel-Ziv Complexity</b>
<b>MCI</b>	<b>Mild Cognitive Impairment</b>
<b>MEG</b>	<b>MagnetoEncephaloGraphy</b>
<b>MEMD</b>	<b>Multivariate Empirical Mode Decomposition</b>
<b>ML</b>	<b>Machine Learning</b>
<b>MLP</b>	<b>Multilayer Perceptron</b>
<b>MLPN</b>	<b>Multilayer Perceptron Network</b>
<b>MMN</b>	<b>MisMatch Negativity</b>
<b>mMSE</b>	<b>minimum Mean Square Error</b>
<b>MRI</b>	<b>Magnetic Resonance Imaging</b>
<b>NB</b>	<b>Naive Bayes</b>
<b>ND</b>	<b>Neurological Disorder</b>
<b>NN</b>	<b>Neural Networks</b>
<b>NPD</b>	<b>NeuroPsychiatric Disorders</b>
<b>OELM</b>	<b>Optimized Extreme Learning Machine</b>
<b>PCA</b>	<b>Principal Component Analysis</b>
<b>PCC</b>	<b>Pearson Correlation Coefficient</b>

<b>PD</b>	<b>P</b> arkinson's <b>D</b> isease
<b>PET</b>	<b>P</b> ositron <b>E</b> mission <b>T</b> omography
<b>PLV</b>	<b>P</b> hase- <b>L</b> ocking <b>V</b> alue
<b>PNN</b>	<b>P</b> robabilistic <b>N</b> eural <b>N</b> etwork
<b>Prec</b>	<b>P</b> recision
<b>PSD</b>	<b>P</b> ower <b>S</b> pectral <b>D</b> ensity
<b>PSP</b>	<b>P</b> ost <b>S</b> ynaptic <b>P</b> otentials
<b>PSVG</b>	<b>P</b> ower of <b>S</b> cale-freeness of <b>V</b> G
<b>qEEG</b>	<b>Q</b> uantitative <b>E</b> EG
<b>RBFNN</b>	<b>R</b> adial <b>B</b> asis <b>F</b> unction <b>N</b> eural <b>N</b> etwork
<b>ReEn</b>	<b>R</b> eyni's <b>E</b> ntropy
<b>ReLU</b>	<b>R</b> ectified <b>L</b> inear <b>U</b> nit
<b>RF</b>	<b>R</b> andom <b>F</b> orest
<b>RFLD</b>	<b>R</b> egulated <b>F</b> isher <b>L</b> inear <b>D</b> iscriminant
<b>RGB</b>	<b>R</b> ed- <b>G</b> reen- <b>B</b> lue
<b>ROC</b>	<b>R</b> eceiver <b>O</b> perating <b>C</b> haracteristic
<b>RQA</b>	<b>R</b> ecurrence <b>Q</b> uantification <b>A</b> nalysis
<b>RVMD</b>	<b>R</b> obust <b>V</b> ariational <b>M</b> ode <b>D</b> ecomposition
<b>SA</b>	<b>S</b> pectral <b>A</b> nalysis
<b>SampEn</b>	<b>S</b> ample <b>E</b> ntropy
<b>SD</b>	<b>S</b> tandard <b>D</b> eviation
<b>SE</b>	<b>S</b> hannon <b>E</b> ntropy
<b>Sen</b>	<b>S</b> ensitivity
<b>SGD</b>	<b>S</b> tochastic <b>G</b> radient <b>D</b> escent
<b>ShanEn</b>	<b>S</b> hannon <b>E</b> ntropy
<b>SISDNet</b>	<b>S</b> ubject <b>I</b> ndependent <b>S</b> chizophrenia <b>D</b> etection <b>N</b> etwork
<b>SLBP</b>	<b>S</b> ymmetrically <b>W</b> eighted- <b>L</b> ocal <b>B</b> inary <b>P</b> atterns
<b>SMO</b>	<b>S</b> equential <b>M</b> inimal <b>O</b> ptimisation
<b>Sn</b>	<b>S</b> ine net neural networks
<b>SoA</b>	<b>S</b> tate- <b>o</b> f-the- <b>A</b> rt
<b>SP</b>	<b>S</b> patial <b>P</b> yramid
<b>Spec</b>	<b>S</b> pecificity
<b>SpEn</b>	<b>S</b> pectral <b>E</b> ntropy
<b>SPM</b>	<b>S</b> patial <b>P</b> yramid <b>M</b> atching
<b>SPWVD</b>	<b>S</b> moothed <b>P</b> seudo- <b>W</b> igner <b>V</b> ille <b>D</b> istribution
<b>SSD</b>	<b>S</b> um of <b>S</b> igned <b>D</b> ifferences
<b>STFT</b>	<b>S</b> hort- <b>T</b> ime <b>F</b> ourier <b>T</b> ransform
<b>SVM</b>	<b>S</b> upport <b>V</b> ector <b>M</b> achine
<b>SVM-RBF</b>	<b>S</b> VM with <b>R</b> adial <b>B</b> asis <b>F</b> unction
<b>SZ</b>	<b>S</b> chi <b>Z</b> ophrenia
<b>tCENTRIST</b>	<b>t</b> ernary <b>C</b> ENsus <b>T</b> Ranform <b>h</b> ISTogram
<b>TD</b>	<b>T</b> ypically <b>D</b> eveloping

<b>T-F</b>	<b>T</b> ime- <b>F</b> requency
<b>TFR</b>	<b>T</b> ime- <b>F</b> requency <b>R</b> epresentation
<b>TN</b>	<b>T</b> rue <b>N</b> egative
<b>TP</b>	<b>T</b> rue <b>P</b> ositive
<b>t-SNE</b>	<b>t</b> -distributed <b>S</b> tochastic <b>N</b> eighbor <b>E</b> mbedding
<b>VG</b>	<b>V</b> isibility <b>G</b> raph
<b>WHO</b>	<b>W</b> orld <b>H</b> ealth <b>O</b> rganization
<b>WT</b>	<b>W</b> avelet <b>T</b> ransform
<b>ZMUV</b>	<b>Z</b> ero <b>M</b> ean <b>U</b> nit <b>V</b> ariance
$\mu\text{V}$	micro <b>V</b> olts

*Dedicated to my family...*

# Contents

<b>Abstract</b>	<b>i</b>
<b>Declaration of Authenticity</b>	<b>iii</b>
<b>Ethics Declaration</b>	<b>iv</b>
<b>Acknowledgements</b>	<b>v</b>
<b>List of Publications</b>	<b>vii</b>
<b>List of abbreviations</b>	<b>vii</b>
<b>1 Introduction</b>	<b>1</b>
1.1 Research challenges and motivation . . . . .	2
1.2 Research problem statements . . . . .	3
1.3 Research objectives . . . . .	5
1.4 Significance of the study . . . . .	5
1.5 Contributions of the dissertation . . . . .	6
1.6 Structure of the Dissertation . . . . .	8
<b>2 Background</b>	<b>11</b>
2.1 Human brain anatomy . . . . .	11
2.1.1 Brain structures and their functions . . . . .	11
2.1.1.1 Cerebrum . . . . .	12
2.1.1.2 cerebellum . . . . .	14
2.1.1.3 brainstem . . . . .	14
2.1.2 Communication system of human brain . . . . .	15
2.1.2.1 Dendrites . . . . .	15
2.1.2.2 Soma (Cell Body) . . . . .	15
2.1.2.3 Axon . . . . .	16
2.1.2.4 Axon (synaptic) terminals . . . . .	16
2.1.2.5 Neuron’s communication system and the synapse . . . . .	16
2.1.3 Electroencephalography (EEG) . . . . .	18
2.1.3.1 History of EEG . . . . .	18
2.1.3.2 EEG Recording system . . . . .	19
2.1.3.3 EEG electrode placement style . . . . .	20
2.1.3.4 EEG Brainwaves . . . . .	22

2.2	Autism spectrum disorder and its effect on EEG . . . . .	25
2.3	Schizophrenia and its effect on EEG . . . . .	26
2.4	Automated EEG analysis . . . . .	28
2.4.1	Methods for analysing EEG signals . . . . .	28
2.4.1.1	Time domain analysis . . . . .	29
2.4.1.2	Frequency domain analysis . . . . .	30
2.4.1.3	Time-Frequency domain analysis . . . . .	31
2.4.2	EEG signal classification techniques . . . . .	32
2.4.2.1	Machine learning based classification . . . . .	33
2.4.2.2	Deep learning based classification . . . . .	33
2.4.2.3	Supervised Classification . . . . .	34
2.4.2.4	Unsupervised Classification . . . . .	35
2.5	Existing research works for ASD and SZ detection and their limitations . . . . .	35
2.5.1	Existing EEG signal classification Methods for ASD detection . . . . .	36
2.5.2	Existing EEG signal classification Methods for Schizophrenia Detection . . . . .	41
2.5.3	Limitations of the existing studies . . . . .	45
2.6	Summary . . . . .	46
<b>3</b>	<b>Spectrogram Image Based Autism Spectrum Disorder Classification</b>	<b>51</b>
3.1	Introduction . . . . .	51
3.2	Methodology . . . . .	55
3.2.1	Pre-processing and spectrogram image generation . . . . .	56
3.2.2	Machine learning based process . . . . .	56
3.2.3	Deep learning based process . . . . .	57
3.3	Performance evaluation . . . . .	58
3.3.1	Dataset . . . . .	59
3.3.2	Performance evaluation parameters . . . . .	60
3.4	Result and discussion . . . . .	61
3.4.1	Results for machine learning based process . . . . .	62
3.4.2	Results of deep learning based process . . . . .	64
3.5	Summary . . . . .	68
<b>4</b>	<b>Topographic Image Based EEG Signal Classification</b>	<b>72</b>
4.1	Introduction . . . . .	72
4.2	Methodology of the proposed mining framework . . . . .	74
4.2.1	Pre-processing of the raw data . . . . .	75
4.2.2	Creation of topographic images for signal segments . . . . .	75
4.2.3	Training and classification using a deep learning-based model . . . . .	76
4.3	Materials and parameters used for evaluating performance . . . . .	77
4.3.1	Data Acquisition . . . . .	77
4.3.2	Performance evaluation criteria . . . . .	77
4.4	The outcomes of the proposed framework . . . . .	78

4.4.1	Experimental configuration . . . . .	78
4.4.2	Experimental Outcomes of the Proposed Framework . . . . .	78
4.5	Summary . . . . .	84
<b>5</b>	<b>Multiple Disease Classification Using a Single Framework</b>	<b>92</b>
5.1	Introduction . . . . .	93
5.2	Methodology . . . . .	97
5.2.1	Workflow of the proposed machine learning based framework . . . . .	97
5.2.1.1	EEG data acquisition . . . . .	98
5.2.1.2	Data pre-processing and artefact removal . . . . .	99
5.2.1.3	Generation of spectrogram image . . . . .	101
5.2.1.4	Feature extraction and dimension reduction . . . . .	102
5.2.1.5	Classification of the extracted features . . . . .	105
5.2.2	Workflow of the proposed deep learning based framework . . . . .	106
5.2.2.1	CNN model training for feature extraction . . . . .	106
5.2.2.2	Classification of different diseases . . . . .	107
5.2.2.3	Performance comparison with popular models . . . . .	108
5.2.2.4	Performance evaluation materials and parameters . . . . .	109
5.3	Results and discussion . . . . .	110
5.3.1	Experimental setup . . . . .	110
5.3.2	Results . . . . .	111
5.3.2.1	Machine learning based classification results . . . . .	111
5.3.2.2	Deep learning based classification results . . . . .	118
5.3.3	Discussion of the deep learning based classification . . . . .	126
5.3.3.1	Performance . . . . .	126
5.3.3.2	Model Complexity . . . . .	126
5.3.3.3	Execution Time . . . . .	127
5.3.3.4	Loss vs. accuracy graph . . . . .	127
5.3.3.5	Binary classification using the proposed model . . . . .	128
5.3.3.6	Comparison with existing researches . . . . .	130
5.4	Summary . . . . .	130
<b>6</b>	<b>Convolutional Neural Network Based Generic EEG Classification Framework</b>	<b>132</b>
6.1	Introduction . . . . .	132
6.2	Materials and proposed methods . . . . .	135
6.2.1	EEG data collection . . . . .	135
6.2.2	Preparing data for the proposed model . . . . .	136
6.2.2.1	Channel reduction to use standard channel data . . . . .	137
6.2.2.2	Resampling the signals to a standard frequency . . . . .	138
6.2.2.3	Segmentation of the EEG signals . . . . .	138
6.2.3	Proposed Generic EEG neural Network (GENet) model . . . . .	138
6.2.4	Classification using proposed GENet model . . . . .	140

6.2.5	Performance evaluation criteria . . . . .	141
6.3	Results and discussion . . . . .	142
6.3.1	Experimental setup . . . . .	142
6.3.2	Layer-wise feature visualisation of GENet . . . . .	142
6.3.3	Results . . . . .	143
6.3.3.1	Binary classification . . . . .	143
6.3.3.2	Multi-class classification . . . . .	146
6.3.4	Discussion . . . . .	148
6.3.4.1	Ablation study . . . . .	149
6.3.4.2	Time complexity analysis . . . . .	150
6.3.4.3	Data augmentation . . . . .	151
6.3.4.4	Comparison with existing studies . . . . .	151
6.4	Summary . . . . .	152
<b>7</b>	<b>Web Based System for Schizophrenia Detection using ConvLSTM based Subject Independent Analysis</b>	<b>153</b>
7.1	Introduction . . . . .	153
7.2	Methods and materials . . . . .	157
7.2.1	EEG data collection . . . . .	157
7.2.2	Segmentation of the EEG signals . . . . .	158
7.2.3	Proposed Subject Independent Schizophrenia Detection neural Network (SISDNet) model . . . . .	159
7.2.4	Classification using proposed SISDNet model . . . . .	160
7.2.5	Performance evaluation matrices . . . . .	161
7.3	Results and discussion . . . . .	162
7.3.1	Experimental setup . . . . .	162
7.3.2	Results . . . . .	162
7.3.2.1	Subject independent analysis . . . . .	162
7.3.2.2	Subject dependent analysis . . . . .	164
7.3.3	Discussion . . . . .	166
7.3.3.1	Layer-wise feature visualisation using t-SNE . . . . .	166
7.3.3.2	Ablation study . . . . .	166
7.3.3.3	Comparison with existing studies . . . . .	167
7.3.3.4	Web-based system for schizophrenia classification . . . . .	168
7.4	Summary . . . . .	182
<b>8</b>	<b>Conclusions and Future Work</b>	<b>183</b>
8.1	Summary of the dissertation . . . . .	183
8.2	Limitations of this research work . . . . .	185
8.3	Future work . . . . .	186
	<b>Bibliography</b>	<b>188</b>

# List of Figures

1.1	Chapter overview of the dissertation . . . . .	9
2.1	Main parts of a human brain [26]. . . . .	12
2.2	Anatomical areas of a human brain [26]. . . . .	13
2.3	Anatomy of a neuron [30]. . . . .	15
2.4	The <b>synapse</b> is where signals pass from one neuron to another. When the signal reaches the end of the axon, it triggers the release of neurotransmitters from tiny vesicles. These neurotransmitters cross the synapse and attach to receptors on the neighbouring cell, potentially altering the receiving cell's properties. If the receiving cell is also a neuron, the signal can continue transmission to the next cell [33]. . . . .	17
2.5	Hans Berger and his first recording of EEG signals in 1920s [37], [38]. . . . .	18
2.6	Electrodes divided into six scalp regions: frontal, central, parietal, occipital, right temporal, and left temporal [40]. . . . .	21
2.7	The international 10-20 electrode placement system [43]. . . . .	21
2.8	Sample EEG signals of five frequency bands [49]. . . . .	23
3.1	An overview of the proposed classification framework. . . . .	56
3.2	First CNN model. . . . .	57
3.3	Second CNN model. . . . .	58
3.4	Third CNN model. . . . .	58
3.5	Electrode placement to collect the EEG data [177]. . . . .	59
3.6	Sample spectrogram images generated by the proposed method: (a) ASD group, (b) non-ASD group . . . . .	60
3.7	Fold-wise sensitivity comparison for different ML-based classifiers. . . . .	63
3.8	Fold-wise specificity comparison for different ML-based classifiers. . . . .	63
3.9	Fold-wise accuracy comparison for different ML-based classifiers. . . . .	64
3.10	ROC graph for different ML-based classifiers. . . . .	65
3.11	Fold-wise AUC value comparison for different ML-based classifiers. . . . .	65
3.12	ROC graph of different CNN Models with different tested batch sizes for CNN model 3. . . . .	66
3.13	Training and validation loss vs. accuracy graph of third CNN Model with training batch size of 64. . . . .	67
4.1	A schematic diagram of the proposed classification framework combining topographic images and deep learning-based CNN model. . . . .	75

4.2	Proposed CNN model for the topographic image classification. . . . .	76
4.3	Examples of topographic images for the tested datasets. For HC and SZ individuals, 4.3a and 4.3b are from dataset 1 while 4.3c and 4.3d, respectively, are from dataset 2. . . . .	78
4.4	Fold-wise comparison of sensitivity value for different training batch sizes for the tested two datasets. . . . .	79
4.5	Fold-wise comparison of specificity value for different training batch sizes for the tested two datasets. . . . .	80
4.6	Fold-wise comparison of precision value for different training batch sizes for the tested two datasets. . . . .	81
4.7	Fold-wise comparison of accuracy value for different training batch sizes for the tested two datasets. . . . .	82
4.8	ROC curve for different training batch sizes of two datasets. . . . .	83
5.1	Schematic diagram of the proposed ML-based categorisation framework. . .	98
5.2	A typical 2000 sample EEG signal data points from the Fp1 channel of the four evaluated datasets. . . . .	100
5.3	CENTRIST applies the Census Transform (CT) calculating method. If the centre pixel is greater than (or equal to) one of its neighbours, a bit 1 is set in the appropriate location. Bit 0 is set if it is not. . . . .	102
5.4	An outline of the proposed DL-based multi-disease categorisation system. .	106
5.5	An structural outline of the proposed DL-based CNN model. . . . .	107
5.6	Overview of the used five-fold cross-validation technique. . . . .	109
5.7	Confusion matrix used for calculating the evaluation parameters for five class classification. . . . .	110
5.8	Sample spectrogram images generated by the proposed method for different datasets. . . . .	111
5.9	Round-wise accuracy comparison for different ML-based classifiers tested in this study. . . . .	112
5.10	Five-fold average accuracy with standard deviation for different ML-based classifiers. . . . .	114
5.11	Round-wise comparison of sensitivity values for different ML-based classifiers.	115
5.12	Round wise comparison of specificity values for different ML-based classifiers.	115
5.13	Round wise comparison of precision values for different classifiers. . . . .	116
5.14	Round wise comparison of F1 score values for different ML-based classifiers.	117
5.15	Comparison of ROC graphs for different ML-based classifiers tested in this study. . . . .	118
5.16	Fold-wise comparison of the sensitivity values for the three tested DL-based models with different training batch sizes. . . . .	120
5.17	Fold-wise comparison of the specificity values for the three tested DL-based models with different training batch sizes. . . . .	121

5.18	Fold-wise comparison of the precision values for the three tested DL-based models with different training batch sizes. . . . .	122
5.19	Fold-wise comparison of the F1 score values for the three tested DL-based models with different training batch sizes. . . . .	123
5.20	Fold-wise comparison of the accuracy values for the three tested DL-based models with different training batch sizes. . . . .	124
5.21	Five-fold average accuracy with standard deviation for the three tested DL-based models with different training batch sizes. . . . .	125
5.22	Comparison of ROC graphs for the three tested DL-based models with different training batch sizes. . . . .	126
5.23	Comparison of the execution times of the three evaluated CNN models for different training batch sizes. . . . .	127
5.24	The evolution of accuracy and loss across epochs during the training and validation of the proposed model. . . . .	128
5.25	The evolution of accuracy and loss across epochs during the training and validation of the ResNet50 model. . . . .	129
5.26	The evolution of accuracy and loss across epochs during the training and validation of the AlexNet model. . . . .	129
6.1	An schematic diagram of the developed framework and steps involved in the process. Four modules of the framework are discussed in four subsections 7.2.1, 6.2.2, 6.2.3, and 6.2.4. . . . .	135
6.2	Standard electrode locations used for EEG data recording using the international 10-20 system. . . . .	137
6.3	GENet: the proposed CNN model. . . . .	139
6.4	Layer-wise classification process visualisation of the GENet model using t-SNE images. Here, features from test subjects are plotted from the input layer to the output layer for the tested SZ2 dataset. At the input layer, there was no clear cluster between two classes (SZ vs. Normal), but as the data progressed from the hidden layers to the output layer, it formed two clearly separable clusters of two classes. . . . .	143
6.5	Accuracy comparison of the GENet model for the three tested signal segment lengths (1s, 2s, and 3s). Seven subplots represent seven tested datasets (SZ1, SZ2, MCI, ADHD, EP, PD, and ASD). In each subplot, four groups of bars represent four training batch sizes (32, 64, 128, and 256). . . . .	144
6.6	A comparison graph of the four evaluation parameters (Sen, Spec, Prec, and F1) with standard deviation for the GENet model. Each subplot represents an evaluation parameter, and the x-axis has the seven assessed datasets. For each dataset, we have four bars for four different training batch sizes (32, 64, 128, and 256). . . . .	145
6.7	ROC graph of the GENet model on tested datasets. . . . .	147

6.8	Spider plot visualisation for fold wise sensitivity, specificity, precision, and accuracy comparison of the GENet model for multi-class classification with different tested batch sizes. Data has five folds (Fold 1,2,...,5) and each polygon is a multivariate data point for a training batch size. . . . .	149
7.1	An overview illustration of the proposed framework and steps involved in the classification process. . . . .	157
7.2	Proposed ConvLSTM based SISDNet model layout. . . . .	160
7.3	Subject-wise accuracy comparison of the SISDNet model for the three training batch sizes on the Kaggle dataset. . . . .	163
7.4	Subject-wise accuracy comparison of the SISDNet model for the three training batch sizes on the Warsaw dataset. . . . .	163
7.5	Fold and batch size-wise comparison of the evaluation parameters for the Kaggle dataset. . . . .	164
7.6	Fold and batch size-wise comparison of the evaluation parameters for the Warsaw dataset. . . . .	165
7.7	Visualisation of the layer-wise classification process in the SISDNet model using t-SNE images. Here visualisation is plotted from the input layer to the output layer for the tested Warsaw dataset with batch size 64. At the input layer, there was no clear cluster between two classes (SZ vs. Normal), but as the data progressed from the hidden layers to the output layer, it formed two clearly separable clusters of two classes. . . . .	167
7.8	Workflow of the developed web-based system using the proposed SISDNet framework. The user uploads EEG data to the web server using a computer device. The server uses two services to perform the classification task: 1) the data processing service pre-processes the uploaded data, and 2) the classification service performs the classification on the processed data. . . .	170
7.9	The Homepage of the developed web-based classification system. . . . .	171
7.10	Information page of the developed web-based classification system. It contains information about the developer and the supervisor panel of the project, as well as links to their profiles on different social and institutional sites. . . . .	172
7.11	Contact page of the website. On this page, an user can contact the system support team with any issues or suggestions regarding the website. . . . .	173
7.12	Login page of the website. Users need to have an account to use the classification service of the system. By using the email and password, they can login to the system. . . . .	174
7.13	Login page of the website. Users need to have an account to use the classification service of the system. By using the email and password, they can login to the system. . . . .	175
7.14	This page is for resetting the account password. If the user forgets her or his password, then she or he can request to reset it by using this page. . . .	176

7.15	This page is for changing the account password. The user needs to put the current password and the new password for changing the account password.	177
7.16	This page shows the data preparation instruction before uploading to the classification service. . . . .	178
7.17	Web page for uploading the data to the classification server. . . . .	179
7.18	This page shows the list of classification request an user have made till now. They can also see the details result of the classification by clicking on the view result button at the end of each row. . . . .	180
7.19	Details result page of a classification request displayed using different charts and tables. . . . .	181

# List of Tables

3.1	Overall classification performance of different ML-based classifiers. . . . .	62
3.2	Overall classification performance of different tested CNN models. . . . .	66
3.3	Performance comparison of the proposed framework with existing methods using the same EEG dataset. . . . .	67
3.4	Performance comparison of the proposed framework with existing methods using different EEG datasets. . . . .	68
4.1	Results of the proposed method’s ten-fold average performance (mean±std) on two test datasets for various batch sizes. . . . .	79
4.2	Comparison of performance with previous research using the same datasets.	84
5.1	Demographic information pertaining to the datasets in use. . . . .	99
5.2	Average sensitivity, specificity, precision, F1 score, and accuracy results for the two distinct feature extractors (cCENTRIST and tCENTRIST) combined with four distinct classifiers (SVM, RF, LDA, and $k$ NN with $k=9$ ) across five rounds . . . . .	113
5.3	The average performance results using a five-fold cross-validation approach for the proposed model in a multi-class classification scenario. . . . .	118
5.4	The average performance results using a five-fold cross-validation approach for the AlexNet model in a multi-class classification scenario. . . . .	119
5.5	The average performance results using a five-fold cross-validation approach for the ResNet50 model in a multi-class classification scenario. . . . .	119
5.6	Comparative analysis of the architectural aspects among the evaluated CNN models. . . . .	127
5.7	The mean performance outcomes of the proposed model using a five-fold cross-validation approach, while employing various batch sizes, in a binary classification setting. . . . .	130
5.8	Comparing our study with prior binary classification research on four specific diseases that utilised same datasets. . . . .	130
6.1	Demographic information related to the datasets used in this research. . . .	137
6.2	Architectural details of the GENet model. . . . .	141
6.3	The GENet model’s performance, averaged over five-fold cross-validation and presented with standard deviations, across seven evaluated datasets while using four different training batch sizes. . . . .	145

6.4	The average performance results of the GENet model in a multi-class classification scenario, obtained through five-fold cross-validation. . . . .	148
6.5	Ablation study results on dataset SZ1 and SZ2. . . . .	150
6.6	Analysis of the proposed GENet model’s time complexity for two SZ datasets evaluated with various batch size configurations. . . . .	151
6.7	Comparison of the accuracy of various data augmentation methods applied to the SZ1 and SZ2 datasets. . . . .	151
6.8	Assessing the proposed GENet model in comparison to the pre-existing state-of-the-art (SoA) studies that utilised the same datasets. . . . .	152
7.1	Demographic data for the datasets used in this study. . . . .	158
7.2	SISDNet model’s architectural specifics. . . . .	160
7.3	Performance of the proposed SISDNet model in subject independent analysis on the Kaggle and Warsaw datasets with different training batch sizes. . . . .	163
7.4	Ten-fold average performance results of the SISDNet model on multi-class classification. . . . .	164
7.5	Ablation study results on tested Kaggle and Warsaw datasets for 10-fold cross-validation Here, we have conducted the ablation study using a training batch size of 32 for both datasets and compared the results of other tested models with the base model’s results. . . . .	167
7.6	Comparative analysis of the proposed model with Kaggle dataset’s existing research. . . . .	168
7.7	Comparative analysis of the proposed model with Warsaw dataset’s existing research. . . . .	169

## Chapter 1

# Introduction

Brain health is a concept that is always changing, gaining attention from the health industry as well as from the general public, and this engenders extensive discussions for valid reasons. The human body's command centre is the brain and central nervous system, which regulate both conscious and unconscious bodily processes and so have an impact on every area of existence [1]. When our brains are impaired by illness or other reasons, there are serious hazards involved for not just the general health and wellbeing of an individual but also for the production and growth of the entire world [1]. As per predictions, it is estimated that approximately one out of every three individuals could potentially encounter the onset of a neurological condition during their lifetime. This places neurological conditions as the second leading cause of mortality and the primary contributor to disability [1]. In addition, it is thought that extreme poverty and growth impairment cause 43% of children under the age of five in low- and middle-income nations to fall short of their developmental potential, which would result in financial losses and anticipated yearly earnings that are 26% lower when they reach adulthood [1].

Neurological disorders are diseases related to the brain, spinal cord, nervous system, neuromuscular junction, and muscles [2]. 10% of the global disease burden and 30% of the non-fatal disease burden come from mental, neurological, and substance use disorders [3]. Neurological conditions were the fourth-highest contributor to the fatal burden of disease in Australia in 2022 [4]. The overall worldwide social cost of dementia in 2019 was anticipated to reach US\$ 1.3 trillion, approximately 1.5% of global GDP [5]. Dementia, depression, bipolar disorder, schizophrenia, and other psychoses, as well as developmental disorders including autism spectrum disorder, are the major neurological disorders. In this study, we will mainly consider two diseases for our research: autism spectrum disorder and schizophrenia.

Autism spectrum disorder (ASD) comprises a range of intricate neurological developmental conditions, encompassing autism, childhood disintegrative disorder, Asperger's syndrome, and an unspecified variant of pervasive developmental disorder [6]. The scope and intensity of ASD symptoms can exhibit significant variation, but frequently encompass challenges in social communication and interaction, intense preoccupations, diminished eye contact, and repetitive behaviours. ASD typically emerges in early childhood, often manifesting by the age of five, and tends to endure into adulthood [7]. The World Health Organisation (WHO) reported that globally, in every 100 children, one child is diagnosed

with ASD [7], [8]. In Australia, the prevalence of autism increases by approximately 40%, transitioning from one in 100 individuals to approximately one in 70 individuals falling within the autism spectrum [9]. According to data from the Centers for Disease Control and Prevention (CDC), as of 2020, roughly one in 54 children in the United States received a diagnosis of an ASD [10]. ASDs can markedly impede an individual's ability to engage in daily routines and participate fully in society. They frequently have adverse effects on a person's educational and social accomplishments, employment prospects, daily life functioning, and integration into the community. Worldwide, individuals with ASD often face challenges such as discrimination, stigmatisation, and violations of their human rights [7]. To date, there is no known cure for ASD; however, early intervention has the potential to enhance brain development and improve learning, communication, and social skills [7].

Schizophrenia (SZ) is a chronic brain disorder that affects a person's thinking, feelings, behaviours, and normal functionality. Symptoms can include hallucinations, delusions, disorganised talking, trouble with thinking, and a lack of motivation [11]. According to WHO, worldwide, 24 million people are affected by it, and in Australia, between 150,000 and 200,000 people are affected by it [12]. Schizophrenic people are vulnerable and 2-3 times more likely to die early than the general population [13]. SZ is treatable with medicines and psychosocial support. So, detection of ASD and SZ is important for treatment and intervention.

## 1.1 Research challenges and motivation

Comprising approximately 86 billion neurons, the human brain is widely regarded the most complicated biological structure within the observable universe. It has a storage capacity of about  $1.25 \times 10^{12}$  bytes and an interconnection distance of at least 100,000 kilometres [14], [15]. It controls perception, thinking, paying attention, emotion, memory, and doing actions [15], [16]. It serves as the central controller of the body by transmitting and receiving information as electrical impulses known as action potentials. The human brain responds to every stimulus by creating action potentials, or electrical impulses. The primary challenge is to capture those electrical impulses and use that knowledge to advance a better understanding of several brain disorders. However, the extraction of insights from vast datasets and the identification of psychiatric disorders represent pivotal and expansive domains within the realm of biomedical science. The assessment of neurological disorders necessitates an examination of the functional aspects of the brain. Various methodologies are available for studying the functional states of the brain, including magnetic resonance imaging (MRI), functional magnetic resonance imaging (fMRI), positron emission tomography (PET), electrocorticography (ECoG), and electroencephalography (EEG) [17].

EEG is a highly employed method for capturing brain signals due to its exceptional temporal precision, non-invasive nature, user-friendliness, and cost-effectiveness [18]. It yields huge amounts of multi-channel EEG signals that neurologists traditionally analyse visually in order to detect and comprehend neurological irregularities. Nevertheless, the

absence of standardised assessment criteria renders this visual inspection an impractical and time-consuming process, marked by the potential for errors, exhaustive effort, subjectivity, high costs, and reliability concerns [19]. Moreover, some neurological disorders share overlapping features in EEG signals, which may lead to misdiagnosis.

As such, there is a need for developing an automated system to evaluate and diagnose neurological disorder from EEG signals in real-time to help the neurologist. This PhD research study builds analysis techniques to automatically detect neurological biomarkers from brain signal data and help clinicians properly diagnose their patients suffering from ASD and SZ.

## 1.2 Research problem statements

EEG recording produces a large volume of data comprising diverse categories, especially when the recordings span a prolonged time period. Despite the amount of brain function-related information present in EEG recordings, the procedures for classifying and evaluating these signals have not been adequately developed. To effectively extract valuable insights from such extensive data, automated methods become indispensable for analysing and classifying the information using appropriate techniques. Traditionally, EEG recordings are evaluated visually by experienced clinicians who manually scan the EEG records to detect abnormalities in them, but this is error-prone, subjective, and unsatisfactory due to the lack of standardised criteria for assessments and the inherent time-consuming nature that can lead to errors stemming from fatigue [20], [21]. As a result, there is a need to develop automatic systems capable of classifying the recorded EEG signals more efficiently.

After reviewing an extensive amount of research papers, we have found some gaps that can be articulated as some research problems. This research study aims to analyse the EEG brain signal data to find solutions for the following research problems:

**Research Problem 1 (RP1):** *Detecting neurological disorders like ASD and SZ from EEG data is an ongoing challenge for researchers and neurologists. EEG is a huge volume of data that holds the functional state of the brain. Currently, the examination of EEG recordings to identify ASD and SZ is still reliant on manual investigations conducted by expert clinicians. Also, EEG signals have huge data quantities and high spatial variability, so it is very difficult to extract valuable information from EEG signals using traditional machine learning or data mining approaches. Despite much investigation of EEG data, researchers are as yet unable to use it to its fullest in a continuous decision-making process. Hence, there is a need to develop methods that can extract additional valuable information from EEG signals and improve classification performance.*

**Research Problem 2 (RP2):** *The second research gap we have found is the scarcity of multi-disease classifiers. The majority of current research has focused on classifying a single disease in comparison to healthy controls (HC). However, even in the few studies that address multi-class classification, they typically involve no more than two diseases. Consequently, diagnosing a patient's EEG signal for multiple diseases necessitates the*

use of multiple CAD systems, which can be both costly and time-consuming. Therefore, there is a pressing need for an effective, reliable, and high-accuracy CAD system that can diagnose multiple neurological diseases within a single framework, i.e., a multi-disease classifier. This approach would help overcome the scarcity of expert neurologists and reduce the diagnostic costs associated with handling multiple diseases.

**Research Problem 3 (RP3):** The next research gap we have found is related to the generalisability of the developed methods. Despite numerous published studies on EEG signal classification in recent years, they suffer from a significant limitation in adaptability, i.e., the developed methods are mostly tested on a particular dataset of a particular disease. This is because methods designed to handle specific EEG classification problems may not be fully efficient when applied to classify EEG signals associated with different diseases. The challenges arise from the nonstationarity, non-linearity, and strong localisation present in the temporal, spectral, and spatial dimensions of EEG signals. Each neurological disorder exhibits distinct periodic and statistical properties in the underlying EEG characteristics, making it difficult to employ a detection method created for one disorder to effectively examine another. So, there is a need for developing a generalised framework that is dataset- and disease-independent.

**Research Problem 4 (RP4):** Although several studies have been done on EEG signal classification in the past few years, there is still a scarcity of CAD systems to help clinicians in their diagnosis process. An automated and efficient CAD system can reduce the manual process for the clinician and also curtail the cost of diagnosing neurological disorders.

Based on the above research problems, in this study, we have proposed five different methods:

- First two methods are proposed to address the first research problem for classifying ASD and SZ from HC subjects using EEG data. In the first method, We have differentiated ASD participants from HC subjects using the spectrogram image representation of the EEG data. We have applied both ML- and DL-based approaches to the spectrogram images to do the categorization. In the second proposed method, we have used the entropy topography based visual representation of the EEG signal with DL-based models to classify SZ from HC subjects. **(RP1)**
- To address the second research problem we have proposed the third method which is a single framework for classifying four neurological disorders from HC subjects. In this developed method we have used the spectrogram images of EEG data from the four neurological disorders with both ML and DL-based classification techniques to carry out the classification task. **(RP2)**
- In the fourth method, we have tried to address the third research issue. Here, a generic CNN based framework is proposed for classifying EEG signals from different neurological disorders and also from different data sources for the same disorders. We have tested the proposed model on seven different datasets from six different neurological disorders. **(RP3)**

- Finally, the fifth method is for developing a CAD system for classifying SZ subjects from HC subjects using EEG data. In this method, we have used DL-based Convolutional Long Short-Term Memory (ConvLSTM) model to perform classification of SZ from HC subject using leave-one-subject-out cross-validation technique. Then, we have used the trained model to develop a web-based system for identification of SZ from user uploaded data. **(RP4)**

### 1.3 Research objectives

In this research study, different DL-based techniques are used in EEG signal analysis for the detection or classification of neurological abnormalities. Five different methods have been proposed to address the four research questions in this dissertation. The performance of the newly developed methods is compared with the existing techniques in the same EEG disorder domain. The following list summarises the objectives of this dissertation:

- To develop DL-based EEG signal classification techniques for ASD and SZ detection.
- To explore the feasibility of time-frequency (T-F) spectrogram image representation of EEG signal for different neurological disorder classifications.
- To evaluate the viability of topographic image representation of EEG signals for SZ classification.
- To develop a single framework for multiple neurological disorder classifications.
- To explore the feasibility of a generic framework for disease- and dataset-independent EEG signal classification.
- To develop a web-based system to provide services for neurological disorder detection.
- To research state-of-the-art EEG data processing techniques for the identification of neurological disorders and to improve their performance.
- To provide automated EEG analysis and classification methods for the identification of anomalies in EEG.

### 1.4 Significance of the study

Diagnosis of mental disorders is typically carried out using clinical interviews designed based on the two standard diagnosis systems: the Diagnostic and Statistical Manual of Mental Disorders (DSM-5) and the International Classification of Diseases, 11th Revision (ICD-11). These systems are based on symptoms related to individual diseases, which can include behavioural, cognitive, emotional, or physical disturbances. However, this subjective assessment approach can be error-prone and vary from expert to expert as the symptoms overlap across the diseases. That is why researchers have been trying to develop new ways to help clinical diagnosis using computerised automated systems.

This research project will address the lack of knowledge in this area by examining various aspects, such as why these algorithms are dataset-specific in nature. Although lots of remarkable research has been conducted in this field, there is still a need to develop systems that can automatically detect abnormalities in EEG signals and reduce false positive and false negative rates. The data mining approach developed by this study will help in the diagnosis and identification of abnormalities in patients in real-time.

The detection of various types of anomalies from biomedical data through the recognition of abnormal period patterns is valuable for many applications. This research will be significant by developing a new technique for ASD and SZ detection, which will offer considerable importance in the medical field as well as future research in this area. The main significance of the study is:

- Will significantly advance the current data mining techniques used at various levels of EEG data analysis, such as data pre-processing, feature extraction, and recognition of brain potential abnormalities.
- Will help technologists build up a computer-assisted analysis system for accurately identifying ASD and SZ.
- Will be beneficial to the medical field while at the same time contributing to the academic world of ASD and SZ-related research.
- Will be helpful for clinical diagnosis.
  - To help the expert neurologist identify ASD and SZ
  - Aids for improving the diagnosis of ASD and SZ from EEG signals
- By correlating the information gained by these techniques with different medication regimens, a physician can more quickly decide on a treatment plan that maximally benefits the patient.

It is hoped that the output of this research work will be beneficial to the medical field while at the same time contributing to knowledge enhancement in the academic world.

## 1.5 Contributions of the dissertation

The research described in this dissertation focuses on the classification of EEG signals from various brain activities for the analysis of various brain disorders. In this dissertation, we have presented five methods for the identification of various kinds of neurological disorders. The major goal of this work is to provide methodologies and procedures for the classification of ASD and SZ EEG signals from healthy subjects. We have also compared our proposed algorithms with other recently published works to see how well those approaches function. The following points illustrate the dissertation's contributions:

1. Introduce the spectrogram representation of the EEG signals for ASD classification.

2. Introduce the topographic representation of the EEG signals for SZ classification.
3. Develop a multi-disease classification framework using EEG data to classify different neurological disorders.
4. Develop a generic framework for classifying EEG signals for various neurological disorders.
5. Develop a web-based system for SZ identification from EEG data.

Below, we cover some quick facts about the contribution points.

### **1. Introduce the spectrogram representation of the EEG signals for ASD classification:**

In our first proposed method, we have used the spectrogram image representation of the EEG data to classify ASD subjects from HC subjects. To perform classification on the spectrogram images, we have used both ML- and DL-based techniques. In the ML-based approach, a histogram-based feature extraction technique is used, and then the dimensions of the extracted features are reduced using principle component analysis (PCA). Finally, four different ML-based classifiers are used to perform the classification on those extracted features. In the DL-based approach, three different convolutional neural networks (CNN) are developed to carry out the classification task on those images. The experimental results demonstrate that the proposed approach has significant advantages over other existing methods.

### **2. Introduce the topographic representation of the EEG signals for SZ classification:**

The second method we have proposed is based on the topographic representation of the EEG data for SZ detection. Here, we have used the Shannon entropy (ShanEn) of the EEG signals to calculate the channel-wise entropy value and the topographic plotting technique to generate the visual representation of the signal data entropy. Then we have proposed a CNN model to perform classification on those topographic images for SZ detection. The experimental results demonstrate that the proposed approach has significant advantages over many other existing methods.

### **3. Develop a multi-disease classification framework using EEG data to classify different neurological disorders:**

In our third proposed method, we have developed a multi-disease classification framework to classify four different neurological disorders using EEG data. In this framework, we have used the spectrogram representation of the EEG data and then used both ML and DL-based processes for classification. In the ML-based approach, we have used two different histogram-based feature extraction methods in combination with PCA and four different

ML-based classifiers to check their performance. In the DL-based approach, a CNN model is developed and used to perform the classification. We have also used two existing popular CNN models to compare the performance of the proposed CNN model with those existing popular models and obtained better results than those popular models using the proposed model.

#### **4. Develop a generic framework for classifying EEG signals for various neurological disorders:**

In this proposed approach, we tried to work around the existing dataset and disorder-dependent solutions by developing a CNN-based generic framework named GENet to classify EEG signal data from different neurological disorders. In this method, EEG data are segmented, and then the GENet model is used to perform feature extraction and classification of those signal data. Seven different EEG datasets for six different neurological disorders are used to validate the proposed model. We have performed both binary classification on those datasets and a multi-class classification using four of those seven datasets. Both the binary and multi-class classification results have shown promising results in the existing studies.

#### **5. Develop a web-based system for SZ identification from EEG data:**

In this fifth method, we have developed a web-based system for SZ detection from EEG signal data. To perform the classification task, we have developed a framework using a DL-based Convolutional Long Short-Term Memory (ConvLSTM) model, performed the classification using the leave-one-out-cross validation (LOOCV) technique, and used the trained model in the back-end of the website to perform SZ detection on the uploaded user data. In this framework, EEG data are segmented, and the proposed ConvLSTM model is trained using those data. Finally, the trained model is used to perform classification on the test data. The developed web-based system will be helpful in the clinical diagnosis process for SZ disorder.

In this research work, we have tried to develop some new approaches for the classification of EEG data to identify ASD and SZ and hope that the proposed methods contribute to successful classification approaches. Finally, the developed web-based system can be used in the clinical diagnosis process of SZ disorder and can be extended for other neurological disorder diagnosis purposes.

## **1.6 Structure of the Dissertation**

This dissertation consists of eight chapters, each containing important information related to our research. Figure 1.1 shows an overview of this thesis structure.

A brief discussion about those chapters is given below:

- **Chapter 2** provides an overview of EEG signal classification techniques and research related to EEG signal analysis. This chapter briefly introduces the background

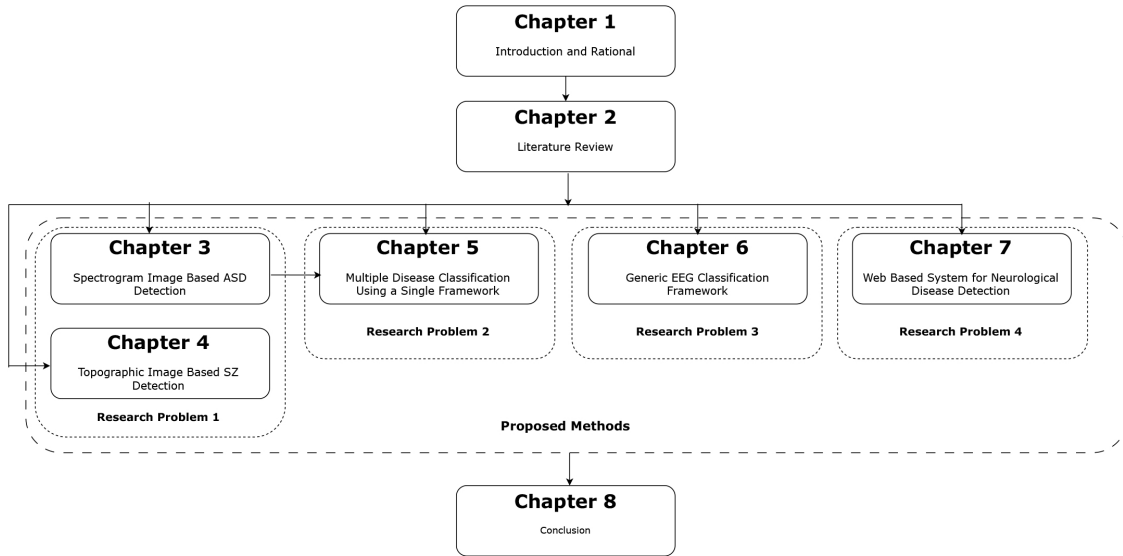


FIGURE 1.1: Chapter overview of the dissertation

knowledge and related information for this research and studies related to ASD and SZ.

- **Chapter 3** introduces the first method of this dissertation, which is a spectrogram image-based EEG signal classification technique for ASD disorder. This research study was the first in the field of ASD detection to introduce the spectrogram image-based classification technique. In this process, EEG signals are first converted to spectrogram images, and then classification operations are carried out on those images using different image categorisation techniques. This classification technique can be used to distinguish ASD subjects from HC subjects.
- **Chapter 4** reports the second proposed method, which is a topographic image-based EEG signal classification technique for SZ disease. This classification technique was also the first in the field of SZ classification from EEG data. This categorisation technique combines Shannon entropy-based topographic images with a convolutional neural network to differentiate between SZ and HC participants. The proposed model is evaluated using two different datasets with different deep learning configurations, and the obtained results showed that the developed method is promising for SZ detection.
- **Chapter 5** introduces a spectrogram image-based EEG signal classification technique for multiple neurological disorders. This classification technique is proposed to perform a multi-class classification task for four neurological disorders, namely, ASD, EP, PD, and SZ, from HC subjects.
- **Chapter 6** presents a generic CNN-based model named GENet for classifying raw EEG data of different neurological diseases. It is developed to work on disease-independent EEG signal categorisation.

- **Chapter 7** introduces a ConvLSTM-based framework for subject-independent SZ classification. It will also present the web platform that is developed using the subject-independent ConvLSTM model to provide support for the clinicians.
- **Chapter 8** gives a summary of the study presented by this research as well as the findings. This chapter also contains details on future works.

## Chapter 2

# Background

This research will build on the existing literature in the area of detecting ASD and SZ from brain signals. EEG reflects the electrical activity of the human brain and provides evidence of brain's function over time, which makes EEG as widely used to study brain functions and to diagnose neurological disorders like SZ, epilepsy, brain tumours, head injury, sleep disorders, dementia etc. by physicians and scientists. It is also helpful for the treatment of abnormalities, behavioural disturbances (e.g., ASD), attention disorders, learning problems and language delay [22]. Several studies have been accomplished to detect different mental disorders from which some of the reported literature are discussed in this chapter.

To create an effective automated system for EEG data classification, a comprehensive understanding of EEG signals is crucial. Therefore, this chapter provides essential and overarching information on the generation of EEG signals and their significance in diagnosing brain disorders.

### 2.1 Human brain anatomy

The human brain is an intricate organ responsible for regulating not only essential bodily functions but also cognitive processes, memory, emotions, sensory perception, motor skills, vision, respiration, temperature control, and hunger. At the core of this complex system is the central nervous system, which includes the spinal cord originating from the brain [23]–[25]. It also controls heart and respiration rates, which affects how people react to stressful events. The brain's weight varies throughout life. At birth, it weighs around one pound, increasing to about two pounds during childhood. In adulthood, the average female brain weighs about 2.7 pounds, while an adult male's brain weighs around three pounds. It is composed of approximately 60% fat and 40% water, carbohydrates, protein, and salts [26]. It includes blood vessels and nerves, consisting of neurons and glial cells [26].

#### 2.1.1 Brain structures and their functions

On a high level, the brain can be divided into three major parts named cerebellum, brainstem and cerebrum [23], [26] as shown in Figure 2.1. A brief description of those parts are given below:

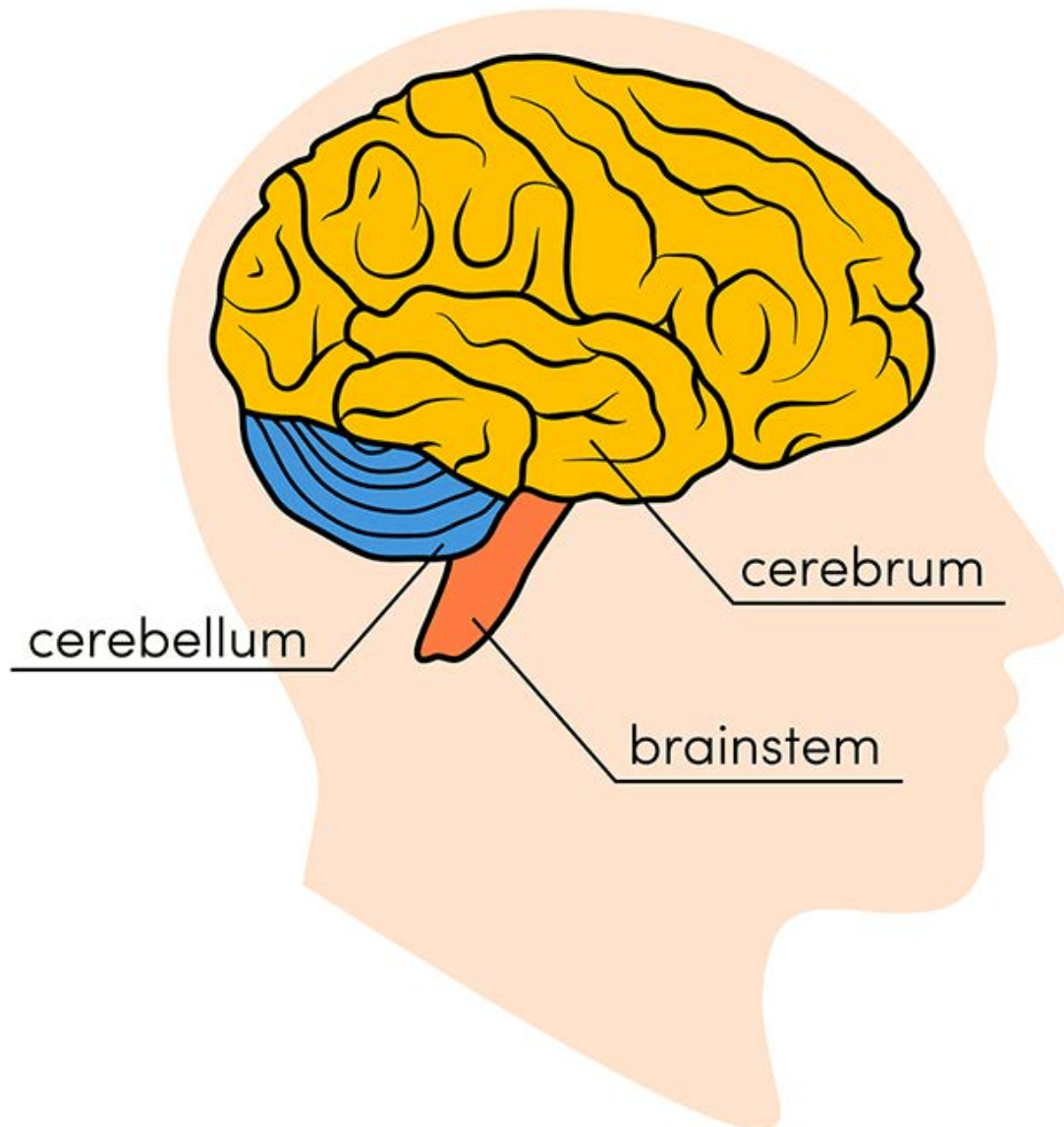


FIGURE 2.1: Main parts of a human brain [26].

#### 2.1.1.1 Cerebrum

The cerebrum is the largest and most important part of the human brain, and is essential to many higher-order cognitive operations. It is split into two hemispheres, the left and the right, and is situated at the front and top of the brain [16], [27]. A network of nerve fibres known as the corpus callosum connects the two hemispheres and enables communication and information sharing between them [16], [27]. Numerous cognitive processes are carried out by the cerebrum, including [16], [23], [27]:

- **Conscious Thought:** It contributes to our awareness, perception, and comprehension of our surroundings. We can think, explain, and make decisions because of this area.
- **Sensory Processing:** It takes in and interprets sensory data from its surroundings,

such as touch, vision, hearing, taste, and smell. The cerebrum's several sections are each tailored for processing particular sensory inputs.

- **Language:** Language comprehension and production are predominantly located in certain areas of the cerebrum, typically in the left hemisphere in most individuals.
- **Motor Control:** The cerebrum is in charge of directing the body's voluntary motions. It contains the main motor cortex, which communicates with the muscles to initiate movement.
- **Emotions:** Through links with other brain areas, it contributes to the regulation of emotions and responses to emotions.
- **Memory:** The cerebrum has a role in the creation of memories as well as short-term, long-term, and general memory functions.
- **Problem-Solving and Learning:** The cerebrum plays a critical role in problem-solving, skill acquisition, and situational adaptation.

The cerebrum's outermost layer comprises neural tissues referred to as the cerebral cortex. Within each hemisphere of the brain, there exist four distinct sections known as lobes: frontal, parietal, temporal, and occipital, each assigned specific functions and roles [16]. Figure 2.1 shows those four lobes with other parts of the brain.

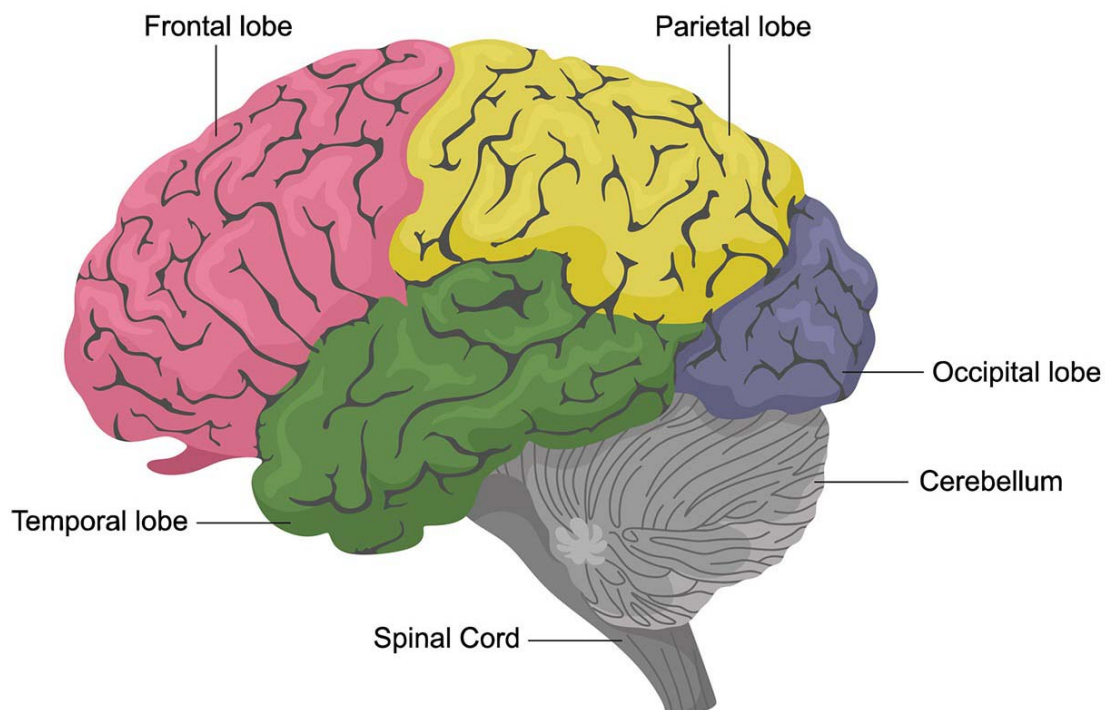


FIGURE 2.2: Anatomical areas of a human brain [26].

Details of the lobes are discussed below [16]:

- **Frontal Lobe:** The largest segment of the brain, known as the frontal lobe, oversees personality traits, decision-making processes, and motor functions. It is situated in the front of the cranial region. Within the frontal lobe, there is also an area associated with smell recognition and the Broca's region, which plays a role in language and speech abilities.
- **Parietal Lobe:** Positioned at the centre of the brain, the parietal lobe plays a vital role in object recognition and the understanding of spatial relationships. Additionally, it is involved in processing tactile sensations and pain perception from the body. Furthermore, within the parietal lobe, one can find Wernicke's area, which contributes to the brain's comprehension of spoken language.
- **Temporal Lobe:** Situated on the lateral sides of the brain, it plays roles in short-term memory, speech processing, musical rhythm perception, and, to a certain degree, smell recognition.
- **Occipital Lobe:** The posterior part of the brain is responsible for visual processing.

#### 2.1.1.2 cerebellum

The cerebellum, often referred to as the "small brain," is a compact structure located at the posterior part of the head, situated above the brainstem and below the temporal and occipital lobes [28]. Comprising two hemispheres similar to the cerebral cortex, the inner region interfaces with the cerebral cortex, while the outer region contains neurons. Remarkably, it constitutes approximately 10% of the brain's total weight but houses roughly 80% of all neurons in the brain [29]. Its primary functions encompass maintaining posture, balance, and coordination of voluntary muscle movements. However, recent research, as explored in [26], has delved into the cerebellum's potential involvement in emotional regulation, cognitive processes, social behaviour, and its conceivable roles in conditions such as addiction, autism, and schizophrenia.

#### 2.1.1.3 brainstem

The brainstem, situated at the base of the brain, forms the critical link between the cerebrum and the spinal cord. Comprising three distinct structures - the midbrain, pons, and medulla oblongata - it operates as a vital relay station, facilitating the transmission of signals between various regions of the body and the cerebral cortex [26]. This intricate structure plays a pivotal role in regulating several fundamental physiological processes, including respiration, awareness, control of eye and mouth movements, as well as the relay of sensory information such as pain, temperature, and auditory stimuli. Furthermore, it exerts control over essential bodily functions like heart rate, blood pressure, and appetite [26].

### 2.1.2 Communication system of human brain

The communication system of the human brain is a complex network of neurons (nerve cells) and glial cells (supporting cells) that work collectively to send and process information. Electrical and chemical signals are used to communicate inside and among various brain areas. Billions of neurons possess the remarkable ability to engage in rapid communication with one another by means of chemical messengers known as neurotransmitters. Neurons vary in shape and size, but they all have four components: dendrites, a soma (cell body), an axon, and axon (synaptic) terminals [15], [16]. Figure 2.3 shows the structure of a neurone with its components. A brief description of those parts is given below:

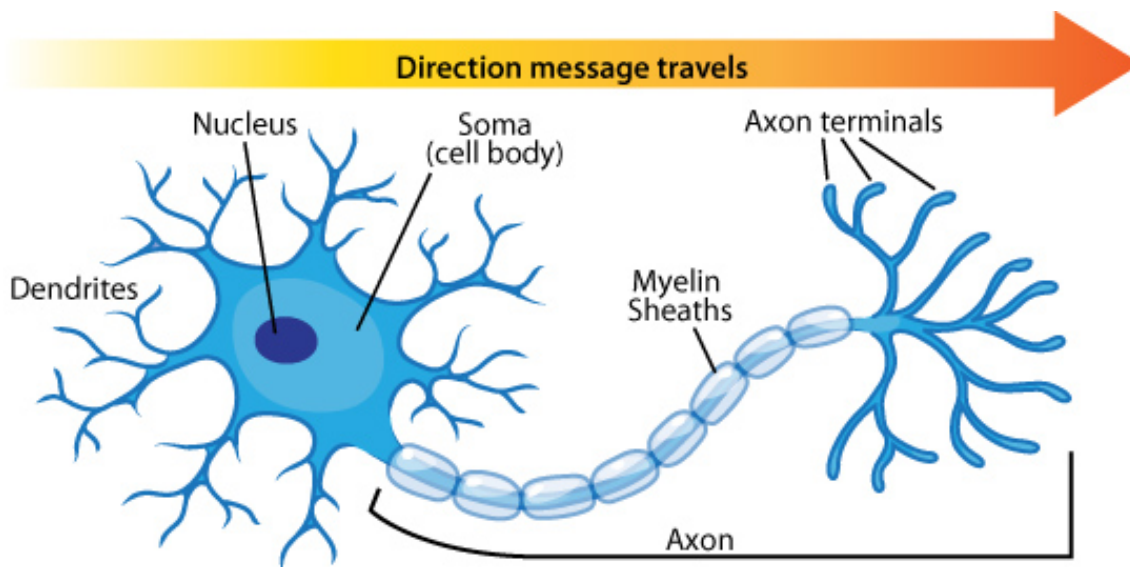


FIGURE 2.3: Anatomy of a neuron [30].

#### 2.1.2.1 Dendrites

Dendrites are branch-like extensions of neurons, resembling the roots of a tree, that extend from the cell body. They play a vital role in receiving information from other neurons and transmitting electrical signals back to the cell body. Covered in synapses, dendrites facilitate communication between neurons. It's worth noting that dendrites can vary in length among neurons, with some having longer dendritic extensions than others. In the central nervous system, neurons often exhibit long, intricate dendrites, enabling them to receive signals from a multitude of other neurons.

#### 2.1.2.2 Soma (Cell Body)

Fundamentally, the soma, often referred to as the cell body, serves as the core of the neuron. Its primary function is to uphold the overall well-being of the cell and ensure the proper functioning of the neuron [31]. Housed within the soma is the cell nucleus, responsible for the generation of genetic information and the orchestration of protein synthesis. These essential proteins, in turn, play a critical role in facilitating the operation

of other components within the neuron. Encasing the soma is a membrane that not only provides protection but also enables communication between the soma and its immediate surroundings.

### 2.1.2.3 Axon

The axon, also known as a nerve fibre, extends from the cell body of the neuron at a region called the axon hillock. Its primary function is to convey signals away from the cell body and toward terminal buttons, facilitating the transmission of electrical impulses to other neurons. In terms of size, axons can vary widely, ranging from as small as 0.1 millimetres to exceeding 3 feet in length [32]. Some axons are enveloped in myelin, a fatty substance that serves as insulation, thereby enhancing the speed of signal transmission. These long nerve processes have the capacity to branch out, enabling the relay of signals to multiple destinations before ultimately terminating at synapses.

### 2.1.2.4 Axon (synaptic) terminals

Situated at the extremity of the neuron, the axon terminals, often referred to as terminal buttons, play a crucial role in transmitting signals to other neurons. At the termination of the terminal button, there exists a gap known as a synapse. Within these terminal buttons, there are reservoirs containing neurotransmitters. These neurotransmitters are subsequently released from the terminal buttons into the synapse, facilitating the transmission of signals to other neurons. During this process, electrical signals undergo a transformation into chemical signals [32]. Following this transmission, any surplus neurotransmitters that were not transferred to the next neuron are reabsorbed by the terminal buttons [32].

### 2.1.2.5 Neuron's communication system and the synapse

Neurons establish communication among themselves through the connection between axons and dendrites. When a neuron communicates with another neuron, it sends an electrical signal known as an action potential (AP) along the length of its axon. This electrical signal undergoes a transformation into a chemical signal at the axon's termination point. The synapse, which is the region between the end of an axon and the tip of a dendrite from another neuron, is where the axon releases this chemical signal along with chemical messengers called neurotransmitters. These neurotransmitters are stored in small vesicles (tiny sacs) within the synaptic terminals. The neurotransmitters convey the signal to the nearby dendrite of the postsynaptic neuron via the synapse, where the dendrite converts the chemical signal back into an electrical one. Importantly, receptors on the postsynaptic neuron are specific to the neurotransmitters released by the presynaptic neuron [31]–[33].

Postsynaptic potentials (PSPs) are generated by the postsynaptic neuron when neurotransmitters bind to its receptors. These PSPs can be categorised into two primary types: excitatory postsynaptic potentials (EPSPs), which increase the likelihood of the postsynaptic neuron generating an action potential, and inhibitory postsynaptic potentials

(IPSPs), which decrease this likelihood. If the PSP reaches its threshold for conduction, the postsynaptic neuron becomes activated, initiating an action potential. This action potential then propagates through the neuron and undergoes similar conversions when it reaches neighbouring neurons [34]. Essentially, this action potential carries the information transmitted by nerve cells. Figure 2.4 shows the synapse and the neuron's communication process.

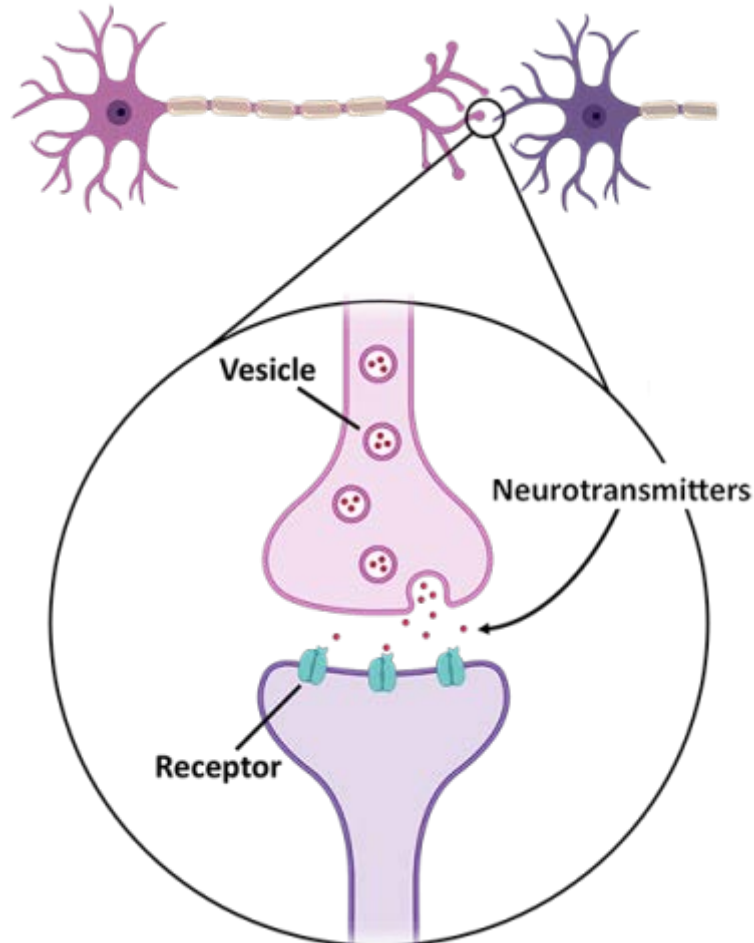


FIGURE 2.4: The **synapse** is where signals pass from one neuron to another. When the signal reaches the end of the axon, it triggers the release of neurotransmitters from tiny vesicles. These neurotransmitters cross the synapse and attach to receptors on the neighbouring cell, potentially altering the receiving cell's properties. If the receiving cell is also a neuron, the signal can continue transmission to the next cell [33].

This synaptic transmission mechanism enables information to be transferred and integrated across the neural network, enabling complex brain activities such as thoughts, feelings, movements, and emotions. Therefore, by monitoring the brain's electrical activity, it becomes easy to reveal the brain's operational mechanisms and mental states and to diagnose or address various neurological conditions.

### 2.1.3 Electroencephalography (EEG)

Electroencephalography (EEG) is a non-invasive neurophysiological technology that captures and analyses electrical activity in the brain. Electrodes are placed on the scalp to detect electrical signals generated by the collective activity of neurons in the brain. EEG is frequently used for many different purposes, including the diagnosis and monitoring of neurological diseases, such as epilepsy, brain tumour, head injury, sleep disorder, dementia, schizophrenia, and monitoring depth of anaesthesia during surgery; treatment of abnormalities; behavioural disturbances (e.g. Autism), attention disorders, learning problems, language delay, etc.; evaluation of sleep patterns; and study of brain function. It offers insightful information on brain activity and aids in comprehending the dynamics of the brain under various settings and stages.

#### 2.1.3.1 History of EEG

EEG has a long history that began in the late 19th and early 20th centuries. Richard Caton, a British biologist, carried out one of the earliest studies on brain electrical activity in 1875. He noticed that electrical currents in animals' exposed brains changed according to brain activity and sensory stimuli [35]. The revolutionary discovery of the first human EEG was made in 1924 by German psychiatrist Hans Berger. The recordings of Berger's 17-year-old son's scalp were made using a Siemens double coil galvanometer, and the recordings showed rhythmic brainwave activity that he called "alpha waves" [36], [37]. Berger published his research in 1929 and popularised the term "electroencephalogram" to refer to the process of capturing brain electrical activity. Figure 2.5 shows the first recording of the EEG signals made by Hans Berger.

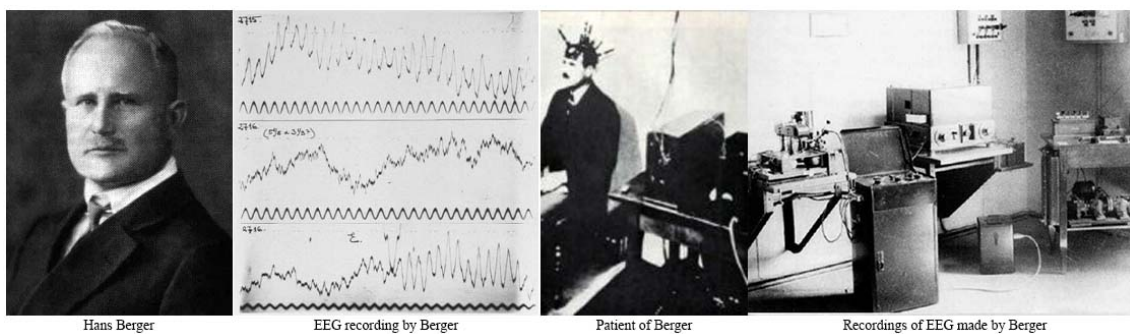


FIGURE 2.5: Hans Berger and his first recording of EEG signals in 1920s [37], [38].

### 2.1.3.2 EEG Recording system

EEG recording system consists of several key components working together to ensure accurate and reliable EEG data acquisition. The major components of an EEG recording system include:

- **Electrodes:** During the EEG test, a number of small discs called electrodes are placed on the scalp at specific locations on the surface of the scalp with temporary glues. These electrodes are conductive sensors that detect the electrical signals generated by the brain during its activities.
- **Electrode cap or headgear:** Many EEG recording methods include electrode caps or helmets to guarantee accurate and consistent electrode placement. The setup procedure is more effective with these caps since they have prearranged electrode placements.
- **Electrode paste or gel:** The electrodes are coated with a conductive paste or gel before being put on the scalp. With less resistance and noise, this paste enhances the electrical connection between the electrodes and the skin.
- **Amplifiers:** The electrodes can only detect very weak electrical impulses in the microvolt ( $\mu\text{V}$ ) range. These signals are amplified while retaining their quality using EEG amplifiers. Additionally, filters are built into amplifiers to cut out unwanted frequencies like those from muscle movement and background noise.
- **Analog-to-Digital converter (ADC):** An ADC is used to transform the amplified analogue EEG signals into digital data. Then, this digital material is prepared and stored for investigation. Initially, EEG recordings were made on paper, but today, digital EEG is thought to be a viable method for capturing EEG signals since it solves the issue of paper storage.

EEG signals are obtained by strategically placing multiple electrodes inside the brain, on the scalp, and over the cortex. These electrodes capture the collective neuronal activity, which results from the combined effects of EPSPs and IPSPs generated by numerous pyramidal neurons located near each electrode [39]. There are two types of EEG recordings based on their location on the head: scalp EEG and intracranial EEG (iEEG). Scalp EEG involves placing small electrodes on the scalp to establish good mechanical and electrical contact. In contrast, intracranial EEG uses special electrodes implanted directly into the brain during surgery. Another variation is the ECoG, where EEG is measured directly from the cortical surface using subdural electrodes.

The amplitude of EEG signals varies depending on the recording method. In a normal adult, scalp EEG signals typically range from about 1 to 100  $\mu\text{V}$ , while measurements with subdural electrodes, like needle electrodes, result in approximately 10 to 20 mV amplitudes. The non-uniform brain architecture and functional organisation of the cortex lead to variability in EEG signals depending on the location of the recording electrodes.

### 2.1.3.3 EEG electrode placement style

Depending on their intended application, EEG recordings can include 1 to 256 electrodes recorded simultaneously, which is known as multichannel EEG recording. Each channel typically consists of a pair of electrodes that produce a signal during the recording. Figure 2.6 shows the alignment of the electrodes over the six scalp regions [40]. The primary regions of the scalp where electrodes are placed are as follows:

- **Frontal (F):** These electrodes cover the front part of the head.
- **Temporal (T):** These electrodes cover the sides of the head.
- **Central (C):** These electrodes cover the central part of the head.
- **Parietal (P):** These electrodes cover the top and back of the head.
- **Occipital (O):** These electrodes cover the back of the head.

The naming of each electrode is comprised of letters from the scalp region and the numbers 1, 2, 3, 4, 5, 6, 7, 8, 9, and 10. A "z" in place of a number refers to an electrode placed on the midline. The numbers represent the locations of the electrodes within each region, with odd numbers on the left side and even numbers on the right side of the head. For example, F7 and F8 are frontal electrodes on the left and right sides of the head, respectively. Fz is a frontal electrode at the vertex of the head. Pz is a parietal electrode at the top and back of the head.

Different electrode localisation configurations, such as 10-20, 10-10, and 10-5 international systems, have been suggested. However, the 10-20 system is widely recognised as the most commonly used [41], [42]. The numbers "10" and "20" indicate that the actual spacing between surrounding electrodes is 10% or 20% of the skull's overall front-to-back or right-to-left distance, respectively. The positions are defined by two points: the inion, which is the crest point of the back of the skull, often indicated by a bump (the prominent occipital ridge, which can usually be located with mild palpation), and the nasion, which is the point between the forehead and the nose level with the eyes. Figure 2.7 shows the electrode location on the brain using the international 10-20 approach.

The EEG voltage signal reflects voltage differences between electrodes, allowing multiple display configurations on the EEG recording. These arrangements, known as montages, determine how the EEG signals detected by different electrodes are combined and displayed. There are various types of montage, each with its own unique purpose and advantages:

- **Bipolar montage:** Adjacent electrodes are coupled in a bipolar montage to produce differential signals. The voltage difference between these coupled electrodes is presented, emphasising localised brain activity and minimising interference from distant sources [44], [45]. The complete montage comprises a sequence of such channels. For instance, the channel labelled "Fp1-F3" represents the voltage difference between the Fp1 electrode and the F3 electrode. Subsequently, the next channel in

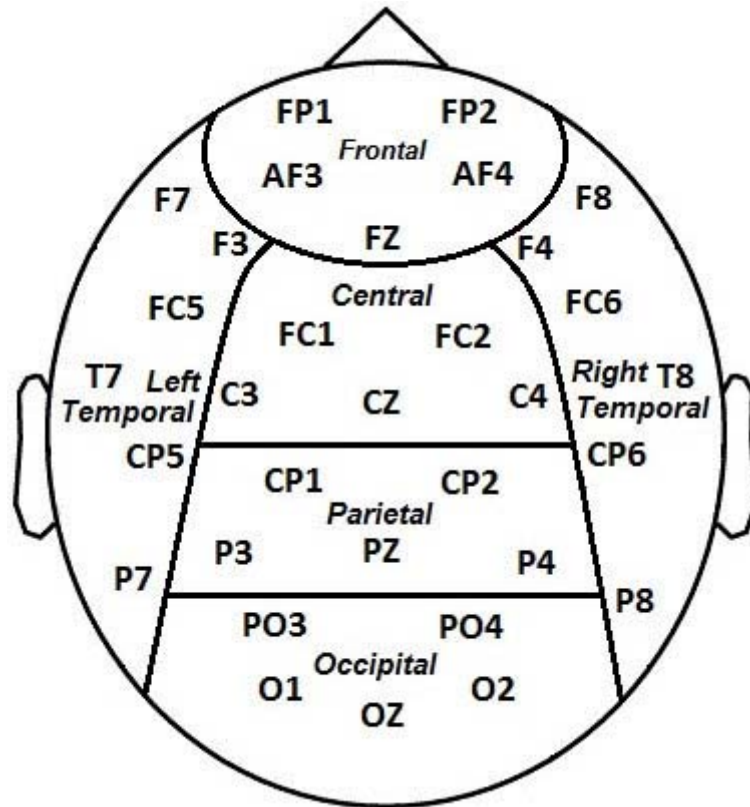


FIGURE 2.6: Electrodes divided into six scalp regions: frontal, central, parietal, occipital, right temporal, and left temporal [40].

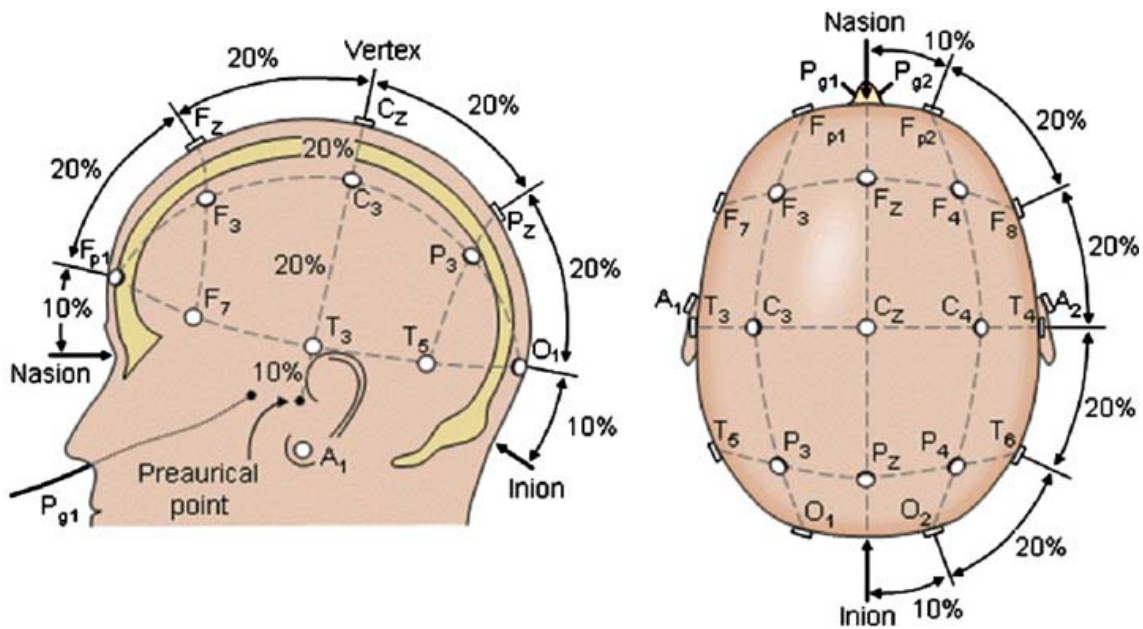


FIGURE 2.7: The international 10-20 electrode placement system [43].

the montage, "F3-C3," represents the voltage difference between F3 and C3, and this pattern continues throughout the entire array of electrodes.

- **Referential montage:** A referential montage selects one electrode as the reference

and compares the EEG signals from all other electrodes to this reference [44], [45]. Although it is not in the same location as the "recording" electrodes, this reference does not have an ensemble position. Because they do not enhance the signal in one hemisphere more than the other, midline placements are frequently employed. Another common term is "linked ears," which refers to an average of electrodes that are physically or mathematically tied to both the earlobes and the mastoids. Although this kind of montage gives a more complete picture of general brain activity, it might not be as good at capturing localised changes as bipolar montages.

- **Laplacian montage:** The Laplacian montage draws attention to spatial gradients in EEG data and can help pinpoint where brain activity is occurring. It measures the voltage variation between each electrode and the mean voltage of the electrodes nearby [44], [45].
- **Average reference montage:** The average of all EEG electrodes is used as the reference point for each electrode in the average reference montage. It is frequently used in clinical EEG recordings and aids in reducing the influence of common noise [44], [45].

In digital EEG, all signals are digitised and stored in a specific montage. As montages can be mathematically constructed from one another, EEGs can be displayed in any desired montage on an EEG machine.

#### 2.1.3.4 EEG Brainwaves

The electrical patterns created by the simultaneous activity of neurons in the brain are known as EEG brainwaves. These brainwaves are divided into a number of frequency bands, each of which is connected to certain mental states, abilities, and actions. EEG brainwaves are recorded in Hertz (Hz) and can be seen in a variety of mental states, including awakesness, sleepiness, and drowsiness. The frequency bands of brain rhythms can be divided into five categories: 0.5-4 Hz (delta,  $\delta$ ), 4-8 Hz (theta,  $\theta$ ), 8-13 Hz (alpha,  $\alpha$ ), 13-30 Hz (beta,  $\beta$ ) and >30 Hz (gamma,  $\gamma$ ) [44]. Details of those bands are discussed below:

- **Delta** waves have a rhythmic band range of 0.5 to 4 Hz and are the slowest brainwaves with the highest amplitude. It is primarily observed during deep sleep, in states of unconsciousness, in serious brain disorders, and in the waking state. It predominates in situations including learning disabilities, severe attention deficit hyperactivity disorder (ADHD), brain traumas, cognitive difficulties, etc [46].
- **Theta** waves have frequencies between 4 and 8 Hz and typically have amplitudes larger than 20 V. In calm or sleepy states, such as during meditation or light sleep, theta waves are frequently observed. It is also linked to creativity, emotional feeling, sensation, and memory. It mostly affects young children and the elderly. Theta wave overexposure can cause depression, ADHD, hyperactivity, and other conditions [47].

- **Alpha** has a frequency range of 8 to 13 Hz with an amplitude of 30-50m  $\mu$ V. It appears when the brain is in a wakeful relaxation state with the eyes closed. They are commonly observed when individuals are in a relaxed and calm state. It is commonly connected with strong mental activity, stress, and anxiety. It is associated with momentary memory storage and cognitive processes [48].
- **Beta** is in the rhythmic range of 13 Hz to 30 Hz. It appears as low-amplitude oscillations with symmetrical frequencies in the frontal region. When the brain is alert and immersed in mental tasks, it produces beta waves. These waves signify a highly focused mental state, often connected with dynamic actions, attentive focus, and problem-solving related to the external environment [44].
- **Gamma** waves have a frequency band ranging from 30 Hz and up. The maximum frequency of this rhythm is occasionally specified as 80 Hz or 100 Hz. It is the fastest brainwave and is associated with high-level cognitive processing, perception, and consciousness [44].

Figure 2.8 shows sample signals from those five frequency bands.

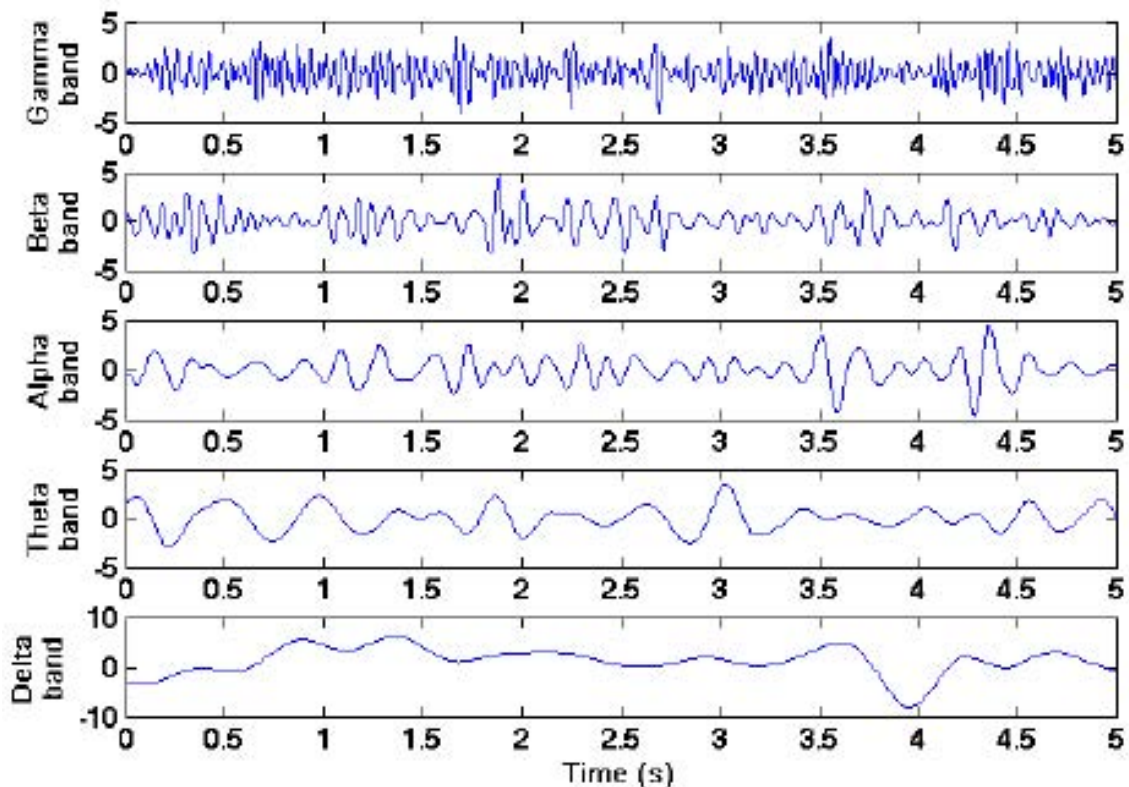


FIGURE 2.8: Sample EEG signals of five frequency bands [49].

External or non-neural electrical impulses that interfere with the proper recording of brain activity are referred to as artefacts in EEG. These artefacts can be caused by a variety of things, including electrical equipment, surrounding factors, perspiration, eye blinking, and muscle movements. The EEG signals may be distorted by artefacts, which makes it difficult to determine the underlying brainwave activity with accuracy.

In EEG recordings, common artefact types include:

- **Muscle artefacts:** Muscle movements, including eye blinks, jaw clenching, and facial expressions, can introduce electrical noise into the EEG recordings.
- **Electrode artefacts:** Poor electrode contact, movement, or displacement can lead to sudden changes in voltage that are not related to brain activity.
- **Eye movement artefacts:** Rapid eye movements, such as saccades and eye blinks, can generate electrical signals that resemble brainwave activity.
- **Sweat and skin artefacts:** Sweat on the scalp or changes in skin conductivity can create unwanted electrical signals.
- **Cardiac artefacts:** Heartbeat-related electrical signals can occasionally interfere with EEG recordings.
- **Environmental interference:** Electrical equipment, power lines, and other electromagnetic sources in the environment can introduce unwanted signals.
- **Electromyographic artefacts:** Electrical activity from nearby muscles, especially in the neck and face, can contaminate EEG recordings.

To get precise EEG data for analysis, these artefacts need to be minimised or eliminated. Artefacts are detected and their effects are reduced using signal processing techniques, including filtering and artefact rejection algorithms. EEG data must be carefully analysed by trained technicians and academics to distinguish between real brainwave activity and signals caused by artefacts.

Abnormal EEG signal patterns can be an indication of a number of neurological disorders. Some examples of abnormal patterns that can be seen in EEG recordings are as follows [44], [50]:

- **Spike-and-Wave complexes:** These are sharp, high-amplitude spikes followed by slow waves. They are often seen in epilepsy, particularly in absence seizures.
- **Sharp waves:** Similar to spikes but with a slightly broader waveform. Sharp waves can be associated with epileptic activity or other brain abnormalities.
- **Slow waves:** Abnormally slow and high-amplitude waves, often observed in cases of brain injury, encephalopathy, or during certain stages of sleep.
- **Burst suppression:** Alternating periods of low and high amplitudes are seen in conditions like hypoxic-ischemic encephalopathy or during deep anaesthesia.
- **Theta-Delta coma:** Predominance of theta and delta waves in comatose patients, indicating severe brain dysfunction.
- **Alpha coma:** Absence of alpha waves despite open eyes, suggesting significant brain dysfunction.

- **Focal slow activity:** Abnormal slow wave activity localised to a specific brain region, indicating a possible focal brain lesion or dysfunction.
- **Periodic patterns:** A repetitive and periodic waveform that can be seen in conditions like Creutzfeldt-Jakob disease or certain drug intoxication.

These unusual patterns offer important information for identifying and tracking different neurological disorders like epilepsy, dementia, bipolar disorder, sleep problems, insomnia, schizophrenia, attention deficit hyperactivity disorder, autism spectrum disorder, and migraines. In order to provide accurate clinical diagnoses and direct the selection of the most appropriate treatments, skilled neurologists and EEG technicians analyse these patterns.

In this dissertation, we have focused on two neurological disorder research problems using EEG data. Those are autism spectrum disorder and schizophrenia, which are briefly introduced in the sections below.

## 2.2 Autism spectrum disorder and its effect on EEG

Autism spectrum disorder (ASD) is a complicated neurodevelopmental disease characterised by social communication difficulties, repetitive behaviours, and restricted interests. Since it spans a broad spectrum of symptoms and severity levels that might differ from person to person, which is why it is known as a "spectrum" disorder. The key characteristics of ASD include social communication challenges, restricted interests, sensory sensitivities, repetitive behaviours, difficulty with transitions, etc [51], [52].

ASD is often identified in childhood, and early intervention and specialised therapy can considerably improve results. The specific causes of ASD are still being researched, although it is most likely a mix of genetic, environmental, and developmental factors [51], [52]. According to the Centers for Disease Control and Prevention (CDC), around 1% of the world's population has ASD, which is around 75 million people [53]. In the US, 1 in 36 children is diagnosed with an ASD [53]. Since 2000, the prevalence of autism has increased by 178%. According to the CDC, boys are four times more likely than girls to get an autism diagnosis. Nearly four out of every five children with autism experience a mental health problem, with ADHD being the most frequent. Autistic people may have co-occurring health problems such as digestive difficulties, seizures, epilepsy, and sleep problems. Approximately 4 out of every 5 autistic children have some difficulty with their motor abilities, such as walking, balancing, or writing [53].

There are certain EEG patterns and modifications connected to autism that have been found in research. These findings contribute to our knowledge of the disorder's neurological foundations. Some significant EEG pattern alterations that have been noted in people with autism are:

- **Increased theta activity:** Theta brainwaves are linked to profound relaxation, daydreaming, and creativity. According to certain research, people with autism

show more theta activity, primarily in the right posterior regions, especially while performing tasks that require social contact [54], [55]. This may be due to variations in how people with autism interpret social cues and use social cognition [54], [55].

- **Unusual alpha activity:** Alpha brainwaves are linked to relaxed wakefulness and a reduction in sensory input. Unusual alpha activity has been seen in several investigations of people with autism, pointing to possible abnormalities in attention control and sensory processing [56], [57].
- **Decrease in gamma synchronisation:** Cognitive activities, including perception, memory, and attention, are associated with gamma brainwaves. Autism individuals have been shown to have decreased gamma synchronisation, which might be a factor in their inability to absorb complex information and integrate sensory data [58], [59].
- **Changed functional connectivity:** Autism-related variations in functional connectivity across brain areas have been identified by EEG connectivity research. This altered connection may lead to difficulties in coordinating brain networks involved in social communication [60], [61].
- **Sensory responses:** Few studies have found changes in sensory responses in the EEG signals of individuals with ASD [62]. They may show altered EEG responses to certain sensory stimuli, which is consistent with the sensory sensitivity frequently seen in autistic people [63].

It's crucial to remember that while certain EEG patterns are linked to autism, they are not unique to the condition and might differ greatly across people. Furthermore, these patterns fit into a bigger picture that entails intricate connections between genes, brain development, and environmental variables. EEG results are only one piece of the puzzle when it comes to understanding the neurological causes of autism. To assist in the diagnosis and treatment of ASD, this dissertation aims to develop methods that can identify EEG signals from ASD individuals and separate them from healthy individuals.

The second neurological disorder that we have considered in this study is schizophrenia. In the next section, we will introduce schizophrenia disorder and its effect on EEG signal data.

## 2.3 Schizophrenia and its effect on EEG

Schizophrenia (SZ) is a complex and multifaceted mental disorder that profoundly affects an individual's cognition, emotions, perception, and behaviour, leading to an altered perception of reality. Individuals with SZ may frequently experience delusions and hallucinations, which at times can result in aggressive behaviour. Tragically, the incidence of suicide is notably higher among individuals with SZ when compared to the general population. SZ typically manifests in patients between the ages of 16 and 30, and if left untreated, it can lead to prolonged psychosis. Key symptoms of SZ encompass hallucinations, delusions, disordered thinking, motor abnormalities, reduced motivation, difficulties

with memory and attention, and diminished emotional expression, as described in [11], [13].

Globally, an estimated 24 million people, or approximately 1 in 300 individuals (0.32%), grapple with SZ. Among adults, the prevalence stands at one in every 222 individuals (0.45%) [64]. While not as common as certain other mental health conditions, SZ frequently emerges during late adolescence and early adulthood, with an earlier onset often observed in males as opposed to females [13]. Below, we outline some of the economic repercussions associated with SZ, as detailed in [65]:

- SZ demands ongoing medical attention with substantial direct healthcare costs, burdening healthcare systems, insurance, and government budgets.
- SZ often starts in early adulthood, disrupting education, careers, and work, causing productivity loss for individuals and the economy.
- Treatment, medications, and support for SZ patients put a financial burden on the family members of that person.
- SZ significantly impacts the quality of life. Individuals may deal with stigma, limited social engagement, and impaired daily functioning, resulting in lower life satisfaction.

Schizophrenia has a complicated economic effect that is difficult to quantify because of a variety of causes and varying levels of severity across people. However, studies reveal significant expenses for support services, lost productivity, and healthcare. Enhancing early intervention, access to mental healthcare, and social inclusion may be able to lessen some of these financial consequences. Researchers have long been interested in discovering the underlying neurological causes of SZ, and EEG has proven to be a useful technique in investigating the brain activity of those suffering from the condition. Here are some important details about the connection between SZ and EEG:

- **Patterns of EEG in SZ:** Research has indicated that individuals diagnosed with SZ frequently demonstrate distinct EEG abnormalities in comparison to individuals without the disorder. These anomalies manifest as alterations in various aspects of brainwave activity, encompassing changes in frequency, amplitude, and synchronisation. Specifically, deviations can be observed in key brainwave oscillations, such as gamma, alpha, and theta waves, providing valuable insights into the neurophysiological differences associated with SZ [66].
- **Gamma oscillations:** SZ frequently exhibits decreased gamma oscillations, which are high-frequency brainwaves that occur between 30 and 80 Hz. Gamma oscillations are essential for working memory, perception, and information processing. Cognitive problems may be a result of abnormalities in gamma activity in people with SZ [67]–[69].

- **Sensory processing:** EEG research has shed light on the sensory processing patterns of people with SZ. The P50 suppression paradigm suggests deficiencies in sensory gating, which make it difficult to filter out unimportant sensory inputs, resulting in sensory overload and attentional interruptions [70]–[72].
- **Mismatch negativity:** Mismatch Negativity (MMN) is an auditory event-related potential that reveals the brain’s capacity to recognise and interpret changes in auditory input. SZ patients have been found to have decreased MMN amplitude, which is a sign of impaired automatic auditory processing and sensory discrimination [73]–[75].
- **Connectivity and synchronisation:** SZ patients show different functional connections between different brain areas, according to EEG connectivity research. These alterations in connection may underpin the disorder’s disturbed integration of information across multiple brain regions, contributing to cognitive and perceptual impairments [76]–[78].

While the findings of EEG analysis in SZ give useful information, they represent only one part of a complex condition. The underlying causes of SZ are likely caused by a mix of neurological, environmental, and genetic factors. Our comprehension of these aspects is helped by EEG research, but further studies are required to completely understand how EEG patterns relate to the many symptoms and cognitive deficiencies associated with SZ.

In the next section, we will introduce the different automated EEG signal analysis techniques used by the researchers for different neurological disorder detection.

## 2.4 Automated EEG analysis

In general, expert clinicians visually analyse the EEG recordings to look for abnormalities in the signal data and identify the disorder. Due to the non-stationary and complex nature of the EEG signal, this process of visual analysis is expensive, error-prone, time-consuming, tiresome, subjective, and has some reliability issues due to the overlapping characteristics of the disorders [22], [79], [80]. Additionally, EEG analysis is essential for all brain-related neurosurgeries as well as helping with the diagnosis and treatment of brain diseases. The neurologist will effectively diagnose a greater number of patients if the time and cost of the EEG analysis process are reduced by automated analysis technologies.

### 2.4.1 Methods for analysing EEG signals

EEG analysis methods can be classified into three categories based on the analysis domain: time domain analysis, frequency domain analysis, and time-frequency domain analysis. A detailed discussion of those analysis methods is given in the following subsections:

### 2.4.1.1 Time domain analysis

EEG time-domain analysis focuses on assessing the features and patterns of EEG signals in their original state without transforming them into frequency or other domains. The temporal features of brain activity can be better understood by this kind of investigation. Some commonly used time-domain analysis techniques are given below [81]–[84]:

- **Amplitude analysis** is a measurement of the deviation of EEG signals from the mean value, commonly given as the difference between the maximum and minimum deviation (i.e., peak-to-peak) or in rectified EEG from baseline-to-peak. It is often measured in microvolts ( $\mu\text{V}$ ). This can reveal details about the level of brain activity as well as any potential anomalies.
- **Statistical measures** of EEG data are used to quantify various aspects of the brain's electrical activity. Some commonly used statistical measures are mean, median, standard deviation, variance, skewness, percentile values, entropy measures, power spectral density, kurtosis, etc. These statistics are essential for comprehending the properties of EEG signals, spotting anomalies, monitoring changes over time, and researching the functional connections and dynamics of the brain.
- **Event-Related potential (ERP) analysis** involves averaging EEG responses that are time-locked to certain triggers, events, or stimuli. This investigation reveals the typical brain activity linked to cognitive functions such as sensory perception, paying attention, and making decisions.
- **Burst detection** identifies EEG bursts, which are short bursts of oscillations with a high frequency and amplitude. For analysing certain brain states and developmental changes in EEG patterns, burst detection is especially helpful.
- **Spike and sharp wave detection** finds sudden, abrupt spikes or waveforms in the EEG data that may represent aberrant brain activity, including epileptic discharges.
- **Signal complexity measures** uses metrics like approximate entropy or sample entropy to quantify the complexity of EEG signals. These measurements can shed light on whether brain activity is random or predictable.

In the early stages of processing and analysing EEG signals, time-domain analysis is frequently employed. It assists researchers in identifying remarkable characteristics, anomalies, and patterns in raw EEG data, which may then be used to lead further exploration with frequency-domain, time-frequency, or other advanced analytic approaches. However, time-domain analysis has some advantages and disadvantages as follows:

**Advantages:** Time-domain analysis of EEG data offers a direct view of brain activity dynamics. It tracks changes in electrical potentials over time, aiding in understanding neural event timing and sequencing. Moreover, this analysis is often easier to

interpret and visualise as it deals with raw signal values over time. It uses less computationally demanding techniques like amplitude measurements or basic statistical analysis. It is especially useful for studying event-related potentials, providing high temporal precision in studying brain responses to specific events or stimuli.

**Disadvantages:** However, time-domain analysis lacks detailed frequency information in EEG signals, potentially missing crucial frequency-related characteristics. Additionally, it can be challenging to separate meaningful signals from noise, impacting accuracy. Also, detecting complex interactions between different frequency components or phase relationships might be harder. The analysis quality heavily depends on the quality of the recorded EEG signals, and issues like poor electrode contact could distort interpretations.

#### 2.4.1.2 Frequency domain analysis

The distribution of frequencies contained in the EEG signal is examined during a frequency-domain analysis of the EEG. This analysis offers insights into the spectral content of brain activity and assists in identifying dominant frequency components linked to various cognitive processes and brain states.

- **Power spectral density (PSD) analysis** uses methods like the Fourier Transform to determine the EEG signal's strength in various frequency bands (such as delta, theta, alpha, beta, and gamma). The energy distribution across frequencies is displayed using a PSD analysis, indicating the frequencies that are most important to the signal [81], [83], [84].
- **Relative power analysis** expresses each frequency band's power in terms of the overall power across all frequency bands. This study reveals the relative prominence of various frequency components.
- **Peak frequency analysis** reveals the frequency where the EEG signal is most powerful. Peak frequencies can be connected to various mental states and cognitive functions.
- **Coherence analysis** investigates the level of synchronisation between EEG signals captured from various electrode pairings. Information on the functional connection between different brain areas is available via coherence analysis.
- **Spectral entropy analysis** determines how unpredictable or complicated the frequency distribution of the EEG signal is. Spectral entropy can shed light on potential modifications to cognitive processes as well as changes in brain dynamics.

Frequency-domain analysis is valuable for studying brain states, cognition, and EEG signal abnormalities. It helps researchers understand frequency distribution and how brain regions function and communicate. Frequency-domain analysis also has some advantages and disadvantages as follows:

**Advantages:** Frequency-domain analysis of EEG signals identifies specific frequency bands linked to different brain activities. It helps understand brain states and functions, identify oscillatory patterns and rhythms crucial for studying cognitive processes and neurological conditions. Different frequency bands correspond to different brain states, like alpha waves during relaxation. This analysis characterizes and quantifies different brain states as different frequency bands correspond to different brain states. Frequency-based filtering techniques improve signal quality by removing noise or artifacts.

**Disadvantages:** Frequency-domain analysis transforms time domain signals into frequency domain, possibly losing some temporal details. It requires understanding of frequency bands and their implications, and the interpretation can be complex. The choice of parameters like window size and frequency bands can greatly affect the results. Despite aiding in noise removal, artifacts or non-brain signals might still interfere with frequency-specific interpretations.

#### 2.4.1.3 Time-Frequency domain analysis

EEG time-frequency domain analysis combines frequency and time information to show how the spectral content of EEG signals varies over time. The complex nature of brain activities that take place across a range of time scales may not be fully captured by conventional time-domain or frequency-domain analysis alone. By demonstrating how various frequency components change over time and providing insights into short-term cognitive processes and their frequency features, time-frequency analysis fills in this gap. By using techniques like sliding windows, time-frequency analysis is used to identify changes in frequency content over shorter time intervals. The most commonly used methods include [81], [84], [85].:

- **Short-Time Fourier transform (STFT)** breaks down an EEG signal into smaller segments (windows) and computes the Fourier Transform for each segment. This reveals the frequency components present in the signal at different time points. STFT provides a valuable insight into the temporal dynamics of EEG signals by showing how frequency components evolve over time. However, its fixed window length limits its ability to capture both high- and low-frequency changes simultaneously.
- **Wavelet transform** is a powerful time-frequency analysis technique used in EEG signal processing to capture frequency changes over time more effectively compared to methods like the STFT. An EEG signal is divided into a number of wavelet functions with various scales (frequencies), and the wavelet transform evaluates how well these functions match the signal at various time points. Compared to fixed-size windows in STFT, it offers higher versatility to catch localised frequency fluctuations.
- **Continuous wavelet transform (CWT)** is a useful technique for studying EEG signals with varying frequency content over time. It extends the concept of the

traditional Fourier transform to provide a time-frequency representation of a signal. It employs wavelet functions that are scaled and shifted to match different frequency components of the signal at various time points. The CWT is particularly well-suited for EEG analysis due to its ability to capture localised frequency changes.

In essence, time-frequency domain analysis of EEG extends beyond conventional time and frequency studies, allowing for a fuller comprehension of how brain activity changes over time and throughout various frequency ranges. Some advantages and disadvantages of time-frequency domain analysis are given below:

**Advantages:** It provides both temporal and frequency information at once, localizing transient frequency changes over time. This is useful for capturing non-stationary events in EEG signals, like ERPs or frequency band changes during tasks. It gives a detailed view of oscillatory dynamics by showing how frequency components change over time. Techniques like wavelet transforms or spectrograms are effective for signals where frequency content changes over time.

**Disadvantages:** Analyzing time-frequency data needs expertise in interpreting joint representations. Simultaneously interpreting changes in both domains can be challenging. The choice of parameters like window size and time-frequency resolution can greatly affect the results. Balancing high time resolution with frequency resolution can be challenging. Artifacts or noise in EEG signals can interfere with time-frequency representations, potentially affecting the analysis accuracy.

### 2.4.2 EEG signal classification techniques

In biomedical research, the categorisation of EEG data is crucial in order to diagnose brain disorders and contribute to a better understanding of cognitive processes. In biomedical research, the categorisation of EEG data is crucial. An effective classification approach aids in the differentiation of EEG segments and in the assessment of a person's health. Classification is an activity that occurs throughout daily life and simply involves making judgements based on the information that is currently accessible. In essence, classification is an algorithmic procedure that divides unclassified sets of observations (the testing class) into the proper categories based on previously determined observations (the training class). In the context of pattern recognition and machine learning, classification refers to an algorithmic process for categorising a given piece of input data into one of a set of categories [86]–[88]. The categories are referred to as classes, while the input data is technically referred to as an instance. A vector of features that collectively represent all of the instance's known properties serves as its formal description [86]–[88].

Assigning class labels to the characteristics obtained from the observations of a collection of data on a particular topic is the aim of classification. A classifier is an algorithm that executes classification, particularly in a practical implementation. The mathematical function used by a classification algorithm to assign input data to a category is sometimes referred to as a classifier. Training sets enable classifiers to acquire the knowledge

necessary to determine the class of a feature vector. These sets are made up of feature vectors that have been tagged with the classes to which they belong. A feature vector is a reduced-dimensional representation of a pattern's defining traits. Signal classification analyses distinct features in a signal to categorise it. This categorisation uncovers insights about the underlying process that produced the signal [86], [88].

The EEG classification process can be broadly categorised into two groups, primarily based on their approaches to feature extraction and classification techniques: machine learning (ML) based classification and deep learning (DL) based classification.

#### 2.4.2.1 Machine learning based classification

ML algorithms rely on manually crafted features and statistical techniques to learn patterns in data. Feature engineering is a crucial step in ML, where domain experts select or engineer relevant features. In EEG classification using machine learning, the focus is on extracting relevant features from EEG signals to represent various patterns associated with different neurological conditions. Feature extraction methods often include time-domain and frequency-domain analysis, statistical measures, or other signal processing techniques.

A wide range of traditional machine learning and pattern recognition algorithms have been employed in EEG data analysis. For instance, independent component analysis (ICA) is a commonly used technique for eliminating artefacts [89]. Principal component analysis (PCA) and local Fisher's discriminant analysis (LFDA) are often applied to reduce the dimensionality of features [79], [89]–[93]. Classic supervised learning methods like linear discriminant analysis (LDA), support vector machines (SVM),  $k$ -Nearest Neighbours ( $k$ -NN), Random Forests, Naive Bayes, and decision trees are commonly utilised for neural classification [79], [90]–[92], [94]–[98]. Additionally, canonical correlation analysis (CCA) is frequently employed to detect and analyse steady-state visual evoked potentials (SSVEPs). These methods play essential roles in various aspects of EEG data processing and classification.

Machine learning models are often interpretable, and feature engineering plays a crucial role in achieving accurate classifications. ML models are typically less complex than deep learning models, making them easier to train and deploy in some cases. Additionally, ML models can often be trained on standard CPUs and may not require specialised hardware. These approaches may be computationally efficient and require less data compared to deep learning methods, but their performance may plateau as data volume increases. Moreover, ML often relies on domain knowledge and human-crafted features, which can be time-consuming and may limit the model's performance [99].

#### 2.4.2.2 Deep learning based classification

DL algorithms, specifically artificial neural networks, aim to learn feature representations directly from raw data. They automatically extract hierarchical features in an end-to-end manner, reducing the need for extensive feature engineering. Among the DL methods, Convolutional Neural Networks (CNNs) and Recurrent Neural Networks (RNNs), are

gaining popularity in EEG classification. DL models can automatically learn hierarchical features from raw EEG data without extensive manual feature engineering. CNNs excel at capturing spatial patterns in EEG signals, making them well-suited for image-like data representations of EEG [79], [90]–[92]. RNNs and its variants, on the other hand, are valuable for capturing temporal dependencies in EEG sequences, such as those found in time-series data [100]–[102].

DL models can automatically learn relevant features from raw data, potentially reducing the need for manual feature engineering. Those models often require large amounts of labelled data and substantial computational resources for training but have the potential to achieve high classification accuracy. Deep learning models can be highly complex and act as "black boxes," making it less interpretable compared to traditional machine learning models. Deep learning models, especially deep neural networks with many layers, are highly complex and require substantial computational resources [99].

Researchers choose between these two approaches depending on factors such as the availability of data, computational resources, interpretability requirements, and the specific EEG classification problem they aim to solve. Hybrid approaches that combine elements of both machine learning and deep learning are also explored to harness the strengths of each methodology [103]–[107].

Again, the classification of EEG signals can be grouped into two main strategies: supervised classification and unsupervised classification. The subsequent section provides a concise overview of these two approaches for EEG classification.

### 2.4.2.3 Supervised Classification

The supervised classification approach involves developing a function by assessing the features present in predefined feature sets, and then that function is used to predict the class label for a test set [108]–[113]. This process consists of two stages: initially, a learning model is developed to describe established class categories within a dataset. This prototype is built based on data sample analysis and pre-existing class labels known as the training set. In the subsequent stage, the learned prototype is applied to new (test) data samples to predict their respective class labels. The supervised approach depends on a set of training data (the training set), which consists of a collection of cases that have been manually marked with the appropriate output [86], [87], [114]–[117].

In general, supervised classification approaches include training the classifier using a pre-defined set of training samples, and when new data samples are presented to the classifier, it will differentiate those new data samples based on the training experience [114]. In this approach, the training set consists of pairs of data points that can be mathematically represented as  $T_s = (x_1, y_1), (x_2, y_2), \dots, (x_n, y_n)$ , where  $x$  is the real value feature set, i.e.,  $x \in X$  and  $y$  denotes the class label usually represented by real numbers, i.e.,  $y \in Y$ . The aim of the supervised classification is to find a mapping function  $f$ , which will find the mapping between the feature space ( $X$ ) and label space ( $Y$ ), i.e.

$f : X \rightarrow Y$ . If the class label set contains a finite number of elements like  $y \in 1, 2, 3, \dots, m$  then it is considered a classification task. For example, if the class labels have two classes, then it is considered a binary classification, with one in the intended class and the other in the non-intended class [86], [88], [112], [118]–[120].

The removal of outliers from the training data sets is crucial since outliers are the main cause of mistakes in supervised classification. A data point that deviates from the entire pattern of the training data is referred to as an outlier. Human error, measurement mistakes, experimental errors, etc. are the main causes of outliers. The effectiveness of the classifier can be improved by identifying and removing outliers [121]. Commonly known supervised classification algorithms are support vector machine (SVM), and linear discriminant analysis (LDA), decision trees, Naive Bayes (NB), logistic regression (LR), linear regression, Gaussian process regression, Kalman filters,  $k$ -nearest-neighbour ( $k$ NN) algorithms, kernel estimation, neural networks (NN) etc.

#### 2.4.2.4 Unsupervised Classification

The process of unsupervised classification includes classifying data according to some indicator of innate ability, such as the distance between examples, which can be viewed as a vector in a multi-dimensional vector space. By assuming that training data has not been manually labelled, this approach looks for underlying patterns in the data that may be utilised to identify the right output class label for fresh data instances [86], [87].

In unsupervised classification, the classifier is given data that are both unlabelled and categorised, and it must predict the class of the testing data without any prior training. As a result, in unsupervised classification, the classifier cannot learn from a pre-defined set of training examples [122]. The more difficult tasks that cannot be evaluated using supervised classification techniques are evaluated using unsupervised classification. The main goal of unsupervised classification is to categorise complicated data by discovering its underlying dynamics or distribution.

Some of the commonly known unsupervised classification approaches are K-means clustering, density-based spatial clustering of applications with noise (DBSCAN), hierarchical clustering, expectation maximisation (EM), generative adversarial network classifiers, hidden Markov models, categorical mixture models, deep belief nets-based classification, and blind signal separation-based classification like Kernel Principal Component Analysis (Kernel PCA), Independent Component Analysis (ICA) etc.

## 2.5 Existing research works for ASD and SZ detection and their limitations

In this section, we have discussed several existing studies for ASD and SZ classification using EEG data, and later, we have identified a few limitations of those studies that we have tried to address in this dissertation.

### 2.5.1 Existing EEG signal classification Methods for ASD detection

As technological advancement grows day by day, computer-aided diagnosis (CAD) has become a necessary part of the medical industry. Several studies have been carried out to diagnose ASD using EEG signals.

Sheikhani et al. [123] used a technique called the short-time Fourier transform (STFT) on EEG signals collected from 19 different channels. The participants consisted of 10 individuals with ASD, aged between 6 and 11 years, and 7 age-matched control subjects without ASD. The goal was to analyse the EEG data and determine potential differences between these two groups. They used variance analysis to evaluate the obtained values. The results of their analysis highlighted a significant finding: the beta frequency band (ranging from 14 to 34 Hz) demonstrated a discrimination rate of 82.4% between the two groups. This indicates that the beta frequency band could potentially serve as a distinguishing factor between individuals with ASD and control subjects. Furthermore, they investigated the coherence values between 112 pairs of the 19 EEG channels. Coherence represents the degree of connectivity between different brain regions. Their findings revealed abnormal connectivity patterns primarily within the parietal lobe and temporal lobe. Additionally, they observed anomalies in the connectivity between these lobes and the central lobe of the brain. This suggests potential disruptions in the communication and synchronisation between these specific brain regions among individuals with ASD compared to the control group.

In a later study [124], they harnessed spectrogram and coherence values derived from quantitative electroencephalography (qEEG) to assess 17 children diagnosed with ASD and 11 control children, all falling within the age range of 6 to 11 years. Among the participants, there were 13 boys and 4 girls in the ASD group and 7 boys and 4 girls in the control group. Through statistical analysis, they evaluated the effectiveness of qEEG in distinguishing between the two groups. Their findings indicated that the alpha frequency band exhibited the highest differentiation level, reaching 96.4%, particularly under the relaxed, eye-opened condition using spectrogram criteria. Further examination of the qEEG data revealed notable differences in the ASD group's left brain hemisphere. Specifically, they observed significantly lower spectrogram criteria values at specific electrode locations: F3, T3 ( $p < 0.01$ ), and FP1, F7, C3, Cz, and T5 ( $p < 0.05$ ). These observations highlight distinctive neurophysiological patterns in individuals with ASD compared to the control group. Regarding connectivity, their analysis encompassed coherence values across 171 pairs of EEG electrodes. Notably, the examination of gamma frequency band (ranging from 36 to 44 Hz) coherence values revealed a higher occurrence of abnormalities. These abnormalities were particularly pronounced in the connectivity patterns between the temporal lobes and other brain lobes.

Shams *et al.* [125] classified autism using EEG through principal component analysis (PCA) and neural networks in motor movement and open-eyed tasks. They gathered data from six autistic and six typically developing (TD) children aged 7 to 9, utilising eight electrodes. EEG data from motor movement and open-eyed tasks were collected separately.

Data was pre-processed by channel normalisation, downsampling (250 Hz to 83.3 Hz), and Butterworth band-pass filtering. Averaging smoothed the data, followed by STFT and PCA to reduce dimensions and enhance feature selection. Multilayer perceptron (MLP) models were trained for classification. Testing included two protocols: one mixing all data and dividing it randomly, and another leaving out each subject for testing in turn. In the first protocol, motor tasks predicted autism with 100% accuracy and TD at 85.3%. For open-eyed tasks, autism achieved 86% accuracy, and typically developing children 78.9%. In the second protocol, motor tasks achieved 100% accuracy for autism and 99% for TD. Open-eyed task accuracy for autism ranged from 40% to 80%, and TD was around 90%. The study highlights that motor tasks are more effective in detecting autistic traits than open-eyed tasks. Consequently, the authors suggest that future research should emphasise motor regions for improved prediction accuracy.

Bosl *et al.* [126] proposed a diagnostic approach to use EEG data as a biomarker for children at high risk for ASD. They used minimum mean square error (mMSE) for feature extraction and  $k$ NN, NB, and SVM for classification on the extracted features. They used a dataset of 79 infants (46 at high risk for autism (HRA) and 33 controls) ranging in age from 6 to 24 months. Resting-state EEG signals were recorded using 64 electrodes while the infant was situated on their mother's lap in a softly illuminated room. During this time, a research assistant blew bubbles to capture the infant's attention. The modified multiscale entropy method was used to pre-process the raw data. A feature set of 192 values was produced by calculating the low, high, and mean for each curve in the mMSE collection. The classification of infants at high risk and those who were healthy fit together best around 9 months old, with over 90% accuracy. In a later study [127], they used a data-driven approach for ASD classification in which EEG data from 188 infant (89 low-risk controls (LRC), 99 HRA; ages 3 to 36 months) participants were used. The EEG signal was decomposed into six subbands using the wavelet transform (WT), and nine different non-linear features were extracted from each subband. Using SVM for classification, they achieved a sensitivity and specificity value exceeding 95% at some ages in distinguishing ASD subjects from LRC subjects.

Ahmadlou *et al.* [128] proposed a fractality and wavelet-chaos-neural network-based ASD diagnosis system. To assess the complexity and dynamic changes in the autistic brain, the concept of fractal dimension is introduced. Specifically, two methods for computing fractal dimension are explored: Higuchi's fractal dimension and Katz's fractal dimension. Using eye-closed EEG data from 17 subjects (9 ASD aged 6 to 13, 8 TD aged 7 to 13) with a two-layer radial basis function neural network (RBFNN), they achieved 90% accuracy. Using the same database in their later study [104] where they used an improved visibility graph (VG) for fractality investigation-based features named power of scale-freeness of VG (PSVG). An enhanced probabilistic neural network (EPNN) was used for classification and got an accuracy of 95.5%. In another study, the same authors used the analysis of functional connectivity of the brain using fuzzy synchronisation likelihood and diagnosed ASD based on that [129]. Using EEG data from 18 subjects (9 ASD, 9 TD) with an EPNN classifier, they obtained 95.5% accuracy.

In a separate investigation [130], Jamal *et al.* employed EEG recordings during tasks involving facial perception. Their aim was to employ discriminative analysis and SVM to classify ASD. They derived synchronised EEG patterns from 128 electrodes, involving 12 participants with ASD and control subjects. Through leave-one-out cross-validation, their model exhibited an accuracy of 94.7% in distinguishing between ASD and typical populations. In another study, Eldridge *et al.* [131] used variance in time by computing the sum of signed differences (SSD) and mMSE features from pre-processed signals and feeding them to three different classifiers named SVM, LR, and NB. On a dataset of 49 children (19 ASD and 30 non-ASD), the highest accuracy of 79% was yielded with the NB classifier.

In [132], Grossi *et al.* proposed a complex EEG processing algorithm named MSROM/I-FAST with seven machine learning algorithms, namely: sine net neural networks (Sn), logistic regression (LR), sequential minimal optimisation (SMO), kNN, K-contractive map (K-CM), NB, and random forest (RF), to classify autism. Using 25 subjects' (15 ASD (13 males and 2 females between 7 and 14 years of age) and 10 typically developing (TD) (4 males and 6 females between 7 and 12 years of age) resting state EEG data from 19 electrodes, the highest accuracy of 92.8% was achieved with the RF classifier. In a later study [133], they used the MS-ROM/I-FAST algorithm again to distinguish ASD EEG from children diagnosed with other neuropsychiatric disorders (NPD). They achieved an overall predictive capability in distinguishing ASD from other NPD cases that ranged from 93% to 97.5%. The trained neural network was subsequently applied to fresh data from 10 ASD adolescents, with 9 out of 10 ASD cases being properly identified by the network. In their new study [134], they used two EEG channels, namely, C3 and C4, to classify ASD EEG data. They achieved 100% accuracy for the dataset of the first study and 94.95% for the dataset of the later study.

Abdulhayh *et al.* [135] utilised EEG intrinsic function pulsation to identify autism patterns. They compared the ASD and TD groups, analysing the statistical features of EEG signals. Within ages 4 to 13, 10 children with ASD and 10 TD children were chosen. EEG was recorded using 64 electrodes at 500 Hz during the resting state. After artefact removal and empirical mode decomposition, intrinsic mode functions were derived. Analysing the pulsations of these modes revealed stability differences in certain channels for the ASD and TD groups. Notably, channel 3's first intrinsic mode showed consistent patterns in ASD and TD, while typically developing children exhibited randomness. Similar patterns were observed in specific channels for non-autistic and autistic children. Utilising 3D mapping, they detected and identified unusual brain activity. This computational method successfully distinguished abnormal EEG activity in children with ASD from that in their typically developing peers.

Dejman *et al.* [136] conducted a study using EEG to analyse the brain network in autism. They employed transfer entropy and graph theory, studying 12 high-functioning autistic youths and 19 healthy controls. EEG signals were collected as subjects viewed human faces in a dark room at 1 kHz. Transfer entropy, measuring information flow between EEG channels, was computed after pre-processing raw signals to eliminate noise.

Channels were paired, and transfer entropy between all pairs was calculated, forming a graph with nodes representing channels and edges denoting connections above a threshold. Noisy transfer entropy values were filtered out using the shift test. Further computations were performed on the graph, including the average degree, total clustering coefficient, average path length, and longest path length of the brain network. A comparison utilising independent sample t-tests with permutation highlighted a significant difference in average degrees between ASD and healthy controls. Healthy controls had notably higher average degrees, aligning with ASD's connectivity theory—indicating fewer neural connections and challenging information transfer in the autistic brain. This study suggests that a lower average degree of effective connectivity could serve as an autism biomarker. Future research aims to incorporate additional graph parameters, multivariate effective connectivity measures, and diverse perception tasks during EEG collection.

Heunis *et al.* [137] used recurrence quantification analysis (RQA) as an ASD biomarker, systematically considering technical and demographic factors. They applied RQA to resting-state EEG data, tested linear and nonlinear classifiers, and progressively analysed subsets of ASD and TD individuals to mitigate confounders. A simulated diagnostic scenario used a leave-one-subject-out approach. In the age-matched subset (7 ASD and 7 TD children aged 2-6), a nonlinear support vector machine classifier achieved 92.9% accuracy, 100% sensitivity, and 85.7% specificity in distinguishing ASD from TD. However, potential confounders including age, sex, intellectual ability, training/test segment counts, and repeatability emerged.

Djemal *et al.* [103] proposed a CAD system using discrete wavelet transform (DWT), Shannon entropy (ShanEn), and an artificial neural network (ANN) for ASD diagnosis. Their study gathered resting state EEG data from 16 channels—10 healthy participants aged 9 to 16 years and 9 autistic participants aged 10 to 16 years. Independent component analysis removed eye artefacts, and an elliptic band-pass filter was used for efficient filtering. They generated two datasets: one with overlapping signal segments and the other with non-overlapping segments. These sets underwent wavelet decomposition and entropy calculation. Four entropy functions—log energy, threshold, Renyi, and Shannon—were compared. For classification, they trained two models: one with wavelet statistical values and the other combining wavelet with entropy functions. They used a three-layer neural network for classification with 10-fold cross-validation. The highest accuracy of 96% with a standard deviation was achieved using DWT statistical values. DWT with entropy functions reached 98.4% accuracy with ShanEn, and other entropies also achieved good accuracy above 83%. Further analysis optimised the DWT with the ShanEn method. For segment length, 50 seconds outperformed others within the range of 10 to 180 seconds. Overlapping windows, yielding about 99.7% accuracy, outperformed non-overlapping segments.

Alturki *et al.* [105] used different feature extraction and classification techniques for the diagnosis of ASD. They used both single-channel and multi-channel EEG data for analysis. At first, ICA is used to remove artefacts and then segmented and filtered using an elliptic band-pass filter. Then they decomposed the signal using DWT into delta, theta,

alpha, beta, and gamma sub-bands. They used logarithmic band power (LgBP), standard deviation (SD), variance, kurtosis, and ShanEn to extract features from the segmented decomposed subbands and feed those features to different classifiers, namely: LDA, SVM,  $k$ NN, and ANN. Using a dataset of 19 children (9 ASD, ages 9 to 16 years, and 10 non-ASD, ages 10 to 16 years), they achieved the highest accuracy of 98.2% using the ShanEn and ANN classifiers.

In another study, Alotaibi *et al.* employed phase-based functional brain connectivity from EEG data within a machine learning framework [138]. They used a dataset of 12 ASD and 12 TD children. Specifically, functional brain connectivity networks were quantitatively characterised using graph-theoretic parameters derived from three different approaches based on a standard phase-locking value (PLV). These parameters were used as features in a machine learning setup. The study achieved an accuracy of 95.8%, 100 sensitivity, and 92% specificity using the trial-averaged PLV approach combined with a cubic SVM. Furthermore, the research highlighted significant alterations in functional brain connectivity among ASD children, particularly in the theta frequency band. The analysis of aggregated graph-theoretic features demonstrated these changes, shedding light on the differences in brain connectivity patterns between the two groups.

Linear and nonlinear Event-Related Potential (ERP) analysis of EEG signals for ASD and TD classification was done by Bakheet *et al.* [139]. They used data from participants while they viewed happy, fearful, and neutral facial expressions. To reveal ERP component activity, they used multivariate empirical mode decomposition (MEMD) to extract intrinsic mode functions (IMFs). Then nonlinear features (sample entropy (SampEn)) and standard linear measures (maximum, minimum, and standard deviation) are extracted from IMFs, evaluated through statistical tests, and used to create input vectors for discriminant analysis (DA), SVM, and  $k$ NN classifiers. They achieved the best classification accuracy of 100% for happy stimulus dataset. They also identified the SampEn measurements from the alpha and theta bands, along with linear features from the delta band, as possible biomarkers for disruptions in emotional facial expression (EFE) processing in ASD children.

Kang *et al.* [140] used multi-features (entropy, relative power, coherence, and bicoherence) to distinguish between ASD and TD children. They selected features using the minimum redundancy maximum correlation algorithm and SVM for classification. Using a dataset of 96 children (aged from 3 to 6 years) with 48 low-function ASD children (38 males and 10 females; age:  $4.9 \pm 1.1$  years) and 48 TD children (38 males and 10 females; age:  $4.9 \pm 1.2$  years) and 10-fold cross validation, they achieved an accuracy of 95.67%. Ari *et al.* [141] introduced an innovative automated technique to detect ASD using the Douglas-Peucker (DP) algorithm, a sparse coding-based feature mapping, and deep CNNs. Initially, the DP algorithm reduces the EEG sample count without compromising quality. EEG rhythms are then extracted using the wavelet transform, encoded using sparse representation, and further processed using the matching pursuit algorithm. The resulting sparsely coded rhythms are segmented and translated into decimal numbers to form an image with concatenated histograms. Data augmentation with ELM-based

autoencoders enriches the dataset. Subsequently, pre-trained deep CNN models classify ASD and healthy EEG signals. This method achieved a performance of 98.88% accuracy, 100% sensitivity, 96.4% specificity, and a 99.19% F1-score for automated ASD detection.

Aslam *et al.* [142] conducted in-depth analysis and evaluation of an extensive feature set to identify optimal features for prediction. This selection process involved utilising Least Squares Feature Extraction (LSFE) in combination with feature selection algorithms (FSA). They determined a set of up to eight most relevant channels using various FSA approaches. Moreover, the study explored the significance of channels and individual features on a per-subject basis. The study yielded impressive results for emotion prediction using a linear support vector machine (LSVM) classifier. They used two datasets to validate their proposed model on ASD classification, and they achieved 100% accuracy for one dataset and 95.5% for the other. They reported that this algorithm had significantly lower complexity than the typically used classifiers (i.e., deep neural networks, CNN, NB, and dynamic graph CNN).

Chawla *et al.* [143] proposed a framework using the flexible analytic wavelet transform (FAWT) of the EEG signal for ASD classification. At first, they filtered the signal and segmented it into durations of 5–20 seconds, then decomposed it into various sub-bands using FAWT. After that, feature vectors are created by extracting multiscale permutation entropy values from decomposed sub-bands. They used different classifiers to perform classification on those extracted features, like  $k$ NN, LR, SVM, RF, and CNN, and obtained the best accuracy of 99.19% using CNN with a segment length of 10 seconds.

### 2.5.2 Existing EEG signal classification Methods for Schizophrenia Detection

Sabeti *et al.* [144] tried to classify schizophrenic patients and age-matched control participants using EEG signals. Data from 20 patients and 20 controls are collected, each with 20 EEG channels. Features like Shannon entropy, spectral entropy, approximate entropy, Lempel-Ziv complexity, and Higuchi fractal dimension are extracted. Leave-one-participant-out cross-validation is used for evaluation with two classifiers, LDA and Adaboost. Initially, LDA achieves 86% accuracy, and Adaboost reaches 90%. To enhance performance, genetic programming is employed to select the most relevant features and eliminate redundant ones. The refined features are used with LDA and Adaboost, achieving 89% and 91% accuracy, respectively.

Sabeti *et al.* [145] compared three different EEG analysis methods: complexity, variability, and spectral measures for the classification of individuals with schizophrenia and normal participants. The research involved 15 participants with schizophrenia and 18 age-matched normal individuals. EEG data was recorded from 20 channels for each participant. The study extracted various features from the EEG data of each participant, like spectral entropy (SpEn) and reyni's entropy (ReEn) from the spectral measures group, approximate entropy (ApEn) and lempel-ziv complexity (LZC) from the complexity measures group, and central tendency measure (CTM) from the variability measure. They

used  $k$ NN for distinguishing between the two groups (schizophrenic and normal). Using a leave-one-participant-out cross-validation approach, they achieved an accuracy of 94%.

Santos *et al.* presented a CAD system using an optimised methodology over the P3b wave in order to classify schizophrenia using SVM and neural networks based on the multilayer perceptron (MLP) [146]. EEG signal of the auditory odd-ball (AOD) task was recorded from 47 subjects (16 SZ, 31 healthy controls (HC)). They achieved a mean correct classification rate (CCR) of 93.42%, with 96.73% specificity and 87.27% sensitivity.

An Epsilon-complexity function-based EEG signal classification model was proposed by Piryatinska *et al.* [147]. They used their  $\epsilon$ -complexity of continuous functions to estimate the  $\epsilon$ -complexity coefficients of the original signal and its finite differences, and then used RF and SVM for classification of the extracted features. Using 10-fold cross validation on a dataset of 84 subjects (45 SZ, 39 HC), they obtained an accuracy of 85.3% using RF and 81.07% for SVM.

Thilakvathi *et al.* [148] also utilised the complexity of EEG signals to distinguish individuals with schizophrenia from normal subjects. The research investigates EEG signal complexity in both rest and mental activity conditions. The study involves 55 subjects with schizophrenia and 23 normal subjects, totalling 78 participants. EEG recordings are obtained during resting states with closed eyes and during mental activity stimulation using modified odd-ball paradigms. They used ShanEn, spectral entropy, information entropy, Higuchi's fractal dimension, Kolmogorov complexity, and approximate entropies for feature extraction in both conditions. They found that EEG signal complexity tends to be higher in individuals with schizophrenia compared to the normal group, especially during different mental states. The study's highest classification accuracy of 88.5% is achieved when considering features from both stimulus conditions together. Overall, the research suggests that assessing EEG signal complexity during mental activity can serve as a valuable approach for identifying individuals with schizophrenia.

In the research [149], authors created an Automated Diagnostic Tool (ADT) for analysing EEG signal patterns and classifying them as normal or schizophrenia. The ADT involves steps like EEG series splitting, non-linear feature extraction, t-test-guided feature selection, classification, and validation. It was applied to a 19-channel EEG dataset of 28 subjects (14 SZ patients and 14 HC subjects). The raw EEG data was divided into sequences of 6250 sample points, producing 1142 features for each class. Non-linear feature extraction generated 157 features for each EEG pattern, with 14 principal features identified as significant. Different classification methods were employed, including decision-tree, LDA,  $k$ NN, probabilistic neural network (PNN), and SVM with various kernels. Experimental results indicated that SVM with Radial Basis Function (SVM-RBF) demonstrated the best performance, achieving an average accuracy of 92.91% on the EEG dataset.

Oh *et al.* used an eleven-layer convolutional neural system for diagnosis of SZ [150] using the same dataset as [149]. 14-fold validation for subject-based testing and 10-fold validation for non-subject-based testing were performed. 98.07% and 81.26% classification accuracy were found for non-subject-based testing and subject-based testing, respectively.

A Pearson correlation coefficient (PCC)-based EEG signal classification framework was

reported in [151]. They segmented the signals into a 10-second time frame and then used PCC to represent the relationships between the channels. After that, they used those PCC matrices as input for classification in a CNN model. A dataset of 84 subjects (45 SZ, 39 HC) was used to validate the proposed method and achieved an accuracy of 90%.

A random forest-based SZ classifier using the same 28 subjects' EEG recordings was proposed in [152]. Data were pre-processed using ICA and Fast Fourier Transformation. K-fold cross validation with 10 iterations was performed with 75% of the dataset used for training and 25% for testing. A random forest classifier achieved 96.77% accuracy.

In another piece of research, Shalhaf *et al.* [106] presented an automated diagnostic approach using transfer learning and deep CNNs to differentiate between SZ patients and HCs based on EEG signals. At first, EEG data is transformed into images using the continuous wavelet transform (CWT), and then Pre-trained CNNs, including AlexNet, ResNet-18, VGG-19, and Inception-v3, are applied to the EEG images, and their convolutional and pooling layers' outputs serve as deep features. These features are then used as input for a SVM classifier. The methodology is tested on EEG signals from 14 SZ patients and 14 healthy subjects. The best results are achieved by applying the method to the combination of frontal, central, parietal, and occipital regions using ResNet-18-SVM, yielding accuracy, sensitivity, and specificity of 98.60%, 99.65%, and 96.92%, respectively.

Aslan *et al.* [153] used STFT-based 2D time-frequency (T-F) images and deep learning (DL) for SZ classification. After converting the EEG data to spectrogram images, they used a DL-based VGG-16 CNN model for the classification of those images. Two different EEG datasets of 84 subjects (39 HC and 45 SZ) and 28 subjects (14 HC and 14 SZ) were used to evaluate the proposed model. They achieved an accuracy of 95% and 97.4% for the datasets, respectively.

Siuly *et al.* [154] used the empirical mode decomposition (EMD) technique for the diagnosis of SZ from EEG signals. They decomposed the EEG signal into intrinsic mode functions (IMFs) by the EMD algorithm, and then twenty-two statistical features were calculated from those IMFs. Then, five significant features were selected using the Kruskal-Wallis test. Finally, different classifiers were used for classification and achieved an accuracy of 89.59% using an ensemble bagged tree classifier on a database of 81 subjects, including 49 patients with SZ and 32 HC persons.

In another study, Khare *et al.* [155] proposed an automated approach for identifying SZ by combining T-F analysis and CNNs to address the limitations of feature extraction methods. EEG signals are processed using CWT, STFT, and smoothed pseudo-Wigner-Ville distribution (SPWVD) methods to generate scalograms, spectrograms, and SPWVD-based time-frequency representation (TFR) plots, respectively. These 2-D plots are then used as input for pre-trained AlexNet, VGG16, ResNet50, and a custom CNN model. The results demonstrate an accuracy of 93.36% with the SPWVD-based TFR and CNN models. Compared to benchmark networks like AlexNet, ResNet50, and VGG16, the developed CNN model, featuring four convolutional layers, not only requires fewer learnable parameters but also offers computational efficiency and speed.

Sun *et al.* [156] employed a two-step approach to classify SZ and HC subjects using

EEG data. In the first step, time and frequency features are extracted and transformed into red-green-blue (RGB) images that encode spatial information. The second step involves creating hybrid deep neural networks (DNNs) by combining CNN and LSTM to analyse RGB images for classification. The findings highlight the significance of the fuzzy entropy (FuzzyEn) feature over the FFT feature in capturing brain topography. The proposed DL method was evaluated using a dataset of 109 subjects (54 SZ, 55 HC) and achieved an average accuracy of 99.22% using FuzzyEn and an average accuracy of 96.34% using FFT for classification.

Shoeibi *et al.* [157] developed a DL-based SZ classification framework using EEG signal data. At first, they segmented the signal into a 25-second time frame and then normalised it by z-score and norm L2 methods. They used both ML and DL for classification. ML-based methods include  $k$ NN, DT, SVM, NB, bagging, RF, and Extremely Randomised Trees (ERT), while DL-based models include 1D-CNN, long-short term memory (LSTM), and 1D-CNN-LSTM. Using a dataset of 28 subjects (14 HC and 14 SZ) with five-fold cross validation, they achieved an accuracy of 99.25% using the CNN-LSTM model.

Akbari *et al.* [158] introduced a new framework for automated diagnosis of SZ using phase space dynamics (PSD) of EEG signals. They plotted the two-dimensional PSD of EEG signals in Cartesian space and extracted fifteen graphical features to assess chaotic behaviour and distinguish healthy individuals from those with SZ. The forward selection algorithm (FSA) was utilised to identify significant features and optimal channels. Eight different classifiers are then evaluated for SZ detection, with  $k$ NN and generalised regression neural network (GRNN) demonstrating superior performance. Through 10-fold cross-validation, the  $k$ NN classifier with city-block distance achieves an average classification accuracy of 94.80% on a dataset of 28 subjects (14 SZ and 14 HC).

A cyclic group of prime order with a modulo 17 operator was used by Aydemir *et al.* [159]. They presented a feature extractor named cyclic group of prime order pattern (CGP17Pat) to create a new multilevel feature extraction model. Iterative neighbourhood component analysis (INCA) was used for feature selection, and  $k$ NN was used for classification. They used a dataset of 28 subjects (14 HC and 14 SZ) with ten-fold cross-validation and leave-one-subject-out (LOSO) validation. The proposed model obtained an accuracy of 99.91% for 10-fold and 84.33% for LOSO validation. WeiKoh *et al.* [160] proposed a CAD system for SZ using EEG signal data. They transformed the EEG signals into images through spectrogram analysis. Subsequently, local configuration pattern features are extracted from these images. A 10-fold validation approach is employed, incorporating Student's t-test and z-score standardisation for each fold. The  $k$ NN classifier yielded the highest accuracy of 97.20% for a dataset of 28 subjects (14 SZ and 14 HC).

A local descriptor-based SZ detection framework was presented in [161]. The authors extracted features from the EEG data using both a histogram of local variance (HLV) and a symmetrically weighted-local binary patterns (SLBP)-based histogram, and then a correlation-based feature selection algorithm was used to reduce the length of the feature vector. Finally, the AdaBoost classifier was used for classification. They validated their proposed model using two datasets of 84 subjects (45 SZ and 39 HC) and 28 subjects (14

SZ and 14 HC). The proposed method achieved an accuracy of 92.85% and 99.36% for the tested datasets, respectively.

### 2.5.3 Limitations of the existing studies

Although the above-mentioned methods have achieved different levels of success in certain cases, they are limited in their robustness and generalisation. This is because it is sometimes very difficult to obtain representative features from EEG signals using existing techniques due to their non-stationarity and presence of noise. Again, the classification approaches mentioned above used a feature engineering approach to craft features from raw EEG data for classification, which requires experts with comprehensive knowledge of the target feature domain. On the other hand, DL-based classification approaches are getting popular among researchers due to their ability to learn features from raw data automatically and also perform classification using those features in an automatic process, which provides better performance in most cases with large-scale data like EEG.

Another noteworthy concern pertains to the prevailing trend in research, where the majority of studies focus on constructing classification frameworks specifically tailored to address a single neurological disorder, such as ASD or SZ, among others. This practice results in the creation of individualised systems for each disorder, which can be time-consuming and resource-intensive. In light of this, there is a practical need for a more efficient approach that offers a unified solution capable of classifying multiple neurological disorders. By adopting such a unified system, clinicians would stand to benefit from increased cost-effectiveness and convenience, allowing them to streamline their diagnostic processes across various neurological conditions using a single platform. This shift towards a more versatile and comprehensive approach could greatly enhance the overall diagnostic workflow and resource utilisation in the medical field.

Another significant observation is that many studies tend to validate their developed methods using a single dataset specific to the disorder for which the system was designed. This approach raises concerns about the generalisability of these methods. In other words, it becomes uncertain whether the methods that have shown success on a particular dataset of a given disease would also be effective when applied to different datasets of the same disorder or datasets belonging to entirely different diseases. This lack of cross-dataset validation introduces challenges in determining the robustness and applicability of these methods across varying scenarios and conditions.

Furthermore, it's important to note the absence of a computer-aided diagnosis (CAD) system that can assist clinicians in their diagnostic procedures. Despite the numerous methods that have been devised for classifying various neurological disorders, only a limited number of these methods have been successfully translated into practical CAD systems that can be utilised for real-life diagnostic purposes.

## 2.6 Summary

This chapter offers an overview of EEG signal classification while providing essential background knowledge related to EEG. The initial focus includes an outline of the human brain, the fundamentals of EEG, the impact of ASD and SZ on EEGs, and the EEG measurement techniques from the head surface locations. The next section of the chapter focuses on the categorisation of EEG data, revisiting the techniques used in earlier research to identify ASD and SZ in EEG signals. According to the literature study, current techniques have their limits, making the creation of new classification algorithms necessary to guarantee accurate neurological disorder diagnosis and treatment.

In the next chapter, we will introduce an ASD classification framework using T-F spectrogram images of EEG signals with both ML and DL-based classification techniques. This framework is the first to use the spectrogram image for ASD EEG data classification.

# OFFICE FOR RESEARCH TRAINING, QUALITY AND INTEGRITY

## DECLARATION OF CO-AUTHORSHIP AND CO-CONTRIBUTION: PAPERS INCORPORATED IN THESIS

*This declaration is to be completed for each conjointly authored publication and placed at the beginning of the thesis chapter in which the publication appears.*

### 1. PUBLICATION DETAILS (to be completed by the candidate)

Title of  
Paper/Journal/Book:

Diagnosis of autism spectrum disorder from EEG using a time–frequency spectrogram image-based approach.  
Electronics Letters, 2020

Surname: Tawhid

First name: Md Nurul Ahad

Institute: Institute for Sustainable Industries and Liveab

Candidate's Contribution (%): 75

Status:

Accepted and in press:

Date:

Published:

Date:

08/10/2020

### 2. CANDIDATE DECLARATION

I declare that the publication above meets the requirements to be included in the thesis as outlined in the HDR Policy and related Procedures – [policy.vu.edu.au](http://policy.vu.edu.au).

Md Nurul Ahad  
Tawhid

Digitally signed by Md Nurul Ahad  
Tawhid  
Date: 2023.09.08 13:05:51 +10'00'

06/09/2023

Signature

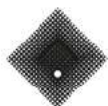
Date

### 3. CO-AUTHOR(S) DECLARATION

In the case of the above publication, the following authors contributed to the work as follows:

The undersigned certify that:

1. They meet criteria for authorship in that they have participated in the conception, execution or interpretation of at least that part of the publication in their field of expertise;
2. They take public responsibility for their part of the publication, except for the responsible author who accepts overall responsibility for the publication;



- 3. There are no other authors of the publication according to these criteria;
- 4. Potential conflicts of interest have been disclosed to a) granting bodies, b) the editor or publisher of journals or other publications, and c) the head of the responsible academic unit; and
- 5. The original data will be held for at least five years from the date indicated below and is stored at the following location(s):

Name(s) of Co-Author(s)	Contribution (%)	Nature of Contribution	Signature	Date
Siuly Siuly	15	Supervision, Formal analysis, Visualization, Manuscript preparation		08/09/23
Hua Wang	10	Supervision, Manuscript preparation, Funding acquisition, Project		08/09/23

Updated: September 2019

# OFFICE FOR RESEARCH TRAINING, QUALITY AND INTEGRITY

## DECLARATION OF CO-AUTHORSHIP AND CO-CONTRIBUTION: PAPERS INCORPORATED IN THESIS

*This declaration is to be completed for each conjointly authored publication and placed at the beginning of the thesis chapter in which the publication appears.*

### 1. PUBLICATION DETAILS (to be completed by the candidate)

Title of  
Paper/Journal/Book:

A spectrogram image based intelligent technique for automatic detection of  
autism spectrum disorder from EEG.

Plos one, 2021

Surname: Tawhid

First name: Md Nurul Ahad

Institute: Institute for Sustainable Industries and Liveab

Candidate's Contribution (%): 70

Status:

Accepted and in press:

Date:

Published:

Date:

25/06/2021

### 2. CANDIDATE DECLARATION

I declare that the publication above meets the requirements to be included in the thesis as outlined in the HDR Policy and related Procedures – [policy.vu.edu.au](http://policy.vu.edu.au).

Md Nurul Ahad  
Tawhid

Digitally signed by Md Nurul Ahad  
Tawhid  
Date: 2023.09.08 13:05:37 +10'00'

08/09/2023

Signature

Date

### 3. CO-AUTHOR(S) DECLARATION

In the case of the above publication, the following authors contributed to the work as follows:

The undersigned certify that:

1. They meet criteria for authorship in that they have participated in the conception, execution or interpretation of at least that part of the publication in their field of expertise;
2. They take public responsibility for their part of the publication, except for the responsible author who accepts overall responsibility for the publication;



3. There are no other authors of the publication according to these criteria;
4. Potential conflicts of interest have been disclosed to a) granting bodies, b) the editor or publisher of journals or other publications, and c) the head of the responsible academic unit; and
5. The original data will be held for at least five years from the date indicated below and is stored at the following location(s):

Name(s) of Co-Author(s)	Contribution (%)	Nature of Contribution	Signature	Date
Siuly Siuly	10	Supervision, Formal analysis, Visualization, Manuscript preparation		08/09/23
Hua Wang	5	Supervision, Manuscript preparation, Funding acquisition, Project		08/09/23
Frank Whittaker	5	Funding acquisition, Manuscript preparation, Project administration		08/09/23
Kate Wang	5	Supervision, Manuscript preparation		08/09/23
Yanchun Zhang	5	Funding acquisition, Manuscript preparation, Project administration		08/09/23

Updated: September 2019

## Chapter 3

# Spectrogram Image Based Autism Spectrum Disorder Classification

Autism spectrum disorder (ASD) is a developmental condition characterised by persistent challenges in social interaction, speech, nonverbal communication, and the presence of restricted or repetitive behaviours. This chapter introduces an efficient diagnostic framework for ASD, centred on the utilisation of time-frequency spectrogram images derived from EEG signals. This method aims to address the first research problem (**RP1**) regarding ASD classification.

In this proposed system, we have utilised short-time Fourier transform (STFT) to convert pre-processed EEG signals into two-dimensional spectrogram images. Subsequently, these images undergo classification using both machine learning (ML) and deep learning (DL) techniques. In the ML approach, we have extracted textural features, selected significant features via principal component analysis (PCA), and then input those into six distinct ML-based classifiers for the classification task. The performance of these models is then evaluated. In the DL-based approach, we have developed three different convolutional neural network (CNN) models and assessed their performance in classifying spectrogram images.

The contents of this chapter have been published in the *Plos One* (Publication 2) [90] and also in the *Electronics Letters* (Publication 1) [79].

### 3.1 Introduction

Autism spectrum disorder (ASD) comprises a group of intricate neurological developmental conditions, including autism, childhood disintegrative disorder, Asperger's syndrome, and an unspecified form of pervasive developmental disorder [6]. The spectrum of ASD symptoms varies widely in terms of range and severity, often encompassing challenges in social communication and interactions, intense fixations, reduced eye contact, and the presence of restricted or repetitive behaviours. ASD typically emerges in early childhood, with onset occurring primarily within the first five years of life, persisting throughout an individual's lifetime [7]. According to the World Health Organisation (WHO), globally, approximately one in 160 children is diagnosed with ASD, as reported in [7]. In Australia, the prevalence of autism increases by approximately 40%, transitioning from one in 100

individuals to approximately one in 70 individuals falling within the autism spectrum [9]. In the United States, the Centers for Disease Control and Prevention (CDC) reported that in 2020, roughly one in 54 children received a diagnosis of ASD [10].

ASDs can significantly impede an individual's capacity to engage in daily activities and participate in social interactions. They often exert adverse effects on a person's educational and social accomplishments, employment opportunities, ability to carry out daily routines, and integration into society [7]. Regrettably, individuals with ASD frequently encounter instances of mistreatment, discrimination, and violations of their human rights on a global scale [7]. To date, there is no known cure for ASD; however, early intervention has the potential to enhance brain development and improve learning, communication, and social skills. To achieve this, the development of an effective, efficient, and highly accurate diagnostic system for ASD is imperative.

The human brain, boasting approximately 86 billion neurons, is widely acknowledged as the most intricate biological system known to science. This awe-inspiring organ governs our thoughts, perceptions, memories, emotions, and actions. The functional state of the brain represents a vast reservoir of data and serves as the primary source of information for diagnosing neurological disorders. Consequently, it stands as a pivotal and expansive area of exploration within the realm of biomedical science. Various methodologies exist for capturing the functional dynamics of the brain, including positron emission tomography (PET), magnetic resonance imaging (MRI), functional magnetic resonance imaging (fMRI), electrocorticography (ECoG), and electroencephalography (EEG) [22], [162], [163].

Among these techniques, EEG stands out as a favoured choice due to its exceptional temporal resolution, user-friendliness, non-invasiveness, cost-effectiveness, and widespread availability for clinicians [18]. Neurons utilise electrical impulses within different frequency bands for their communication, which are recorded in EEG via electrodes affixed to the scalp. This process generates copious volumes of multi-channel EEG signals that neurologists traditionally rely on for visual interpretation to identify and diagnose neurological disorders [88]. However, visual inspection suffers from limitations, including the absence of standardised assessment criteria, rendering it an imperfect evaluation method. It is also characterised by being time-consuming, susceptible to errors, resource-intensive, subjective, human-error-prone, and afflicted with reliability challenges [19].

As technological advancements continue to progress, computer-aided diagnosis (CAD) has become an integral component of the medical field. Numerous studies have been conducted to diagnose autism spectrum disorder (ASD) utilizing EEG signals. These studies can be broadly categorised into two groups based on their feature extraction and classification techniques.

The first approach, known as the machine learning (ML) technique, involves the extraction of various time-frequency-based features from EEG signals. These extracted features are subsequently employed in ASD classification through diverse ML-based classification techniques. The success of ML-based classification relies heavily on the identification of significant features within EEG signals. Several researchers have adopted this approach

to address ASD classification challenges. For instance, Sheikhani *et al.* [123] utilised the short-term Fourier transform (STFT) for feature extraction and the  $k$ -nearest neighbour ( $k$ NN) algorithm, achieving an accuracy of 82.4% with a dataset comprising 17 subjects (10 ASD and 7 control). In a subsequent study [124], they again utilised STFT, combined with statistical analysis and  $k$ NN, achieving an accuracy of 96.4% on a dataset of 28 subjects (17 ASD, 11 control). Bosl *et al.* [126] introduced a diagnostic approach utilising EEG data as a biomarker for high-risk ASD children. They extracted features using minimum mean square error (mMSE) and employed  $k$ NN, naive Bayes (NB), and support vector machine (SVM) classifiers, achieving classification accuracies exceeding 90% with a dataset of 79 infants (46 high-risk for autism (HRA), 33 controls) aged 6 to 24 months. In a subsequent study [127], they employed a data-driven approach for ASD classification using EEG data from 188 infant participants (89 low-risk controls (LRC), 99 HRA) aged 3 to 36 months. The EEG signal underwent wavelet transform (WT) decomposition into six subbands, and nine different non-linear features were extracted from each subband. Employing leave-one-out cross-validation, they assessed these features as inputs to SVM, achieving sensitivity and specificity values exceeding 95% at various ages in distinguishing ASD subjects from LRC subjects.

Eldridge *et al.* [131] leveraged variance in time, computing the sum of signed differences (SSD) and mMSE features from pre-processed signals, and employed various classifiers. They achieved the highest accuracy of 79% with the NB classifier on a dataset of 49 children (19 ASD and 30 non-ASD). In another study by Grossi *et al.* [132], a complex algorithm named MSROM/I-FAST was introduced for EEG processing, along with seven machine learning algorithms, including random forest (RF), logistic regression (LR), and  $k$ -nearest neighbour ( $k$ NN), to classify autism. Using resting-state EEG data from 25 subjects (15 ASD and 10 typically developing (TD)), they achieved the highest accuracy of 92.8% with the RF classifier. Heunis *et al.* [137] employed recurrence quantification analysis (RQA) for feature extraction from resting-state EEG of 14 children (7 ASD and 7 TD), subsequently applying an SVM classifier to achieve a high accuracy of 92.9% using leave-one-subject-out validation. Haputhanthri *et al.* [164] developed a decision support system (DSS) named ASDGenus for ASD diagnosis using EEG data from 15 participants (10 ASD, 5 control). They combined statistical features, such as mean and standard deviation, before and after discrete wavelet transform (DWT) for each channel. Correlation-based feature selection (CFS) was employed for significant feature selection, and four classifiers (LR, SVM, NB, and RF) were applied, with the highest accuracy reaching 93% using the RF classifier. In a later extension [165], they incorporated Shannon entropy for EEG data feature extraction and integrated thermogram face image data from 17 participants (8 ASD, 9 control). This achieved an accuracy of 88% using only EEG data with the RF classifier and 94% accuracy using both EEG and thermogram image data with LR and MLP classifiers. In a recent study [166], Abdolzadegan *et al.* extracted linear and nonlinear data from EEG data of 45 subjects (34 ASD, 11 non-ASD), applying various feature selection techniques and SVM and  $k$ NN classifiers. They achieved an accuracy of 90.57% and 72.77%, respectively. These ML-based classification approaches involve the creation of features from raw EEG data

using feature engineering methods, requiring expertise in the target feature domain [167].

Recently, deep learning (DL)-based classification approaches have gained popularity among researchers due to their capacity to automatically learn features from raw data and perform classification in an automated manner [167]. Ahmadlou *et al.* [128] introduced an ASD diagnosis system based on fractality and a wavelet-chaos-neural network combination. They introduced the concept of utilising fractal dimensions (FDs), which represent the complexity and self-similarity of a signal, as features. Using EEG data recorded with eyes closed from 17 subjects (9 ASD, 8 typically developing (TD)), they achieved an accuracy of 90% with a two-layer radial basis function neural network (RBFNN). In their subsequent study [104], they improved the visibility graph (VG) for fractality assessment and introduced features known as the power of scale-freeness of VG (PSVG). They employed an enhanced probabilistic neural network (EPNN) for classification and achieved an accuracy of 95.5% on the same dataset.

In another study, the same authors explored functional connectivity analysis of the brain using fuzzy synchronisation likelihood-based ASD diagnosis [129]. Using EEG data from 18 subjects (9 ASD, 9 TD), they utilised an EPNN classifier, obtaining an accuracy of 95.5%. Djemal *et al.* [103] introduced an ASD diagnosis system utilising discrete wavelet transform (DWT), Shannon entropy (ShanEn), and an artificial neural network (ANN). They employed a two-layer ANN with ten-fold cross-validation on an EEG dataset comprising 19 subjects (9 ASD and 10 non-ASD). Data were segmented into 50-second segments using two different overlapping techniques. With half-overlapping segmentation, they achieved an impressive classification accuracy of 99.7%, and without any overlapping in segmentation, they achieved an accuracy of 98.6%. Alturki *et al.* [105] also used 50-second segmentation and decomposed the signal into subbands using DWT. They extracted features, including logarithmic band power (LgBP), standard deviation (SD), variance, kurtosis, and ShanEn, from the segmented decomposed subbands. These features were then fed into different classifiers: linear discriminant analysis (LDA), SVM,  $k$ NN, and ANN. Using a dataset of 19 children (9 ASD and 10 non-ASD), they achieved the highest accuracy of 98.2% with the combination of ShanEn and ANN classifiers.

DL-based classification approaches offer the advantage of not requiring domain-specific experts for feature extraction from raw data. DL methods perform both feature extraction and classification automatically, typically yielding superior results compared to ML-based classification processes. However, they are often regarded as black-box models for users [153]. In some cases, researchers use engineered features as inputs for DL models instead of employing raw EEG data on a large scale. This approach can reduce computation time and allow the model to be trained on essential features [103]–[105], [128], [129].

While some state-of-the-art techniques have shown promising results in specific scenarios, their robustness and ability to generalise are often constrained. This limitation stems from the difficulty of extracting representative features from EEG signals using existing methods, primarily due to the non-stationary characteristics of EEG signals and the presence of noise. None of the previous approaches have explored the concept of utilising two-dimensional (2D) time-frequency images to describe EEG data, a perspective that

could potentially reveal exceptional features from diverse angles.

In this chapter, we have introduced a novel approach based on 2D EEG spectrogram images, employing both ML and DL-based techniques for the automatic detection of ASD. These 2D time-frequency (T-F) spectrogram images serve as representations of the non-stationary nature of EEG signals and are subsequently analysed through separate ML and DL processes. Spectrogram images, in the T-F domain, provide a visual representation of EEG signals, where the frequency band evolves over time, and various colours within the image correspond to different energy levels in the EEG signal [168]. While previous studies have explored the use of T-F-based images for classifying neurological disorders such as epilepsy [19], epileptic seizures [169], clinical brain death diagnosis [168], schizophrenia [153], and sleep stage classification [170], this approach has not been applied to ASD classification before. In this chapter, we have proposed a T-F image-based method for ASD classification, employing both ML and DL techniques.

For ML-based classification, we have employed tCENTRIST for feature extraction from spectrogram images due to its computational simplicity and superior performance. The extracted features are then classified using six different classifiers: Naïve Bayes (NB), Linear Discriminant Analysis (LDA), Random Forest (RF),  $k$ -Nearest Neighbours ( $k$ -NN), Logistic Regression (LR), and Support Vector Machine (SVM). We have employed ten-fold cross-validation to assess the performance of the ML-based classification methods.

In the DL-based approach, we have utilised three distinct Convolutional Neural Network (CNN) models to classify the spectrogram images. The dataset is split into three subsets for training (70%), validation (15%), and testing (15%) the models. Obtained results are compared with existing literature that utilises the same dataset for ASD classification.

The major contributions of this study are listed below:

1. For the first time, time-frequency spectrogram image-based EEG signal representation technique is used for ASD classification.
2. performed classification using both ML and DL-based classification with different classifiers.
3. Design and validate a new efficient and automatic CNN-based framework for spectrogram image classification.
4. Explore the framework's performance with a publicly available dataset and outperformed the existing studies.

## 3.2 Methodology

In this research, we have presented an ASD classification method utilising spectrogram images derived from EEG signals. Figure 3.1 offers an overview of the proposed framework, which can be broken down into three components: pre-processing and spectrogram image generation, machine learning-based classification, and deep learning-based classification.

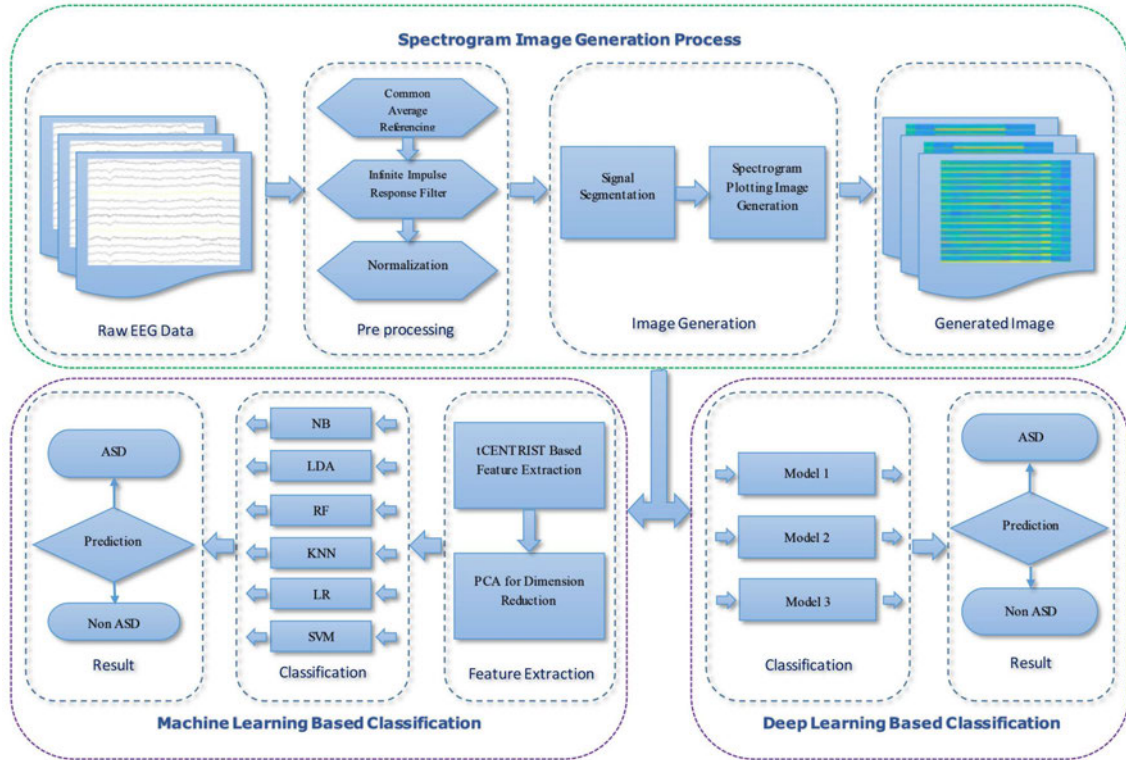


FIGURE 3.1: An overview of the proposed classification framework.

### 3.2.1 Pre-processing and spectrogram image generation

In this section, the raw EEG data undergoes a pre-processing phase to eliminate artefacts. This process involves re-referencing, filtering, and normalisation techniques. To re-reference the data, the Common Average Referencing (CAR) method is applied, which uses the average value of all electrode channels as the reference. Next, an Infinite Impulse Response (IIR) filter is employed to perform a low-pass filtering operation with a cutoff frequency of 40 Hz. Following the filtering step, the signals from each electrode are normalised to fall within the  $[-1, 1]$  range.

The pre-processed signals are then segmented into 3.5-second window frames for each subject in the dataset. Subsequently, the STFT is applied to each of these segments, resulting in the generation of spectrogram plots. These spectrogram images are saved as image files and serve as input data for both the ML and DL-based classification methods.

### 3.2.2 Machine learning based process

The process of ML-based classification involves three distinct stages: feature extraction, dimension reduction, and classification. To extract meaningful features from spectrogram images, we employ the ternary CENTRIST (tCENTRIST) method, which is based on the fusion of Local Ternary Pattern (LTP) and CENSus TRAnformed hISTogram (CENTRIST) techniques initially introduced by Dey *et al.* [171]. Ternary CENTRIST (tCENTRIST) combines LTP in place of the Linear Binary Pattern (LBP) found in CENTRIST [172]. This innovative tCENTRIST approach has demonstrated superior performance in

tasks such as garment texture classification [171] and gender classification from facial images [173]. Moreover, it maintains computational simplicity.

The feature extraction process leverages the Spatial Pyramid Matching (SPM) scheme, dividing images into subregions. Within each of these subregions, LTP-based histograms are generated and concatenated to form a single comprehensive histogram representing the image's features. To manage the high dimensionality of these features, Principal Component Analysis (PCA) is employed to reduce their dimensionality. Consequently, the reduced feature set becomes the input for various ML-based classifiers.

For classification, six distinct classifiers are applied: NB, LDA with pseudolinear discriminant analysis characteristics, RF,  $k$ -NN with a neighbor number set to nine ( $k=9$ ), LR, and SVM with a linear kernel (used LibSVM [174]).

### 3.2.3 Deep learning based process

For the purpose of DL-based classification, the CNN architecture is selected as it is renowned for its effectiveness in addressing image-related challenges [175], [176]. In this study, three distinct CNN models are employed to assess their performance.

The first model comprises three convolutional blocks, each equipped with a max-pooling layer. Additionally, a fully connected layer with 512 units, activated by the rectified linear unit (relu) activation function, is stacked on top of these layers. An illustrative representation of Model 1's structure is depicted in Figure 3.2.

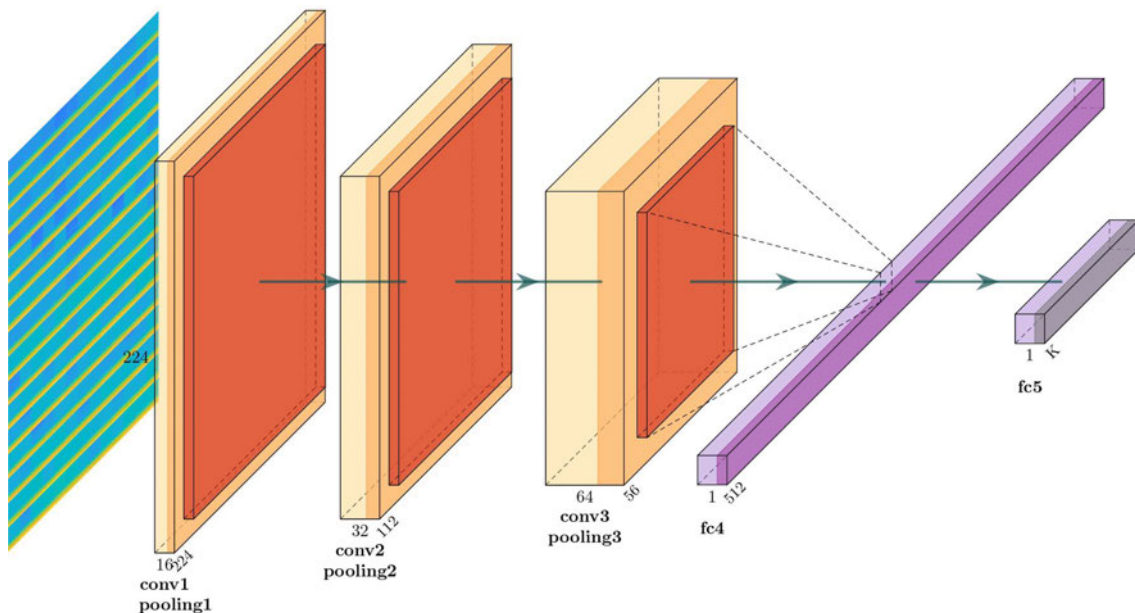


FIGURE 3.2: First CNN model.

The second model closely resembles the first, except for the incorporation of a 20% dropout applied to the final max-pooling layer. The utilisation of dropout entails randomly deactivating 20% of neurons during each training epoch. Model 2's architecture is visually summarised in Figure 3.3.

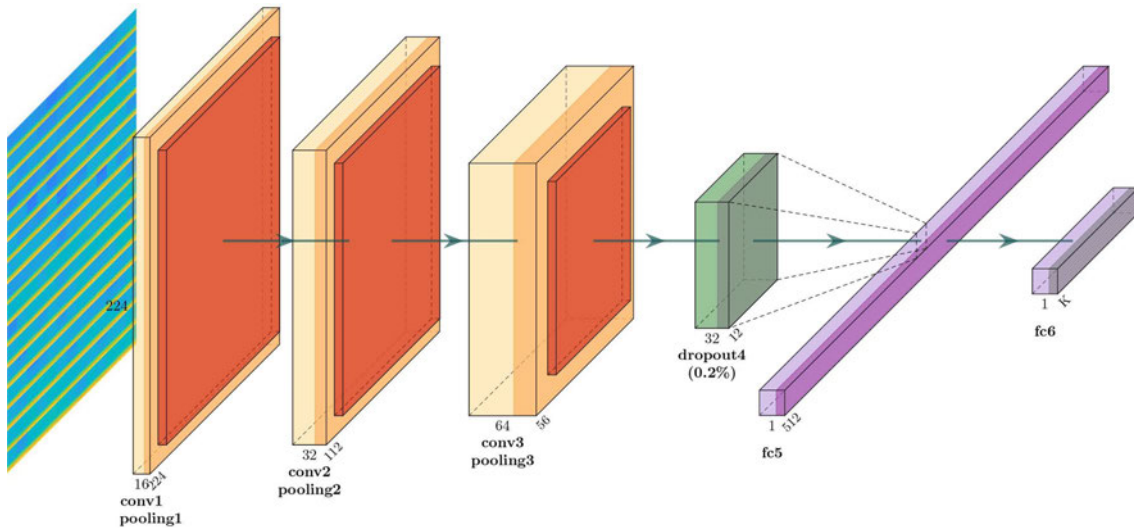


FIGURE 3.3: Second CNN model.

The last CNN model encompasses four consecutive sets of convolutional and max-pooling layers. Following every pair of convolutional and max-pooling operations, a 25% dropout is applied. After the final max-pooling layer, a fully connected layer with 256 neurons is introduced, followed by a 50% dropout layer, culminating in a softmax classification layer designed for handling two classes. A comprehensive layout of Model 3 is provided in Figure 3.4.

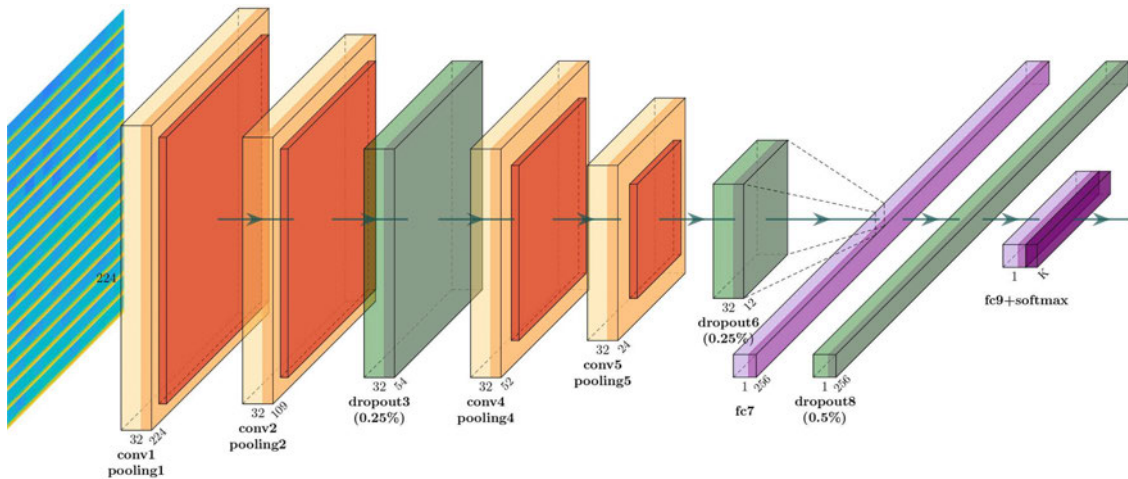


FIGURE 3.4: Third CNN model.

### 3.3 Performance evaluation

This section begins by providing a comprehensive overview of the dataset used in this experiment, along with a detailed description of the pre-processing techniques applied to it. Following this, we delve into the discussion of performance metrics, including the relevant equations used to assess the effectiveness of the proposed system.

### 3.3.1 Dataset

The proposed method is assessed using a dataset obtained from King Abdulaziz University (KAU) Hospital, Jeddah, Saudi Arabia, as detailed in [177]. This dataset is publicly accessible via the following link: <https://malhaddad.kau.edu.sa/Pages-BCI-Datasets.aspx>. To protect the anonymity of participants, no personally identifiable information about the subjects has been disclosed.

The dataset consists of sixteen subjects, comprising twelve individuals from the ASD group (comprising 3 girls and 9 boys, aged between 6 and 20) and four participants from the control group (all boys, aged between 9 and 13), all of whom have no previous history of neurological disorders. EEG signals from these subjects were recorded using Ag/AgCl electrodes, a g.tec EEG cap, g.tec USB amplifiers, and the BCI2000 software. The recordings were conducted while the subjects were in a relaxed state to ensure the acquisition of EEG data free from artefacts. The data were recorded across 16 channels, adhering to the international 10-20 system, as illustrated in Figure 3.5, with the right ear lobe serving as the reference (REF) and AFz as the ground (GND). During the recording process, a band-pass filter with a pass frequency range of 0.1 to 60 Hz was employed, along with a notch filter set at a pass frequency of 60 Hz, to effectively filter the dataset and eliminate unwanted noise. Finally, all EEG signals were digitised at a sampling rate of 256 Hz.

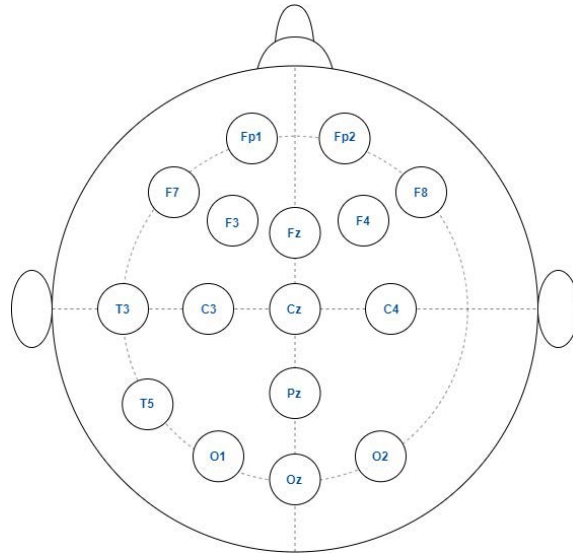


FIGURE 3.5: Electrode placement to collect the EEG data [177].

As per the proposed approach, the data undergoes pre-processing, involving CAR, IIR filtering, and normalisation. Subsequently, the processed signals are divided into 3.5-second time intervals to capture precise information. These signal segments are then used to generate spectrogram plot images through STFT. In total, 4657 images are generated, comprising 3276 images from individuals with ASD and 1381 images from those without ASD. Sample spectrogram images produced by the proposed method are illustrated in Figure 3.6, where Figure 3.6a displays images from the ASD group, and Figure 3.6b showcases

images from non-ASD subjects. These images serve as input data for the classification process, employing both ML and DL techniques.

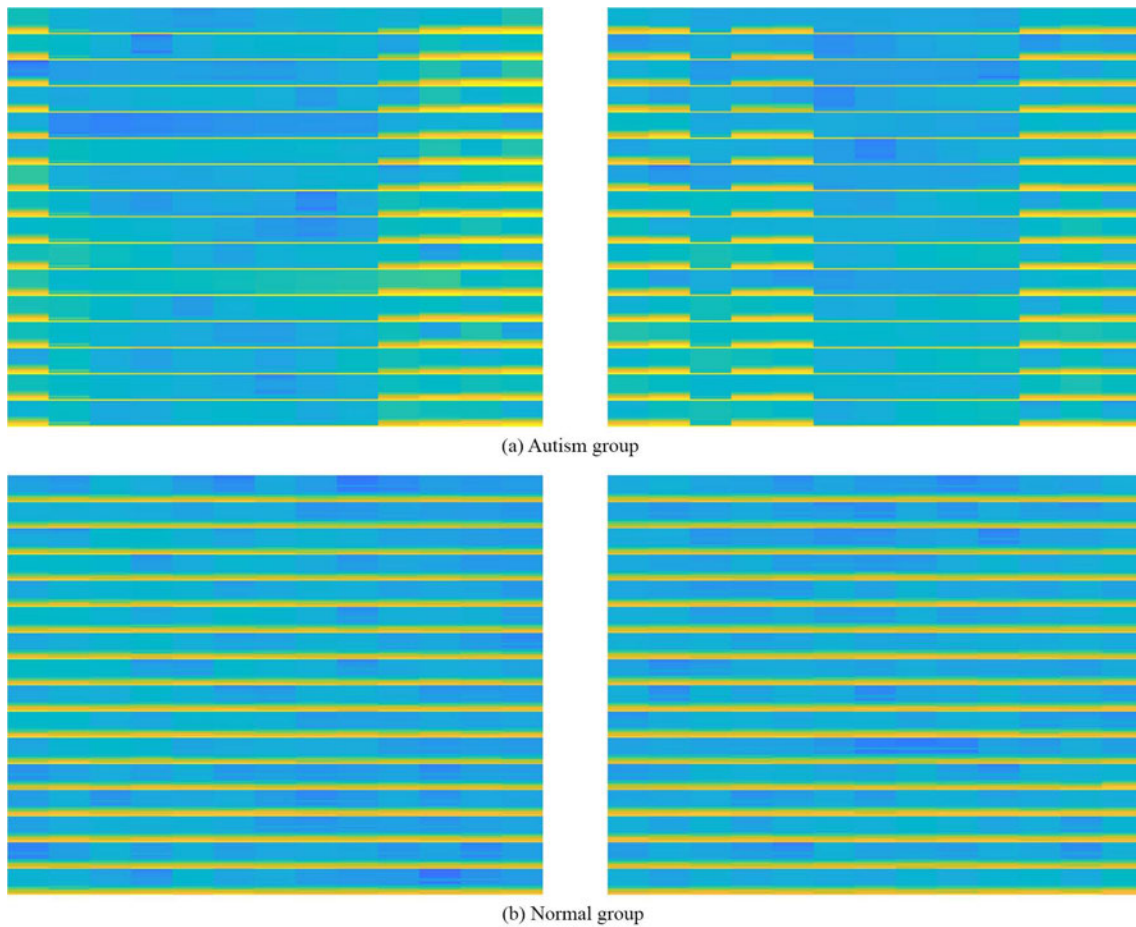


FIGURE 3.6: Sample spectrogram images generated by the proposed method: (a) ASD group, (b) non-ASD group

The generation of images and the execution of machine learning-based experiments take place within the MATLAB (R2020a) environment on a computer equipped with an Intel Core i5 64-bit processor, running at a clock speed of 1.7 GHz, and boasting 8 GB of memory. On the other hand, deep learning-based experiments are conducted within the Google Colab environment [178].

### 3.3.2 Performance evaluation parameters

The performance evaluation of the proposed framework involves the utilisation of Receiver Operating Characteristic (ROC) parameters, which include True Positive (TP), True Negative (TN), False Positive (FP), and False Negative (FN). These parameters are employed to compute critical performance metrics such as sensitivity, specificity, F1 score, and overall accuracy using equations 3.1 through 3.4. Employing these evaluation criteria allows us to assess the performance characteristics of the classifiers, as discussed in prior studies [179]–[184].

$$Sensitivity(Sen) = \frac{TP}{TP + FN} * 100 \quad (3.1)$$

$$Specificity(Spec) = \frac{TN}{TN + FP} * 100 \quad (3.2)$$

$$Accuracy(Acc) = \frac{TP + TN}{TP + FP + TN + FN} * 100 \quad (3.3)$$

$$F1score(F1) = \frac{2 TP}{2 TP + FP + FN} \quad (3.4)$$

Here,

- TP implies that a spectrogram image from an ASD subject is correctly diagnosed as being in the ASD class.
- TN implies that a spectrogram image from a HC subject is correctly diagnosed as being in the HC class.
- FP implies that a spectrogram image from a HC subject is falsely diagnosed as ASD.
- FN implies that a spectrogram image from an ASD subject is falsely diagnosed as HC.

A ROC graph serves as a valuable means to visualise the classifier's reliability. This graph is constructed by plotting sensitivity (true positive rate) along the Y-axis and 1-specificity (false positive rate) along the X-axis. A common metric for assessing the effectiveness of binary classifiers is the Area Under the ROC Curve (AUC). The AUC value adheres to the following inequalities:

$$0 \leq AUC \leq 1 \quad (3.5)$$

As expressed in equation 3.5, an AUC value of 1 signifies that the classifier possesses flawless discrimination capabilities. Conversely, a value equal to or below 0.5 suggests that the classifier lacks any discriminatory capability whatsoever [185].

### 3.4 Result and discussion

Within this section, we delve into the comprehensive outcomes of the proposed classification methods. This exploration is organised into two distinct subsections, each dedicated to one of the two distinct classification processes: the performance of ML-based classification and the performance of DL-based classification.

### 3.4.1 Results for machine learning based process

In the case of ML-based classification, the evaluation of the proposed system's performance employs the  $k$ -fold cross-validation technique. This approach entails the random division of the dataset into  $k$  subsets of equal size. Subsequently, the system is trained using  $k-1$  of these subsets while testing is conducted using the remaining subset. This process repeats  $k$  times (hence " $k$ -fold"), with each subset serving once as the testing set. In this particular analysis, we have employed a ten-fold cross-validation strategy, partitioning spectrogram images into two subsets, with 90% used for training and 10% for testing. This process is repeated ten times to ensure that each image in the dataset is exactly once part of the test subset. Finally, the results obtained from the ten-fold iterations are averaged to yield a comprehensive classification metric.

In the domain of ML-based classification, six distinct classifiers are employed: NB, LDA utilising pseudolinear discriminant analysis, RF,  $k$ -NN with  $k=9$ , LR, and SVM utilising a linear kernel. Table 3.1 presents a comprehensive overview of the overall performance metrics, encompassing equations 3.1 through 3.5, for the six classifiers mentioned above. Among these classifiers, the SVM-based approach exhibits the highest overall performance, achieving an accuracy rate of 95.25%. In contrast, the NB-based method displays the lowest overall performance, yielding an accuracy rate of 72.09%.

TABLE 3.1: Overall classification performance of different ML-based classifiers.

Classifier	Sen %	Spec %	F1	AUC	Acc %
NB	66.83	84.67	0.78	0.77	72.09
LDA	91.54	86.26	0.93	0.96	89.97
RF	<b>99.27</b>	70.02	0.94	0.97	90.59
$k$ NN	90.67	<b>96.13</b>	0.94	<b>0.98</b>	92.29
LR	96.99	90.06	0.96	<b>0.98</b>	94.95
SVM	97.07	90.95	<b>0.97</b>	<b>0.98</b>	<b>95.25</b>

When examining sensitivity, the RF classifier claims the top position with the highest sensitivity rate of 99.27%. The SVM classifier follows closely with the second-highest sensitivity of 97.07%, while the NB classifier trails behind with a sensitivity rate of 66.83%. Fold-wise sensitivity results for these different classifiers are illustrated in Figure 3.7.

Conversely, the  $k$ NN classifier boasts the highest average specificity value at 96.13%, followed by the SVM classifier with 90.95%, and the RF classifier in the last position, registering a specificity rate of 70.02%. Fold-wise specificity outcomes for these diverse classifiers are showcased in Figure 3.8.

It is noteworthy that although SVM and LR may not rank as the best performers in terms of individual sensitivity or specificity, they emerge as the top two classifiers when considering F1 scores and accuracy metrics. This outcome is a result of the RF classifier, which achieves the highest sensitivity rate (99.27%) but exhibits a notably low specificity rate (70.02%). Conversely,  $k$ NN records the highest specificity rate (96.13%) but comparatively lower sensitivity (90.67%) in comparison to the others. In contrast,

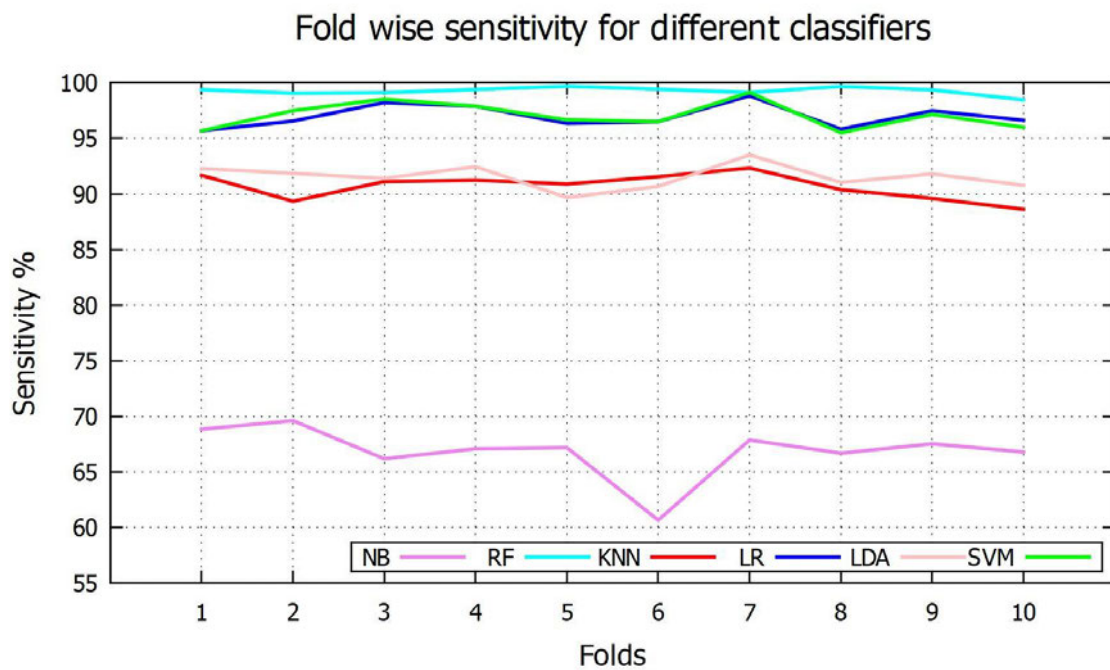


FIGURE 3.7: Fold-wise sensitivity comparison for different ML-based classifiers.

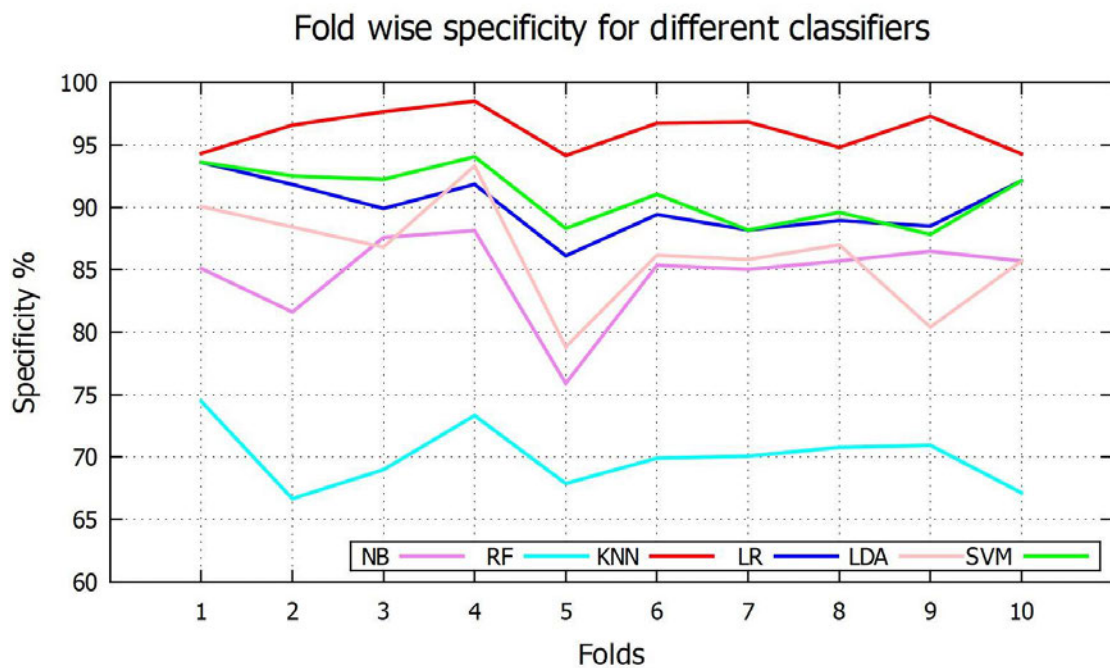


FIGURE 3.8: Fold-wise specificity comparison for different ML-based classifiers.

both SVM and LR maintain a balanced blend of sensitivity and specificity, resulting in impressive F1 scores of 0.97 and accuracy rates of 95.25% and 94.95%, respectively. The fold-wise accuracy results for these various classifiers are displayed in Figure 3.9.

To further assess performance, the ROC curves for different classifiers are depicted in

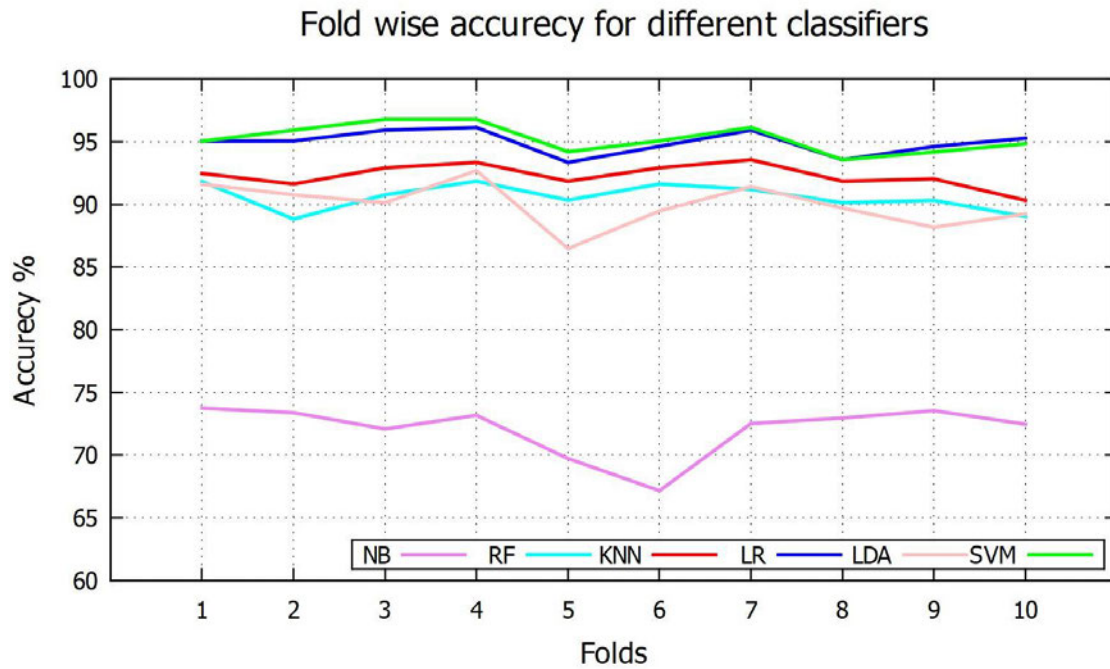


FIGURE 3.9: Fold-wise accuracy comparison for different ML-based classifiers.

Figure 3.10, where the curves for  $k$ NN, LR, and SVM closely overlap. The AUC serves as an indicator of classifier performance, with a larger AUC indicating superior classifier performance. The AUC values for various classifiers are detailed in Table 3.1, with SVM, LR, and  $k$ NN achieving the highest AUC value of 0.98, while NB attains the lowest AUC score of 0.77. For a more granular view of classifier performance, the fold-wise AUCs for different classifiers are presented in Figure 3.11.

### 3.4.2 Results of deep learning based process

As outlined in the methodology section, three distinct CNN models are employed for the DL-based classification process. In this procedure, the complete image dataset is partitioned into three segments, allocating 70% of the images for model training, 15% for validation, and the remaining 15% for testing the trained model. All models undergo training for a duration of 50 epochs to mitigate the risk of overfitting. A uniform batch size of 64 is applied for training all models, with additional batch sizes of 32, 128, and 256 employed during the training of the third model to assess the influence of batch size on the performance of the model. The comprehensive performance metrics for these diverse models are detailed in Table 3.2.

Table 3.2 clearly illustrates that all DL-based models outperform the ML-based classifiers. Among them, Model 3 with a batch size of 64 yields the most impressive results, achieving a remarkable 99.15% accuracy and an exceptional F1 score of 1.00. Models 1 and 2 exhibit commendable sensitivity values; however, due to their relatively lower specificity, their overall F1 scores and accuracy are inferior in comparison to Model 3.

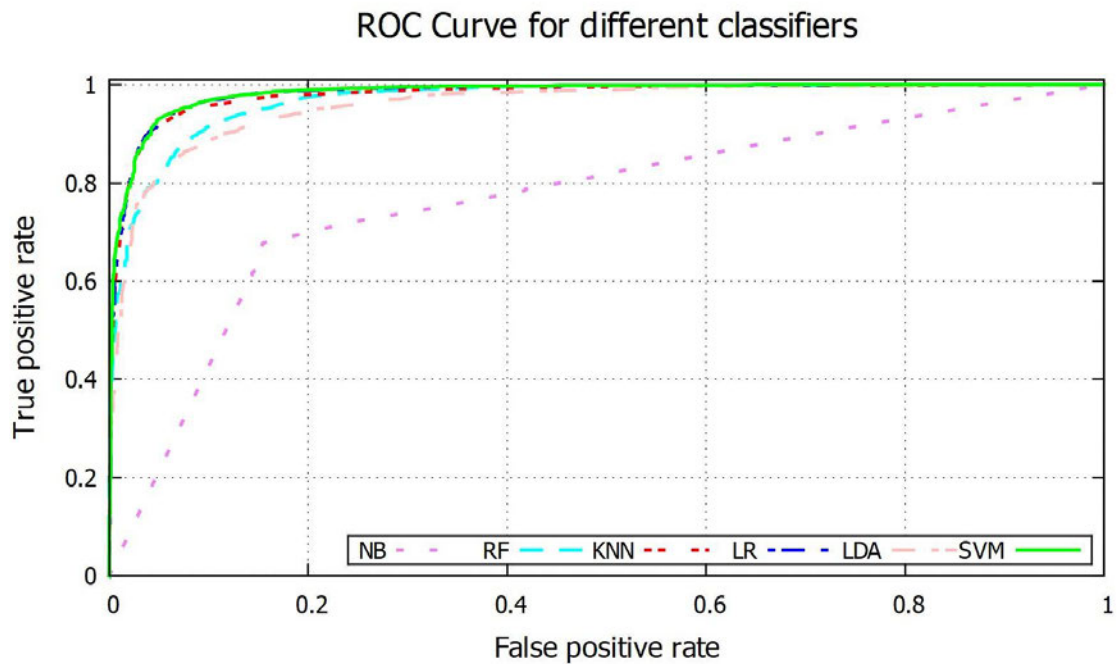


FIGURE 3.10: ROC graph for different ML-based classifiers.

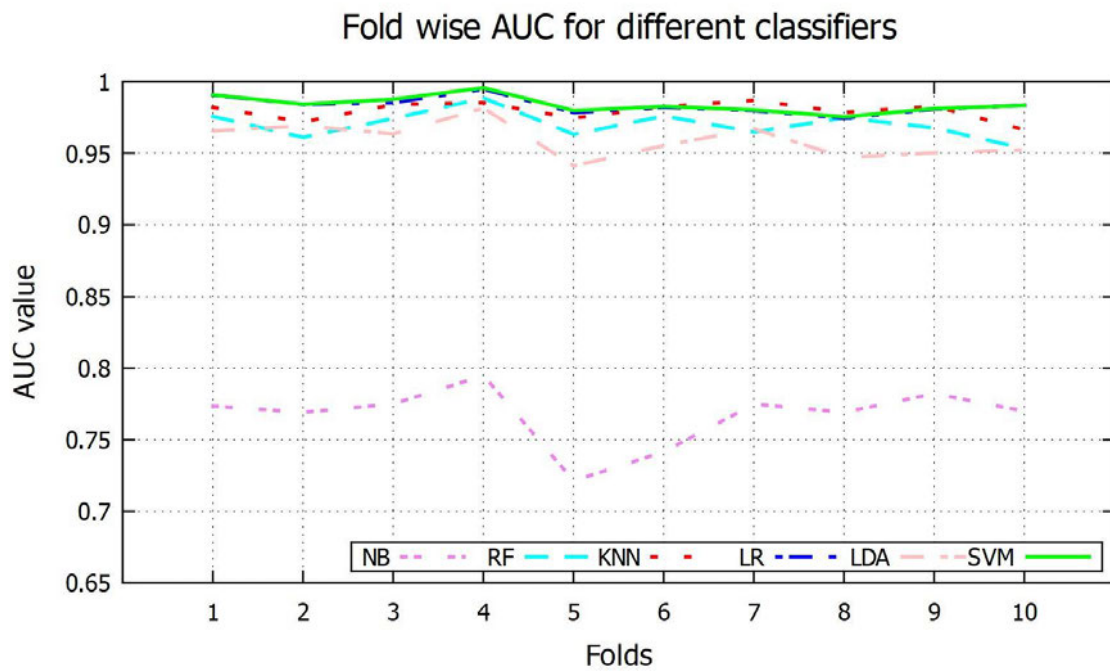


FIGURE 3.11: Fold-wise AUC value comparison for different ML-based classifiers.

In the context of the diverse batch sizes employed for Model 3, a batch size of 128 produces the highest sensitivity at 99.60%, while a batch size of 32 yields the highest specificity at 99.10%. Nevertheless, the overall best performance is achieved by the batch size of 64. Batch size 256 delivers the second-best overall performance, boasting an accuracy rate and F1 score of 99.00% and 0.99, respectively. Batch sizes 128 and 32 occupy

TABLE 3.2: Overall classification performance of different tested CNN models.

Classifier	Sen %	Spec %	F1	AUC	Acc %
Model 1	98.80	89.76	0.97	0.94	96.16
Model 2	98.81	88.94	0.97	0.94	96.02
Model 3 (Batch size 32)	97.71	<b>99.10</b>	0.99	0.98	98.15
Model 3 (Batch size 128)	<b>99.60</b>	96.57	0.99	0.98	98.72
Model 3 (Batch size 256)	99.39	98.12	0.99	<b>0.99</b>	99.00
Model 3 (Batch size 64)	99.19	99.04	<b>1.00</b>	<b>0.99</b>	<b>99.15</b>

the third and fourth positions, each achieving accuracy rates of 98.72% and 98.15%, with identical F1 scores of 0.99. Figure 3.12 depicts the ROC curve for all DL-based models, while Table 3.2 provides the AUC values, where Model 3, with batch sizes of 64 and 256, achieves an AUC of nearly 1 (0.99). Model 3, with batch sizes of 32 and 128, attains an AUC of 0.98, whereas Models 1 and 2 record an AUC of 0.94.

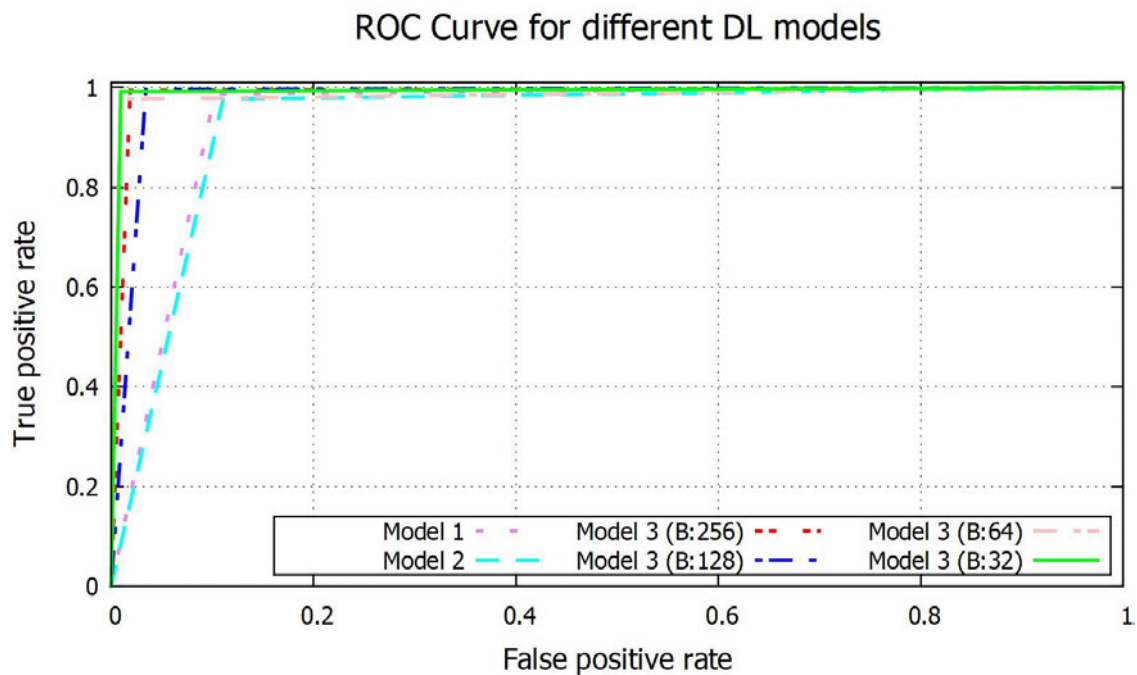


FIGURE 3.12: ROC graph of different CNN Models with different tested batch sizes for CNN model 3.

Since Model 3 with a batch size of 64 has demonstrated superior performance among the three proposed DL models for ASD identification in comparison to TD children, we offer a detailed examination of the loss versus accuracy graph for this model. Figure 3.13 displays epoch-wise trends of training and validation loss versus accuracy for Model 3 with a batch size of 64. In this graph, both training and validation accuracy approach 100% as the losses decrease to nearly zero with the increasing number of epochs. This phenomenon indicates that the CNN model has effectively adapted to the training data, resulting in lower loss values on the validation set.

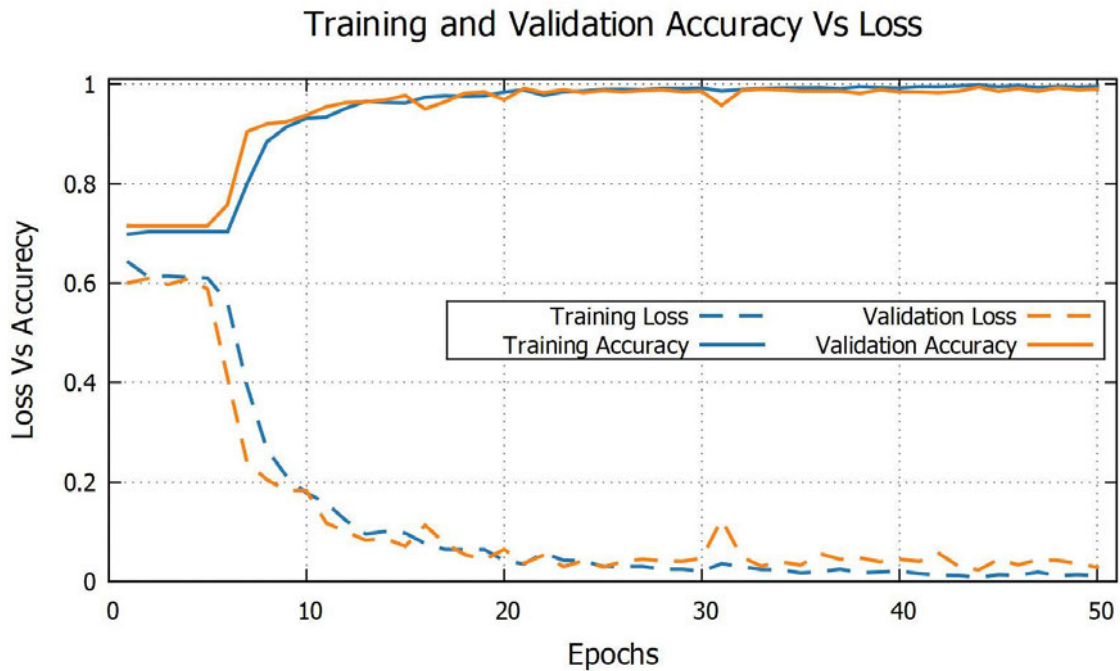


FIGURE 3.13: Training and validation loss vs. accuracy graph of third CNN Model with training batch size of 64.

A comparison between the proposed approach and prior research conducted using the same ASD dataset employed in this analysis is presented in Table 3.3. Notably, some of the prior works, such as [177], [186], [187], adopted ML-based classification methods, while others, including [103], [105], [188], utilised DL techniques for ASD classification.

TABLE 3.3: Performance comparison of the proposed framework with existing methods using the same EEG dataset.

Authors	Feature extraction	Classifier	Accuracy %
Alsaggaf <i>et al.</i> [186]	FFT	FLDA	80.27
Alhaddad <i>et al.</i> [177]	FFT	FLDA	90.00
Kamel <i>et al.</i> [187]	FFT	RFLD	92.06
Nur <i>et al.</i> [188]	MLPN	MLPN	80.00
Djemal <i>et al.</i> [103]	DWT, ShanEn	ANN	98.60
Alturki <i>et al.</i> [105]	DWT, ShanEn	ANN	98.20
<b>Proposed Method</b>	Spectrogram image	CNN	<b>99.15</b>

In the studies conducted by Alsaggaf *et al.* [186], Kamel *et al.* [187], and Alhaddad *et al.* [177], feature extraction from EEG signals involved employing the Fast Fourier Transform (FFT) method. Kamel *et al.* utilised Regulated Fisher Linear Discriminant (RFLD) for classification and achieved an accuracy of 92.06%. Alsaggaf *et al.* and Alhaddad *et al.*, on the other hand, utilised Fisher Linear Discriminant Analysis (FLDA) for classification, resulting in accuracies of 80.27% and 90.00%, respectively.

In a more recent study, Nur *et al.* [188] utilised the Multilayer Perceptron Network (MLPN) classification method and obtained an accuracy of 80%. Djemal *et al.* [103]

employed Discrete Wavelet Transform (DWT) with Shannon Entropy (ShanEn) on 50-second segment lengths in conjunction with an Artificial Neural Network (ANN) classifier, achieving an accuracy of 98.60% for non-overlapping segments. Similarly, Alturki *et al.* [105] used DWT with ShanEn for feature extraction and employed ANN for classification, attaining an accuracy of 98.20%. The proposed technique, which employs spectrogram images in conjunction with a CNN classifier, surpasses all the mentioned approaches, achieving an accuracy of 99.15%.

Table 3.4 offers a comprehensive summary of existing ASD classification studies that employed different datasets. A detailed discussion of these existing methods can be found in Section 3.1. Given the variability in datasets used for validation in these studies, conducting a fair comparison with the proposed method is challenging.

TABLE 3.4: Performance comparison of the proposed framework with existing methods using different EEG datasets.

Authors	Dataset	Feature extraction	Classifier	Accuracy %
Sheikhani <i>et al.</i> , 2008 [123]	Own dataset	STFT	kNN	82.40
Ahmadlou <i>et al.</i> , 2010 [128]	Iranian dataset	Wavelet and fractal dimension	RBNN	90.00
Bosl <i>et al.</i> , 2011 [126]	Own dataset	mMSE	SVM	90.00
Ahmadlou <i>et al.</i> , 2012 [104]	Iranian dataset	Wavelet and visibility graph	EPNN	95.50
Sheikhani <i>et al.</i> , 2012 [124]	Own dataset	STFT and statistical	kNN	96.40
Ahmadlou <i>et al.</i> , 2012 [129]	Iranian dataset	Wavelet and fuzzy logic	EPNN	95.50
Eldridge <i>et al.</i> , 2014 [131]	Own dataset	SSD, mMSE	SVM, LR, NB Sn, LR, SMO, kNN,	79.00
Grossi <i>et al.</i> , 2017 [132]	Own dataset	MSROM/I-FAST	K-CM, NB, RF	92.80
Djermal <i>et al.</i> , 2017 [103]	KAU	DWT, ShanEn	ANN	98.60
Heunis <i>et al.</i> , 2018 [137]	Own dataset	RQA, PCA	SVM	92.90
Haputhanthri <i>et al.</i> , 2019 [164]	Own dataset	DWT and statistical	LR, SVM, NB, RF	93.00
Jayarathna <i>et al.</i> , 2019 [189]	Own dataset	statistical and entropy	RF, LR, JRip, CNN etc.	98.06
Haputhanthri <i>et al.</i> , 2020 [165]	Own dataset	statistical and entropy	LR, MLP, NB, RF	88.00
Abdolzadegan <i>et al.</i> , 2020 [166]	Own dataset	Linear and nonlinear	kNN, SVM	90.57
Alturki <i>et al.</i> , 2020 [105]	KAU	DWT, ShanEn	ANN	98.20
<b>Proposed Method</b>	<b>KAU</b>	<b>Spectrogram image</b>	<b>CNN</b>	<b>99.15</b>

### 3.5 Summary

In this chapter, we have introduced the utilisation of T-F spectrogram images of EEG signals for distinguishing between ASD and TD children. We have generated spectrogram images through STFT from EEG signals and employ both ML and DL techniques for classification. In the ML-based classification, we have used six distinct classifiers to classify the features extracted using the tCENTRIST method. In the DL-based process, we have used three different CNN models to process the spectrogram images.

Our results highlight that SVM exhibits the highest classification accuracy in the ML-based classification process, achieving an accuracy rate of 95.25%. In contrast, in the DL-based classification process, the proposed CNN model demonstrates outstanding performance, achieving an accuracy of 99.15%. To provide context, we also compare our approach with other state-of-the-art methods in the literature that utilised the same dataset employed in this analysis.

These findings underscore the effectiveness of our proposed approach, surpassing the majority of techniques documented in existing literature. This approach can serve as a foundation for CAD systems intended for the detection of various neurological disorders that utilise EEG recordings for diagnosis.

In order to respond to the first research problem related to the classification of SZ, a second methodology has been formulated. This method involves the utilisation of topographic images derived from EEG signal data. The subsequent chapter provides a comprehensive and detailed discussion of this developed approach.

# OFFICE FOR RESEARCH TRAINING, QUALITY AND INTEGRITY

## DECLARATION OF CO-AUTHORSHIP AND CO-CONTRIBUTION: PAPERS INCORPORATED IN THESIS

*This declaration is to be completed for each conjointly authored publication and placed at the beginning of the thesis chapter in which the publication appears.*

### 1. PUBLICATION DETAILS (to be completed by the candidate)

Title of  
Paper/Journal/Book:

Brain data mining framework involving entropy topography and deep learning.  
Databases Theory and Applications: 33rd Australasian Database Conference,  
ADC 2022

Surname: Tawhid

First name: Md Nurul Ahad

Institute: Institute for Sustainable Industries and Liveab

Candidate's Contribution (%): 70

Status:

Accepted and in press:

Date:

Published:

Date:

27/08/2022

### 2. CANDIDATE DECLARATION

I declare that the publication above meets the requirements to be included in the thesis as outlined in the HDR Policy and related Procedures – [policy.vu.edu.au](http://policy.vu.edu.au).

Md Nurul Ahad  
Tawhid

Digitally signed by Md Nurul Ahad  
Tawhid  
Date: 2023.09.08 13:05:12 +10'00'

08/09/2023

Signature

Date

### 3. CO-AUTHOR(S) DECLARATION

In the case of the above publication, the following authors contributed to the work as follows:

The undersigned certify that:

1. They meet criteria for authorship in that they have participated in the conception, execution or interpretation of at least that part of the publication in their field of expertise;
2. They take public responsibility for their part of the publication, except for the responsible author who accepts overall responsibility for the publication;



- 3. There are no other authors of the publication according to these criteria;
- 4. Potential conflicts of interest have been disclosed to a) granting bodies, b) the editor or publisher of journals or other publications, and c) the head of the responsible academic unit; and
- 5. The original data will be held for at least five years from the date indicated below and is stored at the following location(s):

Name(s) of Co-Author(s)	Contribution (%)	Nature of Contribution	Signature	Date
Siuly Siuly	10	Supervision, Formal analysis, Visualization, Manuscript preparation		08/09/23
Kate Wang	10	Supervision, Manuscript preparation		08/09/23
Hua Wang	10	Supervision, Manuscript preparation, Funding acquisition, Project		08/09/23

Updated: September 2019

## Chapter 4

# Topographic Image Based EEG Signal Classification

In response to the first research problem, the preceding chapter introduced a framework aimed at detecting ASD through spectrogram analysis. In continuation, the current chapter is dedicated to the development of an alternative method, specifically tailored to address the same research problem (**RP1**) but in the context of schizophrenia (SZ) disorder.

We have developed a novel approach that utilises deep learning techniques to differentiate individuals with SZ from healthy controls by creating an entropy topography of the EEG signal. Our method involves extracting Shannon entropy values from each channel of the EEG signal and mapping them onto the brain scalp to generate topographic images. Subsequently, these images are subjected to training and classification using our custom convolutional neural network. We assessed the method's performance on two distinct EEG datasets from individuals with SZ, and the results demonstrated its potential for mining brain signal data.

The contents of this chapter have been presented in *33rd Australasian Database Conference, ADC 2022* (Publication 4) [190].

### 4.1 Introduction

Brain signal data is increasingly harnessed to evaluate brain activity, offering significant potential for the diagnosis and treatment of mental and neurological conditions. Among these signals, electroencephalogram (EEG) data is a prominent example. There is a growing global demand for streamlined methods to interpret brain signal data, making healthcare more effective and cost-efficient. In the realm of biomedical research, the development and adoption of advanced signal processing algorithms for EEG data analysis are of paramount importance [22].

EEG, which captures the brain's spontaneous electrical activity in the form of extensive time-series data, is inherently non-linear and non-stationary. It exhibits patterns linked to an individual's mental health state. EEG data serves various purposes, including the creation of brain-computer interfaces (BCIs) [191], exploration of changes in brain

electrical activity in response to external stimuli or internal mental processes [22], recognition of sleep stages [192], detection of emotions and fatigue [193], and the prediction of brain-related health conditions (prognosis) [90], [194].

Traditionally, expert clinicians visually analyse EEG signals, yet discerning subtle but critical changes through visual inspection can prove challenging. Consequently, this has spurred biomedical engineers to explore innovative and efficient algorithms for detecting these changes. Data mining techniques can extract vital biomarkers from brain signal data, facilitating the automatic categorisation of brain states into distinct disorder categories through the development of computer-aided diagnostic (CAD) systems.

Lately, EEG technology has garnered significant attention for its precise monitoring of brain activity. Nevertheless, the raw EEG signal presents challenges, as it is susceptible to artefacts and exhibits complexity due to its temporal and spatial variability. In the process of identifying brain states, the pivotal stages involve feature extraction and classification. Traditional manual feature extraction and selection methods necessitate specific domain expertise. Furthermore, the cost associated with conventional feature selection methods escalates exponentially with the increasing number of features, as discussed in Dash *et al.*'s work [195].

While prior research has predominantly concentrated on feature extraction processes in either the time domain [98], frequency domain [196], or time-frequency domain [154], with relatively limited exploration in the spatial domain. The spatial domain of an EEG signal refers to the physical space where electrical brain activity is measured and recorded. In EEG, electrodes are placed on the scalp to capture electrical potentials generated by neural activity in the brain. The spatial domain, therefore, encompasses the scalp surface where these electrodes are positioned. Techniques such as source localization or scalp topographic mapping help to infer the underlying brain regions generating the recorded electrical signals. Spatial domain analysis in EEG involves interpreting the spatial patterns of electrical potentials across electrodes. Changes in these patterns can indicate variations in brain activity associated with cognitive tasks, stimuli, or neurological conditions. The objective of this study is to leverage a combination of the time, frequency, and spatial domains to achieve accurate detection of anomalies in multichannel EEG recordings.

Over the past decade, numerous studies have delved into the realm of mining extensive EEG datasets, as evidenced by research works [78], [79], [154], [197], [198]. The majority of these investigations have employed diverse statistical metrics as signal features and have employed various classifiers for feature classification. However, conventional approaches often struggle to extract salient and discriminative attributes from vast datasets. Moreover, statistical features applied to lengthy signals may inadvertently overlook short-term properties, which hold paramount importance in identifying abnormalities. This limitation can be addressed by visualising small signal segments' entropy as topographic images.

Furthermore, when it comes to classification, deep learning (DL)-based models outperform machine learning (ML)-based classifiers, especially in scenarios involving large data volumes. DL models possess the capability to autonomously learn features and perform classification [167]. Nevertheless, the majority of studies within the field of data mining

for EEG data have primarily assessed their proposed methodology on a specific dataset, raising questions about their generalisability to other datasets.

Hence, for the purpose of detecting anomalies within this extensive brain signal dataset using time, frequency and spatial domain, this study introduces a novel framework that combines topographic imaging and deep learning, with a specific focus on EEG data mining. EEG multichannel recordings offer insights into the spatial distribution of brain electrical activity. In this context, waveform patterns are transformed into images, providing a visual representation of the electric landscape of brain activity at discrete moments or illustrating the varying frequency characteristics of recorded EEG signals for imaging purposes [199].

In our proposed approach, the signals undergo an initial segmentation into three-second (3s) time windows to facilitate feature extraction from these brief signal segments. Subsequently, Shannon entropy (ShanEn) is employed to extract entropy values from these segments, which are then utilised to generate corresponding topographic images. Following this, a deep learning-based convolutional neural network (CNN) is developed to extract features and conduct classification on these topographic images. To assess the generalisability and performance of the proposed model, we have used two well known publicly available EEG datasets pertaining to schizophrenia disorders. The key contributions of this study encompass the following:

1. Develop a data mining framework for brain signal data, especially EEG.
2. Introduce an entropy-based topographic visualisation of the EEG signal.
3. Design and validate a new efficient and automatic CNN-based framework for topographic image classification.
4. Explore the framework's generalisability and performance with two different EEG datasets.

Details of the proposed method and the obtained results are discussed in the sections below.

## 4.2 Methodology of the proposed mining framework

Here, we have proposed a brain signal data mining framework using topographic images and a deep learning-based CNN model. This framework works in a couple of steps: first, the signals are resampled and segmented into small time windows in the pre-processing step, and then topographic images are generated from those signal segments. Finally, we have trained our proposed CNN model on those generated topographic images to perform classification into different classes, and the classification performance is evaluated using different evaluation parameters. Figure 4.1 shows the overall diagram of the proposed framework. Details of those steps are discussed below:

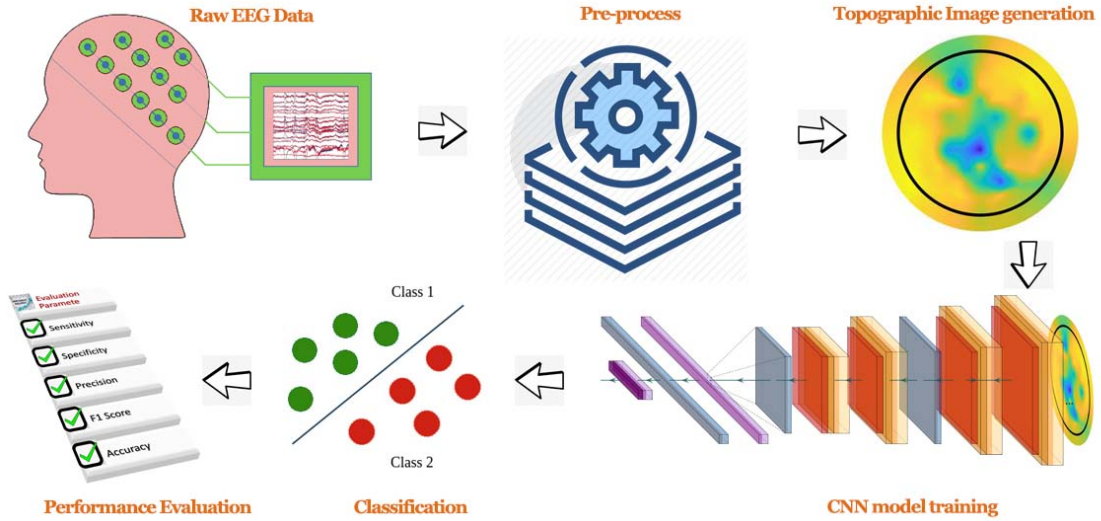


FIGURE 4.1: A schematic diagram of the proposed classification framework combining topographic images and deep learning-based CNN model.

#### 4.2.1 Pre-processing of the raw data

In this phase, we have undertaken pre-processing of the original EEG signal data to create the topographic image. Initially, we applied resampling to the raw data, aligning it with a standardised 256 Hz sampling frequency, which is a commonly utilised frequency range and offers computational advantages over higher frequencies [200]. Subsequently, the data underwent segmentation into compact three-second (3s) segments. This segmentation strategy was employed to maximise feature extraction from these smaller signal portions and to augment the overall dataset size [79], [90], [194].

#### 4.2.2 Creation of topographic images for signal segments

A brain signal topographic image is a neuroimaging technique that is used to plot the activity of the different brain regions using several tones of colour (like black and blue, which could represent low signal amplitudes, whereas yellow and red could represent higher amplitudes.) [201]. This method provides a far more exact and representative picture of the position of rhythm, amplitude, and other changes in relation to the skull's surface and also helps to pinpoint the exact location of signal alteration. Here, we have used entropy topography, where entropy has been extracted from non-overlapping windows of brain signal recordings and plotted to a 2-D map by colour coding of signal features. To extract the entropy values, we have used Shannon entropy (ShanEn), which quantifies the probability density function of the distribution of values using the below equation 4.1:

$$ShanEn = - \sum_i p_i \log p_i \quad (4.1)$$

In this context,  $i$  represents the probability of the occurrence of the amplitude value  $v_i$  within the data time series, while  $p_i$  signifies the likelihood of the amplitude value  $v_i$  appearing at any point throughout the data time series. Consequently,  $p_i$  can be expressed

as the proportion of data points within the data time series that possess the amplitude value  $v_i$  relative to the total number of data points.

After calculating the ShanEn for each recording channel of the segmented brain signal, we have plotted the entropy values into the topographic plotting to get the topographic image for that signal segment. A topographical transformation produces maps that depict the scalp distribution of brain activity at discrete times or at selected frequencies of the spontaneous brain signal. These generated images are used in the next step of CNN model training and classification.

### 4.2.3 Training and classification using a deep learning-based model

We adopted a deep learning-based Convolutional Neural Network (CNN) model for classification purposes, as it is a well-established choice for image-based classification tasks. This model has demonstrated remarkable efficacy in autonomously learning pertinent features and accurately classifying data into diverse categories [175]. In this research, we crafted a CNN model tailored for the classification of the generated topographic images. Our proposed model encompasses four convolutional (Conv) layers, each equipped with 32 filters of size  $5 \times 5$  and activated using the Rectified Linear Unit (ReLU) function. Following each Conv layer, we used a batch normalisation and a max-pooling layer with a pooling size of  $2 \times 2$ . The second and fourth max-pooling layers are supplemented by a 25% dropout layer, while the fully connected layer is followed by a 50% dropout layer. The training of our CNN model utilises the Adam optimiser, employs softmax as the classifier, and categorical cross-entropy as the loss function. Figure 4.2 shows a block diagram of the proposed CNN model.

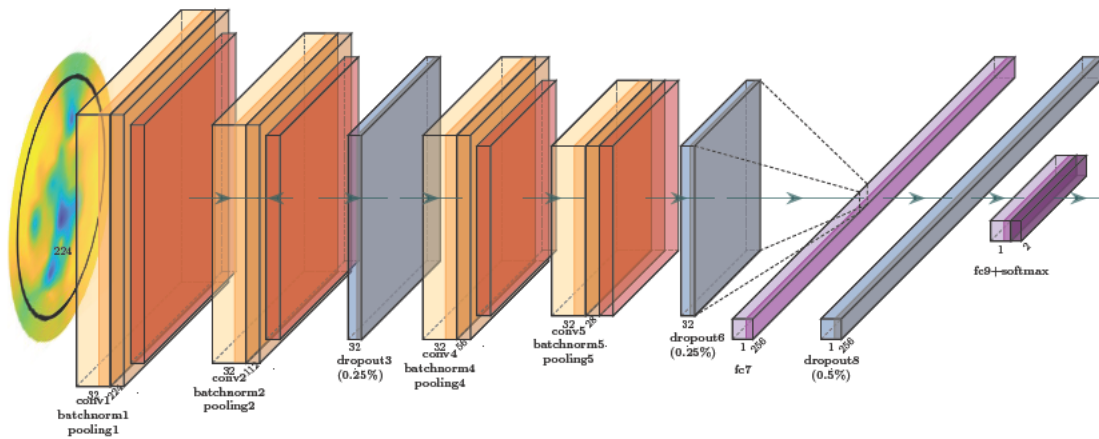


FIGURE 4.2: Proposed CNN model for the topographic image classification.

After training the CNN model, a categorisation process is conducted and a binary classification is performed among patients and normal subjects.

### 4.3 Materials and parameters used for evaluating performance

We have conducted a validation of the proposed brain signal data mining framework using two publicly available EEG brain signal datasets related to schizophrenia (SZ) disease. In our evaluation, we carried out binary classification tasks distinguishing SZ subjects from healthy control (HC) subjects. To assess the performance of our proposed framework, we employed a range of commonly used evaluation metrics within this domain. Further details regarding the datasets and evaluation parameters are provided in the following subsections.

#### 4.3.1 Data Acquisition

In this research, we have used two publicly available EEG datasets of schizophrenia disorders to validate the proposed framework. The first dataset we have used contains 81 subjects (14 females and 67 males; average age 39 years), 49 of whom have SZ and 32 are HC subjects [202]. EEG data was recorded from 64 electrodes at a sampling rate of 1024 Hz. In this study, we have used the same data as the authors of [154] used. Details of the data collection and pre-processing steps can be found in [202].

The second dataset we have used is from the Institute of Psychiatry and Neurology in Warsaw, Poland [78] with 28 subjects. Among those subjects were 14 patients (7 females, 7 males; average age  $28.3 \pm 4.1$  and  $27.9 \pm 3.3$  years, respectively) and 14 HCs within the same age and gender group. Fifteen minutes of resting state EEG data were recorded at a 250 Hz sampling frequency from 19 channels of the 10–20 international standard EEG system. Details of the data can be found in [78].

#### 4.3.2 Performance evaluation criteria

Cross-validation serves as a technique to assess the predictive performance of a model while mitigating the risk of overfitting. Achieving high classification rates may hinge on the specific pairing of training and testing sets. The strategy we employed is known as  $k$ -fold cross-validation, where the dataset is divided into  $k$  subsets of equal or nearly equal size. During each iteration,  $k-1$  subsets are designated for training, while the remaining subset is reserved for testing. This process is repeated  $k$  times, with each subset serving as the test set exactly once. In our study, we adopted 10-fold cross-validation to comprehensively evaluate the performance of our proposed framework.

Subsequently, the system's performance was assessed using six standard evaluation metrics: sensitivity (Sen), specificity (Spec), precision (Prec), F1 score (F1), accuracy (Acc), and the receiver operating characteristic (ROC) curve.

## 4.4 The outcomes of the proposed framework

In this research work, we have introduced a data mining system tailored for EEG signal data, integrating topographic images and a deep learning-based approach. We have tested the proposed model on two distinct EEG datasets of SZ disease to perform a binary classification (SZ vs. HC). Details of the achieved results, along with visualisation and descriptions of experimental setups are discussed in the subsequent subsections.

### 4.4.1 Experimental configuration

We initiated our experimentation by pre-processing the EEG data, which involved resampling it to 256 Hz and segmenting it into 3-second chunks. Subsequently, we computed Shannon Entropy (ShanEn) for these shorter segments and utilised the calculated ShanEn values to generate topographic images. This process resulted in a total of 4,728 images for SZ subjects and 3,108 images for HC subjects in the case of dataset 1. As for dataset 2, these figures amounted to 5,146 images for SZ subjects and 4,235 images for HC subjects. Sample topographic images from both datasets are presented in Figure 4.3.

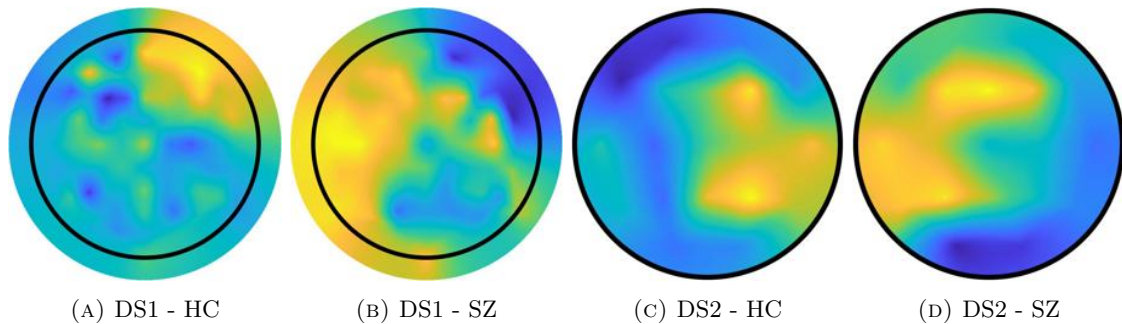


FIGURE 4.3: Examples of topographic images for the tested datasets. For HC and SZ individuals, 4.3a and 4.3b are from dataset 1 while 4.3c and 4.3d, respectively, are from dataset 2.

These images were subsequently employed for training and classification using the CNN model. During the CNN model training phase, we adopted the mini-batch mode and tested four distinct batch sizes: 32, 64, 128, and 256 as part of our experimentation.

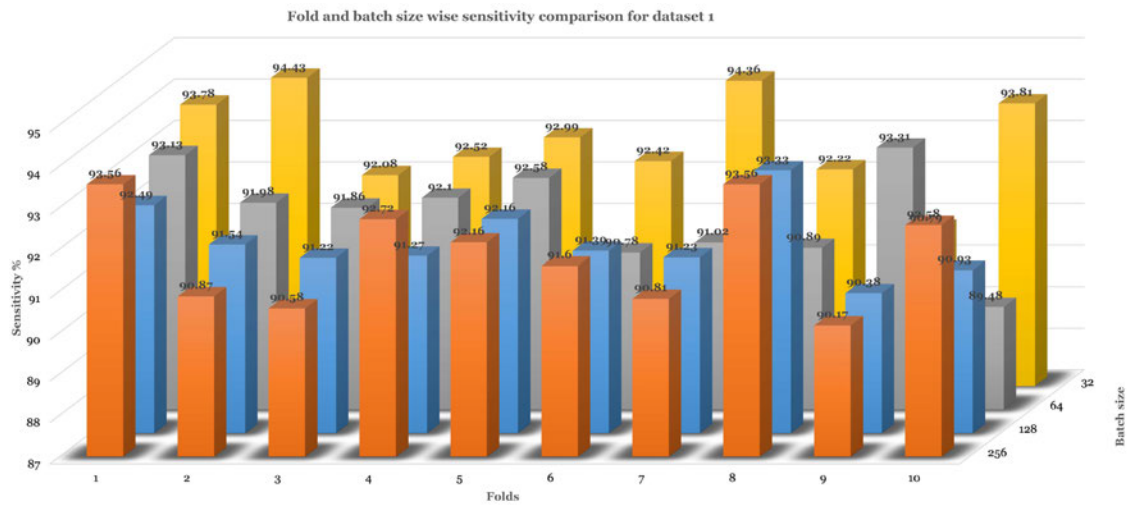
### 4.4.2 Experimental Outcomes of the Proposed Framework

In this study, we have validated our proposed framework using two distinct EEG datasets related to SZ disorder, employing the 10-fold cross-validation technique. We have tested four different training batch sizes to assess their impact on the performance of the CNN model. Table 4.1 presents the average performance metrics for the framework across the tested datasets and batch sizes. The values highlighted in bold represent the highest average performance achieved for each evaluation parameter within the respective dataset, as determined over the 10-fold cross-validation process.

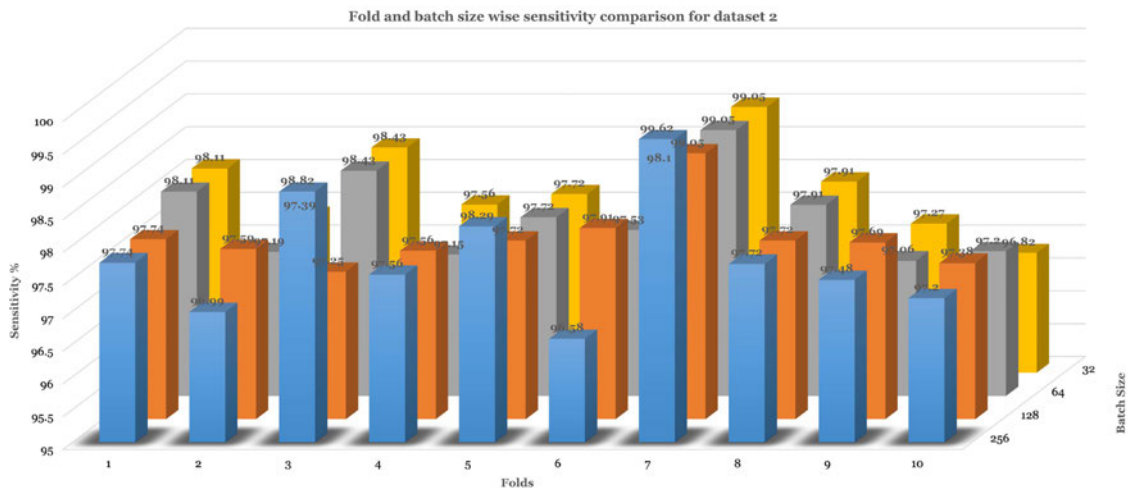
Table 4.1 reveals that the performance of the proposed framework experiences a decline as the training batch size increases. Specifically, for dataset 1, the highest 10-fold average

TABLE 4.1: Results of the proposed method's ten-fold average performance (mean $\pm$ std) on two test datasets for various batch sizes.

Datasets	Parameters	Batch size 256	Batch size 128	Batch size 64	Batch size 32
Dataset 1	Sen%	91.86 $\pm$ 1.17	91.59 $\pm$ 0.81	91.71 $\pm$ 1.12	<b>92.94<math>\pm</math>1.10</b>
	Spec%	81.78 $\pm$ 3.30	83.93 $\pm$ 1.61	<b>84.69<math>\pm</math>2.49</b>	83.49 $\pm$ 1.84
	Prec%	88.50 $\pm$ 1.83	89.64 $\pm$ 1.25	<b>90.14<math>\pm</math>1.46</b>	89.57 $\pm$ 0.84
	F1	0.90 $\pm$ 0.01	<b>0.91<math>\pm</math>0.01</b>	<b>0.91<math>\pm</math>0.01</b>	<b>0.91<math>\pm</math>0.01</b>
	Acc%	87.87 $\pm$ 1.05	88.54 $\pm$ 0.59	88.93 $\pm$ 1.24	<b>89.20<math>\pm</math>0.81</b>
Dataset 2	Sen%	97.80 $\pm$ 0.85	97.76 $\pm$ 0.47	97.74 $\pm$ 0.62	<b>97.84<math>\pm</math>0.60</b>
	Spec%	97.56 $\pm$ 0.66	<b>97.95<math>\pm</math>0.67</b>	97.81 $\pm$ 0.53	97.86 $\pm$ 0.48
	Prec%	97.97 $\pm$ 0.63	<b>98.30<math>\pm</math>0.56</b>	98.18 $\pm$ 0.49	98.22 $\pm$ 0.45
	F1	0.98 $\pm$ 0.01	<b>0.98<math>\pm</math>0.00</b>	0.98 $\pm$ 0.01	<b>0.98<math>\pm</math>0.00</b>
	Acc%	97.69 $\pm$ 0.42	97.85 $\pm$ 0.53	97.77 $\pm$ 0.51	<b>97.85<math>\pm</math>0.45</b>



(A) Dataset 1



(B) Dataset 2

FIGURE 4.4: Fold-wise comparison of sensitivity value for different training batch sizes for the tested two datasets.

sensitivity of  $92.94\pm 1.10\%$  is achieved when utilising a batch size of 32, while for dataset 2, it reaches  $97.84\pm 0.60\%$  with the same batch size. To delve into a more detailed fold-wise

performance analysis, we have depicted fold- and batch-size-specific sensitivity values in Figure 4.4. Figure 4.4a corresponds to dataset 1, whereas Figure 4.4b pertains to dataset 2.

Examining Figure 4.4a, it is evident that for a single fold of dataset 1, the highest sensitivity of 94.43% is attained in fold 2 with a batch size of 32, while the lowest sensitivity of 89.48% is observed in fold 10 with a batch size of 64. In the case of dataset 2, fold 7 with a batch size of 256 and fold 6 with a batch size of 256 yield the highest and lowest single-fold sensitivities, amounting to 99.62% and 96.58%, respectively. High sensitivity is a desirable trait, as it signifies the model's capability in detecting abnormalities.

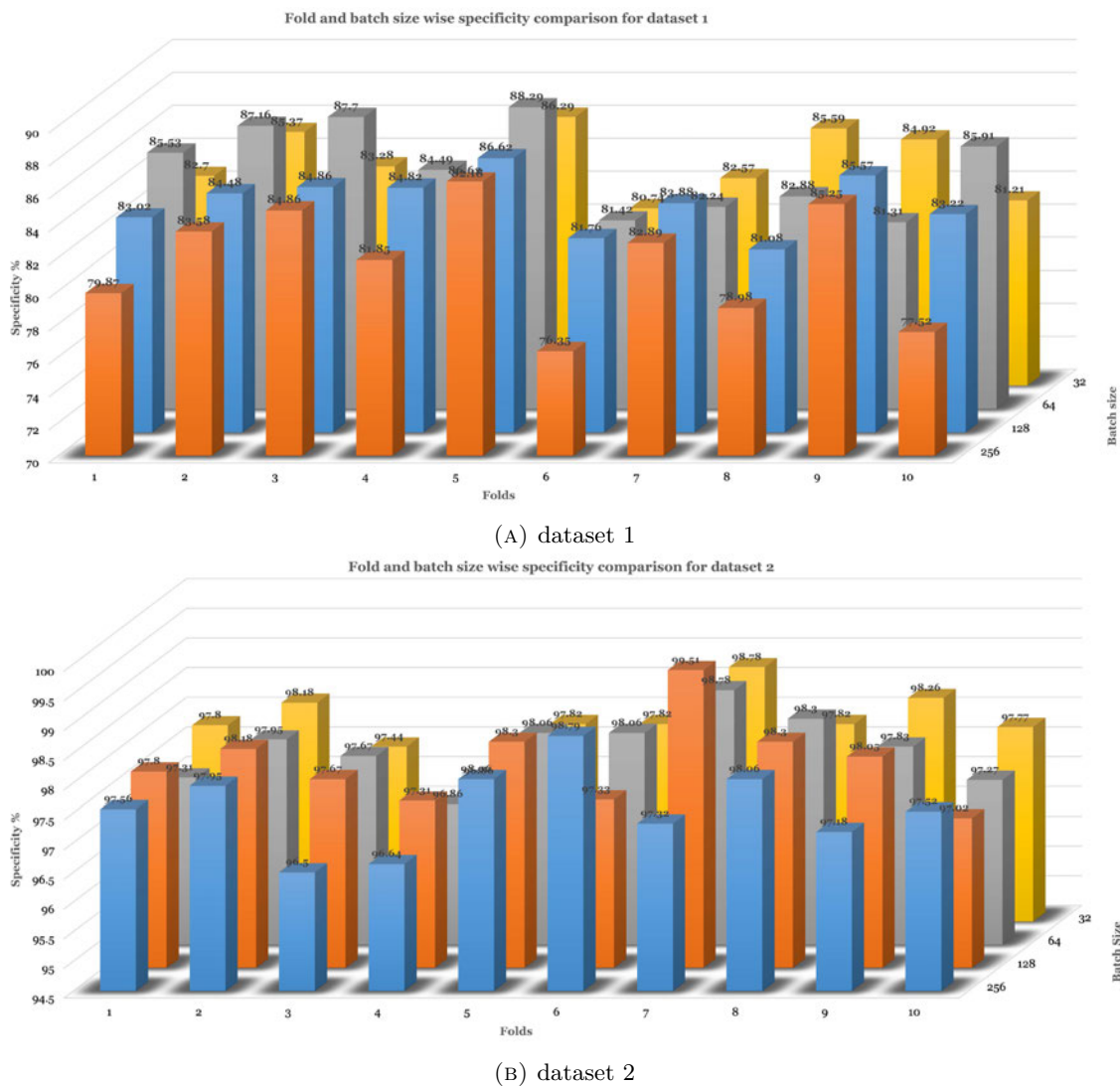
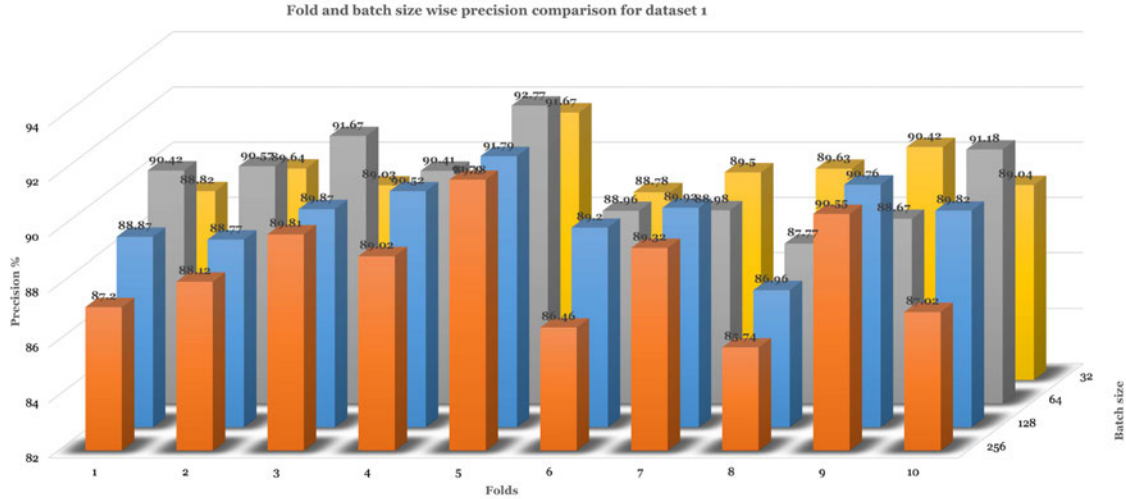


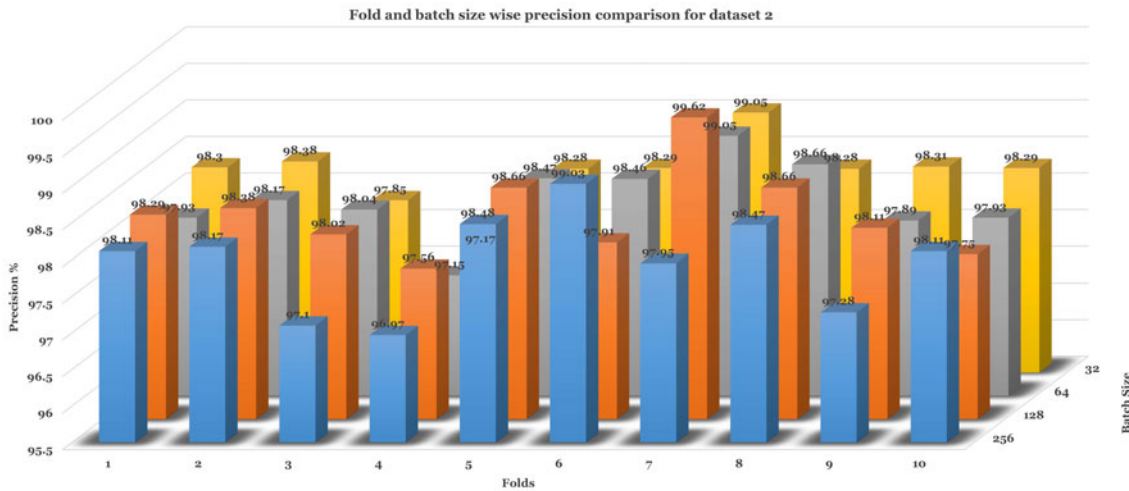
FIGURE 4.5: Fold-wise comparison of specificity value for different training batch sizes for the tested two datasets.

Figure 4.5 illustrates the specificity comparison, considering both fold and batch size, for dataset 1 (Figure 4.5a) and dataset 2 (Figure 4.5a). In the case of dataset 1, the highest and lowest specificity values are 88.29% (fold 5, batch size 64) and 76.35% (fold 6, batch size 256), respectively. As for dataset 2, these values are 99.62% (fold 7, batch size 128) and 96.5% (fold 3, batch size 256), respectively. When considering the mean

specificity over the 10-fold cross-validation, the highest value of  $84.69 \pm 2.49\%$  is observed with a batch size of 64, while the lowest value of  $81.78 \pm 3.30\%$  is associated with a batch size of 256, as displayed in Table 4.1. A higher specificity score implies that the model can effectively differentiate between healthy individuals and those with the disease.



(A) dataset 1



(B) dataset 2

FIGURE 4.6: Fold-wise comparison of precision value for different training batch sizes for the tested two datasets.

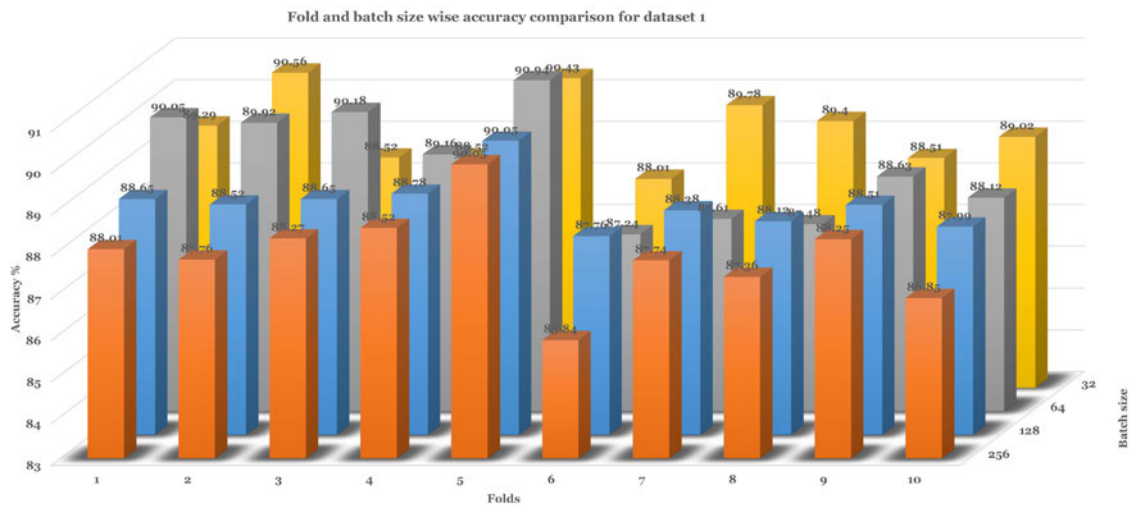
The next performance metric under consideration is precision, which signifies the percentage of relevant instances correctly retrieved. Figure 4.6 provides an overview of precision values, taking into account fold and batch size considerations. Specifically, Figure 4.6a and Figure 4.6b display precision results for datasets 1 and 2, respectively.

From Figure 4.6a, we can see, in dataset 1, the highest and lowest single-fold precision values are achieved in fold 5 ( $92.77\%$  for batch size 64) and fold 8 ( $85.74\%$  for batch size 256), respectively. For dataset 2 in Figure 4.6b, these values are attained in fold 7 ( $99.62\%$  for batch size 128) and fold 4 ( $96.97\%$  for batch size 256), respectively. Looking at the 10-fold average precision from Table 4.1, the highest value for dataset 1 is  $90.14 \pm 1.46\%$  with a batch size of 64, while the lowest is  $88.50 \pm 1.83\%$  with a batch size of 256. As

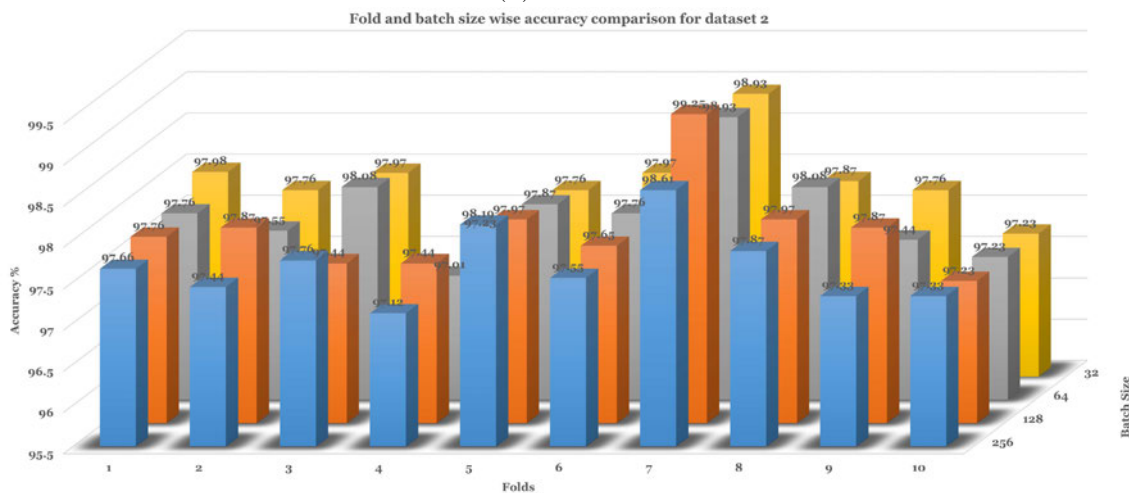
for dataset 2, the corresponding values are  $98.30 \pm 0.56\%$  (batch size 128, highest) and  $97.97 \pm 0.63\%$  (batch size 256, lowest).

We also thoroughly examined the accuracy parameter. As evident from Table 4.1, batch size 32 consistently yielded the highest accuracy for both tested datasets, resulting in values of  $89.20 \pm 0.81\%$  for dataset 1 and  $97.85 \pm 0.45\%$  for dataset 2. Figure 4.7a and Figure 4.7b present the detailed accuracy comparisons, considering fold and batch size, for dataset 1 and dataset 2, respectively.

For dataset 1, the highest single-fold accuracy, 90.94%, was achieved in fold 5 with a batch size of 64, while the lowest, 85.84%, was observed in fold 6 for a batch size of 256. In contrast, for dataset 2, the highest single-fold accuracy reached 99.25% in fold 7 with a batch size of 128, while the lowest accuracy value was 97.12% in fold 4 with a batch size of 256.



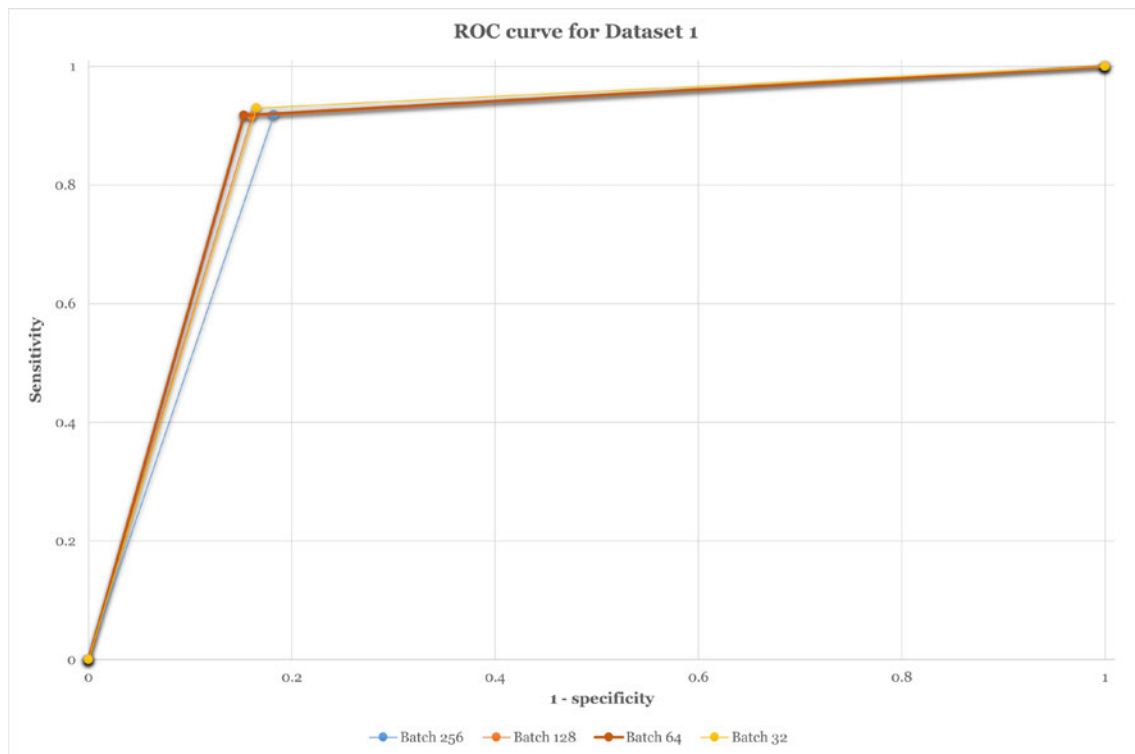
(A) dataset 1



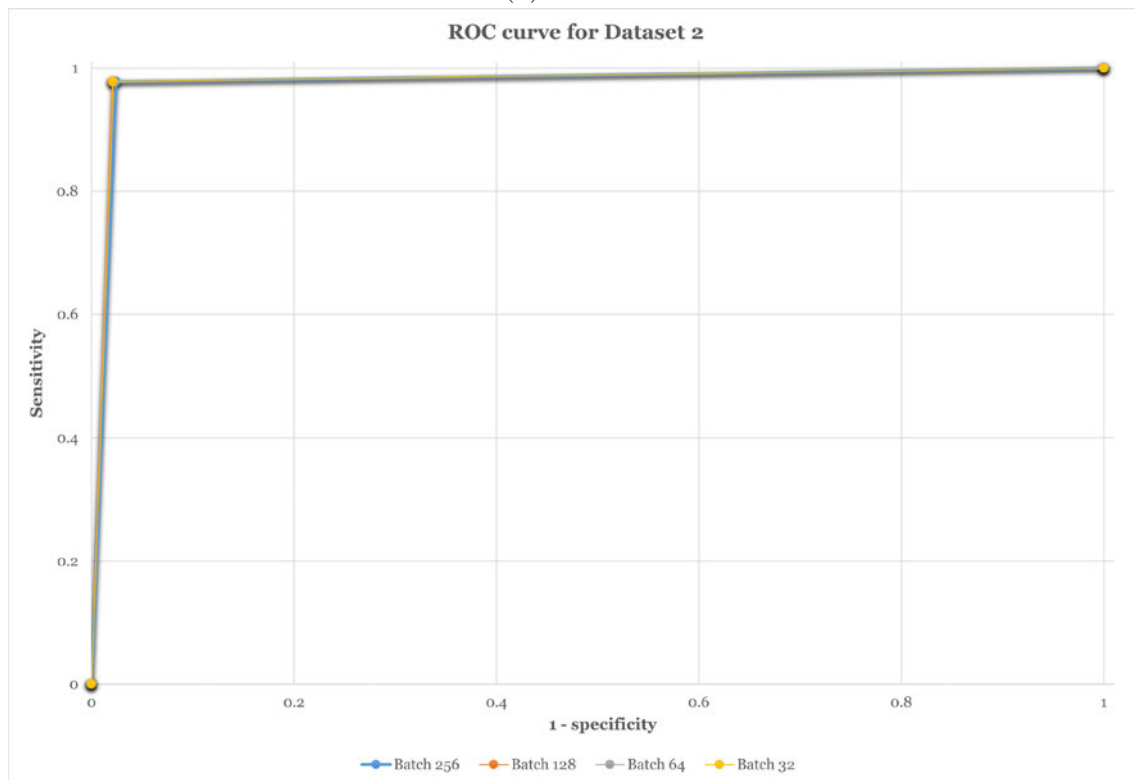
(B) dataset 2

FIGURE 4.7: Fold-wise comparison of accuracy value for different training batch sizes for the tested two datasets.

The ROC graph, which plots sensitivity (true positive rate) on the Y-axis against 1-specificity (false positive rate) on the X-axis, is a valuable tool for visualising the classifier's



(A) dataset 1



(B) dataset 2

FIGURE 4.8: ROC curve for different training batch sizes of two datasets.

performance. A good classifier tends to have a graph closer to the (0, 1) point. We generated ROC graphs for both datasets, employing different training batch sizes, to

assess the performance of the proposed model, as presented in Figure 4.8. Specifically, Figure 4.8a corresponds to dataset 1, while Figure 4.8b pertains to dataset 2.

In Figure 4.8a, we observe that the ROC curve for batch size 32 is slightly closer to the ( $y = 1$ ) line due to its higher sensitivity value. However, its (1-specificity) value (0.1652) is marginally higher than that of batch size 128 (0.1531). Generally, all tested batch sizes exhibit similar ROC curves, as their sensitivity and specificity values exhibit only minor differences, as shown in Figure 4.8a. Likewise, for dataset 2, batch size 32 yields the highest sensitivity, while batch size 128 achieves the highest specificity. Nevertheless, the differences are minimal, resulting in overlapping ROC curves for all batch sizes in dataset 2, as illustrated in Figure 4.8b.

To facilitate a comparison of our proposed model’s performance with existing works related to the datasets used in this study, we have provided a comparative table in Table 4.2. While our proposed model has not attained the highest accuracy among the tested datasets, it underscores the potential of utilising topographic image-based brain signal classification for such tasks. Moreover, this proposed method explores the combined features of time, frequency, and spatial domain in schizophrenia classification. We have also explored the performance of the framework on two well-known EEG datasets to check the generalisability of the proposed model. Furthermore, fine-tuning the CNN model and exploring transfer learning techniques using pre-trained CNN models can potentially enhance the accuracy of the classification process.

TABLE 4.2: Comparison of performance with previous research using the same datasets.

Datasets		Comparison for Classification Accuracy (%)				
<b>dataset 1</b>	Siuly <i>et al.</i> [154]	89.59%	Thilakvathi <i>et al.</i> [148]	88.50%	Proposed model	89.20%
<b>dataset 2</b>	Singh <i>et al.</i> [203]	98.96%	Shoeibi <i>et al.</i> [157]	99.25%	Proposed model	97.85%

## 4.5 Summary

In this research study, we have introduced a novel topographic image-based brain signal data mining framework employing deep learning techniques. Our proposed model was put to the test using well-established EEG brain signal data to perform classification tasks related to schizophrenia neurological disorder. The EEG signals underwent initial segmentation into small time segments, followed by the computation of entropy values using Shannon Entropy for each segment. Subsequently, these entropy values were employed to generate topographic plots corresponding to the signal segments.

We have introduced a CNN model to perform classification on those topographic images, distinguishing between two classes: patients and healthy individuals. The results of our proposed framework demonstrated promising performance, with accuracy rates of 89.20% and 97.85% achieved for dataset 1 and dataset 2, respectively.

Although the proposed model could not beat the existing studies in term of accuracy but have produced an accuracy very close to the existing best studies. The main contribution of this study is that we have explored the spatial domain of the EEG signal for SZ classification. In clinical settings, topographic maps can assist in identifying abnormal brain activity or patterns associated with various neurological disorders, helping in diagnosis and treatment planning. Moreover, we have used Shannon Entropy to produce the topographic images; other kind of entropy methods can be explored to produce the topographic images and check the performance of the categorisation task. Additionally, different CNN models and transfer learning can be explored to improve the performance of the proposed framework.

Chapters 3 and 4 present two of our proposed methods for addressing the first research question. In the next chapter, our third proposed method is presented that is proposed to address the second research question.

# OFFICE FOR RESEARCH TRAINING, QUALITY AND INTEGRITY

## DECLARATION OF CO-AUTHORSHIP AND CO-CONTRIBUTION: PAPERS INCORPORATED IN THESIS

*This declaration is to be completed for each conjointly authored publication and placed at the beginning of the thesis chapter in which the publication appears.*

### 1. PUBLICATION DETAILS (to be completed by the candidate)

Title of  
Paper/Journal/Book:

Data Mining Based Artificial Intelligent Technique for Identifying Abnormalities  
from Brain Signal Data.

International Conference on Web Information Systems Engineering, 2021

Surname: Tawhid

First name: Md Nurul Ahad

Institute: Institute for Sustainable Industries and Liveab

Candidate's Contribution (%): 70

Status:

Accepted and in press:

Date:

Published:

Date:

01/01/2022

### 2. CANDIDATE DECLARATION

I declare that the publication above meets the requirements to be included in the thesis as outlined in the HDR Policy and related Procedures – [policy.vu.edu.au](http://policy.vu.edu.au).

Md Nurul Ahad  
Tawhid

Digitally signed by Md Nurul Ahad  
Tawhid  
Date: 2023.09.08 12:54:06 +10'00'

08/09/2023

Signature

Date

### 3. CO-AUTHOR(S) DECLARATION

In the case of the above publication, the following authors contributed to the work as follows:

The undersigned certify that:

1. They meet criteria for authorship in that they have participated in the conception, execution or interpretation of at least that part of the publication in their field of expertise;
2. They take public responsibility for their part of the publication, except for the responsible author who accepts overall responsibility for the publication;



- 3. There are no other authors of the publication according to these criteria;
- 4. Potential conflicts of interest have been disclosed to a) granting bodies, b) the editor or publisher of journals or other publications, and c) the head of the responsible academic unit; and
- 5. The original data will be held for at least five years from the date indicated below and is stored at the following location(s):

Name(s) of Co-Author(s)	Contribution (%)	Nature of Contribution	Signature	Date
Siuly Siuly	15	Supervision, Formal analysis, Visualization, Manuscript preparation		08/09/23
Kate Wang	5	Supervision, Manuscript preparation		08/09/23
Hua Wang	10	Supervision, Manuscript preparation, Funding acquisition, Project		08/09/23

Updated: September 2019

# OFFICE FOR RESEARCH TRAINING, QUALITY AND INTEGRITY

## DECLARATION OF CO-AUTHORSHIP AND CO-CONTRIBUTION: PAPERS INCORPORATED IN THESIS

*This declaration is to be completed for each conjointly authored publication and placed at the beginning of the thesis chapter in which the publication appears.*

### 1. PUBLICATION DETAILS (to be completed by the candidate)

Title of  
Paper/Journal/Book:

Textural feature based intelligent approach for abnormality detection from  
brain signal data.

Plos one, 2022

Surname: Tawhid

First name: Md Nurul Ahad

Institute: Institute for Sustainable Industries and Liveab

Candidate's Contribution (%): 70

Status:

Accepted and in press:

Date:

Published:

Date:

14/11/2022

### 2. CANDIDATE DECLARATION

I declare that the publication above meets the requirements to be included in the thesis as outlined in the HDR Policy and related Procedures – [policy.vu.edu.au](http://policy.vu.edu.au).

Md Nurul Ahad  
Tawhid

Digitally signed by Md Nurul Ahad  
Tawhid  
Date: 2023.09.08 12:54:22 +10'00'

08/09/2023

Signature

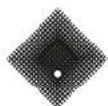
Date

### 3. CO-AUTHOR(S) DECLARATION

In the case of the above publication, the following authors contributed to the work as follows:

The undersigned certify that:

1. They meet criteria for authorship in that they have participated in the conception, execution or interpretation of at least that part of the publication in their field of expertise;
2. They take public responsibility for their part of the publication, except for the responsible author who accepts overall responsibility for the publication;



- 3. There are no other authors of the publication according to these criteria;
- 4. Potential conflicts of interest have been disclosed to a) granting bodies, b) the editor or publisher of journals or other publications, and c) the head of the responsible academic unit; and
- 5. The original data will be held for at least five years from the date indicated below and is stored at the following location(s):

Name(s) of Co-Author(s)	Contribution (%)	Nature of Contribution	Signature	Date
Siuly Siuly	15	Supervision, Formal analysis, Visualization, Manuscript preparation		08/09/23
Kate Wang	5	Supervision, Manuscript preparation		08/09/23
Hua Wang	10	Supervision, Manuscript preparation, Funding acquisition, Project		08/09/23

Updated: September 2019

# OFFICE FOR RESEARCH TRAINING, QUALITY AND INTEGRITY

## DECLARATION OF CO-AUTHORSHIP AND CO-CONTRIBUTION: PAPERS INCORPORATED IN THESIS

*This declaration is to be completed for each conjointly authored publication and placed at the beginning of the thesis chapter in which the publication appears.*

### 1. PUBLICATION DETAILS (to be completed by the candidate)

Title of  
Paper/Journal/Book:

Automatic and Efficient Framework for Identifying Multiple Neurological Disorders from EEG Signals.  
  
IEEE Transactions on Technology and Society, 2023

Surname: Tawhid

First name: Md Nurul Ahad

Institute: Institute for Sustainable Industries and Liveab

Candidate's Contribution (%): 70

Status:

Accepted and in press:

Date:

Published:

Date:

25/01/2023

### 2. CANDIDATE DECLARATION

I declare that the publication above meets the requirements to be included in the thesis as outlined in the HDR Policy and related Procedures – [policy.vu.edu.au](http://policy.vu.edu.au).

Md Nurul Ahad  
Tawhid

Digitally signed by Md Nurul Ahad  
Tawhid  
Date: 2023.09.08 12:55:11 +10'00'

08/09/2023

Signature

Date

### 3. CO-AUTHOR(S) DECLARATION

In the case of the above publication, the following authors contributed to the work as follows:

The undersigned certify that:

1. They meet criteria for authorship in that they have participated in the conception, execution or interpretation of at least that part of the publication in their field of expertise;
2. They take public responsibility for their part of the publication, except for the responsible author who accepts overall responsibility for the publication;



- 3. There are no other authors of the publication according to these criteria;
- 4. Potential conflicts of interest have been disclosed to a) granting bodies, b) the editor or publisher of journals or other publications, and c) the head of the responsible academic unit; and
- 5. The original data will be held for at least five years from the date indicated below and is stored at the following location(s):

Name(s) of Co-Author(s)	Contribution (%)	Nature of Contribution	Signature	Date
Siuly Siuly	15	Supervision, Formal analysis, Visualization, Manuscript preparation		08/09/23
Kate Wang	5	Supervision, Manuscript preparation		08/09/23
Hua Wang	10	Supervision, Manuscript preparation, Funding acquisition, Project		08/09/23

Updated: September 2019

## Chapter 5

# Multiple Disease Classification Using a Single Framework

In this chapter, we have presented our third proposed method to address the second research problem (**RP2**), which is to develop a single system for classifying multiple neurological disorders.

In this research, we have developed a multi-class classification framework for identifying four common neurological disorders – autism, epilepsy, Parkinson’s disease, and schizophrenia – using EEG data. Our approach combines both machine learning (ML) and deep learning (DL) classifiers. The process begins with the removal of noise and artefacts from the EEG signal through filtering techniques, followed by signal normalisation to enhance computational efficiency. Subsequently, the normalised signals are divided into small time segments, and spectrogram images are generated from these segments utilising the short-time Fourier transform.

In the ML-based classification component of our framework, we have employed two histogram-based textural feature extraction methods to compute features independently. Principal component analysis is then applied to select significant features from the extracted feature set. Finally, we have utilised four distinct ML-based classifiers to categorise these selected features into different disorder classes.

In the DL-based approach, we have developed a Convolutional Neural Network (CNN) specifically tailored for classifying the spectrogram images. To assess the performance of our proposed CNN model, we conducted a comparative analysis with two well-known CNN models: AlexNet and ResNet50. Furthermore, we evaluated the performance of our model in binary classification tasks, distinguishing between disorder and healthy states.

The ML-based classification method has been presented in the *International Conference on Web Information Systems Engineering* (Publication 3), and an extension of the work is published in *Plos One* (Publication 5). The DL-based method is published in *IEEE Transactions on Technology and Society* (Publication 6).

## 5.1 Introduction

Neurological disorders encompass a diverse group of conditions that affect both the central and peripheral nervous systems, spanning from neurodegenerative and neurodevelopmental disorders to psychiatric conditions [204]. This category encompasses a wide array of diseases, numbering over 600 in total. Among the most well-known neurological disorders are epilepsy (EP), Parkinson's disease (PD), mild cognitive impairment (MCI), Alzheimer's disease (AD), schizophrenia (SZ), cerebrovascular diseases, including stroke, as well as conditions like migraines and headache-related ailments, brain tumours, and developmental disorders such as autism spectrum disorder (ASD) and attention deficit hyperactivity disorder (ADHD) [204].

These disorders contribute significantly to the global disease burden, accounting for 10% of the overall burden and 30% of the non-fatal disease burden [3]. In Australia, they constitute over 20% of the total disease burden and incur a financial cost of \$74 billion in 2017 [205]. Conditions like depression and anxiety alone impose a substantial economic burden, costing the global economy approximately one trillion USD in lost productivity annually [3]. Neurological disorders have a profound impact on the lives of affected individuals and their families, and in severe cases, they can even lead to mortality. Early diagnosis and medical intervention can significantly improve clinical outcomes, but detecting these diseases in their early stages remains a challenge. Furthermore, access to mental health professionals is inadequate in many regions, with a shortage of such professionals in low-income countries and an overabundance in high-income countries [3].

Currently, the majority of diagnoses for brain disorders are made through manual assessments conducted by neurologists or trained clinicians. These assessments often involve techniques such as administering disease-related questionnaires, observing patient behaviour, or visually inspecting brain functionality captured through various methods like magnetic resonance imaging (MRI), functional magnetic resonance imaging (fMRI), positron emission tomography (PET), electrocorticography (ECoG), and electroencephalogram (EEG) [22], [162], [163]. Among these techniques, EEG is particularly favoured due to its exceptional temporal resolution, accessibility, non-invasiveness, cost-effectiveness, and widespread availability for clinicians [18].

EEG, is a technique employed to record the electrical activity generated by a large number of neurons within the human brain. It is commonly utilised for studying the physiological states of the brain. Typically, expert neurologists visually analyse a substantial amount of EEG signals to detect abnormalities. However, this process is time-consuming, subjective, complex, and prone to human error. Moreover, the intricate nature of EEG signals, including issues such as a poor signal-to-noise ratio, aperiodic patterns, and non-stationarity, coupled with overlapping disease-related features, makes visual diagnosis by neurologists even more challenging. This can sometimes lead to misdiagnosis [19].

To address these challenges, the development of computer-aided diagnostic (CAD) systems aimed at assisting clinicians in their decision-making has been a critical area of research. However, most existing studies have focused on developing individual CAD

systems for single disease classification, typically distinguishing between a specific neurological disorder and healthy controls (HC) [79], [98], [154], [162]. Furthermore, even within the realm of multi-class classification, most studies have considered at most two diseases. Consequently, diagnosing multiple neurological disorders in a single patient's EEG signal often necessitates the use of multiple CAD systems, which can be costly and time-consuming.

Hence, there is a compelling need for an effective, reliable, and high-accuracy CAD system capable of diagnosing multiple neurological diseases within a unified framework. Such a system could help address the shortage of expert neurologists and reduce the diagnostic costs associated with multiple diseases. CAD systems have significant potential in assisting medical professionals during the diagnosis process, particularly in terms of saving time and enhancing diagnostic accuracy. Therefore, the primary objective of this study is to design a novel framework capable of automatically detecting four neurological disorders – namely, ASD, EP, PD, and SZ – from EEG signal data.

It's worth noting that a significant portion of existing studies in the literature has primarily focused on single disease classifications using EEG data, typically distinguishing between a specific neurological disorder and HC subjects [78], [79], [98], [103], [127], [132], [154], [162], [169], [180], [184], [188], [197], [198], [206]–[209]. However, there is a growing interest in developing unified classification systems capable of categorising various neurological conditions from EEG signals.

Some studies have ventured into building single classification systems for distinguishing between multiple neurological disorders, often employing a 3-class classification approach among AD, MCI, and HC subjects. For instance, Akrofi *et al.* [210] developed an automated pattern recognition system based on coherence analysis for distinguishing between AD, MCI, and HC using EEG data, achieving an overall accuracy of 83.99% through techniques like k-means clustering and multiple discriminant analysis. McBride *et al.* [211] proposed an innovative approach involving Sugihara causality analysis, which yielded a high average accuracy rate of 96.5% for separating AD, MCI, and HC classes across three different recording protocols. Ieracitano *et al.* [212] introduced a novel method utilising continuous wavelet transform (CWT) and bispectrum (BiS) representation to distinguish between AD, MCI, and HC classes. They employed a multi-layer perceptron classifier to process the extracted CWT and BiS features and achieved an accuracy of 89.22% for the 3-way classification scheme. In a recent study, Burcu *et al.* [213] presented a methodology based on discrete wavelet transform (DWT), power spectral density (PSD), and coherence measures to classify AD, MCI, and HC EEG data. By using a bagged tree classifier and a 5-fold cross-validation scheme, they achieved an average accuracy of 96.5%.

In addition to the classification of AD, MCI, and HC classes, there have been notable efforts to develop frameworks for distinguishing between other neurological disorders such as ASD and EP from HC subjects.

Ibrahim *et al.* [214] introduced a framework for the classification of ASD and EP against HC. They employed a pre-processing step to decompose the EEG signal into

sub-bands using discrete wavelet transform (DWT) and extracted relevant features, including standard deviation (SD), band power (BP), Shannon entropy (ShanEn), and the largest Lyapunov exponent. These features were subsequently classified using various machine learning algorithms, including artificial neural networks (ANN),  $k$ -nearest neighbour ( $k$ -NN), support vector machines (SVM), and linear discriminant analysis (LDA). Their approach achieved an accuracy of 94.62% for the 3-class classification task using the  $k$ -NN classifier. Alturki *et al.* [105] pursued a similar three-class classification task, distinguishing between ASD, EP, and HC. They used DWT to decompose the EEG signals and extracted features such as logarithmic band power (LBP), SD, variance, kurtosis, and Shannon entropy (ShanEn). Their approach achieved an overall classification accuracy of 99.9% using SVM and 97% using ANN for both single-channel and multi-channel modes.

While these existing studies have demonstrated good classification performance, there remains room for improvement in terms of accuracy, performance, and the number of disease categories considered. Notably, these studies show that it is feasible to develop a unified framework for multi-class EEG classification. However, to the best of our knowledge, no studies have considered more than two disease classifications from healthy subjects within a single framework. Moreover, the development of a single system for diagnosing multiple neurological disorders can help address the shortage of expert clinicians and reduce the cost associated with using multiple CAD systems for diagnosing different diseases. Therefore, there is a substantial research opportunity for the development of a comprehensive CAD system for diagnosing multiple neurological disorders from EEG data.

In the context of existing studies, the data mining process typically involves two primary stages: feature extraction from the signal data and subsequent classification of these extracted features using various classifiers. Many of these studies have traditionally relied on utilising statistical information as features derived from the signal data, and subsequently, these features are subjected to classification using diverse classifiers. However, when dealing with extensive datasets, these conventional approaches often face limitations in effectively extracting meaningful and distinguishing features from EEG data, as noted in the literature [90]. Furthermore, the extraction of statistical features from extended recordings (long-term data) may inadvertently neglect short-term variations in signal characteristics that are pivotal for identifying anomalies [90].

To overcome these challenges, a novel approach has been introduced in recent studies. This approach involves the visual representation of small segments of the signal, using the raw signal data to create visual depictions, and focusing on the analysis of these compact data segments [79], [90]. By adopting this method, researchers aim to address the limitations associated with conventional techniques and obtain a more comprehensive view of the EEG data, particularly when dealing with high volumes or when short-term variations are of significance, such as in anomaly detection tasks.

To achieve the aforementioned objective, we have introduced a data mining approach based on time-frequency (T-F) spectrogram images, specifically designed for analysing

brain signal data, particularly EEG recordings, to identify four distinct neurological disorders: autism spectrum disorder, epilepsy, Parkinson’s disease, and schizophrenia, in addition to healthy control subjects, resulting in a total of five classes. Spectrogram images serve as the basis for visualising EEG signals in the T-F domain, effectively capturing the nonstationary characteristics inherent in the signal data [79]. These spectrogram images portray changes in the frequency spectrum over time, with varying colours representing different energy levels [90]. In comparison to alternative feature extraction methods, spectrogram images possess the advantage of encompassing more unexplored EEG signal characteristics, potentially yielding improved performance when integrated into a classification algorithm [90]. Previous research has successfully employed spectrogram images for the discrimination of patients from HC across various neurological disorders, including epilepsy [19], epileptic seizures [169], ASD [90], and schizophrenia [153], consistently achieving strong classification outcomes. These promising results have motivated the incorporation of spectrogram images in our current study.

In this research, we have harnessed these spectrogram images and employed both machine learning and deep learning techniques for feature extraction and classification to tackle a multi-class classification task. In both classification pipelines, the EEG data underwent pre-processing to eliminate noise and artefacts. Subsequently, the signals were partitioned into smaller time intervals, and spectrogram images were constructed from those segments using STFT.

In the ML-based approach, we have extracted histogram-based textural features from these images using two techniques known as completed CENSus TRAnform hISTogram (cCENTRIST) and ternary CENSus TRAnform hISTogram (tCENTRIST). These histogram-based methods were originally proposed by Dey *et al.* [171] and have exhibited strong performance in texture classification tasks. To reduce the dimensionality of the extracted features, principal component analysis (PCA) was applied. Finally, we employed four ML-based classifiers: SVM,  $k$ -NN, RF, and LDA to categorise the reduced feature set.

On the contrary, in the DL-based classification approach, we adopted the CNN model. CNNs have gained popularity in image-related classification tasks due to their exceptional ability to autonomously learn relevant features and effectively classify data into various categories [175]. In this research, we have introduced a CNN model for the multi-class classification of neurological disorders, utilising T-F-based spectrogram images. To ensure unbiased results and assess the effectiveness of our proposed system, we have employed a five-fold cross-validation strategy. Furthermore, we have compared the performance of our proposed model with two other well-known CNN architectures, namely AlexNet and ResNet50. Additionally, we have assessed the proposed model’s binary classification capabilities using the four datasets included in this study and compared its performance with state-of-the-art literature that utilises the same EEG datasets.

Following are the significant contributions of this study:

1. For the first time, a single, unified framework is designed to classify four neurological abnormalities from brain signal data.

2. Two distinct feature extractors in combination with four different ML-based classifiers are examined in ML-based classification.
3. Design and validate a new efficient and automatic CNN-based framework for both multi- and binary-class neurological disease classification.
4. Explore the performance of the proposed CNN model with other popular CNN models and obtain better performance for multi-class classification. Also, improve the binary classification accuracy compared to existing methods.
5. Build a low-time-cost CNN model for spectrogram image classification.
6. Validate the proposed framework using four EEG signal datasets from four different neurological abnormalities.
7. Obtain improved performance for the multi-disease classification process compared to the existing methods.

The remainder of the chapter contains a detailed discussion of the proposed method and the obtained results.

## 5.2 Methodology

This section contains a detailed discussion of the proposed multi-disease classification framework using both ML and DL-based approaches. Section 5.2.1 contains the discussion of the ML-based classification framework, and Section 5.2.2 contains the discussion of the DL-based classification framework.

### 5.2.1 Workflow of the proposed machine learning based framework

In this research, we have adopted T-F-based spectrogram images for the classification of brain signal data using cCENTRIST and tCENTRIST-based feature extraction techniques with four distinct ML-based classification approaches. The workflow encompassed multiple stages: First, the raw brain signal data underwent initial processing to eliminate artefacts. Then the signals are partitioned into small time frames, and spectrogram images were derived using STFT. After that, we have applied cCENTRIST and tCENTRIST-based techniques to extract relevant features from the spectrogram images, and PCA was employed to reduce the dimensionality of the extracted features. Finally, four different classifiers, namely:  $k$ NN, SVM, RF, and LDA, are employed to categorise the spectrogram images into their respective classes. For a comprehensive understanding of this methodology, Figure 5.1 provides a visual overview of these steps. Further details are elaborated in the subsequent sections.

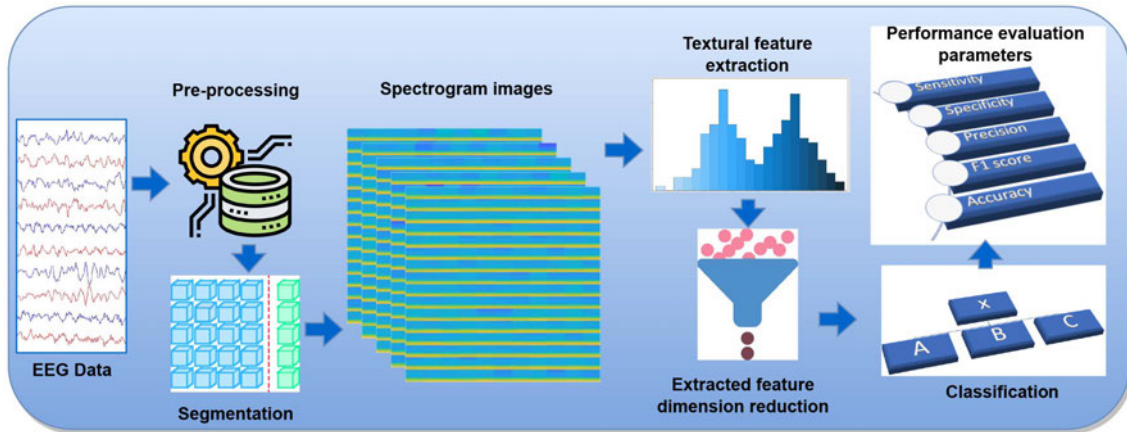


FIGURE 5.1: Schematic diagram of the proposed ML-based categorisation framework.

### 5.2.1.1 EEG data acquisition

In this study, we have used four different datasets of four neurological disorders, namely: ASD, EP, PD, and SZ. These datasets are discussed in detail below:

#### 5.2.1.1.1 Autism spectrum disorder dataset

The ASD dataset employed in this study was obtained from King Abdulaziz University (KAU) Hospital, located in Jeddah, Saudi Arabia [177]. This dataset comprises twelve individuals diagnosed with ASD, consisting of 3 girls and 9 boys, with an average age of  $12.5 \pm 4.84$  years. Additionally, four control group subjects, all boys, were included in the dataset, with an average age of  $11 \pm 1.83$  years and no history of neurological disorders. The EEG data for this study was recorded in a resting state using the international 10–20 systems, encompassing 16 channels. The details of the recording process can be found in [177]. During the recording phase, the EEG data underwent filtering procedures, which included a band-pass filter with a passband of 0.1–60 Hz and a notch filter centred at 60 Hz to eliminate unwanted noise. Subsequently, all EEG signals were digitised at a sampling rate of 256 Hz.

#### 5.2.1.1.2 Epilepsy dataset

The epilepsy dataset used in this study was gathered at Universidade Federal do Para, Brazil, as documented in [215]. This dataset encompasses resting-state EEG signals obtained from 14 subjects. Among these participants, 7 were patients diagnosed with epilepsy, comprising 3 females and 4 males, with average ages of  $24 \pm 7$  and  $39.5 \pm 6.4$  years, respectively. Additionally, there were 7 healthy control subjects, matched for both sex and age with the patient group. The resting-state EEG data was recorded using 20 channels at a sampling rate of 256 Hz.

### 5.2.1.1.3 Parkinson’s disease dataset

For this study, a publicly accessible dataset was obtained from the University of Iowa, Iowa City, Iowa, United States, as described in [197]. This dataset includes data from 14 patients with Parkinson’s disease (PD), consisting of 8 females and 6 males, with average ages of  $72.33 \pm 7.53$  and  $69.13 \pm 9.69$  years, respectively. Additionally, there were 14 control subjects who were matched with the patient group in terms of age and gender. The resting-state EEG data in this dataset was recorded using 64 channels and had a sampling rate of 500 Hz. The Brain Vision system with Pz as the baseline reference channel was employed for the recording process. Further details regarding the data acquisition procedure can be found in [197].

### 5.2.1.1.4 Schizophrenia dataset

The dataset used in this study consists of 28 subjects in total. This group comprises 14 patients, including 7 females and 7 males, with an average age of  $28.3 \pm 4.1$  years for females and  $27.9 \pm 3.3$  years for males. These patients were hospitalised at the Institute of Psychiatry and Neurology in Warsaw, Poland, and were diagnosed with paranoid schizophrenia. Additionally, there are 14 healthy control subjects, also within the same age group and with a similar gender proportion, from the same institute [78]. The EEG data was recorded during a resting state, and each recording spanned 15 minutes. The data was sampled at a rate of 250 Hz and collected from 19 channels following the international standard 10–20 EEG montage.

For a summarised view of the participants’ demographic information across different datasets, please refer to Table 5.1. Figure 5.2 provides an illustrative representation of EEG signals from channel Fp1 for the four neurological disorders under investigation.

TABLE 5.1: Demographic information pertaining to the datasets in use.

Disease	Patient (M/F)	Normal (M/F)	Frequency	Channels
<b>ASD</b>	12 (9/3)	4 (4/0)	256	16
<b>EP</b>	7 (4/3)	7 (4/3)	256	20
<b>PD</b>	14 (6/8)	14 (6/8)	500	64
<b>SZ</b>	14 (7/7)	14 (7/7)	250	19
<b>Total</b>	47 (28/19)	39 (23/16)		

### 5.2.1.2 Data pre-processing and artefact removal

In this research, the pre-processing of the raw EEG data consists of two primary steps: dataset standardisation, aimed at aligning all datasets to a common standard for comparability, followed by filtering to eliminate noise and unwanted signals. Further details of these procedures are elaborated upon in the subsequent sections.

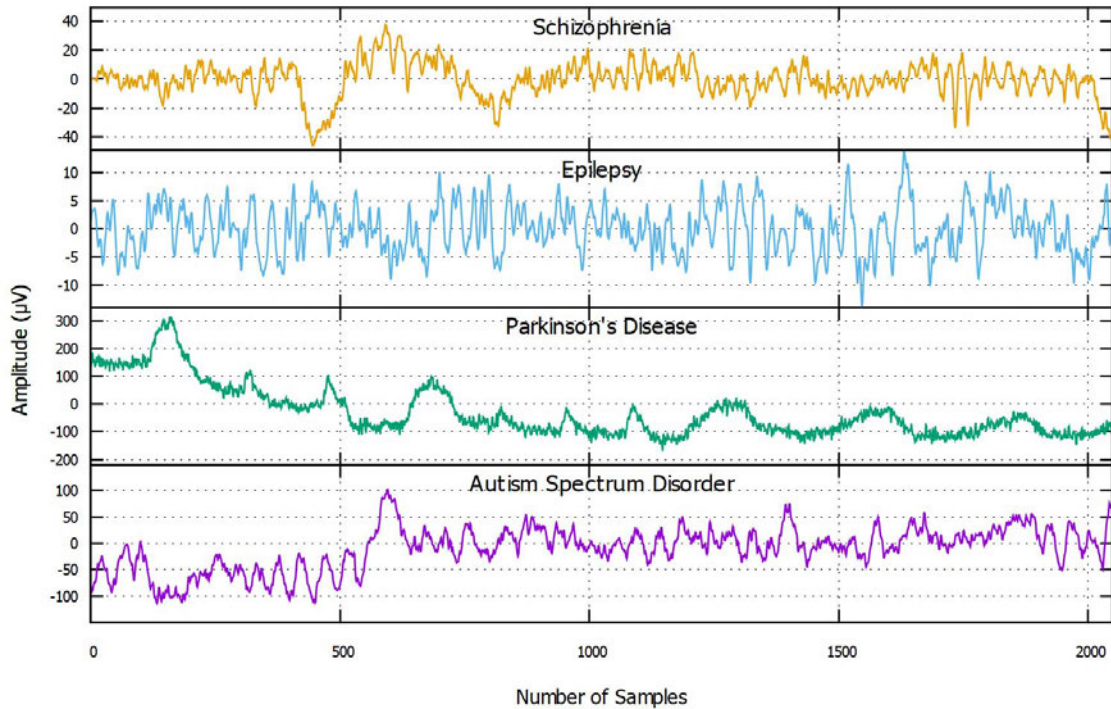


FIGURE 5.2: A typical 2000 sample EEG signal data points from the Fp1 channel of the four evaluated datasets.

#### 5.2.1.2.1 Resampling of datasets for standardisation purposes

To enable a fair comparison of data recorded under different conditions, it is essential to standardise them. As depicted in Table 5.1, all four datasets used in this study are collected with varying sampling frequencies and different numbers of recording channels, making it necessary to bring them to a common standard for accurate comparisons. To achieve this, we selected the ASD dataset, which has 16 channels, as the reference. We then adjusted the other three datasets (EP, PD, and SZ) to match this standard. For consistency, we utilised the standard 16 channels (Fp1, Fp2, F3, F4, F7, F8, C3, C4, T3, T4, P3, P4, T5, T6, O1, O2) typically employed for 16-channel EEG data recordings. Subsequently, we resampled the PD and SZ datasets to 256 Hz, aligning all the datasets with a common sampling frequency of 256 Hz.

#### 5.2.1.2.2 Filtering of data for artefact removal

EEG data are known for their nonlinear, non-stationary, and complex characteristics, often contaminated with various artefacts. These artefacts can significantly impact the diagnosis process, particularly because some artefacts may resemble neurological disorder patterns, potentially leading to biased clinical interpretations [216].

In this study, after aligning all datasets to a common configuration, the next crucial step involves the removal of artefacts from the raw EEG data. To achieve this, three pre-processing techniques have been applied: Common Average Referencing (CAR), Infinite Impulse Response (IIR) filtering, and normalisation.

- **Common Average Referencing (CAR):** CAR is a straightforward re-referencing technique that computes the average of all electrode recordings and uses it as a reference. This reference signal primarily captures the components common to all electrodes, leaving behind the isolated signal from each electrode, which represents individual channel activity.
- **Infinite Impulse Response (IIR) Filtering:** Following CAR, the signal undergoes low-pass IIR filtering with a cut-off frequency set at 40 Hz. This step effectively eliminates artefacts arising from muscle activity, ocular movements, and external noise sources, which often introduce higher-frequency signals.
- **Normalisation:** Normalisation is employed to mitigate variations in individual signal characteristics attributable to fundamental frequency rhythms and reduce computational complexity. In this study, the Zero Mean Unit Variance (ZMUV) method is utilised to normalise signals from each channel. This normalisation approach transforms the signal distribution to have a mean of zero and a variance of one, a widely accepted technique in CNN-based image classification processes [90].

#### 5.2.1.2.3 Segmenting EEG signals

The datasets used in this study have a relatively small number of samples, especially for deep learning-based classification tasks. Addressing this data scarcity challenge, a common strategy employed in previous works is to segment the available data into smaller, informative segments [79], [153]. This segmentation approach has been utilised in various studies to effectively increase the dataset's sample size, maintaining the original data's labels and facilitating more robust analysis.

Given the aperiodic and non-stationary nature of EEG signals, as well as their varying signal magnitudes over time, the pre-processed EEG data from each participant is segmented into three-second (3s) data segments. This segmentation strategy aims to capture representative information from specific time intervals [98]. Consequently, each segmented data segment becomes a 2D vector with dimensions of  $16 \times 768$ , where 16 represents the number of EEG channels, 768 corresponds to 256 samples per second multiplied by 3 seconds, providing a structured format for subsequent analysis and classification.

#### 5.2.1.3 Generation of spectrogram image

This step involves the transformation of pre-processed signal data into spectrogram images. Following the segmentation, spectrogram images are generated from these small segments using the STFT-based spectrogram plotting technique. Spectrograms are a widely used method for analysing the time-frequency domain of EEG signal data. The STFT process converts the time-varying EEG signal into a two-dimensional matrix with time and frequency axes.

To calculate the STFT, the signal is initially divided into overlapping windowed blocks [217]. A Hamming window approach is applied to ensure continuity between the first and

last points in the frames and to mitigate the leakage effect on the spectrum. Subsequently, the Fourier transform (FT) is computed for each segment, resulting in its own local frequency spectrum. The STFT of a signal  $x(t)$  can be calculated using the following equation 5.1:

$$STFT\{x(t)\} = X(\tau, \omega) = \int_{-\infty}^{\infty} x(t)w(t - \tau)e^{-i\omega t} dt \quad (5.1)$$

Here,  $\omega$  is the signal frequency,  $w(\tau)$  is the nonzero window function, and  $X(\tau, \omega)$  is the FT of the product  $x(t)w(t - \tau)$ , reflecting the signal's phase and amplitude with time and frequency. STFT is frequently visualised by its spectrogram, which is an intensity representation of STFT magnitude over time. These images are further used for feature extraction and classification in this study.

#### 5.2.1.4 Feature extraction and dimension reduction

In this phase, features are extracted from the spectrogram images and then reduced in dimensionality for the subsequent classification tasks. The feature extraction process employs two texture-based feature extractors: the completed CENSus TRanform hISTogram (cCENTRIST) and the ternary CENSus TRanform hISTogram (tCENTRIST). These feature extraction methods were introduced by Dey *et al.* [171] and have demonstrated their effectiveness in tasks such as garment texture classification and face image-based gender identification [171], [173].

To provide a brief overview of these feature extractors, let's delve into CENTRIST, cCENTRIST, and tCENTRIST in the following sections:

##### 5.2.1.4.1 CENSus TRanform hISTogram (CENTRIST)

CENTRIST is a non-parametric local transform approach built on the idea of Census Transform (CT) [218], which maps a pixel by comparing intensity values with its eight neighbouring pixels and generates an eight-bit string (CT values). This approach is similar to LBP except that LBP performs interpolation for corner pixels, but CENTRIST considers those pixels as is. A sample CT calculation process is given in Figure 5.3.

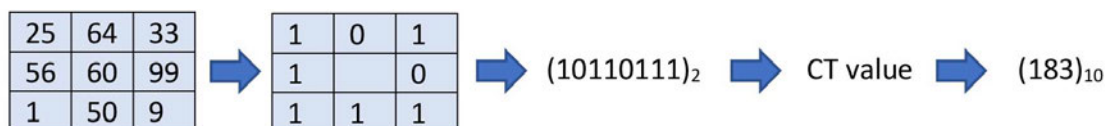


FIGURE 5.3: CENTRIST applies the Census Transform (CT) calculating method. If the centre pixel is greater than (or equal to) one of its neighbours, a bit 1 is set in the appropriate location. Bit 0 is set if it is not.

CENTRIST is designed to capture both local and global information within an image. It does so by constructing a histogram using the CT values of various image patches. Additionally, CENTRIST integrates spatial information based on the Spatial Pyramid

Matching (SPM) approach. SPM involves dividing an image into smaller regions and then aggregating the matching results within those regions to improve recognition accuracy. To further streamline the feature set, PCA is applied to reduce the dimensionality of the extracted CENTRIST features.

#### 5.2.1.4.2 Completed CENTRIST (cCENTRIST)

In this texture extractor, called cCENTRIST, the authors have replaced the traditional Local Binary Pattern (LBP) with a Census Transform-based approach (CLBP) for generating CT (Census Transform) values. When comparing a pixel to its neighbouring pixels, cCENTRIST considers both the magnitude (CLBP\_M) and the signs (CLBP\_S) of the differences. Furthermore, it employs global thresholding to produce a binary code (CLBP\_C) for the center pixel. cCENTRIST generates a uniform and rotation-invariant CT code by incorporating information from the signs, magnitudes, and centre-pixel characteristics of the neighbouring pixels.

For an image of size  $3 \times 3$ , differences ( $d_p$ ) have two different components calculated from the differences between each neighbouring pixel and the central pixel using equation 5.2, where  $s_p$  and  $m_p$  are the sign and magnitude parts of the differences  $d_p$ .

$$d_p = S_P \times m_p \quad \text{and} \quad \begin{cases} S_P = \text{sign}(d_p), [1 \text{ if } d_P \geq 0, \text{ else } -1] \\ m_p = |d_p| \end{cases} \quad (5.2)$$

If  $P$  and  $R$  are the neighbour number and radius of LBP code, respectively, then  $CLBP\_S_{P,R}$ ,  $CLBP\_M_{P,R}$  and  $CLBP\_C_{P,R}$  are calculated using the equations 5.3 - 5.5 as follows:

$$CLBP\_C_{P,R} = t(g_c, c), t(x, c) = \begin{cases} 1, & x \geq c \\ 0, & x < c \end{cases} \quad (5.3)$$

$$CLBP\_S_{P,R} = \sum_{p=0}^{P-1} s(g_p - g_c) 2^p, s(x) = \begin{cases} 1, & x \geq 0 \\ 0, & x < 0 \end{cases} \quad (5.4)$$

$$CLBP\_M_{P,R} = \sum_{p=0}^{P-1} t(m_p, c) 2^p, t(x, c) = \begin{cases} 1, & x \geq c \\ 0, & x < c \end{cases} \quad (5.5)$$

Here  $c$  is a threshold calculated as the average of the whole image,  $g_c$  is the grey value of the centre pixel, and  $g_p (p = 0, 1, \dots, P - 1)$  is the neighbouring pixel's grey value on a circle with radius  $R$ . Finally, a 3D histogram is generated as a CT value using  $CLBP\_S_{P,R}$ ,  $CLBP\_M_{P,R}$  and  $CLBP\_C_{P,R}$  and PCA is applied to reduce the dimension of the feature vector. Algorithm 1 describes the process of cCENTRIST.

#### 5.2.1.4.3 Ternary CENTRIST (tCENTRIST)

In this texture extractor, known as tCENTRIST, the authors replaced the conventional Local Binary Pattern (LBP) with a Local Ternary Pattern (LTP) within the CENTRIST

---

**Algorithm 1:** Feature extraction and dimension reduction using cCENTRIST and PCA

---

**Input:** Spectrogram image  $I$

**Output:** Dimension reduced feature vector of  $I$

- 1 Initialisation;
  - 2 Calculate level 2 Spatial Pyramid (SP) for the image  $I$
  - 3 **for** each block of SP **do**
  - 4     (a) Calculate  $CLBP_{C_{P,R}}$ ,  $CLBP_{S_{P,R}}$  and  $CLBP_{M_{P,R}}$  using equations 5.3, 5.4 and 5.5, respectively
  - 5     (b) Concatenate all histograms from each to form a single histogram feature block
  - 6 Apply PCA to extract M feature points from the extracted features
- 

framework. This modification introduces an additional bit to handle fluctuations in intensity. For a 3x3 image window, tCENTRIST generates a ternary code for each central pixel (c) using the following equation 5.6:

$$LTP_{P,R} = \sum_{p=0}^{P-1} q(g_p - g_c)3^p, q(a) = \begin{cases} 1 & \text{if } a \geq \mu \\ -1 & \text{if } a < \mu \\ 0 & \text{otherwise} \end{cases} \quad (5.6)$$

where,  $\mu$  is a threshold value of  $\pm 5$  and  $g_p$ ,  $g_c$ ,  $P$ , and  $R$  are defined in equation 5.3-5.5. After calculating the LTP values, two histograms are generated using the upper and lower codes of LTP and finally concatenated to build a single histogram. Afterwards, PCA is applied to reduce the dimension of the feature vector. Algorithm 2 describes the process of tCENTRIST.

---

**Algorithm 2:** Feature extraction and dimension reduction using tCENTRIST and PCA

---

**Input:** Spectrogram image  $I$

**Output:** Dimension reduced feature vector of  $I$

- 1 Initialisation;
  - 2 Calculate level 2 Spatial Pyramid (SP) for the image  $I$
  - 3 **for** each block of SP **do**
  - 4     (a) Calculate  $LTP$  value using equation 5.6.
  - 5     (b) Construct a histogram using the LTP value;
  - 6 Concatenate all histograms from each to form a single histogram feature block
  - 7 Apply PCA to extract M feature points from the extracted features
- 

Both the cCENTRIST and tCENTRIST feature extractors incorporate a spatial pyramid (SP) structure that divides the images into a pyramid-like hierarchy of blocks. This SP structure allows them to capture both local and global information from the images. After feature extraction, PCA is employed to reduce the dimensionality of the extracted features. PCA helps in selecting the most informative features while reducing computational complexity. Finally, the reduced features are fed into four machine learning-based

classifiers for classification into different classes. These classifiers are an integral part of the classification process, aiding in distinguishing between neurological disorders based on the extracted features.

### 5.2.1.5 Classification of the extracted features

In this classification step, the features extracted in the previous step using cCENTRIST and tCENTRIST feature extractors are utilised. The classification process employs four different machine learning-based classifiers: SVM,  $k$ NN, RF, and LDA.

- **Support Vector Machine (SVM):** Currently, SVM is a highly effective classifier for detecting abnormalities in brain signal data. It is particularly adept at handling high-dimensional and non-linear data. In this study, we used the same multi-class LibSVM [174] as the authors of cCENTRIST and tCENTRIST [171] used, which is SVM with the following linear kernel function,  $K(x, y)$ :

$$K(x, y) = x^T y \quad (5.7)$$

Here, kernel function is constructed from the dot product of two invariant,  $x$  and  $y$ .

- **$k$ -Nearest Neighbour ( $k$ NN):** Another classifier tested in this study is  $k$ NN, known for its simplicity and robustness, especially when dealing with large-scale datasets. It classifies data points based on the most frequent class among their closest neighbours in the feature space [219]. In  $k$ NN based classification, we have tested for 10 different  $k$  values (1 to 10) with Euclidean distance metrics as defined as follows:

$$D(x_y, s) = \sqrt{\sum_{i=1}^n (s_i - x_y)^2} \quad (5.8)$$

Here,  $s$  denotes the training set, and  $y$  is the unknown test data.

- **Random Forest (RF):** Another classifier evaluated in this study is Random Forest (RF), an ensemble learning method proposed by Leo Breiman [220]. RF comprises multiple decision trees, and the final prediction is based on a majority vote from these trees. In this study, entropy is employed as an impurity metric for constructing the RF model, which is defined as follows:

$$Entropy, I_E = - \sum_{i=1}^n p_i \log_2 p_i \quad (5.9)$$

Here,  $p_i$  refers to the probability of class  $c_i$  in the data sample.

- **Linear Discriminant Analysis (LDA):** The fourth and final classifier we have used is LDA, which performed well in many classification tasks like emotional speech recognition, multimedia information retrieval, face recognition, image identification,

etc. [221]. For each class  $c$  with a mean  $\mu_c$  and covariance  $\Sigma$ , LDA is calculated as follows:

$$y_c = x^T \Sigma^{-1} \mu_c - \frac{1}{2} \mu_c^T \Sigma^{-1} \mu_c + \log \frac{n_c}{n} \quad (5.10)$$

where  $x$  is the test instance,  $n_c$  and  $n$  are the number of instances in class  $c$  and in the whole dataset, respectively.  $x$  is classified with the highest  $y_c$  values.

These classifiers are applied to the spectrogram images to perform multi-class classification, distinguishing between different neurological disorders. The performance of these classifiers is assessed using various evaluation techniques.

### 5.2.2 Workflow of the proposed deep learning based framework

In this approach, the data collection and spectrogram image generation process are the same as in the ML-based approach. However, we introduce a novel CNN model for classification. Figure 5.4 provides an overview of the process. The EEG data acquisition, filtering, and segmentation processes remain consistent with the ML-based framework. The subsequent steps of this framework are discussed in detail in the following subsections:

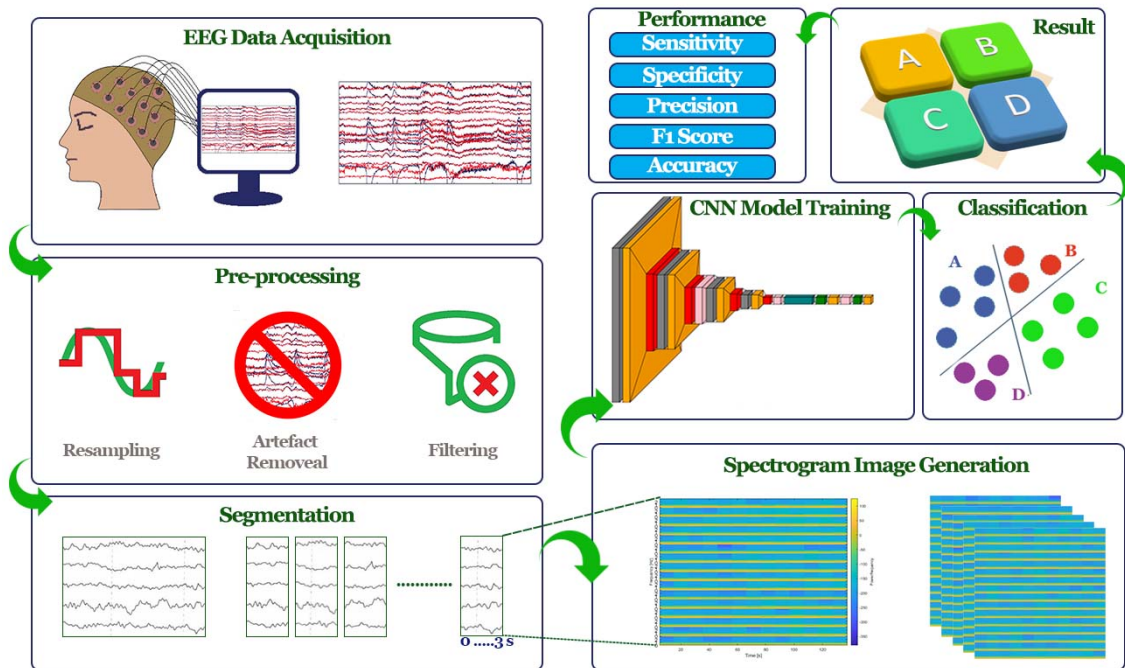


FIGURE 5.4: An outline of the proposed DL-based multi-disease categorisation system.

#### 5.2.2.1 CNN model training for feature extraction

CNN, a popular DL-based classification model for image-related problems, has demonstrated remarkable efficiency in automatically learning relevant features and categorising data into different classes [175]. CNNs are generally less sensitive to noise and capable of

extracting valuable information from noisy data [222]. In this study, we have designed a CNN model for classifying the spectrogram images generated from EEG data. The specific details of the proposed CNN model are outlined below:

The proposed CNN model comprises four convolutional layers, each followed by max-pooling, and a fully connected layer. All convolutional layers consist of 32 filters with a kernel size of  $3 \times 3$  and a stride of 1 pixel, followed by a max-pooling layer with a pool size of  $2 \times 2$ . The second and fourth convolutional layers incorporate dropout layers with a 25% dropout rate. The fully connected layer consists of 256 neurons, followed by a 50% dropout layer. The classification layer employs softmax as the activation function, while relu is used as the activation function in the other five layers. A schematic representation of the proposed model is provided in Figure 5.5. Training of the proposed model involves using categorical cross-entropy as the loss function, the Adam optimiser, and softmax as the classifier.

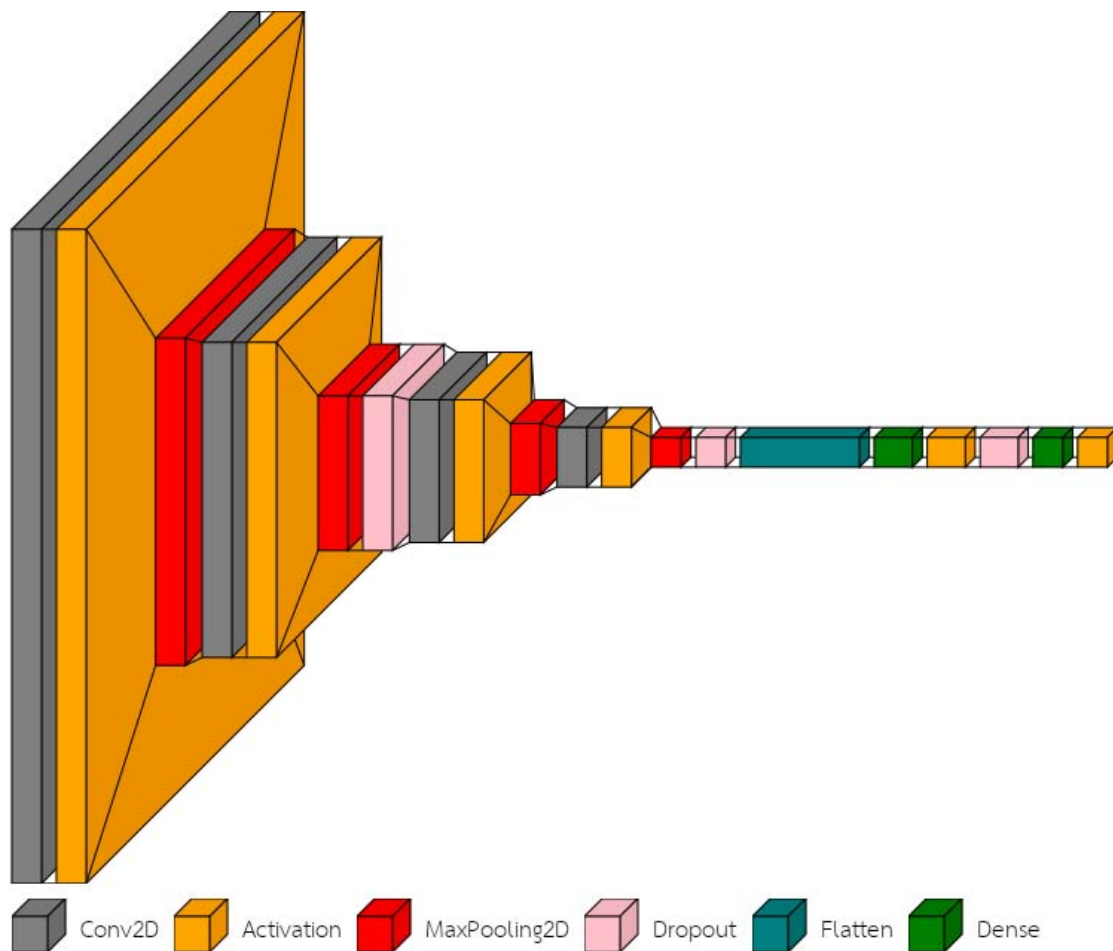


FIGURE 5.5: An structural outline of the proposed DL-based CNN model.

### 5.2.2.2 Classification of different diseases

Following feature extraction and CNN model training, the classification process is carried out on the datasets, encompassing both multi-class and binary-class classifications. In the

multiclass classification, four categories are considered, each corresponding to a neurological disorder (ASD, EP, PD, and SZ), and all images from healthy control subjects across all four datasets are grouped into a single HC class. This results in a total of five classes for the classification task: ASD vs. EP vs. HC vs. PD vs. SZ.

Additionally, to evaluate the performance of the proposed framework for individual disease detection, binary classification is conducted for each of the datasets separately. In this context, each dataset is treated independently, leading to four distinct binary classification tasks: ASD vs. HC, EP vs. HC, PD vs. HC, and SZ vs. HC.

### 5.2.2.3 Performance comparison with popular models

We have evaluated the performance of our proposed CNN model by comparing it to two well-known CNN models, AlexNet and ResNet50, in the context of multi-class classification. Below are some details about these two popular models:

#### 5.2.2.3.1 AlexNet

AlexNet is indeed a groundbreaking CNN architecture developed by Alex Krizhevsky *et al.* in 2012 [223]. Its success in winning the ImageNet Large Scale Visual Recognition Challenge (ILSVRC) was a significant milestone in the field of computer vision and deep learning. AlexNet's architecture includes eight weight layers, with the first five being convolutional layers and the last three fully connected layers. These layers, combined with techniques like ReLU activation, max-pooling, and dropout, contributed to its remarkable recognition accuracy. Researchers have since built upon the principles introduced by AlexNet to develop even more advanced deep learning models for various image classification tasks. Details of the network architecture can be found in [223].

#### 5.2.2.3.2 ResNet50

Indeed, ResNet, short for Residual Network, is a significant advancement in deep learning and convolutional neural networks. It was introduced by Kaiming He and his team in 2015 and played a crucial role in winning the ILSVRC challenge [224]. ResNet is characterised by its deep architecture, and there are several variants with different layer configurations, such as ResNet-18, ResNet-34, ResNet-50, ResNet-101, and ResNet-152. ResNet-50, in particular, contains 50 layers, including 49 convolutional layers and a fully connected layer. The key innovation in ResNet is the use of residual connections, or skip connections, which help address the vanishing gradient problem in very deep networks. This architectural concept has since been adopted and adapted in many other deep learning models to enable training of extremely deep neural networks. Details of the network architecture can be found in [224].

### 5.2.2.4 Performance evaluation materials and parameters

To validate the proposed model, EEG brain signal data from four distinct neurological disorders - ASD, EP, PD, and SZ is utilised. These four datasets are employed to conduct a five-class classification task, distinguishing between ASD, EP, PD, SZ, and HC using the proposed method. The performance of the proposed approach is assessed using various evaluation metrics commonly employed in this field of study. Further details about these evaluation metrics are outlined below:

#### 5.2.2.4.1 Classification performance measure

To mitigate potential bias in the model's classification performance and provide a more reliable estimate of the model's overall accuracy on the entire dataset, a cross-validation scheme is recommended in the literature [98], [182], [225], [226]. In this study, we have employed a five-fold cross-validation technique to validate the performance of the proposed models. In this approach, the dataset is divided into five roughly equal parts, with four parts used for training the classifier and the remaining part for testing the trained system. This process is repeated five times, ensuring that each image in the dataset is included in the test set exactly once. This testing procedure is illustrated in Figure 5.6.

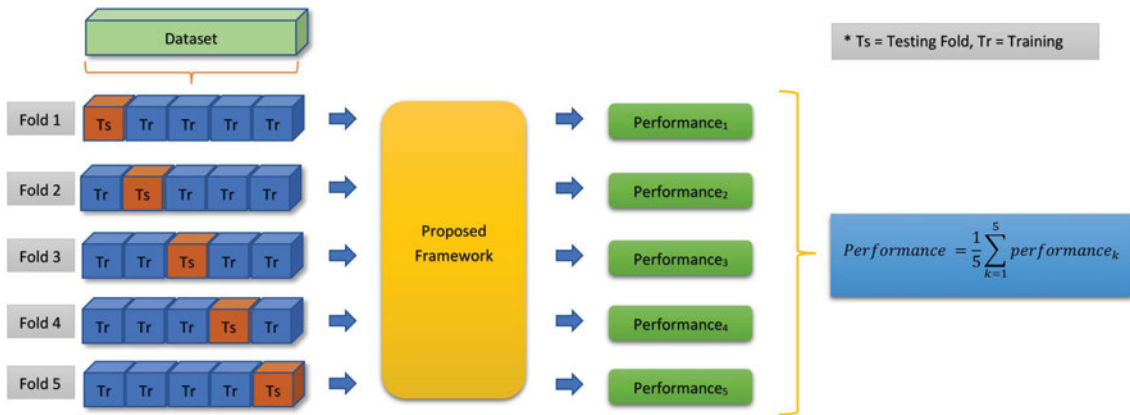


FIGURE 5.6: Overview of the used five-fold cross-validation technique.

The results generated from the five-fold cross-validation are utilised to assess the system's performance using six key parameters: sensitivity (Sen), specificity (Spec), precision (Prec), F1 score (F1), accuracy (Acc), and the receiver operating characteristic (ROC) curve. These metrics provide valuable insights into the classifier's behaviour based on the test data [98], [154], [181], [227]. The calculations for these six parameters involve the use of four key values: true positive (TP), true negative (TN), false positive (FP), and false negative (FN), as described in equations (5.11) through (5.15).

$$Sensitivity(Sen) = \frac{TP}{TP + FN} * 100 \quad (5.11)$$

$$Specificity(Spec) = \frac{TN}{TN + FP} * 100 \quad (5.12)$$

$$Precision(Prec) = \frac{TP}{TP + FP} * 100 \quad (5.13)$$

$$F1score(F1) = \frac{2 TP}{2 TP + FP + FN} \quad (5.14)$$

$$Accuracy(Acc) = \frac{\sum_{i=1}^n TP_i}{TP + FP + TN + FN} * 100 \quad (5.15)$$

The values of TP, TN, FP, and FN for multi-class classification can be determined using the confusion matrix, as illustrated in Figure 5.7. In this figure, for class C, the TP value is represented by green cells, FN is indicated by blue cells, TN is reflected in yellow cells, and FP values are shown in orange cells. These values can be calculated similarly for other classes.

		Predicted Class					
		A	B	C	D	E	
Actual Class	A	TP <sub>A</sub>	E <sub>AB</sub>	E <sub>AC</sub>	E <sub>AD</sub>	E <sub>AE</sub>	
	B	E <sub>BA</sub>	TP <sub>B</sub>	E <sub>BC</sub>	E <sub>BD</sub>	E <sub>BE</sub>	
	C	E <sub>CA</sub>	E <sub>CB</sub>	TP <sub>C</sub>	E <sub>CD</sub>	E <sub>CE</sub>	FN
	D	E <sub>DA</sub>	E <sub>DB</sub>	E <sub>DC</sub>	TP <sub>D</sub>	E <sub>DE</sub>	
	E	E <sub>EA</sub>	E <sub>EB</sub>	E <sub>EC</sub>	E <sub>ED</sub>	TP <sub>E</sub>	TN
			FP		TP		

FIGURE 5.7: Confusion matrix used for calculating the evaluation parameters for five class classification.

The ROC graph is a useful tool for visualising the classifier's reliability. It is made by plotting sensitivity (true positive rate) on the Y-axis and 1-specificity (false positive rate) on the X-axis. These parameters provide insights into how classifiers will perform when dealing with test data [98], [112], [154], [181], [228], [229].

## 5.3 Results and discussion

In this study, we have introduced a data mining framework for brain signal analysis using spectrogram images and both ML and DL-based techniques. We applied this framework to four EEG datasets related to neurological disorders (ASD, EP, PD, SZ) and conducted a five-class classification task (ASD vs. EP vs. PD vs. SZ vs. HC). In this section, we will provide a detailed overview of the results obtained and visualise the outcomes of our experiments along with the experimental settings.

### 5.3.1 Experimental setup

In our methodology, we segmented the EEG data of each subject into 3-second segments and then generated spectrogram images with a size of 112×112 pixels using the Short-Time Fourier Transform (STFT) method. This process resulted in the creation of 5437 images from the ASD dataset (3825 ASD and 1612 HC), 2483 images from the EP dataset

(1248 EP and 1235 HC), 1745 images from the PD dataset (864 PD and 881 HC), and 9752 images from the SZ dataset (5312 SZ and 4440 HC). The combined dataset consisted of 19417 images, with five classes having 3825, 1248, 864, and 5312 images for the ASD, EP, PD, and SZ classes, respectively, and all HC images from the four diseases combined to form the normal class, containing 8168 images. Sample images from these five classes are illustrated in Figure 5.8, where 5.8a, 5.8b, 5.8c, 5.8d, and 5.8e show sample images from the ASD, EP, PD, SZ, and Normal classes, respectively.

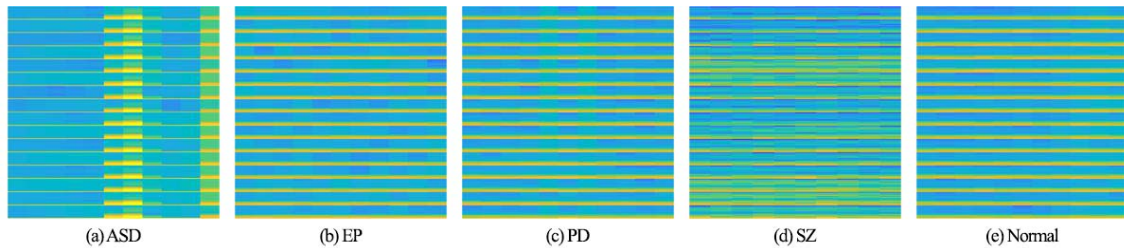


FIGURE 5.8: Sample spectrogram images generated by the proposed method for different datasets.

After generating the spectrogram images, we divided them into five approximately equal sub-parts to facilitate 5-fold cross-validation for the proposed approaches. Each experimental model was trained using four of these sub-parts, with the remaining sub-part used for validation. This process was repeated five times to ensure that each sub-part was used once for model validation. This 5-fold cross-validation approach allowed us to assess the overall performance of the models on the entire dataset while mitigating issues related to overfitting and bias in the results.

Image generation and ML-based classification were conducted using the MATLAB (R2020a) environment on a computer equipped with an Intel Core i5 64-bit processor operating at a frequency of 1.7 GHz and 8 GB of memory. For DL-based classification experiments, we utilised the Google Colab<sup>1</sup> environment. All models were trained for 50 epochs to avoid overfitting, and we employed mini-batch mode for batch size selection, experimenting with three different batch sizes (32, 64, and 128) during the training process of the models.

### 5.3.2 Results

This section comprises two parts, each discussing the results from the two different approaches employed in this proposed method: ML-based classification results and DL-based classification results.

#### 5.3.2.1 Machine learning based classification results

In this proposed brain signal data mining framework, two different histogram-based techniques, cCENTRIST and tCENTRIST, are used to extract textural features from the

<sup>1</sup><https://colab.research.google.com/notebooks/intro.ipynb>

spectrogram images. Subsequently, PCA is employed to reduce the dimension of the extracted features. Finally, four ML-based classification techniques, namely SVM (LibSVM), RF, LDA, and  $k$ NN (with  $k$  values ranging from 1 to 10), are employed to classify the reduced features separately for each feature extractor. A five-fold cross-validation technique is utilised to validate the performance of the classifiers. Table 5.2 presents the average results from five rounds of evaluations based on equations (5.11) to (5.15) for the four classifiers. For  $k$ NN, the results for  $k=9$  are provided as it yielded the best performance among the ten different  $k$  settings tested.

Table 5.2 provides a comprehensive view of our results. Notably, when employing cCENTRIST-based feature extraction,  $k$ NN achieves the highest overall accuracy at 86.28%, while RF demonstrates the lowest overall accuracy among the four classifiers. SVM and  $k$ NN exhibit similar accuracy levels, with LDA delivering moderate performance in comparison. In terms of individual rounds,  $k$ NN reaches its peak accuracy of 86.69% during round 2, while RF exhibits the lowest performance with an accuracy of 77.13% in round 3.

On the other hand, when utilising tCENTRIST-based feature extraction, SVM emerges as the top-performing classifier with the highest overall accuracy of 88.78%. LDA, conversely, yields the lowest overall accuracy at 72.46%, while  $k$ NN and RF achieve accuracy levels of 87.96% and 76.21%, respectively. In individual rounds, SVM attains its highest accuracy of 89.13%, whereas LDA performs less optimally, achieving an accuracy of 72.01%.

Figure 5.9 visually illustrates the accuracy trends for the different classifiers and feature extraction techniques across multiple rounds of the cross-validation process. These findings underscore the critical role of selecting an appropriate combination of feature extraction methods and classifiers to optimise classification performance in this context.

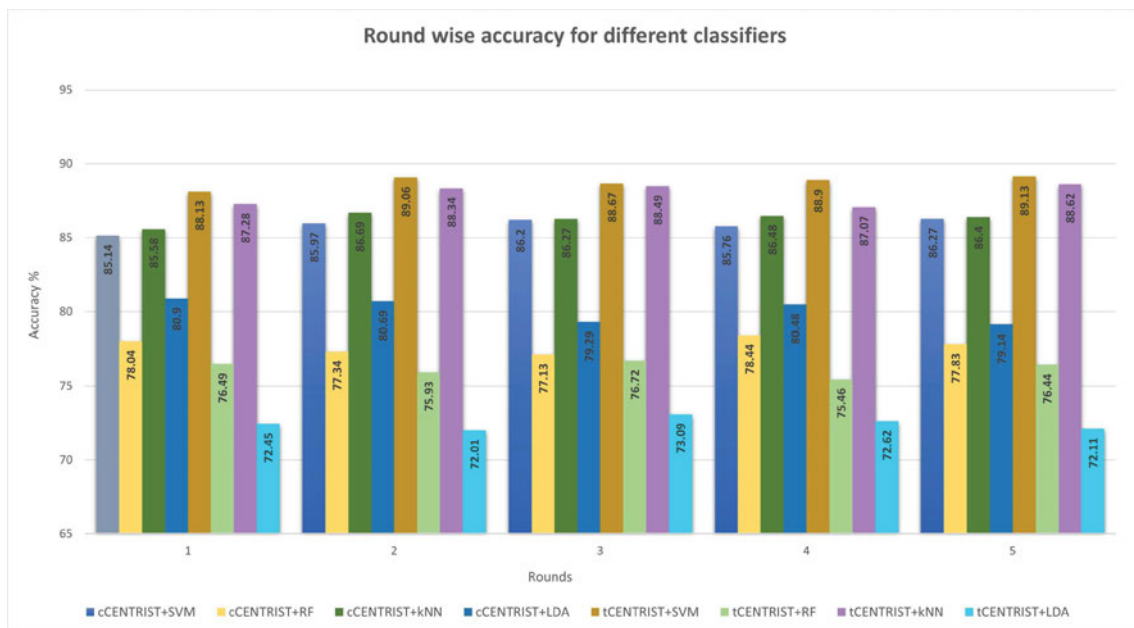


FIGURE 5.9: Round-wise accuracy comparison for different ML-based classifiers tested in this study.

TABLE 5.2: Average sensitivity, specificity, precision, F1 score, and accuracy results for the two distinct feature extractors (cCENTRIST and tCENTRIST) combined with four distinct classifiers (SVM, RF, LDA, and kNN with  $k=9$ ) across five rounds

cCENTRIST based feature extraction																
SVM				kNN				RF				LDA				
Disease	Sen%	Spec%	Prec%	F1	Sen%	Spec%	Prec%	F1	Sen%	Spec%	Prec%	F1				
<b>ASD</b>	90.72	96.80	87.45	0.89	87.59	97.59	90.03	0.89	75.77	97.40	87.69	0.81	79.67	96.92	86.40	0.83
<b>EP</b>	83.59	98.51	79.46	0.81	77.14	98.06	73.29	0.75	31.87	99.97	98.56	0.48	80.70	97.19	66.36	0.73
<b>Normal</b>	84.77	87.83	83.49	0.84	88.89	86.56	82.77	0.86	92.29	70.17	69.20	0.79	78.69	86.33	80.70	0.80
<b>PD</b>	83.99	99.61	91.01	0.87	69.11	99.95	98.37	0.81	24.26	100.00	100.00	0.39	83.47	98.25	69.06	0.76
<b>SZ</b>	84.91	96.22	89.43	0.87	86.27	97.06	91.72	0.89	76.35	96.09	88.02	0.82	81.95	92.84	81.19	0.82
<b>Avg</b>	<b>85.59</b>	<b>95.79</b>	<b>86.17</b>	<b>0.86</b>	<b>81.80</b>	<b>95.85</b>	<b>87.23</b>	<b>0.84</b>	<b>60.11</b>	<b>92.72</b>	<b>88.69</b>	<b>0.66</b>	<b>80.90</b>	<b>94.31</b>	<b>76.74</b>	<b>0.78</b>
<b>Acc</b>	<b>85.87(± 0.45)</b>			<b>86.28(± 0.42)</b>				<b>77.76(± 0.53)</b>				<b>80.1(± 0.74)</b>				
tCENTRIST based feature extraction																
<b>ASD</b>	92.26	97.44	89.88	0.91	91.96	96.64	87.16	0.89	71.88	97.77	88.82	0.79	75.96	93.93	75.39	0.76
<b>EP</b>	86.16	98.96	85.04	0.86	78.74	98.10	73.99	0.76	23.25	99.92	95.45	0.37	74.37	95.92	55.59	0.63
<b>Normal</b>	88.77	89.50	85.99	0.87	88.76	89.49	86.00	0.87	95.96	62.74	65.15	0.78	68.47	83.64	75.24	0.72
<b>PD</b>	87.95	99.73	93.85	0.91	88.94	99.96	99.10	0.94	39.77	99.97	98.35	0.57	80.91	98.36	69.82	0.75
<b>SZ</b>	87.06	97.45	92.78	0.90	85.86	98.02	94.25	0.90	67.36	99.57	98.35	0.80	74.26	89.26	72.26	0.73
<b>Avg</b>	<b>88.44</b>	<b>96.61</b>	<b>89.51</b>	<b>0.89</b>	<b>86.85</b>	<b>96.44</b>	<b>88.10</b>	<b>0.87</b>	<b>59.64</b>	<b>91.99</b>	<b>89.23</b>	<b>0.66</b>	<b>74.79</b>	<b>92.22</b>	<b>69.66</b>	<b>0.72</b>
<b>Acc</b>	<b>88.78(± 0.36)</b>			<b>87.96(± 0.36)</b>				<b>76.21(± 0.45)</b>				<b>72.46(± 0.39)</b>				

Furthermore, for a comprehensive assessment of classifier performance, we computed the average accuracy over the five-fold cross-validation along with the standard deviation (SD) for each combination of feature extraction method and classifier. These results are depicted in Figure 5.10. Notably, SVM combined with the tCENTRIST-based feature extraction method achieves the highest average accuracy at 88.78%, with a relatively low SD value of 0.36, indicating consistent and robust performance. Conversely, LDA in combination with tCENTRIST exhibits the lowest average accuracy of 72.46%, accompanied by a slightly higher SD value of 0.39. These findings further emphasize the effectiveness of SVM with tCENTRIST for classifying neurological disorders using EEG data.

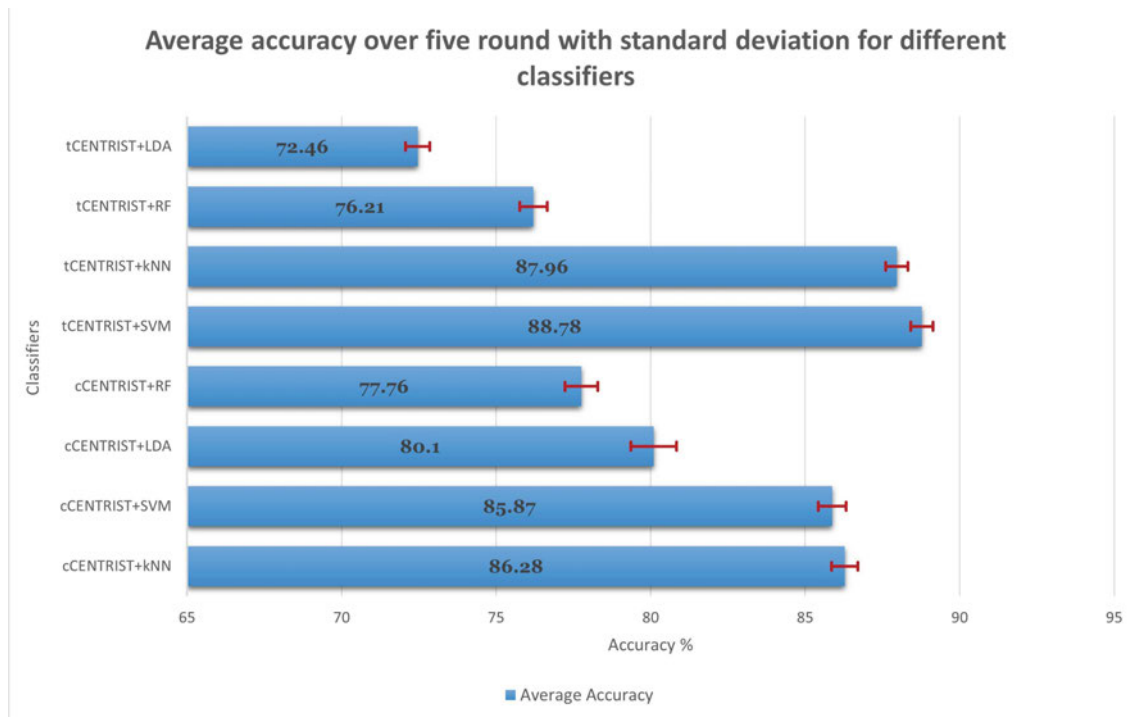


FIGURE 5.10: Five-fold average accuracy with standard deviation for different ML-based classifiers.

To provide a comprehensive evaluation of classifier performance, we computed and visualized sensitivity, specificity, precision, and F1 score for each classifier using the equations 5.11 - 5.15 and have made some comparative visualisations as shown in Figure 5.11, 5.12, 5.13 and 5.14.

The analysis of sensitivity values, as depicted in Figure 5.16, reveals important insights into the performance of the classifiers. For the tCENTRIST-based feature extraction approach, tCENTRIST+SVM achieves the highest single-round sensitivity of 89.58% and an overall 5-fold average sensitivity of 88.44% (with a standard deviation of 0.69). In contrast, tCENTRIST+RF exhibits the lowest single-round sensitivity at 58.95% and an overall 5-fold average sensitivity of 59.64% (with a standard deviation of 0.72).

When considering the cCENTRIST feature extractor, SVM outperforms other classifiers by achieving the highest 5-fold average sensitivity of 85.59% (with a standard deviation of 0.49), while RF produces the lowest average sensitivity of 60.11% (with a standard

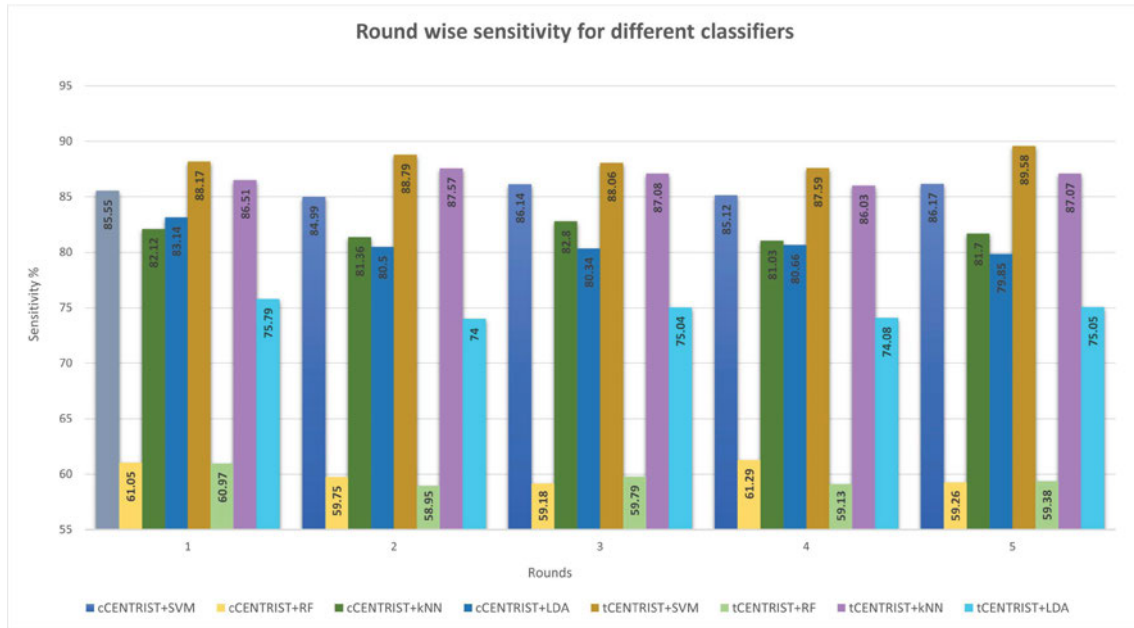


FIGURE 5.11: Round-wise comparison of sensitivity values for different ML-based classifiers.

deviation of 0.89). These results highlight that the tCENTRIST+SVM classifier demonstrates greater sensitivity in detecting diseases compared to other classifiers, which is a desirable characteristic in medical diagnostics. Sensitivity is particularly crucial for minimising false negatives, ensuring that individuals with conditions are correctly identified and referred for further evaluation or treatment.

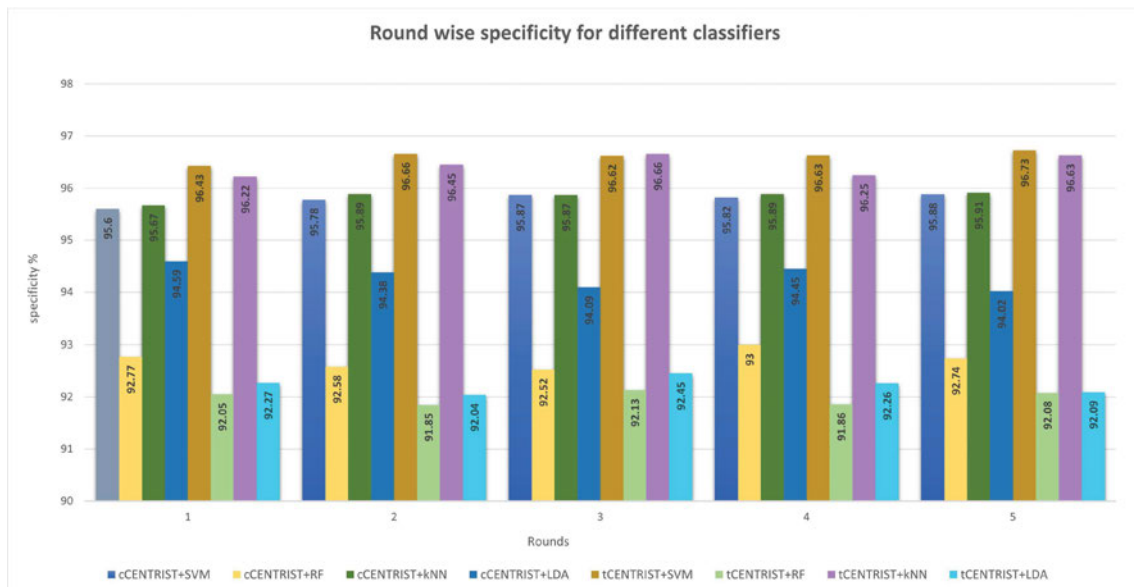


FIGURE 5.12: Round wise comparison of specificity values for different ML-based classifiers.

Figure 5.12 illustrates the round-wise specificity of the ML-based classifiers. It is evident that SVM and kNN exhibit similar specificity values across the rounds for both feature extractors. Specifically, tCENTRIST+SVM achieves the highest single-round specificity

value of 96.73% and an overall 5-fold average specificity of 96.61% (with a standard deviation of  $\pm 0.1$ ).

Conversely, tCENTRIST+RF records the lowest single-round specificity at 91.85% and the lowest overall 5-fold average specificity of 91.99% (with a standard deviation of  $\pm 0.12$ ). A higher specificity value is indicative of the model's ability to effectively distinguish healthy individuals from patients. In medical diagnosis, high specificity is essential to minimise false positives and avoid unnecessary medical interventions for individuals without the condition.

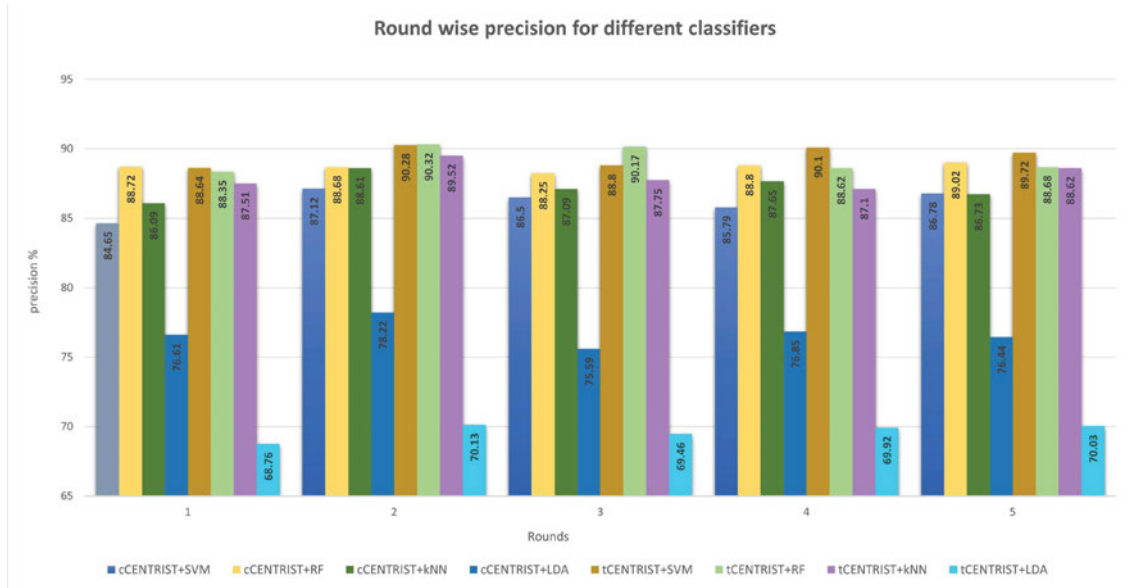


FIGURE 5.13: Round wise comparison of precision values for different classifiers.

Precision, a crucial measure in information retrieval and classification evaluations, reflects the percentage of retrieved instances that are relevant. Figure 5.13 displays the round-wise precision values for the different classifiers. From the plot, it becomes evident that the RF classifier, despite its overall poor performance with both cCENTRIST and tCENTRIST, tends to exhibit higher precision compared to other classifiers in most cases. This phenomenon can be attributed to the fact that while RF has low sensitivity, the images it identifies as patients are often correct, making its precision relatively high in these cases.

Overall, tCENTRIST+SVM yields the highest 5-fold average precision of 89.51% ( $\pm 0.67$ ), followed by tCENTRIST+RF with a precision value of 89.23% ( $\pm 0.84$ ). In contrast, tCENTRIST+LDA produces the lowest average precision, at 69.66% ( $\pm 0.51$ ). Precision is particularly important in the medical context, as it indicates the classifier's ability to correctly identify true positives while minimising false positives. High precision ensures that when the model classifies an individual as having a particular condition, it is highly likely that the individual indeed has the condition, reducing the chances of incorrect diagnoses.

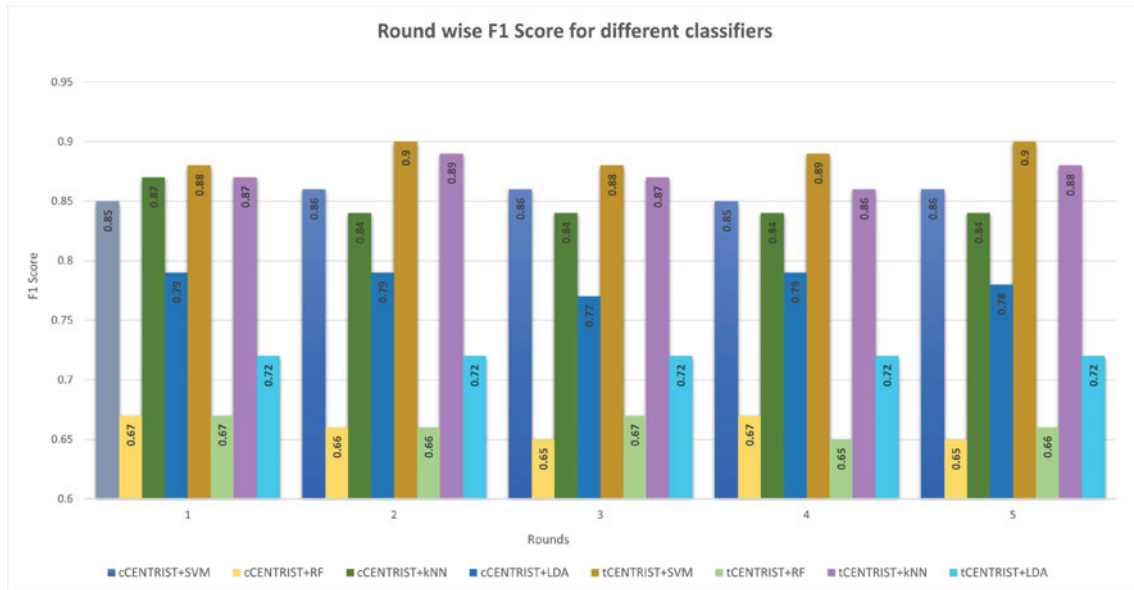


FIGURE 5.14: Round wise comparison of F1 score values for different ML-based classifiers.

The F1 score, which represents the harmonic mean of precision and recall, is a critical measure for evaluating classifier performance. Figure 5.14 illustrates the round-wise F1 scores for the tested classifiers. The F1 score is particularly valuable in situations where there is an imbalance between positive and negative classes or when both precision and recall need to be considered.

From the plot, it is evident that the SVM classifier consistently outperforms the other classifiers in terms of F1 scores across all rounds. Overall, tCENTRIST+SVM achieves an average F1 score of 0.89 ( $\pm 0.009$ ), demonstrating its robustness in achieving a balance between precision and recall. In contrast, kNN exhibits an average F1 score of 0.84 ( $\pm 0.005$ ), and RF lags behind with the lowest average F1 score of 0.66 ( $\pm 0.01$ ). A high F1 score indicates that the classifier effectively combines precision and recall, making it a suitable choice for applications where both false positives and false negatives need to be minimised.

To assess the classifiers' performance comprehensively, we have constructed ROC curves by plotting sensitivity (true positive rate) against 1-specificity (false positive rate). Figure 5.15 displays the ROC curves for the classifiers employed in this study.

From the ROC curves, it is evident that the curve for the tCENTRIST+SVM classifier is positioned at the top, indicating the highest sensitivity among all the classifiers. This suggests that tCENTRIST+SVM excels at correctly identifying positive cases (patients) while minimising false negatives. In contrast, the ROC curve for tCENTRIST+RF is situated lower, reflecting its lower sensitivity compared to other classifiers, resulting in a lower true positive rate. The ROC curve analysis provides valuable insights into each classifier's ability to discriminate between different classes and make informed predictions.

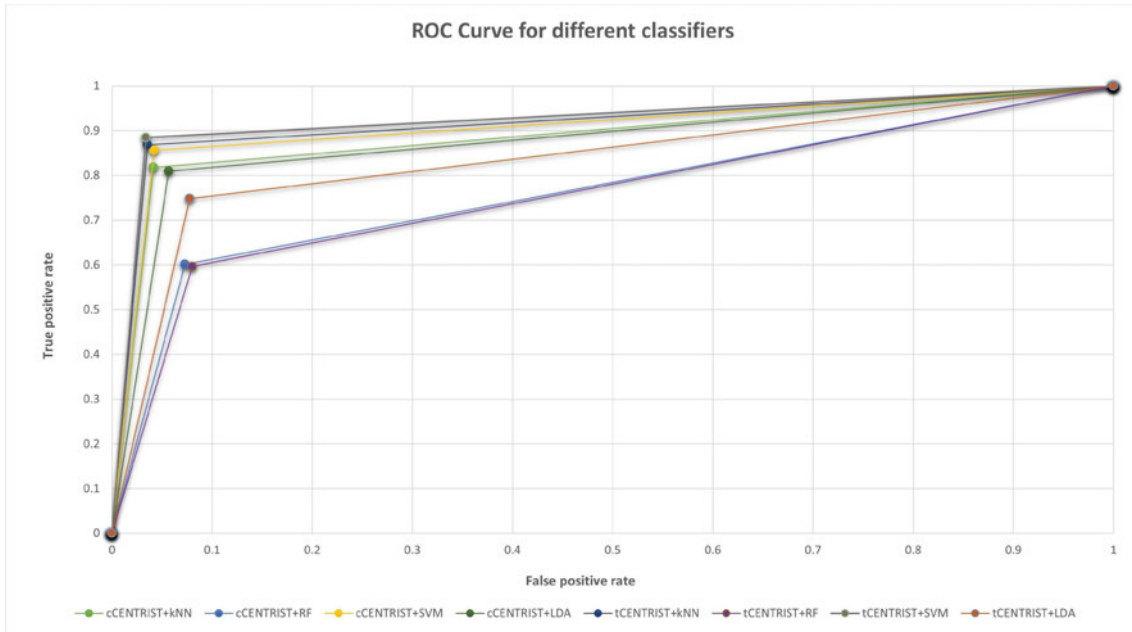


FIGURE 5.15: Comparison of ROC graphs for different ML-based classifiers tested in this study.

### 5.3.2.2 Deep learning based classification results

In our study, we have conducted experiments using three different models: the proposed model, AlexNet, and ResNet50, applying a five-fold cross-validation technique. The models were trained for 50 epochs to optimise their performance while avoiding overfitting. We have also investigated the impact of different batch sizes (32, 64, and 128) on the models' results and compared their performance. To evaluate the results comprehensively, we computed five key metrics: sensitivity (Sen), specificity (Spec), precision (Prec), F1 score (F1), and accuracy (Acc). Tables 5.3, 5.4 and 5.5 provide disease-specific, batch-wise average sensitivity, specificity, precision, F1 score, and accuracy values over five-fold for the proposed models, AlexNet and ResNet50, respectively. Overall average values are highlighted in bold.

TABLE 5.3: The average performance results using a five-fold cross-validation approach for the proposed model in a multi-class classification scenario.

Diseases	Batch Size 128					Batch Size 64					Batch Size 32				
	Sen%	Spec%	Prec%	F1	Acc%	Sen%	Spec%	Prec%	F1	Acc%	Sen%	Spec%	Prec%	F1	Acc%
ASD	98.82	99.59	98.33	0.99		99.03	99.6	98.39	0.99		98.7	99.61	98.44	0.99	
EP	97.77	99.91	98.73	0.98		98.08	99.86	97.94	0.98		96.47	99.85	97.73	0.97	
Normal	98.43	98.88	98.46	0.98	<b>98.49</b>	98.28	98.93	98.52	0.98	<b>98.49</b>	98.35	98.44	97.87	0.98	<b>98.20</b>
PD	99.08	99.92	98.42	0.99	$\pm 0.19$	98.38	99.95	98.97	0.99	$\pm 0.21$	97.71	99.94	98.83	0.98	$\pm 0.28$
SZ	98.42	99.48	98.63	0.99		98.52	99.46	98.57	0.99		98.12	99.46	98.57	0.98	
Avg	<b>98.5</b>	<b>99.56</b>	<b>98.51</b>	<b>0.98</b>		<b>98.46</b>	<b>99.56</b>	<b>98.48</b>	<b>0.99</b>		<b>97.87</b>	<b>99.46</b>	<b>98.29</b>	<b>0.98</b>	

Table 5.3 provides insights into the performance of the proposed model with different batch sizes. Here are the key observations:

**Accuracy Improvement:** The proposed model exhibits an increase in accuracy as the batch size increases. Specifically, it achieves an accuracy of 98.20% ( $\pm 0.28$ ) for a batch

size of 32. This accuracy improves to 98.49% ( $\pm 0.21$ ) when the batch size is increased to 64. Interestingly, even with a batch size of 128, the accuracy remains at 98.49%, but the standard deviation (SD) decreases to  $\pm 0.19$  from  $\pm 0.21$ .

**Batch Size Effect:** This suggests that the proposed model’s performance benefits from larger batch sizes, as indicated by the improved accuracy and reduced variability (SD) with batch size 64 and 128. However, there is no further accuracy improvement beyond a batch size of 64.

Overall, increasing the batch size appears to enhance the performance stability of the proposed model without compromising accuracy, as demonstrated by the reduced SD for larger batch sizes.

TABLE 5.4: The average performance results using a five-fold cross-validation approach for the AlexNet model in a multi-class classification scenario.

Diseases	Batch Size 128					Batch Size 64					Batch Size 32				
	Sen%	Spec%	Prec%	F1	Acc%	Sen%	Spec%	Prec%	F1	Acc%	Sen%	Spec%	Prec%	F1	Acc%
ASD	89.77	92.81	81.66	0.84		87.06	96.72	87.09	0.87		91.24	98.88	95.65	0.93	
EP	51.96	96.42	84.41	0.49		69.26	99.13	86.00	0.75		76.95	99.74	96.26	0.84	
Normal	80.18	74.45	69.82	0.74	<b>72.98</b>	81.93	88.35	84.88	0.82	<b>82.52</b>	95.18	88.28	85.98	0.90	<b>90.07</b>
PD	48.19	98.35	81.00	0.50	<b><math>\pm 7.30</math></b>	62.09	99.62	91.10	0.72	<b><math>\pm 4.47</math></b>	81.06	99.39	90.13	0.84	<b><math>\pm 2.85</math></b>
SZ	58.97	97.88	92.14	0.71		86.54	90.48	80.84	0.82		86.10	98.07	94.89	0.90	
Avg	<b>65.82</b>	<b>91.98</b>	<b>81.8</b>	<b>0.65</b>		<b>77.37</b>	<b>94.86</b>	<b>85.98</b>	<b>0.8</b>		<b>86.1</b>	<b>96.87</b>	<b>92.58</b>	<b>0.88</b>	

Table 5.4 provides insights into the performance of AlexNet with different batch sizes. Here are the key observations:

**Accuracy Variation:** AlexNet achieves the highest accuracy of 90.07% with a batch size of 32. However, as the batch size increases to 64 and 128, the accuracy decreases significantly to 82.52% and 72.98%, respectively.

**Standard Deviation:** The SD of the accuracy increases as the batch size increases. For batch size 32, the SD is 2.85, which rises to 4.47 for batch size 64 and further increases to 7.30 for batch size 128.

Overall, these results indicate that, in the case of AlexNet with this dataset, increasing the batch size not only leads to a decrease in accuracy but also results in higher variability (SD) across the five-fold cross-validation, suggesting that a smaller batch size may be more suitable for this model and dataset combination.

TABLE 5.5: The average performance results using a five-fold cross-validation approach for the ResNet50 model in a multi-class classification scenario.

Diseases	Batch Size 128					Batch Size 64					Batch Size 32				
	Sen%	Spec%	Prec%	F1	Acc%	Sen%	Spec%	Prec%	F1	Acc%	Sen%	Spec%	Prec%	F1	Acc%
ASD	97.74	99.04	96.25	0.97		95.43	99.20	96.76	0.96		98.65	99.46	97.81	0.98	
EP	93.84	99.23	91.12	0.92		90.47	99.65	94.48	0.92		95.86	99.89	98.33	0.97	
Normal	96.74	97.18	96.14	0.97	<b>96.41</b>	95.12	95.18	93.93	0.94	<b>94.78</b>	98.62	98.45	97.93	0.98	<b>98.23</b>
PD	95.07	99.92	98.31	0.97	<b><math>\pm 1.45</math></b>	93.79	99.32	86.69	0.90	<b><math>\pm 4.15</math></b>	97.19	99.92	98.28	0.98	<b><math>\pm 0.95</math></b>
SZ	95.79	99.46	98.57	0.97		94.95	98.90	97.09	0.96		98.03	99.65	99.05	0.99	
Avg	<b>95.83</b>	<b>98.97</b>	<b>96.08</b>	<b>0.96</b>		<b>93.95</b>	<b>98.45</b>	<b>93.79</b>	<b>0.94</b>		<b>97.67</b>	<b>99.47</b>	<b>98.28</b>	<b>0.98</b>	

The performance of ResNet50 with different batch sizes is summarised in Table 5.5. Here are the key observations:

**Accuracy Variation:** ResNet50 achieves the highest accuracy of 98.23% with a batch size of 32. However, as the batch size increases to 64, the accuracy decreases to 94.78%. Surprisingly, with a batch size of 128, the accuracy increases slightly to 96.41%.

**Standard Deviation:** The SD of the accuracy remains relatively stable across different batch sizes, indicating consistent performance over the five-fold cross-validation.

Overall, these results suggest that ResNet50 is less sensitive to changes in batch size compared to AlexNet with this dataset. However, a batch size of 32 appears to yield the highest accuracy for ResNet50.

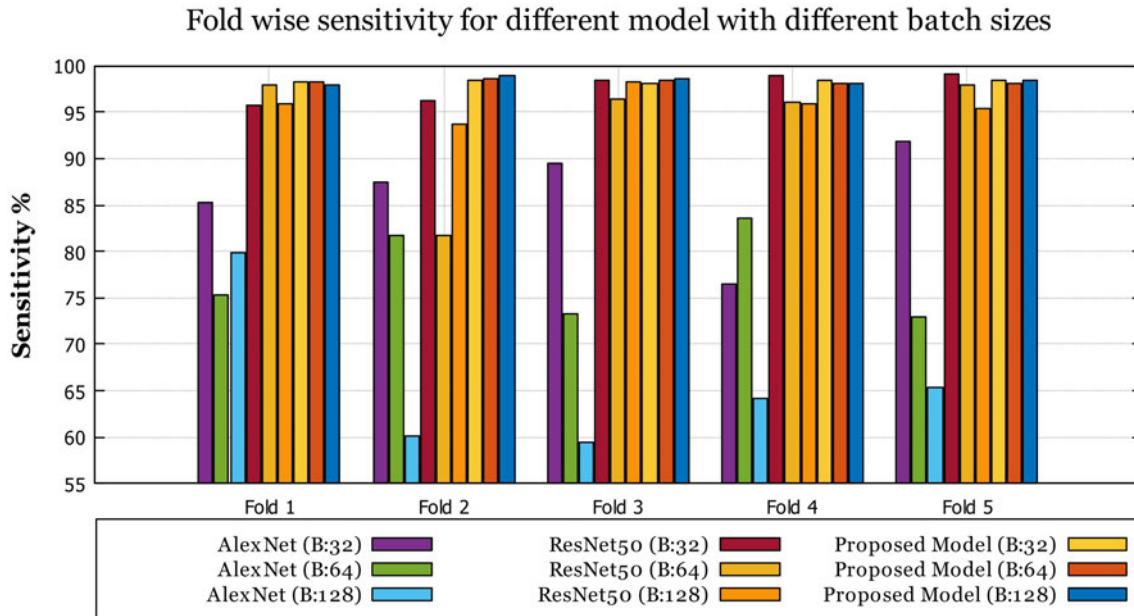


FIGURE 5.16: Fold-wise comparison of the sensitivity values for the three tested DL-based models with different training batch sizes.

The sensitivity results for the proposed model, AlexNet, and ResNet50 for different batch sizes are visualised in Figure 5.16. Here are the key observations:

**Proposed Model Sensitivity:** The proposed model consistently exhibits high sensitivity across all batch sizes, with five-fold average sensitivity values of approximately 98.28% (batch size 32), 98.26% (batch size 64), and 98.33% (batch size 128). These values indicate the model's strong ability to correctly identify patients among the subjects.

**ResNet50 Sensitivity:** ResNet50 also maintains high sensitivity, particularly with a batch size of 32, where it achieves a five-fold average sensitivity of approximately 97.67%. The sensitivity slightly decreases with larger batch sizes (93.95% for batch size 64 and 95.83% for batch size 128). ResNet50 demonstrates robust performance in patient identification.

**AlexNet Sensitivity:** AlexNet, on the other hand, has lower sensitivity compared to the proposed model and ResNet50. It exhibits the lowest single-fold sensitivity (59.54%) for batch size 128, indicating a higher likelihood of misclassifying patients as healthy subjects. The five-fold average sensitivities for AlexNet range from 65.82% (batch size 128) to 86.10% (batch size 32).

Overall, these results highlight the superior sensitivity of the proposed model compared to AlexNet and its competitive performance with ResNet50, especially when utilising larger batch sizes.

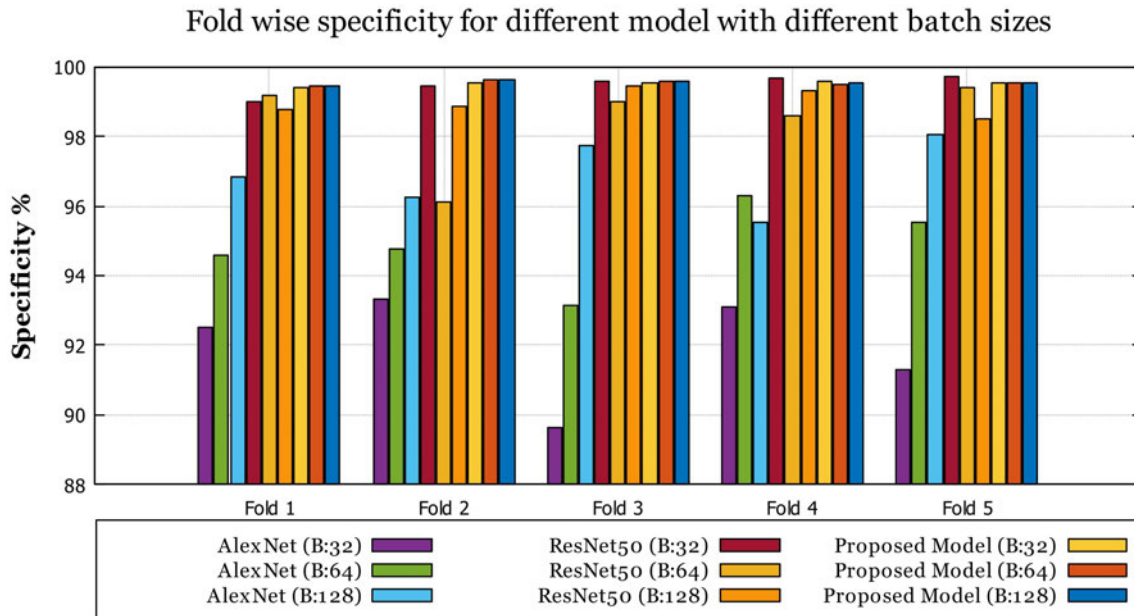


FIGURE 5.17: Fold-wise comparison of the specificity values for the three tested DL-based models with different training batch sizes.

Specificity, which measures the ability to correctly classify healthy subjects as such, is crucial in medical diagnosis. Here's an analysis of the specificity results for the proposed model, AlexNet, and ResNet50 with different batch sizes, as shown in Figure 5.17:

**AlexNet Specificity:** AlexNet achieves a single-fold specificity as low as 89.65% (batch size 32, fold 3) and as high as 99.70% (batch size 32, fold 5). However, its performance varies significantly. The five-fold average specificity values for AlexNet are 96.87% (batch size 32), 98.45% (batch size 64), and 98.97% (batch size 128). Although the average specificity values are relatively high, the model exhibits variability in its performance.

**ResNet50 Specificity:** ResNet50 demonstrates a strong ability to correctly classify healthy subjects, with a single-fold specificity ranging from 94.13% (batch size 128, fold 1) to 99.70% (batch size 32, fold 5). The five-fold average specificities for ResNet50 are 94.86% (batch size 32), 98.13% (batch size 64), and 98.98% (batch size 128). ResNet50 consistently delivers high specificity values.

**Proposed Model Specificity:** The proposed model consistently outperforms both AlexNet and ResNet50 in terms of specificity. It achieves the highest single-fold specificity values for all batch sizes and maintains very high specificity across the board. The five-fold average specificities for the proposed model are 99.51% (batch size 32), 99.52% (batch size 64), and 99.55% (batch size 128). These results indicate that the proposed model excels at correctly classifying healthy subjects, making it highly suitable for medical diagnosis.

Overall, the proposed model exhibits superior specificity compared to AlexNet and ResNet50, demonstrating its effectiveness in ruling out healthy subjects from patients.

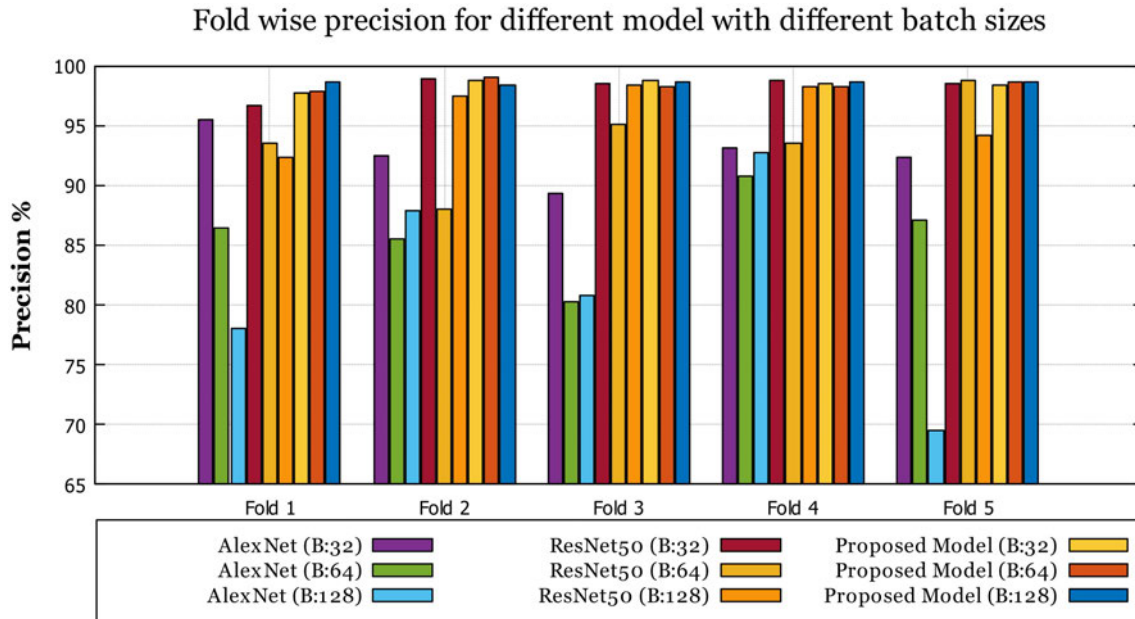


FIGURE 5.18: Fold-wise comparison of the precision values for the three tested DL-based models with different training batch sizes.

Precision, also known as positive predictive value, is crucial in classification tasks as it indicates the validity of the results by measuring the percentage of correctly identified patients among the retrieved group of patients. Here's an analysis of precision results for the proposed model, AlexNet, and ResNet50 with different batch sizes, as shown in Figure 5.18:

**AlexNet Precision:** AlexNet exhibits variable precision values across different batch sizes, with the lowest precision of 81.80% (batch size 128) and the highest precision of 92.58% (batch size 32). The five-fold average precisions for AlexNet are 85.98% (batch size 64), 85.97% (batch size 128), and 92.13% (batch size 32). While the average precision values are moderate, AlexNet's performance varies significantly.

**ResNet50 Precision:** ResNet50 demonstrates a higher and more consistent precision compared to AlexNet. Its precision values range from 93.79% (batch size 64) to 98.28% (batch size 32). The five-fold average precisions for ResNet50 are 96.08% (batch size 32), 94.93% (batch size 64), and 96.75% (batch size 128). ResNet50 consistently delivers high precision values.

**Proposed Model Precision:** The proposed model consistently outperforms both AlexNet and ResNet50 in precision, regardless of batch size. It achieves high and consistent precision values, with an average precision of 98.60% (batch size 32), 98.41% (batch size 64), and 98.40% (batch size 128). The proposed model's high precision indicates that it correctly identifies patients with a very low rate of misclassification.

Overall, the proposed model exhibits superior precision compared to AlexNet and ResNet50, demonstrating its ability to accurately identify patients while minimising the misclassification of healthy subjects as patients.

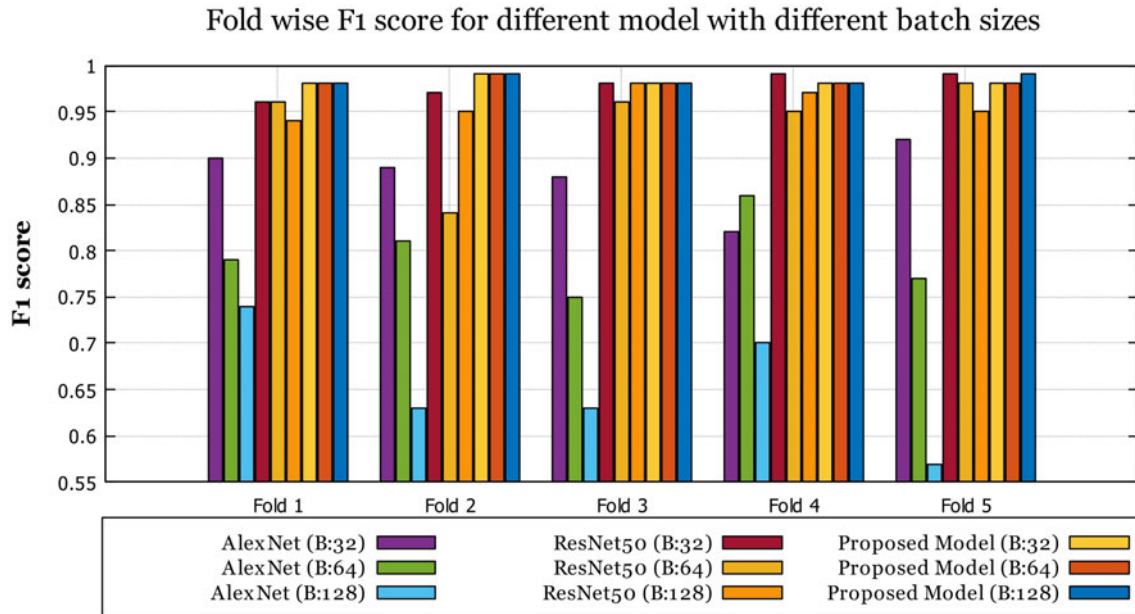


FIGURE 5.19: Fold-wise comparison of the F1 score values for the three tested DL-based models with different training batch sizes.

The F1 score, which combines precision and recall, provides a comprehensive performance measure for detecting patients in classification tasks. It is the harmonic mean of precision and recall. Here's an analysis of F1 score results for the proposed model, AlexNet, and ResNet50 with different batch sizes, as shown in Figure 5.19:

**AlexNet F1 Score:** AlexNet exhibits varying F1 scores across different batch sizes. The lowest F1 score is 0.654 ( $\pm 0.067$ ) achieved with batch size 128, indicating relatively poor performance. The five-fold average F1 scores for AlexNet are 0.723 (batch size 64), 0.676 (batch size 128), and 0.793 (batch size 32). These values suggest that AlexNet's performance is inconsistent and less robust.

**ResNet50 F1 Score:** ResNet50 delivers higher and more consistent F1 scores compared to AlexNet. The highest F1 score for ResNet50 is 0.978 ( $\pm 0.013$ ), indicating excellent performance, while the lowest F1 score is 0.834 ( $\pm 0.041$ ) for batch size 128. The five-fold average F1 scores for ResNet50 are 0.946 (batch size 64), 0.915 (batch size 128), and 0.969 (batch size 32). ResNet50 consistently provides robust F1 scores.

**Proposed Model F1 Score:** The proposed model consistently outperforms both AlexNet and ResNet50 in F1 score, regardless of batch size. It achieves high and consistent F1 scores, with an average F1 score of 0.984 ( $\pm 0.005$ ) for batch size 128, 0.981 ( $\pm 0.004$ ) for batch size 64, and 0.982 ( $\pm 0.004$ ) for batch size 32. The proposed model's F1 scores indicate excellent and robust performance in detecting patients.

In summary, the proposed model consistently outperforms AlexNet and ResNet50 in F1 score, demonstrating its ability to provide robust and reliable results in detecting patients across different batch sizes.

Figure 5.20 provides a comparison of fold-wise accuracy for the three tested models with different batch sizes. Here's an analysis of the accuracy results:

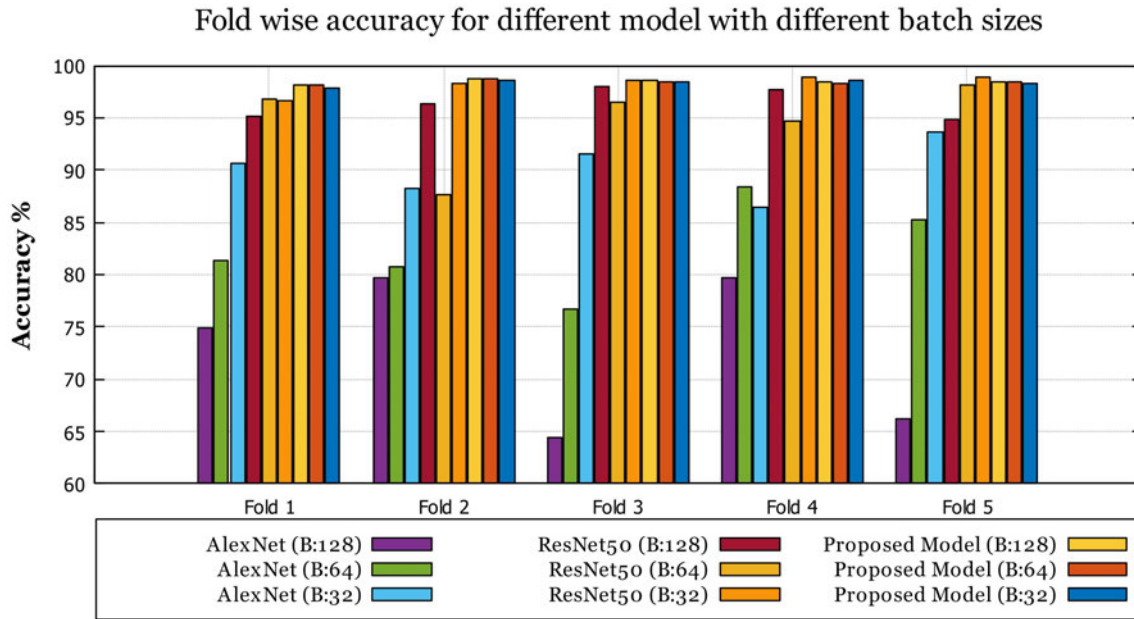


FIGURE 5.20: Fold-wise comparison of the accuracy values for the three tested DL-based models with different training batch sizes.

**AlexNet Accuracy:** AlexNet exhibits varying accuracy across different batch sizes and folds. The lowest single-fold accuracy is 64.46% (batch size 128) in fold 3, while the highest single-fold accuracy is 93.66% (batch size 32) in fold 5. AlexNet’s accuracy ranges from 64.46% to 93.66% across different batch sizes and folds.

**ResNet50 Accuracy:** ResNet50 consistently delivers higher accuracy compared to AlexNet. The lowest single-fold accuracy for ResNet50 is 87.69% (batch size 64), while the highest single-fold accuracy is 98.92% (batch size 32). ResNet50’s accuracy ranges from 87.69% to 98.92% across different batch sizes and folds.

**Proposed Model Accuracy:** The proposed model consistently outperforms both AlexNet and ResNet50 in accuracy, regardless of batch size. The lowest accuracy for a single fold is 98.09% (batch size 32) in fold 3, while the highest accuracy is 98.74% (batch size 64) in fold 1. The proposed model’s accuracy ranges from 98.09% to 98.74% across different batch sizes and folds.

In summary, the proposed model consistently outperforms AlexNet and ResNet50 in accuracy, demonstrating its superior performance in accurately classifying patients and healthy subjects. It provides high and consistent accuracy results across different batch sizes and folds, indicating its robustness and reliability in detecting patients.

Figure 5.21 provides a comparison of the average accuracy with standard deviation over the 5-fold for all the experiments. Here’s an analysis of the plot:

**Green Bars (Average Accuracy):** The green bars represent the average accuracy for the three tested models (AlexNet, ResNet50, and the proposed model) with different batch sizes. The proposed model consistently exhibits the highest average accuracy among the three models, followed by ResNet50 and AlexNet.

**Red Line (Standard Deviation):** The red line shows the standard deviation of the

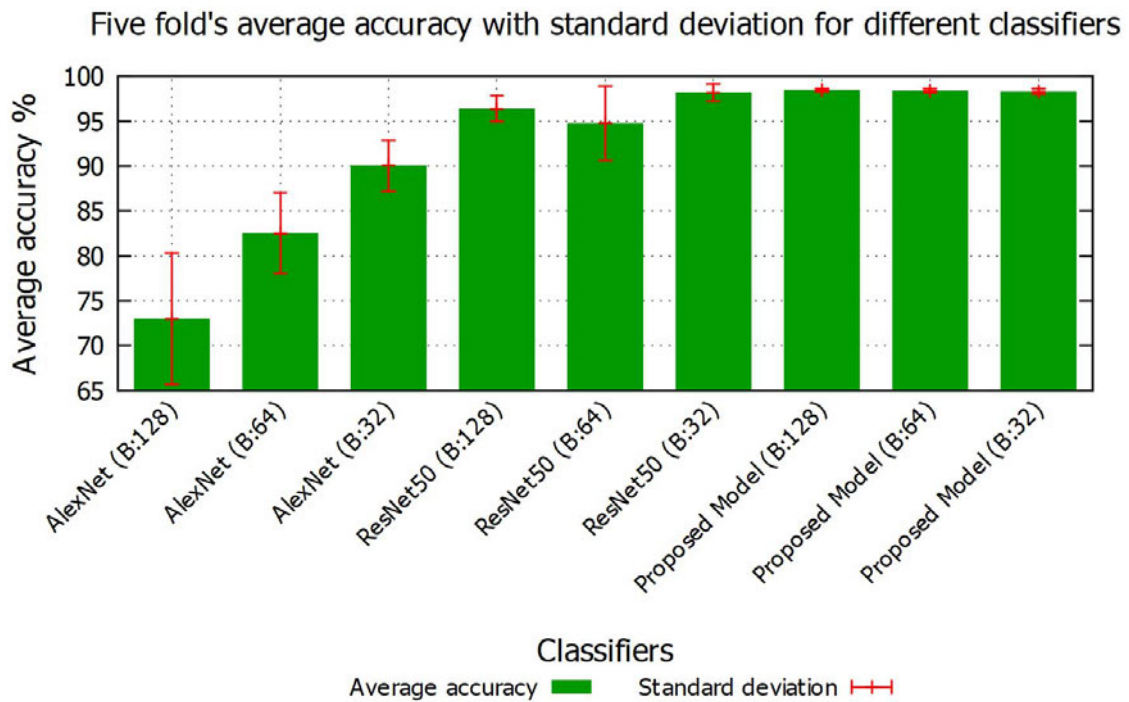


FIGURE 5.21: Five-fold average accuracy with standard deviation for the three tested DL-based models with different training batch sizes.

accuracy values over the five folds for each model and batch size combination. It provides a measure of the variability or stability of the accuracy results. Notably, the proposed model has a significantly lower standard deviation (0.19) compared to ResNet50 (0.95), indicating that the proposed model's classification results are more consistent and stable over the full dataset.

In summary, the plot demonstrates that while ResNet50 achieves a similar average accuracy to the proposed model, the proposed model outperforms ResNet50 in terms of classification stability and consistency. This suggests that the proposed model is a robust choice for classifying patients and healthy subjects with minimal variability in its accuracy results.

Figure 5.22 presents the Receiver Operating Characteristic (ROC) curves for all the models tested in the study. Here's an analysis of the plot:

**Proposed Model:** The ROC curves for the proposed model with three different batch sizes (32, 64, and 128) are shown. These curves are close to the ideal (0,1) point, indicating that the proposed model performs well as a classifier for the dataset. ROC curves close to the (0,1) point typically indicate strong classification performance.

**ResNet50 and AlexNet:** The ROC curve for ResNet50 with a batch size of 32 is also close to the ideal point, suggesting good classification performance. However, for other batch sizes of ResNet50 and for AlexNet, the ROC curves are noticeably below the (0,1) point. This indicates that the performance of ResNet50 varies with batch size, and AlexNet performs less effectively in classifying the dataset according to ROC analysis.

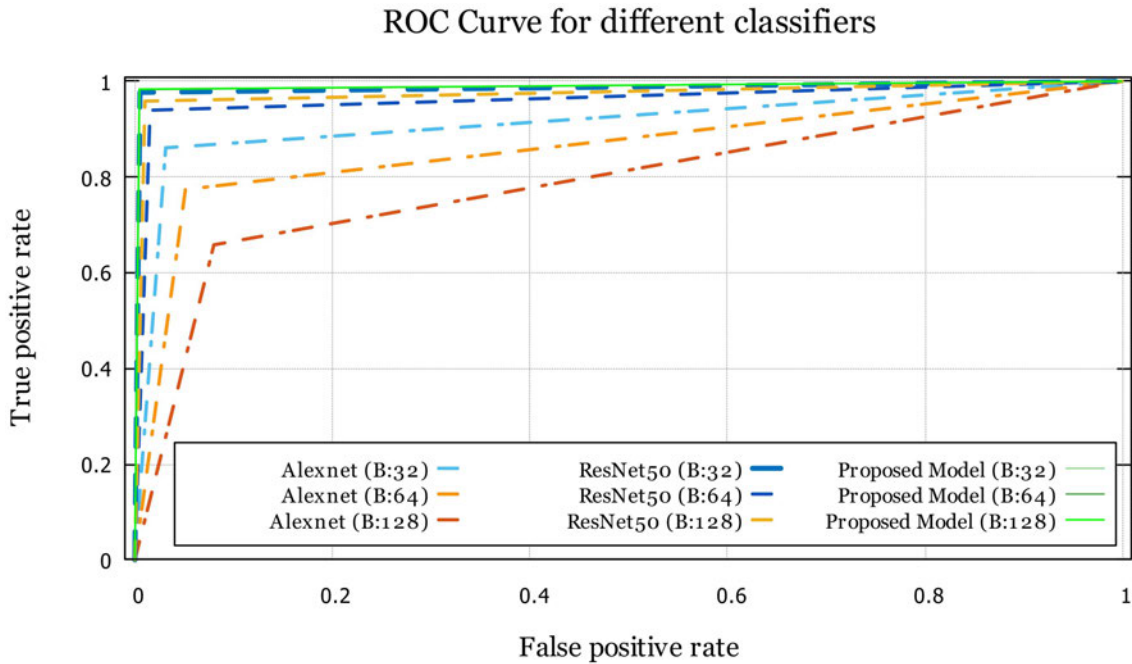


FIGURE 5.22: Comparison of ROC graphs for the three tested DL-based models with different training batch sizes.

In summary, the ROC curve analysis reinforces the idea that the proposed model is a strong classifier for the dataset, particularly when compared to other models like ResNet50 and AlexNet, which exhibit varying performance depending on batch size.

### 5.3.3 Discussion of the deep learning based classification

The results of the three models clearly indicate that the proposed model outperforms the other two models in terms of various performance evaluation criteria. Additionally, the proposed model demonstrates its superiority in terms of model complexity and execution time. Here's a summary of the key findings:

#### 5.3.3.1 Performance

The proposed model consistently outperforms ResNet50 and AlexNet in terms of sensitivity, specificity, precision, F1 score, and accuracy. It achieves the highest average accuracy with a low standard deviation, indicating stable and robust performance.

#### 5.3.3.2 Model Complexity

The proposed model has significantly lower complexity compared to ResNet50 and AlexNet. Table 5.6 summarizes the architectural aspects of the three CNN models. While ResNet50 has 50 hidden layers and over 23 million trainable parameters, AlexNet has 8 hidden layers with over 41 million trainable parameters. In contrast, the proposed model has 5 hidden layers with only 234,981 trainable parameters. This highlights the efficiency and simplicity of the proposed model.

TABLE 5.6: Comparative analysis of the architectural aspects among the evaluated CNN models.

Model	Layer	Trainable parameters	Training time/epoch
Alexnet	8	41,454,121	8-13s
ResNet50	50	23,628,677	25-56s
Proposed Model	5	234,981	5-6s

### 5.3.3.3 Execution Time

The proposed model demonstrates faster execution times compared to ResNet50 and AlexNet. A comparison of the single epoch execution time of the three models is done in the Google Colab environment and depicted in Figure 5.23. In a single epoch, ResNet50 with batch size 32 requires the highest execution time of 56 seconds, which reduces to 30 seconds for batch size 64 and 25 seconds for batch size 128. AlexNet's execution times are also higher, with 13, 10, and 8 seconds for batch sizes 32, 64, and 128, respectively. On the other hand, the proposed model achieves much faster execution times, with 6, 5, and 5 seconds for the same batch sizes.

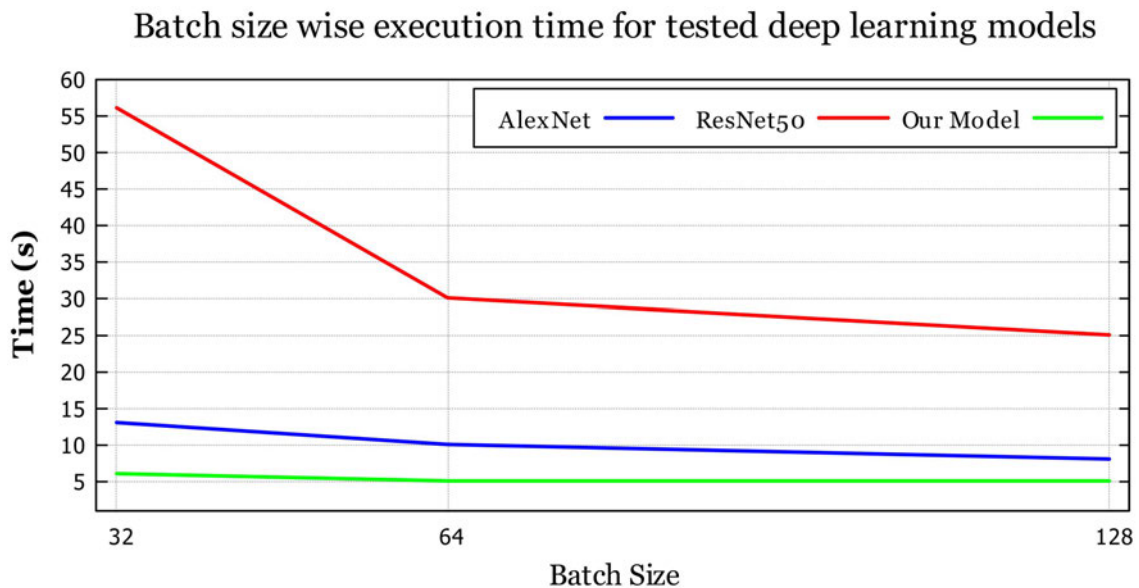


FIGURE 5.23: Comparison of the execution times of the three evaluated CNN models for different training batch sizes.

In summary, the proposed model offers superior classification performance with a simpler architecture and faster execution times compared to ResNet50 and AlexNet. These findings highlight the efficiency and effectiveness of the proposed model for brain signal data classification tasks.

### 5.3.3.4 Loss vs. accuracy graph

The loss vs. accuracy curves for the proposed model, ResNet50, and AlexNet provide further insights into their performance and stability on the spectrogram image dataset.

Figs. 5.24, 5.25 and 5.26 show the loss vs. accuracy graph for the proposed models, ResNet50 and AlexNet, respectively. Figure 5.24 depicts that the proposed model exhibits a smooth learning curve, with both training and validation losses steadily decreasing as the number of epochs increases. Accuracy also shows a consistent improvement, approaching 1 (100%) as the epochs progress. These characteristics indicate the stability of the proposed model on the dataset, and the convergence of loss and accuracy suggests that the model effectively learns from the data without overfitting.

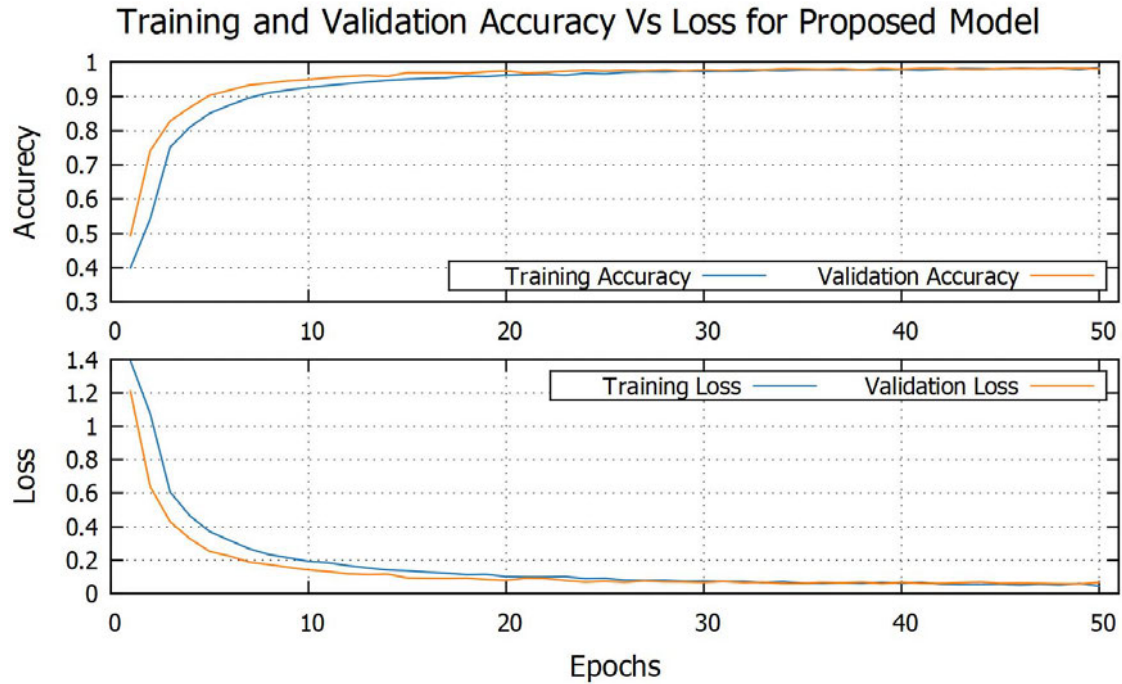


FIGURE 5.24: The evolution of accuracy and loss across epochs during the training and validation of the proposed model.

In contrast, AlexNet and ResNet50 exhibit consistent and gradually improving training losses and accuracy as epochs progress. However, their validation losses and accuracy exhibit pronounced fluctuations, indicating instability. When comparing the two models, it becomes evident that ResNet50 displays relatively lower instability in validation loss changes over epochs compared to AlexNet. Nevertheless, both models experience considerable fluctuations in validation accuracy throughout the training process.

### 5.3.3.5 Binary classification using the proposed model

Finally, to further evaluate the proposed model's performance, we have conducted individual binary classification tasks on four disease datasets, namely PD vs. HC, ASD vs. HC, EP vs. HC, and SZ vs. HC, using 5-fold cross-validation. Table 5.7 presents the fold-wise sensitivity, specificity, precision, accuracy, and F1 score for the four binary classifications, employing the proposed model with three different batch sizes.

From Table 5.7, it's evident that the proposed model achieves exceptional performance in these binary classifications. For instance, in the PD vs. HC task, it achieves 100%

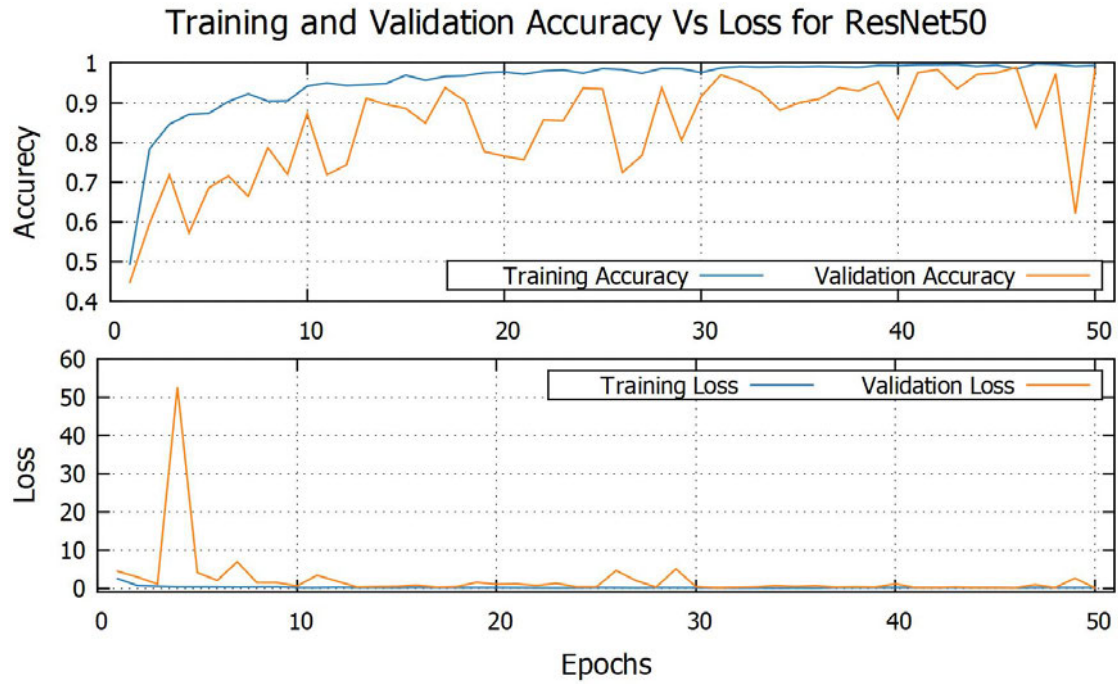


FIGURE 5.25: The evolution of accuracy and loss across epochs during the training and validation of the ResNet50 model.

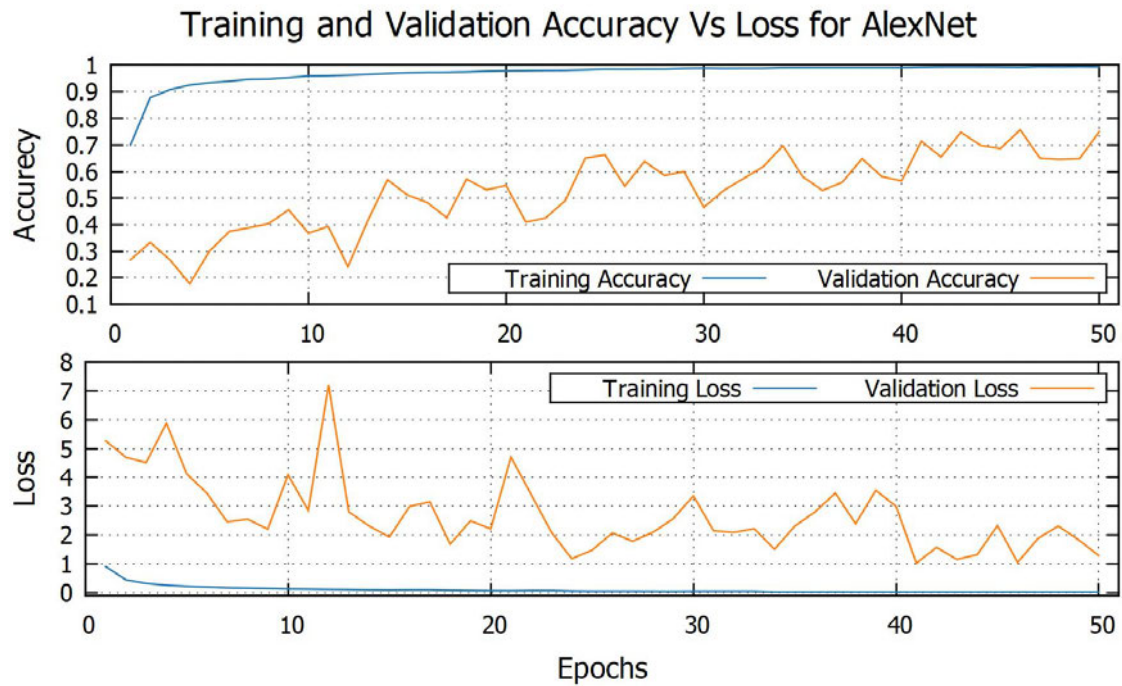


FIGURE 5.26: The evolution of accuracy and loss across epochs during the training and validation of the AlexNet model.

accuracy in fold 3 and 4 across all batch sizes. Similarly, in the ASD vs. HC classification, it achieves 99.91% accuracy in fold 3 with batch sizes 128 and 64. The EP vs. HC classification demonstrates the highest accuracy of 99.80% in fold 5 with batch size 64, while the SZ classification performs best with 99.49% accuracy in fold 2 with batch size

TABLE 5.7: The mean performance outcomes of the proposed model using a five-fold cross-validation approach, while employing various batch sizes, in a binary classification setting.

Disease	Batch Size 128					Batch Size 64					Batch Size 32				
	Sen%	Spec%	Prec%	F1	Acc%	Sen%	Spec%	Prec%	F1	Acc%	Sen%	Spec%	Prec%	F1	Acc%
PD vs Normal	99.64	99.88	99.89	1.00	99.77	99.64	99.89	99.88	1.00	99.77	99.75	99.64	99.68	1.00	99.71
ASD vs Normal	99.58	98.96	99.55	1.00	99.39	99.74	98.58	99.40	1.00	99.39	99.53	98.70	99.45	0.99	99.28
EP vs Normal	98.46	99.37	99.34	0.99	98.91	98.96	99.20	99.18	0.99	99.08	98.95	98.30	98.33	0.99	98.63
SZ vs Normal	99.11	98.96	98.77	0.99	99.02	99.08	99.01	98.85	0.99	99.05	98.76	99.06	98.87	0.99	98.92

64. These results underscore the model’s robustness and effectiveness in binary disease classification.

### 5.3.3.6 Comparison with existing researches

Table 5.8 presents a comprehensive comparison of the proposed model’s binary classification performance with existing works that have utilised the same datasets. It is evident that the proposed method has achieved superior results across all diseases when compared to the state-of-the-art approaches. This demonstrates the effectiveness and advancements provided by the proposed model in the field of binary disease classification using EEG data.

TABLE 5.8: Comparing our study with prior binary classification research on four specific diseases that utilised same datasets.

Task	Authors	Method	Accuracy%
ASD vs Normal	Alturki <i>et al.</i> [105]	DWT, ShanEn, ANN	98.20
	Ari <i>et al.</i> [141]	sparse coding image, CNN	98.88
	<b>This study</b>	<b>Spectrogram image, CNN</b>	<b>99.39</b>
EP vs Normal	Tawhid <i>et al.</i> [100]	ConvLSTM	98.79
	<b>This study</b>	<b>Spectrogram image, CNN</b>	<b>99.08</b>
PD vs Normal	Anjum <i>et al.</i> [197]	Linear-predictive-coding	85.70
	Qiu <i>et al.</i> [230]	Power spectral density, LeNet-5	96.31
	<b>This study</b>	<b>Spectrogram image, CNN</b>	<b>99.77</b>
SZ vs Normal	S.L. Oh <i>et al.</i> [150]	CNN	98.07
	Zülfikar <i>et al.</i> [231]	Hilbert Spectrum image, VGG16	98.20
	<b>This study</b>	<b>Spectrogram image, CNN</b>	<b>99.05</b>

## 5.4 Summary

In this chapter, a comprehensive system has been developed for the multi-classification of brain signal data related to multiple neurological disorders using a combination of T-F spectrogram images and both ML and DL techniques. The unique aspect of this system is its ability to classify multiple diseases within a single framework, addressing a gap in existing research.

The process begins with pre-processing the EEG data, including filtering for noise reduction and artefact removal, followed by segmentation into smaller segments. T-F-based spectrogram images are then generated from these segments using STFT, providing a visual representation of the EEG data.

In the ML-based approach, textural features are extracted from these spectrogram images using two histogram-based feature extractors, cCENTRIST and tCENTRIST. PCA is applied to reduce the dimensionality of these extracted features. Classification is carried out using a variety of ML algorithms, including  $k$ NN with different  $k$  values, SVM, LDA, and RF. The goal is to classify the features into one of five classes: ASD, EP, PD, SZ, or HC. The results indicate that the tCENTRIST feature extractor, coupled with SVM, achieved the highest classification accuracy of 88.78%. This was followed closely by  $k$ NN with an accuracy of 87.96%. These outcomes highlight the effectiveness of the system in accurately categorising EEG data related to neurological disorders.

In contrast, the DL-based approach, we have employed the spectrogram images as input data for a novel CNN model, which is evaluated using three different batch sizes for both multi-class (ASD vs. EP vs. HC vs. PD vs. SZ) and binary classification tasks (ASD vs. HC; EP vs. HC; PD vs. HC; and SZ vs. HC). The proposed CNN model is compared against two well-known CNN architectures, namely AlexNet and ResNet50, utilising the same three batch sizes. Extensive experimentation is conducted using a five-fold cross-validation approach to thoroughly evaluate the proposed method.

The experimental findings has revealed that the proposed CNN model has consistently outperformed the other two popular CNN models. It has achieved an impressive overall correct classification rate of 98.33% for four neurological disorders and an overall accuracy of 98.49% for multi-class classification, demonstrating its superior performance. Furthermore, the proposed CNN model has exhibited significantly shorter training times compared to AlexNet and ResNet50, making it a more efficient choice for practical applications. Additionally, the stability of the loss vs. accuracy graphs for the proposed CNN model has indicated its suitability for building a diagnostic system for multiple neurological disorders.

To further assess the performance of the proposed framework, binary classification tasks are conducted using the datasets related to the four diseases considered in this study. The results have showed that the proposed framework consistently outperformed state-of-the-art techniques that utilised the same datasets, highlighting its effectiveness and potential for clinical applications.

In conclusion, the obtained results reveal that this approach is robust and extensible and can be used in studies involving EEG data and signal processing techniques. Notwithstanding, the framework's high classification accuracy indicates that an EEG data segment as short as 3 seconds is enough for identifying these four diseases.

In the next chapter, we have addressed the third research question by developing a generic framework for EEG signal classification that will work irrespective of disease or dataset.

## Chapter 6

# Convolutional Neural Network Based Generic EEG Classification Framework

In this chapter, we have developed a unified standard platform for diagnosing different types of neurological disorders utilising electroencephalogram (EEG) signal data to address the third research problem (**RP3**). Here, we have developed a Generic EEG neural Network (GENet) framework based on convolutional neural networks that can identify various NDs from EEG. The proposed framework consists of several parts: (1) preparing data using channel reduction, resampling, and segmentation for the GENet model; (2) designing and training the GENet model to carry out important features for the classification task; and (3) assessing the proposed model's performance using different signal segment lengths, several training batch sizes, and the cross-validation technique on seven different EEG datasets of six distinct NDs named schizophrenia, autism spectrum disorder, epilepsy, Parkinson's disease, mild cognitive impairment, and attention-deficit/hyperactivity disorder. In addition, this study also investigates whether the proposed GENet model can identify multiple NDs from EEG. The proposed model achieved much better performance for both binary and multi-class classification compared to state-of-the-art methods.

The contents of this chapter is under review in *IEEE Transactions on Cognitive and Developmental Systems*.

### 6.1 Introduction

Neurological disorders (NDs) are a set of diseases that damage both the central and peripheral nervous systems and include everything from neurodegenerative to neurodevelopmental and psychiatric conditions [204]. There are more than 600 types of NDs in the world [1]. Commonly known NDs include schizophrenia (SZ), Parkinson's disease (PD), mild cognitive impairment (MCI), epilepsy (EP), Alzheimer's disease (AD), and dementia [204]. Additionally, cerebrovascular diseases such as stroke, migraine and headache-related diseases, brain tumours, and developmental disorders such as autism spectrum disorder (ASD) and attention deficit/hyperactivity disorder (ADHD) are also classified as NDs [204]. NDs have a huge impact on patients' quality of life and increase their mortality

risks. According to the World Health Organisation (WHO), one in three people may experience the onset of a neurological disorder (ND) at some stage of their lives, making it the second biggest cause of mortality and the primary source of disability [1]. In addition, it is believed that extreme poverty and growth stunting cause 43% of children under the age of five in middle and low-income countries to fall short of their developmental potential, which will result in financial losses and projected annual earnings that are 26% lower in their adulthood [1]. Early detection and treatment can improve the health status of ND patients; however, diagnosing ND at an early stage is difficult due to the lack of computer-aided diagnosis (CAD) systems and the shortage of mental health professionals.

The majority of these brain diseases are typically diagnosed by expert clinicians using visual examination of brain activity captured by various methods such as magnetic resonance imaging (MRI), functional magnetic resonance imaging (fMRI), positron emission tomography (PET), electrocorticography (ECoG), and EEG [22], [162], [163]. EEG is the most extensively utilised of these techniques due to its excellent temporal resolution, availability, non-invasiveness, economical set-up costs, and widespread availability for professionals [18]. EEG captures the electrical activities of neurones in the human brain as signal data, and those signals are then visually analysed by the expert clinicians for identification of NDs. This visual analysis process is subjective, lengthy, error-prone, and difficult due to the overlapping features for different diseases, which may lead to misdiagnosis [19]. Additionally, the availability of neurologically trained workers differs by a factor of 70 between high- and low-income countries (1 versus 70 for 100,000 people) [1]. As a result, the development of CAD systems will aid doctors and improve ND diagnosis at earlier stages.

Several researchers have published a number of studies on EEG signal classification in recent years [98], [141], [154], [155], [232]–[236], but they have a major drawback of adaptability. Because of the disease-specific features, a method proposed to deal with a specific EEG classification problem may not be totally efficient in its identical configurations for the EEG signal classification problem of another disease. This is due to the nonstationarity, non-linearity, and strong localisation in the temporal, spectral, and spatial dimensions of the EEG signal [22]. For every ND like SZ, PD, ADHD, MCI, EP, and ASD, the underlying characteristic of EEG has distinct periodical and statistical properties, making it challenging to examine with a detection method created for a different ND. Therefore, the motivation of this research is to provide a unified process for EEG signal classification that is adaptable and effective for a wide range of EEG challenges.

With the advancement of technology, CAD has become an important part of the medical industry. Several studies have been conducted to diagnose NDs using EEG data. EEG signal classification techniques can be broadly classified into two categories based on the used feature extraction and classification approaches, namely machine learning (ML)-based classification and deep learning (DL)-based classification. In ML-based techniques, handcrafted features like statistical and nonlinear parameters are extracted from the time, frequency, and time-frequency domains, and different ML-based classifiers are used to perform categorisation on those extracted features. ML-based classification of EEG signals

is carried out in several studies for identification of SZ [92], [154], [190], MCI [98], PD [232], ASD [79] and ADHD [237]. This process requires experts in those feature domains for the analysis of EEG data.

In DL-based classification, several DL models exist, like convolutional neural networks (CNN), long short-term memory (LSTM), recurrent neural networks (RNN), and gated recurrent units (GRU), among which CNN is widely used for image and signal processing, natural language processing, and data analytics [90]. CNN is generally less sensitive to noise and can extract useful information from noisy input [222]. Although CNN has been proven extremely effective for image classification, it has also demonstrated efficiency in EEG signal categorisation. Previously, CNN-based EEG data classification was completed for SZ [155], EP [92], [233], PD [92], [198], [234], ASD [90], [92], [141], MCI [235] and ADHD [236] and had good classification accuracy. However, those studies focused on single disease identification, which makes their multi-disease applicability an issue. Moreover, most of the studies have converted the EEG signals to visual representations or extracted handcrafted features before classifying them using the CNN model. Due to this handcrafted feature extraction and signal visualisation, the CNN model cannot learn the significant features that it can extract from the raw EEG data. This study addresses this gap by using raw EEG signal data as input for the CNN model.

In this study, we have developed a CNN model based on the Generic EEG Neural Network (GENet) that can categorise EEG signals from different NDs. Furthermore, we have used the raw EEG data as an input to the GENet model so that the deep learning process can self-learn the significant features from the EEG signal. At first, the raw EEG data are pre-processed to make those signals ready for input into the GENet model. To do that, we have reduced the total number of channels to 19 channels according to the international 10-20 standard [42], [238] and resampled the signals to 256 Hz. Then, to use the short-term features of the EEG signal, we have segmented the signals into small time frames. Here, we have tested three different segment lengths to check the impact of the signal segment length on the detection process. Finally, the GENet model was trained using those signals and performed the classification task. Seven different EEG datasets from six different NDs have been used to validate the proposed model. We have also performed a five-class classification using four datasets from among those seven datasets. A five-fold cross-validation technique is used to remove any biases in the results. Results from this study are compared with existing state-of-the-art studies that have used the same EEG datasets.

The major contributions of this study are compiled as follows:

1. A new framework is developed to address the challenge of multi-disease scalability in existing studies.
2. For the first time, a generic EEG classification framework using the CNN model is introduced for identifying different NDs, and the scalability of the framework is validated using seven distinct datasets representing six major NDs.

3. The proposed framework is extended for multi-disease classification problems to address the gap in this study type.
4. The proposed computerised system is validated using extensive experiments, including classifier performance evaluations, layer-wise classification feature visualisation, ablation studies, and comparative analysis with noteworthy recent research.
5. In both binary and multi-class classification situations, the suggested GENet model outperforms the existing methods.

Details of the proposed method and results are discussed in the sections below.

## 6.2 Materials and proposed methods

In this section, the proposed framework, the datasets used to validate the framework, and the evaluation parameters are introduced in detail. In subsection 6.2.1, we have discussed details of the datasets that are used in this study, followed by the different processing steps of the proposed framework in subsection 6.2.2. The proposed classification model is presented in subsections 6.2.3 and 6.2.4 and finally, different evaluation parameters and approaches are discussed in the subsection 6.2.5. Figure 6.1 illustrates the schematic diagram of the proposed framework. A detailed discussion of those steps is given in the below subsections.

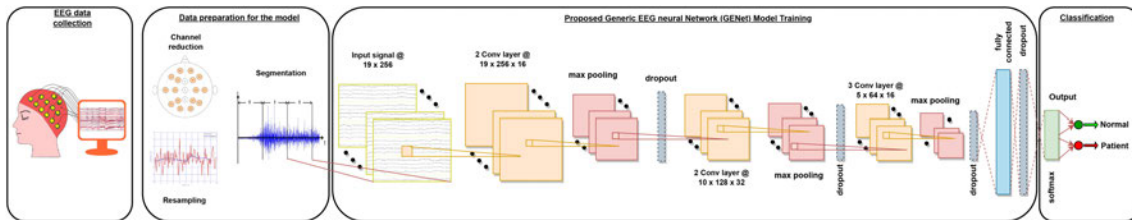


FIGURE 6.1: An schematic diagram of the developed framework and steps involved in the process. Four modules of the framework are discussed in four subsections 7.2.1, 6.2.2, 6.2.3, and 6.2.4.

### 6.2.1 EEG data collection

In this research, we have used seven different publicly available datasets for six different NDs, namely: ASD, ADHD, EP, PD, MCI, and two datasets for SZ. A brief description of those datasets is given below:

- The first schizophrenia dataset (hereafter referred to as SZ1) that we have used in this study was collected from the Kaggle website [239]. It contains 81 subjects (49 SZ and 32 HC). EEG data are recorded from 64 channels at a sampling rate of 1024 Hz during the task of pressing a button.
- The second Schizophrenia Dataset (hereafter referred to as SZ2) is comprised of 28 subjects (14 age- and sex-matched subjects from the SZ and HC groups) that were

collected at the Institute of Psychiatry and Neurology in Warsaw, Poland [78]. The signals are recorded in their resting state at a sampling rate of 250 Hz from 19 channels of a standard 10-20 EEG electrode system.

- Dataset of MCI is collected from cardiac catheterisation units of Sina and Nour Hospitals, Isfahan, Iran [240]. This dataset consists of 27 subjects' resting-state EEG signals (11 MCI and 16 HC) that were recorded from 19 electrodes at a sampling rate of 256 Hz.
- The ADHD dataset is recorded in the Psychology and Psychiatry Research Centre at Roozbeh Hospital (Tehran, Iran). It has a total of 121 subjects, with 61 from the ADHD group and 60 from the control group. Visual attention task-based EEG recording is carried out on 19 channels using the standard EEG 10–20 system at a sampling frequency of 128 Hz.
- The epilepsy dataset is collected at Universidade Federal do Para, Brazil, with 14 subjects (7 EP, 7 HC) [215]. EEG data is recorded at a 256 Hz sampling rate from 20 channels while the subjects are in a resting state.
- For PD, a dataset from the University of Iowa, United States, is used here [197]. This dataset has a total of 28 subjects (14 age- and sex-matched subjects from each group). EEG signal data in the resting state is recorded from 64 channels at a sampling rate of 500 Hz.
- The autism spectrum disorder dataset consists of 16 subjects (12 ASD, 4 non-ASD), which were collected from King Abdulaziz University (KAU) Hospital, Saudi Arabia [177]. Resting-state EEG data is collected from 16 channels at a sampling frequency of 256 Hz.

Each dataset is chosen because of its distinctive underlying temporal and spectral characteristics, which are critical for the development of a uniform EEG categorisation model. But due to limited space availability, thorough descriptions of these datasets have been excluded. Table 6.1 provides a summary of the participants' demographic data for different datasets. Details of those datasets can be found in [78], [177], [197], [215], [239], [240].

### 6.2.2 Preparing data for the proposed model

In this step, we have completed some pre-processing of the EEG signals to make the data ready for input into the proposed model. Here, the pre-processing of the raw EEG signal consists of three sub-tasks: (i) picking the standard common channels to use in the classification process. (ii) resampling the signals, and finally (iii) segmenting the signals into small time-frame blocks. Details of those steps are discussed in the following subsections:

TABLE 6.1: Demographic information related to the datasets used in this research.

	SZ1 [239]	SZ2 [78]	MCI [240]	ADHD [241]	EP [215]	PD [197]	ASD [177]
Patients(P) (Male/Female)	49 (41/8)	14 (7/7)	11	61 (48/13)	7 (4/3)	14 (6/8)	12 (9/3)
Normal(N) (Male/Female)	32 (26/6)	14 (7/7)	16	60 (50/10)	7 (4/3)	14 (6/8)	4 (4/0)
Patients Age range	40.02 ± 13.7	28.1 ± 3.7	66.4 ± 4.6	9.62 ± 1.75	32.86 ± 9.51	70.5 ± 8.35	12.5 ± 3.91
HCs Age range	38.38 ± 13.7	27.75 ± 3.15	65.3 ± 3.9	9.85 ± 1.77	32.86 ± 9.51	70.5 ± 8.35	11 ± 2.49
Sampling Frequency	1024	256	256	128	256	500	256
Resampled Frequency	256	256	256	256	256	256	256
Recorded no of channel	64	19	19	19	20	64	16
Used no of channel	19	19	19	19	19	18	16
<b>Number of samples generated after signal segmentation</b>							
1 second segment (P/N)	14184/9324	15457/12716	21009/29931	9404/7466	3744/3707	2606/2657	11486/4848
2 second segment (P/N)	7083/4655	7725/6356	10503/14960	4683/3717	1872/1853	1299/1326	5737/2421
3 second segment (P/N)	4728/3108	5146/4235	6999/9972	3117/2471	1248/1235	864/881	3825/1612

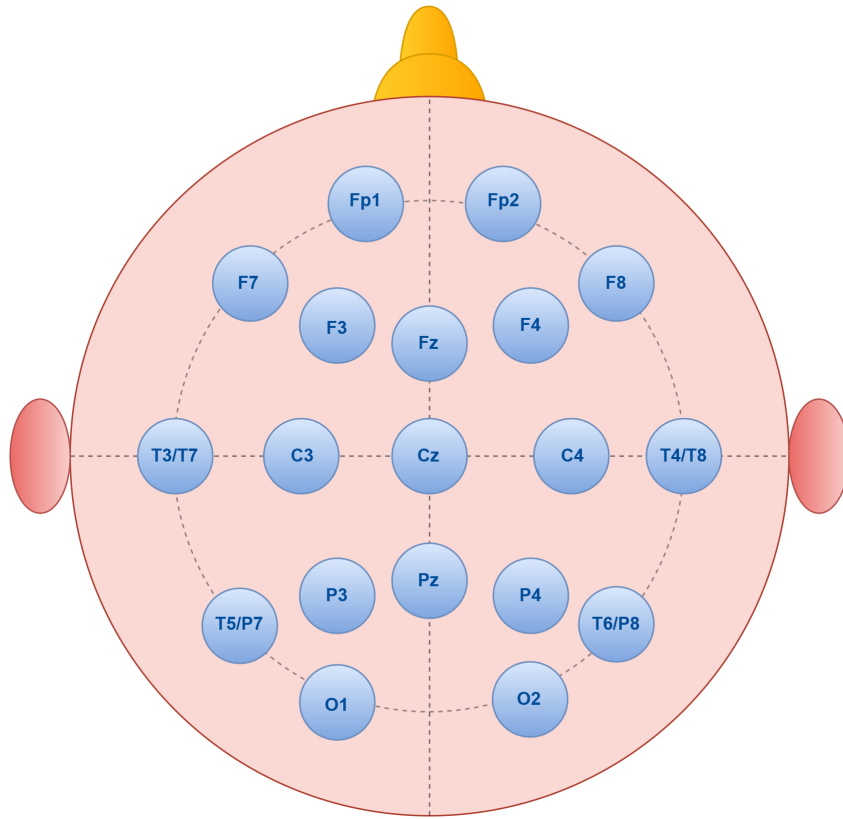


FIGURE 6.2: Standard electrode locations used for EEG data recording using the international 10-20 system.

### 6.2.2.1 Channel reduction to use standard channel data

From Table 7.1, we see that the number and position of the recording channels vary from dataset to dataset. To prepare those data for input into the proposed CNN model, we have selected the channels that are common to the datasets and also standard for EEG signal analysis. To do so, we have selected the most widely used 19 channels (Fp1, Fp2, F3, F4, F7, F8, C3, C4, T3/T7, T4/T8, P3, P4, T5/P7, T6/P8, O1, O2, Fz, Cz, Pz) from the international 10-20 system [42], [238] as shown in Fig 6.2. For the PD dataset, although it has recorded 64 channels, it was missing the Pz channel in those 64 channels,

and for the ASD dataset, the original dataset only contains 16 channels of EEG recording. As a result, we modified our proposed model to accept 18 and 16-channel data as input for the classification of PD and ASD, respectively.

### 6.2.2.2 Resampling the signals to a standard frequency

After channel selection, the next thing we did was resample all the datasets to a common frequency band so that they could be input into the proposed model. From Table 7.1 we can see that four datasets have a 256 Hz sampling rate, which is a widely used sampling frequency for EEG data and computationally less expensive compared to high-frequency bands [200]. We have also chosen this frequency band as the standard for the proposed model and converted all other datasets to a 256 Hz sampling rate.

### 6.2.2.3 Segmentation of the EEG signals

Data scarcity is a major issue in the field of EEG signal analysis using deep learning-based techniques. This issue is often solved by researchers using segmentation techniques. In this process, original EEG data are segmented into small informative segments and given the same level as the original one, which results in an increase in data sample size with an equal ratio [79], [153]. In this study, we have tested three different segment lengths (one second (1s), two seconds (2s), and three seconds (3s)) to check the effect of segments on the classification process as well as the minimum length of the EEG signal, which is enough for representative feature extraction and disease classification. In the bottom three rows of Table 7.1, we have given the total number of samples generated after segmentation of 1s, 2s, and 3s, respectively.

### 6.2.3 Proposed Generic EEG neural Network (GENet) model

In this study, we have developed a CNN model named GENet to perform classification of the raw EEG signal data. We have used the CNN model as it is usually less sensitive to noise and can extract useful information from noisy input by learning suitable features on its own using convolutional kernels, filtering, pooling, and nonlinear activation operations, and classifying data into different categories [222]. An architectural diagram of the proposed GENet model is shown in Figure 6.3.

The GENet model contains seven convolution (Conv2D) layers, three max-pooling (MaxPooling2D) layers, four dropout layers, and a fully connected (FC) layer. Table 6.2 lists the details of the configuration of those layers. The Conv2D layer consists of multiple kernels for feature extraction, and the local connection and weight sharing characteristics are used to reduce network parameters and overfitting. Conv2D layer operations can be defined using (6.1) which involves multiplying input data with a convolutional kernel and adding an offset, with the kernels sequentially scanning the input data of the upper layer [242].

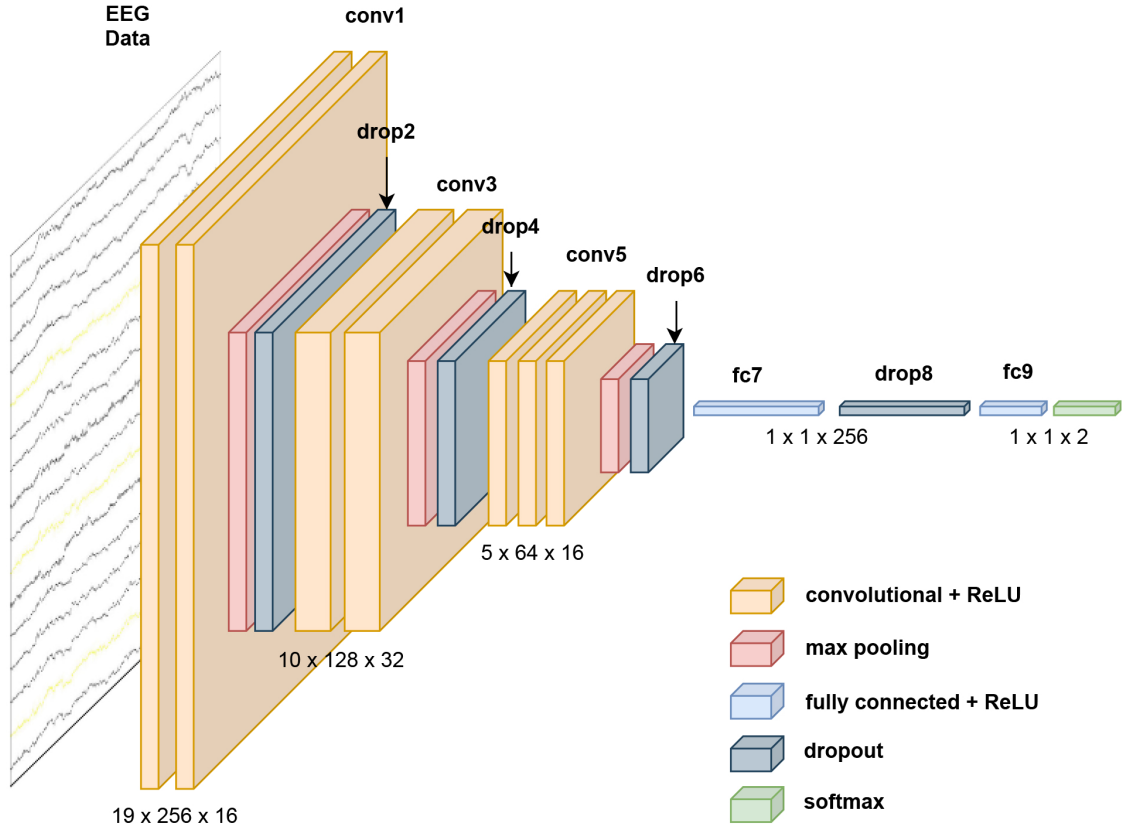


FIGURE 6.3: GENet: the proposed CNN model.

$$y(i, j) = \sum_{k=1}^n \sum_{l=1}^m \omega(k, l)x(i - k, j - l) + b \quad (6.1)$$

Where  $y(i, j)$  is the  $i^{\text{th}}$  row and  $j^{\text{th}}$  column output feature map,  $w(k, l)$  is the filter weights,  $x(i - k, j - l)$  is the input data, and  $b$  is the bias term. The first two Conv2D layers of the GENet model have 16 filters with a kernel size of  $(3 \times 3)$  and a stride of one pixel. After each convolutional layer, the activation function is utilised to activate the node's summed input. Here, Rectified Linear Unit (ReLU) is used, which has a linear identity for all positive values and assigns zero to all negative values using (6.2) on input  $x$  [242]. ReLU has the benefit of good generalisation with less computational cost.

$$R(x) = \max(0, x) \quad (6.2)$$

Following those two Conv2D layers is a max-pooling layer with a pool size of  $(1 \times 2)$  and a stride of  $(2 \times 2)$ . Pooling layers are used to downsample the output from the convolution layer to reduce the dimensionality of the feature maps and introduce some degree of translation invariance [242]. The most common pooling operation is max pooling, which selects the maximum value from a local neighbourhood using (6.3).

$$y_{i,j,k} = \max_{m,n} x_{i \times s + m, j \times s + n, k} \quad (6.3)$$

where  $y_{i,j,k}$  is the output of the  $k^{th}$  feature map at position  $(i, j)$ ,  $x_{i \times s + m, j \times s + n, k}$  is the input at position  $(i \times s + m, j \times s + n)$  and the  $k^{th}$  feature map, and  $s$  is the stride.

Following the pooling layer, we have used a 25% dropout layer to regularise the CNN model and avoid overfitting issues. At each training epoch, a random portion of the layer's nodes are dropped out (set to zero) via Dropout. As a result, the risk of overfitting is reduced, and the network is forced to learn more robust features.

The third and fourth Conv2D layers have 32 filters with  $(3 \times 3)$  kernels and one pixel stride. These two Conv2D layers are also followed by a MaxPooling2D layer with pool size and stride, both of which are  $(2 \times 2)$ , and a 25% dropout layer. The fifth, sixth, and seventh Conv2D layers have 16 filters each with a kernel of  $(3 \times 3)$  and one pixel stride. Then there is a MaxPooling2D layer with a pool and stride of  $(2 \times 2)$ , followed by a dropout layer of 25%.

The FC layer connects all the neurons from the previous layer to the output layer. It accepts flattened output from the convolutional layers and performs a linear transformation of the input followed by an activation function [242]. The internal equation of the FC layer can be denoted as (6.4).

$$y_k = \sigma\left(\sum_i w_{i,k}x_i + b_k\right) \quad (6.4)$$

where  $y_k$  is the  $k^{th}$  neuron's output,  $\sigma$  is the activation function,  $w_{i,k}$  is the weight parameter connecting the  $i^{th}$  input neuron to the  $k^{th}$  output neuron,  $x_i$  is the  $i^{th}$  neuron's input, and  $b_k$  is the bias parameter for the  $k^{th}$  output neuron. We have used an FC layer with 256 neurons that is activated by ReLU functions, followed by a 50% dropout layer. Finally, the classification layer uses 2 or 5 neurons, based on the number of classes for classification (binary or multi). The softmax activation function is used for this layer, which uses (6.5) for internal calculation.

$$y_i = \frac{e^{x_i}}{\sum_{j=1}^n e^{x_j}} \quad (6.5)$$

where  $y_i$  is the  $i^{th}$  element of the output vector,  $x_i$  is the  $i^{th}$  element of the input vector, and  $n$  is the size of the input vector.

We have used categorical cross-entropy as the loss function that measures the cross-entropy loss between the labels and predictions and is used in classification problems with two or more label classes. To minimise the loss function, the Adam algorithm, a stochastic gradient descent (SGD) technique based on the adaptive learning rate of the first- and second-order moments of the gradient average, is used as the optimiser. This approach typically accelerates the model's convergence and is more resistant to noise and sparse gradients.

#### 6.2.4 Classification using proposed GENet model

After feature extraction and GENet model training, the classification process is carried out on the test cases in the final dense layer. For binary classification, this layer contains

TABLE 6.2: Architectural details of the GENet model.

Layer	# Filter	Size	Activation	Option
Conv2D	16	3x3	ReLU	padding=same
Conv2D	16	3x3	ReLU	padding=same
MaxPooling2D		1x2		stride=2x2
Dropout				25%
Conv2D	32	3x3	ReLU	padding=same
Conv2D	32	3x3	ReLU	padding=same
MaxPooling2D		2x2		stride=2x2
Dropout				25%
Conv2D	16	3x3	ReLU	padding=same
Conv2D	16	3x3	ReLU	padding=same
Conv2D	16	3x3	ReLU	padding=same
MaxPooling2D		2x2		stride=2x2
Dropout				25%
Flatten				
Dense	256		ReLU	
Dropout				50%
Dense (classifier)	2 (binary)/ 5(multi)		softmax	
Total trainable params: 943,906				

two neurons, while for multi-class classification, it has five neurons, as we have conducted a five-class classification process by modifying the last layer. To evaluate the performance of the GENet model in binary classification, we have tested it on seven different EEG datasets from six distinct NDs shown in Table 7.1. Furthermore, to assess the performance of the proposed framework on multi-class classification, we have performed a multi-disease detection using four of the tested datasets (SZ2, MCI, EP, and ADHD) from Table 7.1. In this case, we have merged all the HC subjects from those four datasets into one group (HC) and performed a five-class classification process (SZ vs. MCI vs. EP vs. ADHD vs. HC).

### 6.2.5 Performance evaluation criteria

The number of correct classifications may depend on the training set and the test set, so cross-validation is one way to identify a model's prediction accuracy and decrease overfitting [90]. A technique to achieve this is known as the  $k$ -fold cross-validation, which starts by randomly dividing the dataset into  $k$  subsets of equal or nearly equal size, with  $k-1$  subsets used for training and the rest used for testing. This training and testing process is repeated  $k$  times ( $k$ -fold), using a different subset for testing every time. Here, we have evaluated the models' performance using a 5-fold cross-validation technique.

Finally, to report the performance of the proposed framework, we have used five well-known evaluation parameters in this field, which are sensitivity (Sen) or recall, specificity

(Spec) or selectivity, precision (Prec), F1 score (F1), and accuracy (Acc). We have also considered the receiver operating characteristic (ROC) curve for validation purposes. These criteria can be used to anticipate how classifiers would behave on test data [91], [98], [154], [181], [194], [243].

## 6.3 Results and discussion

In this research, a generic framework is proposed for the classification of EEG data from patients and healthy subjects. To validate the proposed model's scalability, we have tested it on seven distinct EEG datasets from six different NDs. The next subsection discusses the detailed experimental setup for the proposed system, and the detailed results of the experiments are discussed in the later subsections.

### 6.3.1 Experimental setup

As stated previously in the methodology section, after pre-processing, we have segmented the EEG signals into small time frames. To check the impact of the segment length on the proposed model, we tested three different segment lengths: 1s, 2s, and 3s. After segmentation, an EEG signal trial forms a matrix of  $s \times c$ , where  $s$  is the signal length and  $c$  is the number of channels.  $s$  can be defined by  $l \times f$ , where  $l$  is the segment length (1s, 2s, or 3s) and  $f$  is the sampling frequency (256 Hz). Therefore, the CNN input matrix sizes for 1s, 2s, and 3s segment lengths are  $256 \times 19$ ,  $512 \times 19$ , and  $768 \times 19$ , respectively.

Afterward, the resulting signal populations are arbitrarily divided into five equal or nearly equal subparts to carry out the 5-fold cross-validation for all the datasets. In this cross-validation scheme, four out of five subparts are used to train the proposed model, and the rest are used to validate it. This approach is repeated five times to verify that each segment is used exactly once for testing the models. The results of this 5-fold cross-validation method demonstrate the model's overall performance on the entire dataset while also reducing over-fitting and biasing issues.

The experiments are performed on a computer equipped with an Intel(R) Core(TM) i5 CPU @ 1.7 GHz processor, 8 GB of memory, Windows 10 64-bit operating system, and Google Colab<sup>1</sup>. The GENet model is trained for 50 epochs, as it starts overfitting after that. Training batch size selection is done using mini-batch mode, a popular batch size selection approach for faster learning [90]. We have tested four different batch sizes (32, 64, 128, and 256) during the training process of the proposed model.

### 6.3.2 Layer-wise feature visualisation of GENet

T-distributed stochastic neighbour embedding (t-SNE) is a non-linear dimension reduction approach that projects multivariate data on a 2D or 3D space in an unsupervised manner [244]. We have used t-SNE visualisation to generate two-dimensional (2D) representations of the extracted features from each layer of the GENet model. This technique helps to

---

<sup>1</sup><https://colab.research.google.com/notebooks/intro.ipynb>

visualise the model’s layer-wise extracted features in the classification process. Figure 6.4 illustrates the feature visualisation from input to output layer of the GENet model for the tested SZ2 dataset. For the sake of convenience, we have included a single fold’s t-SNE plot with 300 test subjects. The figures show the 2D map of the multidimensional feature vectors, with each symbol representing an individual sample from the test set.

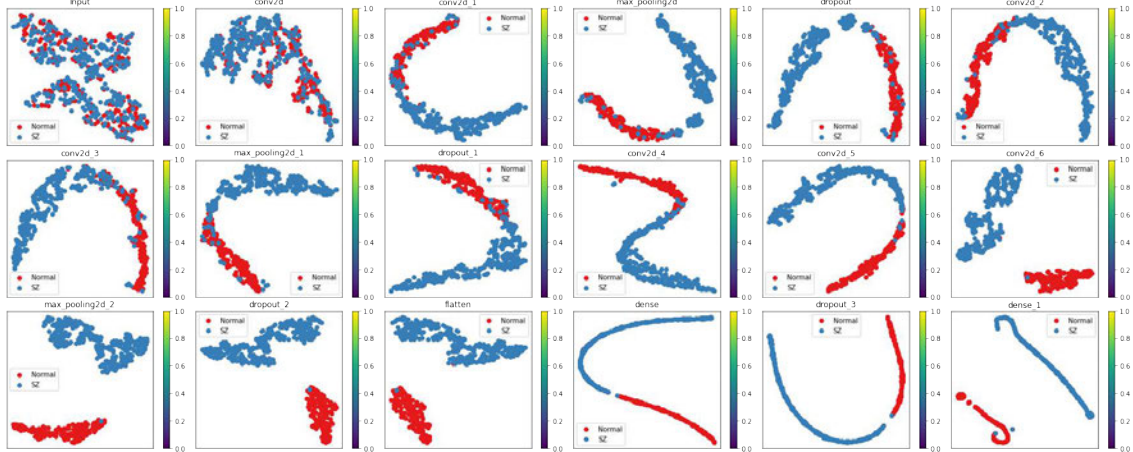


FIGURE 6.4: Layer-wise classification process visualisation of the GENet model using t-SNE images. Here, features from test subjects are plotted from the input layer to the output layer for the tested SZ2 dataset. At the input layer, there was no clear cluster between two classes (SZ vs. Normal), but as the data progressed from the hidden layers to the output layer, it formed two clearly separable clusters of two classes.

A t-SNE plot is a useful way to visualise how the extracted features of a classifier from different categories cluster together and are well separable or not [244]. From Figure 6.4, we can see that in the input layer projection, all of the feature points from the two classes are randomly mixed up, and as the data passes through the layers of the GENet model, it is clustered into two classes. Finally, in the t-SNE plot of the output layer, we can see the completely separable clusters of the two groups (SZ vs. HC). Hence, from these t-SNE images, we can claim that our proposed GENet model performs well on EEG data analysis for anomaly detection.

### 6.3.3 Results

We have performed two types of classification tasks: binary and multi-class classification. The detailed results of these two experiments are discussed below:

#### 6.3.3.1 Binary classification

For binary classification, we have tested the performance of the proposed model on seven different datasets from six distinct NDs. To check the impact of segment length, three different segment lengths are tested: 1s, 2s, and 3s, and those results are compared. Furthermore, to test the impact of the training batch size on the GENet model, we have used four separate batch sizes (32, 64, 128, and 256) to train the model. Figure 6.5 plots

the 5-fold average accuracy comparison for three segment lengths and four batch sizes on the tested datasets. From the figure, we can see that for most of the cases, a segment length of 1s produces the best classification accuracy compared to the other two segment lengths. For this reason, further discussions of this study are based on 1s segment length.

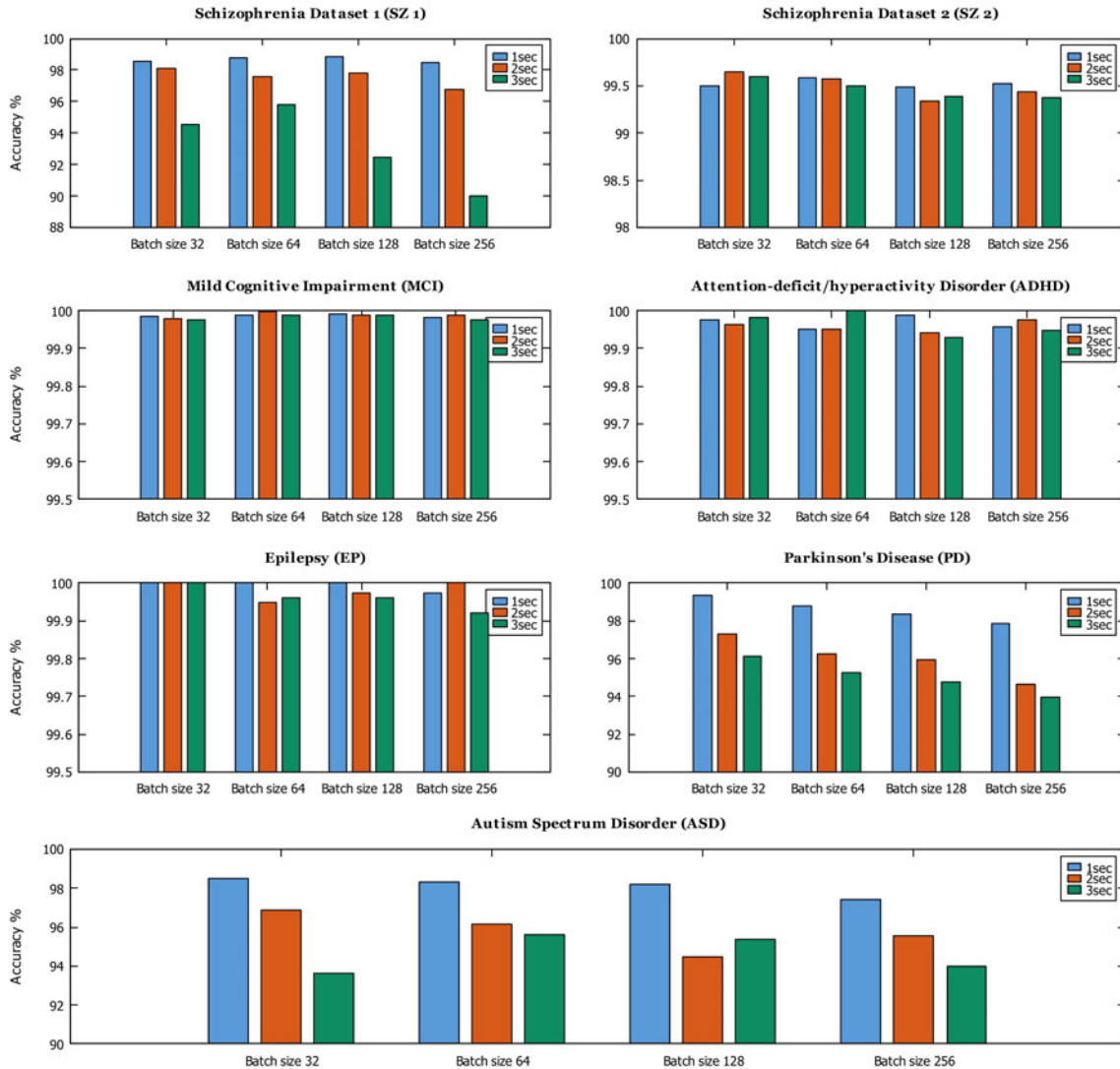


FIGURE 6.5: Accuracy comparison of the GENet model for the three tested signal segment lengths (1s, 2s, and 3s). Seven subplots represent seven tested datasets (SZ1, SZ2, MCI, ADHD, EP, PD, and ASD). In each subplot, four groups of bars represent four training batch sizes (32, 64, 128, and 256).

To further evaluate the performance of the GENet, we have used four evaluation parameters that are popular in this field of study: sensitivity, specificity, precision, and F1 score. An experiment's sensitivity (also known as recall, hit rate, or true positive rate) refers to the classifier's ability to correctly distinguish patients from healthy people. On the other hand, the capacity of a test to correctly separate healthy participants from patients is referred to as specificity (also known as true negative rate or selectivity). Precision, also known as "positive predictive value" in the classification context, refers to the percentage

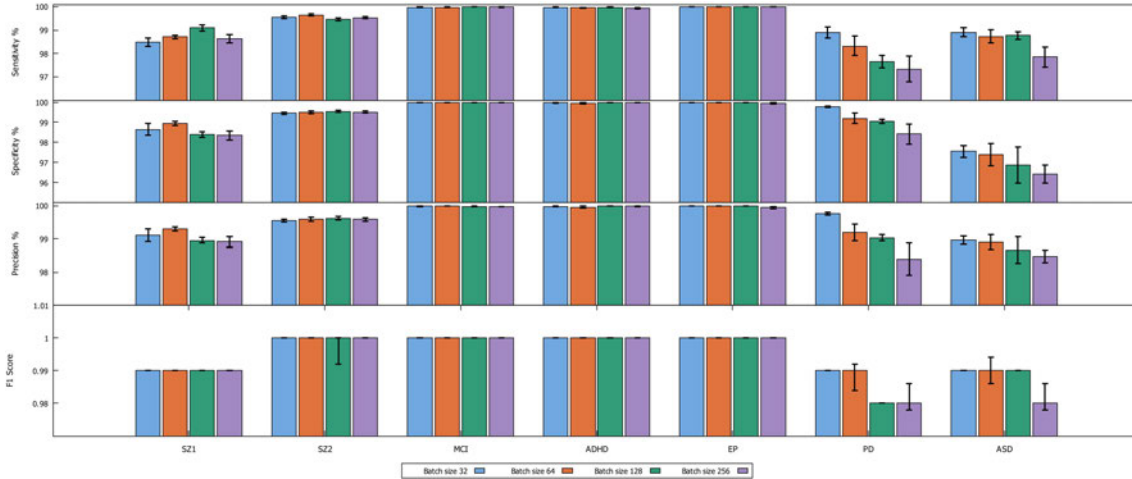


FIGURE 6.6: A comparison graph of the four evaluation parameters (Sen, Spec, Prec, and F1) with standard deviation for the GENet model. Each subplot represents an evaluation parameter, and the x-axis has the seven assessed datasets. For each dataset, we have four bars for four different training batch sizes (32, 64, 128, and 256).

of true patients in the retrieved patient group. Finally, the F1 score is calculated by combining the precision and recall values of a test result to determine the test’s performance in finding patients. It is the harmonic mean of precision and recall. The performance of a classification framework expects high values for those parameters.

TABLE 6.3: The GENet model’s performance, averaged over five-fold cross-validation and presented with standard deviations, across seven evaluated datasets while using four different training batch sizes.

Batch size	Datasets							
		SZ1	SZ2	MCI	ADHD	EP	PD	ASD
32	Sen%	98.49±0.41	99.54±0.14	99.98±0.01	99.98±0.03	100.00±0.00	98.90±0.54	98.91±0.42
	Spec%	98.64±0.65	99.45±0.14	99.99±0.01	99.97±0.04	100.00±0.00	99.77±0.09	97.55±0.65
	Prec%	99.10±0.42	99.55±0.11	99.99±0.01	99.98±0.03	100.00±0.00	99.77±0.08	98.96±0.28
	F1	0.99±0.00	1.00±0.00	1.00±0.00	1.00±0.00	1.00±0.00	0.99±0.01	0.99±0.00
	Acc%	<b>98.55±0.18</b>	<b>99.50±0.04</b>	<b>99.99±0.01</b>	<b>99.98±0.01</b>	<b>100.00±0.00</b>	<b>99.34±0.33</b>	<b>98.51±0.43</b>
64	Sen%	98.71±0.15	99.65±0.11	99.98±0.01	99.96±0.05	100.00±0.00	98.32±0.92	98.73±0.63
	Spec%	98.94±0.24	99.50±0.18	99.99±0.01	99.95±0.09	100.00±0.00	99.20±0.58	97.39±1.24
	Prec%	99.30±0.15	99.59±0.14	99.99±0.01	99.96±0.07	100.00±0.00	99.19±0.59	98.90±0.51
	F1	0.99±0.00	1.00±0.00	1.00±0.00	1.00±0.00	1.00±0.00	0.99±0.01	0.99±0.01
	Acc%	<b>98.80±0.08</b>	<b>99.58±0.11</b>	<b>99.99±0.01</b>	<b>99.95±0.06</b>	<b>100.00±0.00</b>	<b>98.76±0.72</b>	<b>98.34±0.63</b>
128	Sen%	99.10±0.31	99.45±0.14	100.00±0.00	99.98±0.03	100.00±0.00	97.66±0.60	98.77±0.38
	Spec%	98.40±0.29	99.54±0.12	99.99±0.01	100.00±0.00	100.00±0.00	99.05±0.27	96.87±2.03
	Prec%	98.95±0.19	99.62±0.10	99.98±0.02	100.00±0.00	100.00±0.00	99.03±0.20	98.67±0.89
	F1	0.99±0.00	1.00±0.00	1.00±0.00	1.00±0.00	1.00±0.00	0.98±0.00	0.99±0.00
	Acc%	<b>98.82±0.29</b>	<b>99.49±0.12</b>	<b>99.99±0.01</b>	<b>99.99±0.02</b>	<b>100.00±0.00</b>	<b>98.37±0.31</b>	<b>98.19±0.66</b>
256	Sen%	98.63±0.42	99.53±0.09	99.99±0.02	99.94±0.07	100.00±0.00	97.34±1.21	97.85±0.98
	Spec%	98.35±0.52	99.51±0.13	99.98±0.00	99.99±0.03	99.95±0.07	98.41±1.12	96.41±1.03
	Prec%	98.91±0.34	99.59±0.11	99.97±0.01	99.99±0.02	99.95±0.07	98.39±1.08	98.48±0.44
	F1	0.99±0.00	1.00±0.00	1.00±0.00	1.00±0.00	1.00±0.00	0.98±0.01	0.98±0.01
	Acc%	<b>98.51±0.22</b>	<b>99.52±0.03</b>	<b>99.98±0.01</b>	<b>99.96±0.03</b>	<b>99.97±0.04</b>	<b>97.87±0.76</b>	<b>97.42±0.91</b>

Table 6.3 lists the five-fold average values with standard deviation (SD) of the performance parameters for the tested datasets with four different training batch sizes. From

Table 6.3, we can see that for most of the datasets, batch size variation has not had that much impact on the model’s performance except for PD and ASD, where parameter values decrease with the increase in training batch size. For the tested dataset SZ 1, the highest sensitivity value of  $99.10(\pm 0.31)\%$  is achieved for batch size 128 while the best specificity and precision values of  $98.94(\pm 0.24)\%$  and  $99.30(\pm 0.15)\%$  ( $pm0.15$ ) are obtained for training batch size 64. A five-fold average highest accuracy  $98.82(\pm 0.29)\%$  is achieved using the training batch size of 128. In the case of the F1 score, all the tested training sizes produce the same value of 0.99. For dataset SZ 2, the highest values for the five evaluation parameters are  $99.65(\pm 0.11)\%$ ,  $99.54(\pm 0.12)\%$ ,  $99.62(\pm 0.1)\%$ ,  $1.00(\pm 0.00)$  and  $99.58(\pm 0.11)\%$  for the training batch sizes of 64, 128, 128, 256, and 64, respectively.

In MCI and ADHD datasets, our proposed model has achieved a five-fold highest accuracy of 99.99% with SDs of  $(\pm 0.01)$  and  $(\pm 0.02)$ , respectively. It has obtained  $100(\pm 0.00)\%$  sensitivity and 99.99% specificity and precision with SD  $(\pm 0.02)$  and  $(\pm 0.01)$ , respectively, in the classification performance for the MCI dataset. On the other hand, for the ADHD dataset, sensitivity is  $99.98(\pm 0.03)\%$  and specificity and precision values are  $100(\pm 0.00)\%$ . For both datasets, F1 scores are 1.00. Among the tested datasets, for the EP dataset, we have achieved an overall  $100(\pm 0.00)\%$  classification accuracy for three batch sizes (32, 64, and 128). For batch size 256, the performance of the model has decreased to  $99.97(\pm 0.04)\%$ .

As mentioned in Table 6.1, both the PD and ASD datasets have a smaller number of channels than other datasets (18 and 16 channels for PD and ASD, respectively), so we have modified the input layer of the GENet model to perform the training and classification processes. For those two datasets, categorisation performance decreases with the increase in training batch size. For the PD dataset, the highest average accuracy  $99.34(\pm 0.33)\%$  is achieved using batch size 32, and for ASD it is  $98.51(\pm 0.43)\%$ . The highest sensitivity, specificity, precision, and F1 score values are  $98.90(\pm 0.54)\%$ ,  $99.77(\pm 0.09)\%$ ,  $99.77(\pm 0.08)\%$  and  $0.99(\pm 0.01)$ , respectively, for the PD dataset and  $98.91(\pm 0.42)\%$ ,  $97.55(\pm 0.65)\%$ ,  $98.96(\pm 0.28)\%$  and  $0.99(\pm 0.00)$ , respectively, for the ASD dataset.

The ROC curve is a good indicator of the classifier’s performance. If the curve of a classifier is close to the point (0, 1), then it is considered to be a good classifier, while if the curve is close to or below the diagonal line, then it is considered to be a poor classifier. We have plotted the ROC curve of the GENet model for the seven tested datasets, as shown in Figure 6.7. From the figure, we can see that for EP, MCI, and ADHD datasets, the proposed model achieved perfect classification performance, and for other datasets, the performance is near perfect. Such large areas under the ROC curves also prove the scalability of the proposed EEG classification framework.

### 6.3.3.2 Multi-class classification

To further assess the performance of the proposed GENet model, we have performed a multi-class classification using four datasets among the seven tested datasets that have similar data sampling records. For this purpose, we have used the SZ 2, MCI, EP, and ADHD datasets and modified the final layer of the GENet model to perform a five-class

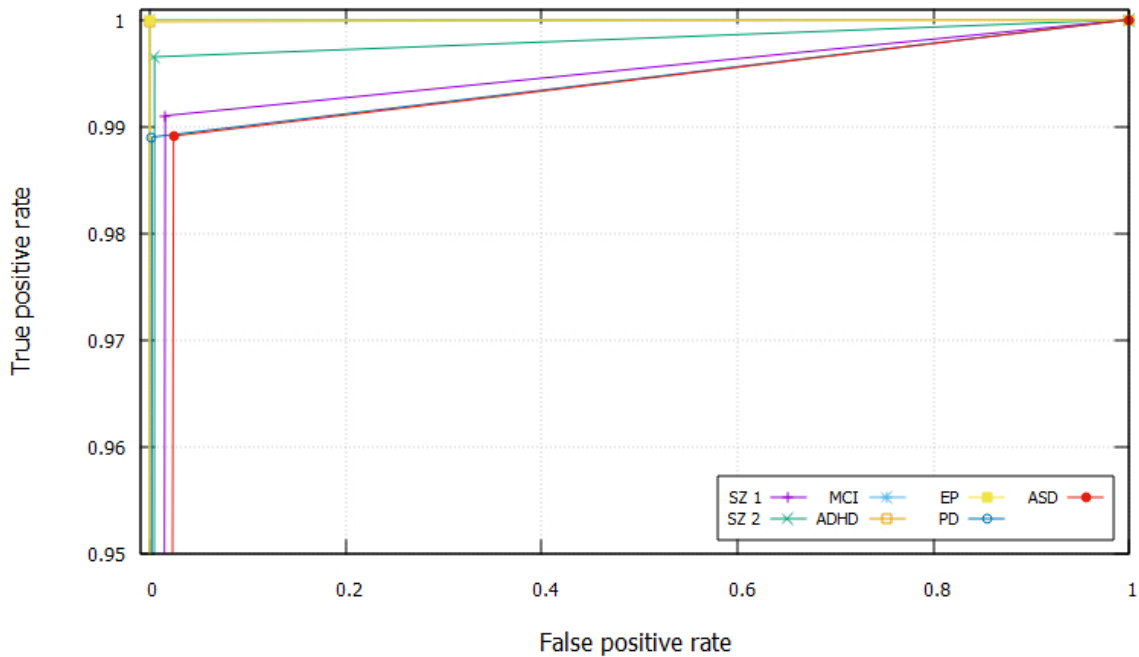


FIGURE 6.7: ROC graph of the GENet model on tested datasets.

(SZ vs. MCI vs. EP vs. ADHD vs. Normal) categorisation task. This multi-class classification task is also evaluated using the five-fold cross-validation technique. The performance of this classification task is also measured using the same five parameters as for binary classification. Table 6.4 summarises the performance result of the GENet model for multi-class classification over five-fold and for four different batch sizes (32, 64, 128 and 256).

From Table 6.4, we can see that for multi-class categorisation using GENet, increasing the batch size increases the performance of the model. The proposed model has achieved an accuracy of  $99.75(\pm 0.07)\%$  with batch size 32, which has increased to  $99.81(\pm 0.04)\%$ ,  $99.83(\pm 0.02)\%$  and  $99.84(\pm 0.05)\%$  for batch sizes 64, 128, and 256, respectively. To further inspect the impact of batch sizes on the individual folds, we have plotted the sensitivity, specificity, precision, and accuracy values as a spider plot in Figure 6.8.

In the Figure 6.8, each axis of the graphs represents a testing fold, and the four coloured areas represent four different tested batch sizes. From the Figure 6.8, we can see that for a single fold, the highest sensitivity of  $99.87\%$  is achieved for fold 5 of batch size 256 and fold 2 of batch size 64, while the lowest sensitivity value of  $99.55\%$  is obtained for fold 1 of batch size 32. In case of specificity, the highest and lowest values are  $99.96\%$  for fold 2 with batch size 256 and  $99.88\%$  for fold 1 with batch size 32, respectively. Fold 4 of batch size 64 has produced the highest precision of  $99.92\%$  and fold 5 of batch size 32 has given the lowest precision value of  $99.64\%$ . A single fold with the highest accuracy of  $99.88\%$  is achieved for fold 2 of batch size 256, and the lowest accuracy of  $99.68\%$  is obtained for both folds 1 and 5 of batch size 32.

TABLE 6.4: The average performance results of the GENet model in a multi-class classification scenario, obtained through five-fold cross-validation.

<b>Batch Size</b>		<b>Sen%</b>	<b>Spec%</b>	<b>Prec%</b>	<b>F1</b>	<b>Acc%</b>
<b>256</b>	Normal	99.86	99.83	99.84	1.00	<b>99.84</b>
	SZ	99.59	99.93	99.60	1.00	
	MCI	99.95	99.99	99.96	1.00	
	EP	99.76	99.99	99.90	1.00	
	ADHD	99.90	99.99	99.92	1.00	
	<b>AVG</b>	<b>99.81</b>	<b>99.94</b>	<b>99.84</b>	<b>1.00</b>	
<b>128</b>	Normal	99.86	99.80	99.81	1.00	<b>99.83</b>
	SZ	99.46	99.94	99.68	1.00	
	MCI	99.96	99.98	99.94	1.00	
	EP	99.79	99.99	99.89	1.00	
	ADHD	99.95	99.98	99.86	1.00	
	<b>AVG</b>	<b>99.80</b>	<b>99.94</b>	<b>99.84</b>	<b>1.00</b>	
<b>64</b>	Normal	99.86	99.78	99.80	1.00	<b>99.81</b>
	SZ	99.43	99.93	99.62	1.00	
	MCI	99.94	99.99	99.96	1.00	
	EP	99.79	99.99	99.89	1.00	
	ADHD	99.90	99.99	99.88	1.00	
	<b>AVG</b>	<b>99.78</b>	<b>99.94</b>	<b>99.83</b>	<b>1.00</b>	
<b>32</b>	Normal	99.78	99.74	99.76	1.00	<b>99.75</b>
	SZ	99.27	99.91	99.51	1.00	
	MCI	99.91	99.98	99.94	1.00	
	EP	99.78	99.99	99.87	1.00	
	ADHD	99.92	99.96	99.60	1.00	
	<b>AVG</b>	<b>99.73</b>	<b>99.92</b>	<b>99.74</b>	<b>1.00</b>	

### 6.3.4 Discussion

In this study, a generic framework using the GENet model is proposed to classify NDs using EEG data. GENet is a CNN-based model that is designed to take raw EEG signal data as input and train its internal layers with the significant features of the data to perform classification tasks. To reduce the manual process in the classification steps, we have tried to develop a DL-based system so that it will extract and classify the features automatically. We have also tried to minimise the pre-processing steps by just segmenting the signals into small chunks and reducing the recording channels to make the EEG signals ready for the GENet model. To prove the multi-disease scalability of the proposed GENet model, we have evaluated it using seven different EEG datasets from six distinct NDs. We have tested two different datasets (SZ1 and SZ2) of the same disease (SZ) as well as five other datasets from five different diseases (MCI, ADHD, EP, PD, and ASD).

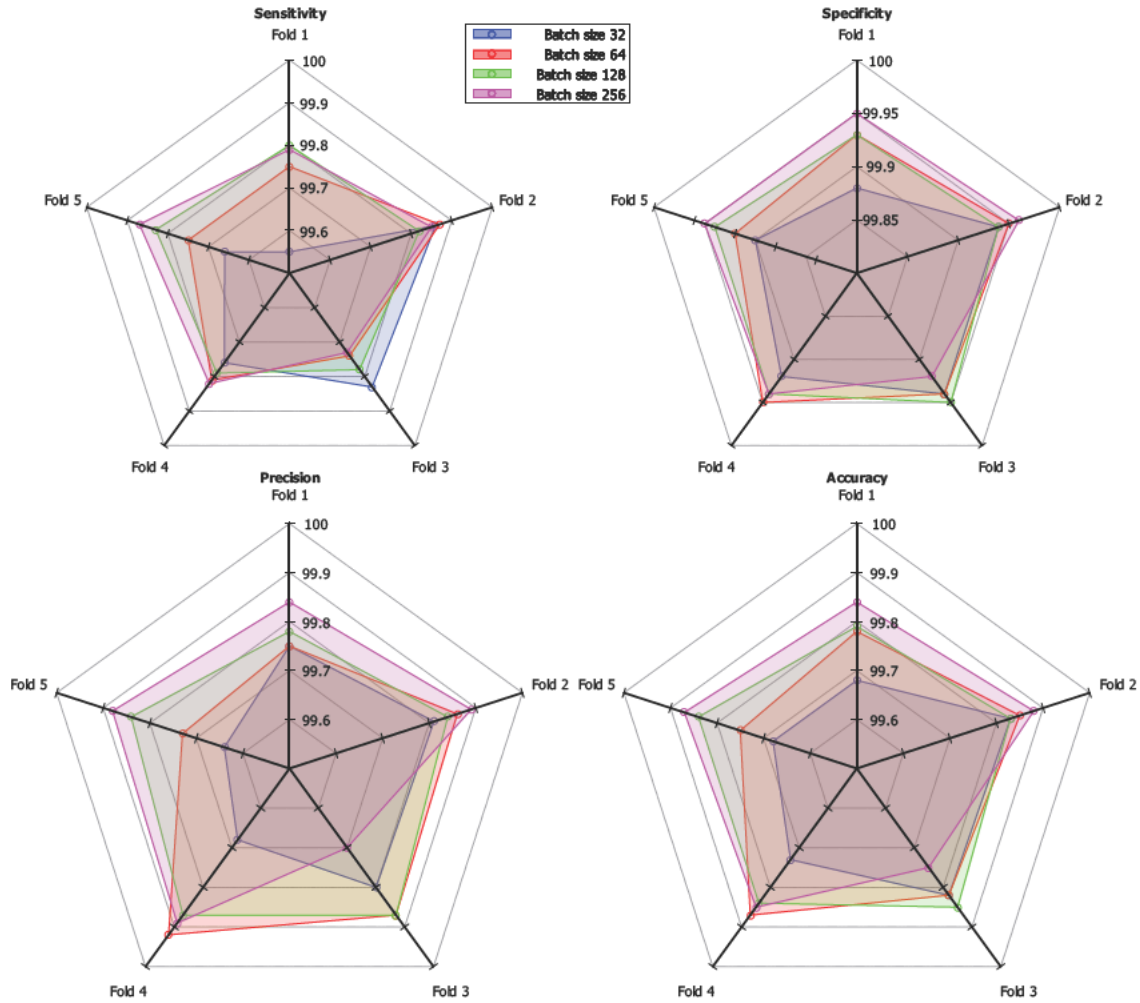


FIGURE 6.8: Spider plot visualisation for fold wise sensitivity, specificity, precision, and accuracy comparison of the GENet model for multi-class classification with different tested batch sizes. Data has five folds (Fold 1,2,...,5) and each polygon is a multivariate data point for a training batch size.

#### 6.3.4.1 Ablation study

Generally, an ablation study is a series of experiments in which parts of a machine learning system are removed or replaced to assess the effect of these parts on the system's performance. To validate the structure of the proposed GENet model, we have conducted ten different ablation studies using datasets SZ 1 and SZ 2, considering that the model will behave similarly for other datasets. In this ablation study, we have used the results of the GENet model on datasets SZ1 and SZ2 for batch sizes 64 and 128, respectively, as the baseline result and performed those ablation studies using the same setup. To conduct the ablation process, we have divided the proposed model into four different blocks for ease of experimentation. As shown in Table 6.2, every dropout layer divides the model into a block, so the first block consists of the first two Conv2D layers, the maxpooling2D layer, and the dropout layer. The second block consists of the second two Conv2D layers, the second maxpooling2D layer, the second dropout layer, and so on. The ablation experiment

settings and the obtained results are given in Table 6.5.

TABLE 6.5: Ablation study results on dataset SZ1 and SZ2.

Ablation methods	Accuracy %	
	SZ1	SZ2
<b>Baseline (no ablation)</b>	<b>98.82</b>	<b>99.58</b>
Removed 2nd block	97.57	99.13
Removed 3rd block	97.40	99.07
Removed both 2nd and 3rd block	81.05	97.63
Added a duplicate of 2nd block before 3rd block	98.12	98.94
Doubled the filters in first block	98.13	98.95
Doubled the filters in 2nd block	98.05	98.96
Doubled the filters in last block	98.16	98.97
Halved the filters in first block	98.13	99.03
Halved the filters in 2nd block	98.37	99.09
Halved the filters in last block	98.10	98.94
Added a conv2d layer in first block	98.14	98.99
Added a conv2d layer in second block	98.09	98.98
SGDM optimiser used in place of Adam	98.62	99.45
AlexNet	91.62	99.03
ResNet18	93.83	98.94

Different types of ablation processes were tested, including adding or removing blocks, increasing or decreasing the filters of the convolution layers of different blocks, and adding convolution layers in different blocks. From Table 6.5, we can see that adding or removing the blocks has a negative impact on the accuracy of the proposed system. For example, removing both the 2nd and 3rd blocks drops the accuracy from 98.82% to 81.05% for SZ1, while for SZ2, it drops from 99.58% to 97.63%. In the case of adding a single convolution layer, adding it in the first block gives a better result than adding it in the second block. On the other hand, changing the filters in the different blocks has a different effect. We have tried both halving and doubling the filters in each block. Among the three blocks, doubling the filters in the last block produces the best results, while halving the filters in the second block produces the best results. We have also tested the SGDM optimiser in place of Adam and got an accuracy of 98.62% and 99.45% for SZ1 and SZ2, respectively. Moreover, we have also tested and reported on two popular CNN models, AlexNet and ResNet18. All the tested ablation methods prove that the proposed GENet model gives a better result than the other tested models.

#### 6.3.4.2 Time complexity analysis

Table 6.6 shows the time-complexity analysis of the proposed GENet model on the two tested SZ datasets. From the table, we can see that, with the increase in training batch size, the time per epoch decreases, but there is not much of a steady pattern in the accuracy and loss values of training and validation. Yet, considering the time complexity analysis, batch size 128 may gain good classification accuracy with a smaller training time.

TABLE 6.6: Analysis of the proposed GENet model’s time complexity for two SZ datasets evaluated with various batch size configurations.

Dataset	Batch size	Time / epoch	Training		Validation	
			Acc.%	Loss	Acc.%	Loss
SZ1	32	6s	98.46	0.05	98.55	0.05
	64	5s	98.94	0.03	98.80	0.05
	128	4s	98.96	0.03	98.82	0.05
	256	4s	98.77	0.04	98.52	0.06
SZ2	32	14s	99.49	0.01	99.50	0.04
	64	6s	99.56	0.01	99.58	0.02
	128	4s	99.57	0.01	99.49	0.02
	256	4s	99.63	0.01	99.52	0.02

### 6.3.4.3 Data augmentation

Data augmentation is a quick way to add more labelled data to train a network and has been extensively used in the context of deep learning [100]. Due to the structure of the EEG signal, relatively few data augmentation methods can be applied while maintaining equal power, frequency, and spatial components. We have employed the same seven data augmentation methods as the authors in [100]: multiplication, frequency shift, adding noise, flipping data, and a combination of those four approaches on the SZ1 and SZ2 datasets, and the obtained results on those augmented data are given in Table 6.7.

TABLE 6.7: Comparison of the accuracy of various data augmentation methods applied to the SZ1 and SZ2 datasets.

Data augmentation methods	Accuracy %	
	SZ1	SZ2
No augmentation	99.58	98.82
Multiplied signal (Multi)	99.88	99.67
Adding noise (Noise)	99.76	99.37
Flipping the data (Flip)	99.66	99.27
Frequency shifting (Freq)	99.82	99.47
Noise + Flip	99.83	99.53
Noise + Multi	99.86	99.70
Flip + Freq	99.84	99.56

Table 6.7 shows that data augmentation improves the proposed model’s performance and demonstrates its robustness to perturbations.

### 6.3.4.4 Comparison with existing studies

Finally, to compare the performance of the proposed GENet model with existing state-of-the-art (SoA) research work that has used the same datasets as we have used in this study, we have listed the SoA works with our accuracy in Table 6.8.

TABLE 6.8: Assessing the proposed GENet model in comparison to the pre-existing state-of-the-art (SoA) studies that utilised the same datasets.

Dataset	SoA Authors	SoA Accuracy %	Our Accuracy %
<b>SZ1</b>	Xiaojun <i>et al.</i> [245]	92.00	<b>98.82</b>
<b>SZ2</b>	Mehmet <i>et al.</i> [246]	99.47	<b>99.58</b>
<b>MCI</b>	Siuly <i>et al.</i> [98]	98.78	<b>99.99</b>
<b>ADHD</b>	Ali <i>et al.</i> [247]	89.70	<b>99.99</b>
<b>EP</b>	Tawhid <i>et al.</i> [100]	98.79	<b>100.00</b>
<b>PD</b>	Anjum <i>et al.</i> [197]	85.70	<b>99.77</b>
<b>ASD</b>	Tawhid <i>et al.</i> [90]	99.15	<b>98.51</b>

From Table 6.8, we can see that, for datasets SZ1, SZ2, MCI, ADHD, EP, and PD, our proposed model has outperformed the SoA’s accuracy. For the ASD dataset, our proposed model produces an accuracy close to the SoA, which is maybe due to the fact that it has fewer data channels (16) than other datasets (19) for which this GENet model is proposed.

## 6.4 Summary

Here, we have proposed a DL-based generic framework for classifying ND from EEG data. Firstly, we have pre-processed the EEG signal data and segmented the EEG signals into short time fragments. We have tested three different time segments (1s, 2s, and 3s) to check the impact of the segment length on the detection process. Then, we have proposed a CNN model named GENet to classify the segmented signals into healthy or disordered groups. To assess the performance and scalability of the proposed framework, we tested it on seven different EEG datasets from six different NDs and performed extensive experimental work using 5-fold cross-validation.

Among the tested segment lengths, 1s data segment gives the highest classification accuracy compared to the other two time segments. The proposed GENet model offers higher classification performance for the seven tested datasets. For six of the seven tested datasets, our proposed model achieved higher accuracy than state-of-the-art work using those datasets. We have achieved an accuracy of 98.82%, 99.58%, 99.99%, 99.99%, 100%, 99.77% and 98.51% for datasets SZ1, SZ2, MCI, ADHD, EP, PD, and ASD, respectively. We have also tested the proposed model for multi-class classification using four (SZ2, MCI, EP, and ADHD) of the seven datasets to perform a five-class (SZ vs. MCI vs. EP vs. ADHD vs. Normal) classification task and achieved an accuracy of 99.84%. Moreover, we have analysed the t-SNE images of the proposed GENet model to check the extracted features’ plotting and found that those features are clustered into separable classes. We have also completed several ablation studies to validate the proposed GENet model.

Finally, the findings show that this method is versatile and may be applied to multi-disease classification tasks using EEG data and other signal processing tasks.

## Chapter 7

# Web Based System for Schizophrenia Detection using ConvLSTM based Subject Independent Analysis

In this chapter, we have developed a web-based system for diagnosing SZ from EEG data to address both the fourth and first research problem (**RP1**, **RP4**). Convolutional LSTM (ConvLSTM) is a type of deep learning architecture that combines the concepts of convolutional neural networks (CNNs) and long short-term memory (LSTM) networks [248]. It is particularly well-suited for image and video processing tasks where spatial and temporal dependencies need to be considered.

In a ConvLSTM, the convolutional operations are used to extract spatial features from the input sequence, while the LSTM operations are used to model temporal dependencies and to maintain a memory of the information over time. By combining these two types of operations, the ConvLSTM can effectively capture both the spatial and temporal patterns in sequential data, making it a useful tool for many applications, such as video prediction, anomaly detection, and weather forecasting [248].

The structure of a ConvLSTM network typically consists of an input layer, one or more ConvLSTM layers, and an output layer. The input layer receives the input sequence, which is then processed by the ConvLSTM layers. Each ConvLSTM layer has two components: the convolutional component and the LSTM component. The convolutional component uses convolutional filters to extract spatial features from the input, while the LSTM component uses gates to control the flow of information and to maintain a memory of the information over time.

### 7.1 Introduction

Schizophrenia (SZ) is a severe mental disorder that impairs a person's capability for clear thinking, feeling, and behaviour [190]. It is characterised by a variety of symptoms, including hallucinations, delusions, disordered thinking, and abnormal behaviour. Schizophrenia symptoms can be chronic or episodic, and they often first arise in late adolescence or early

adulthood [249]. People with schizophrenia may experience auditory or visual hallucinations, where they see or hear things that aren't there, as well as delusions, where they hold strong, false beliefs that are not based in reality. Worldwide, 24 million people are affected by it, which 0.32% (1 in 300 people) of the total population, and in adults, this rate is 0.45% [13]. SZ reduces the life expectancy of people by 2 to 3 times that of the normal population due to physical illnesses like cardiovascular, metabolic, and infectious diseases [13]. SZ can be treated using long-term medication, but it puts a severe cost burden on their families and on the health systems [249]. Moreover, it requires timely detection of the severity and stage of the SZ to provide treatment [13]. As a result, there is an increasing need to create an effective and automatic diagnostic system for differentiating SZ patients from healthy control (HC) individuals.

Usually, SZ is diagnosed primarily through interviews and observations of patient behaviour by a qualified psychiatrist, but it takes time, is sometimes biased, and is subject to errors [249]. Therefore, recently, various brain activity imaging methods such as magnetic resonance imaging, functional magnetic resonance imaging, positron emission tomography, electrocorticography, and electroencephalography (EEG) have been used to diagnose SZ [22], [91], [92], [162], [190]. EEG is the most widely used of these techniques because of its excellent temporal resolution, availability, non-invasiveness, relatively low financial costs, and general availability for professionals [79], [90]. The electrical activity of neurons in the human brain is recorded by the EEG as signal data, and the signals are then visually analysed by experienced clinicians to identify SZ. This visual analysis process is time-consuming, subjective, error-prone, and difficult due to the overlapping features for different diseases, which may lead to misdiagnosis [19]. Furthermore, the availability of expert clinicians varies by a ratio of 70 between high-income and low-income nations (1 versus 70 per 100,000 people) [1]. As a result, a computer-aided automatic data analysis system is necessary to produce an accurate and reliable diagnosis of SZ.

With the advent of technology, CAD has become a key component of the medical business. In recent years, a number of studies on the classification of SZ from EEG signals have been published by various academics [101], [150], [152], [154], [155], [157]–[159], [203], [249]–[257]. Based on the feature extraction and classification methods used, EEG signal classification techniques can be roughly divided into two categories: machine learning (ML)-based classification and deep learning (DL)-based classification.

In ML-based approaches, statistical and nonlinear parameters are manually retrieved from the time, frequency, and time-frequency domains of EEG data, and various ML-based classifiers are then employed to categorise the extracted features. For example, Zhang [251] used a combination of different statistical features with a random forest (RF) classifier to perform classification on a dataset of 81 subjects using 10-fold cross validation (CV) and achieved an accuracy of 81.10%. Khare *et al.* [250] used empirical wavelet transformation (EWT) to extract the amplitude modulation-frequency modulation (AM-FM) components of the signal, and then different time domain features were extracted and selected using the Kruskal-Wallis test. Finally, different ML-based classifiers are used to perform the classification, among which support vector machine (SVM) achieved the highest accuracy

of 88.70% on the same dataset and cross-validation technique. Siuly *et al.* used empirical mode decomposition (EMD)-based features with an ensemble bagged tree (EBT) classifier to obtain a 10-fold average accuracy of 89.59% on the same database. Khare *et al.* used flexible tuneable Q wavelet transform (FTQWT) scheme-based statistical features with flexible least squares SVM (FLSSVM) to classify SZ from healthy controls (HC). 91.39% average accuracy was obtained over a 10-fold CV for the same dataset. In another approach, Khare *et al.* developed an optimised model by combining robust variational mode decomposition (RVMD) and an optimised extreme learning machine (OELM) classifier. The proposed model obtained the highest accuracy of 92.93% over a 10-fold CV on an 81-subject dataset.

Buettner *et al.* used spectral analysis (SA) with an RF classifier and obtained an accuracy of 96.77% on a dataset with 28 subjects using a 10-fold CV [152]. In order to achieve instantaneous amplitude- and frequency-based mode functions, Krishnan *et al.* [255] investigated the use of multivariate empirical model decomposition (MEMD). From these mode functions, a number of entropy-based features are derived and chosen using recursive feature selection. Using a 10-fold CV, they achieved an average accuracy of 93% on the same dataset. Aydemir *et al.* [159] used the analysis of the complexity and Higuchi fractal dimension (HFD) features to classify it with the  $k$ -NN classifier and reported an accuracy of 99.91% in 10-fold CV and 84.33% in leave one subject out (LOSO) validation. This ML-based study used handcrafted feature extraction methods before classification, which were chosen based on the expertise of the researcher. This manual feature extraction approach is costly, time-consuming, and biased. Additionally, if data sizes are huge, these approaches might not work correctly and occasionally perform poorly [249].

On the other hand, very few studies have used DL-based classification of SZ from HC subjects. In this process, both the feature extraction and classification processes are carried out automatically. Moreover, for large-scale data, DL-based models can automatically extract and learn important features and use those features for classification. Khare *et al.* [155] used smoothed pseudo-Wigner Ville distribution (SPWVD) to generate the time-frequency representations (TFR) from EEG signals and feed them into a convolutional neural network (CNN) model. Using a 10-fold CV on a dataset of 81 subjects, they achieved an accuracy of 93.36%. Guo *et al.* [253] used CNN to classify electrical markers of the EEG signal of SZ from HC and obtained an accuracy of 92% on the same dataset. Siuly *et al.* [249] used filtering and deep learning feature extraction and classification using GoogLeNet and achieved an accuracy of 95.09% with a 10-fold CV on a dataset of 81 subjects. Oh *et al.* [150] used a custom CNN model to automatically extract and classify features of EEG signals and obtained an accuracy of 98.07% for 10-fold CV and 81.26% for LOSO validation on a dataset of 28 subjects. Singh *et al.* [203] developed a spectral feature-based model using Fast Fourier transform (FFT) and fed it into both CNN and long short-term memory network (LSTM) models for classification of SZ. On a dataset of 28 subjects with the holdout validation method, they achieved the best accuracy of 98.96% using the CNN model. Shoeibi *et al.* [157] tested different ML and DL-based models to classify SZ from HC subjects on the same dataset. Among the different models

tested, they achieved the best accuracy of 99.25% using the CNN-LSTM model with a 5-fold CV. Tawhid *et al.* used an entropy topography-based EEG signal presentation technique with CNN to classify SZ patients from HC. They tested their proposed model on two datasets of 81 and 28 subjects and achieved an accuracy of 89.20% and 97.85%, respectively.

Although several deep learning algorithms have been developed for SZ classification, the majority of them concentrate on subject-dependent classifications, where a subset of EEG data collected from a subject is used for training the model and another subset is used for testing the trained model. However, high EEG variability exists between people for the same brain activity due to anatomical and physiological differences between them [258]. When machine learning algorithms are trained with EEG data from all participants except one for performance testing, the individual differences significantly degrade the classification performance. Most of the SZ detection methods did not validate their proposed models for subject-independent analysis. Moreover, the real-life classification performance of a system can be accurately calculated using subject-independent analysis. Additionally, as the DL-based studies are still limited and not all the models are explored in the SZ classification, there is still scope for improvement in terms of efficiency and performance. Therefore, in this research work, we have tried to address these issues by developing a DL-based SZ classification system for subject-independent analysis.

In this study, we have developed a subject-independent SZ detection network (SISDNet) using a DL-based two-dimensional (2D) convolutional long short-term memory (ConvLSTM) model to classify 2D EEG data. We have used ConvLSTM, which combines CNN and LSTM in a single layer, to extract spatiotemporal information from time-series data, and to the best of our knowledge, this study is the first to use the ConvLSTM model in SZ classification. At first, the raw EEG data are resampled to 256 Hz to make them input-ready for the SISDNet. Then, to use the short-term features of the EEG signal, we have segmented the signals into small time frames of 3 seconds (3s). Finally, the SISDNet model was trained using those signals and performed the classification task. Two different EEG datasets from SZ have been used to validate the proposed model. Along with the subject-independent analysis, we have also evaluated the proposed model using the 10-fold cross validation (CV) technique to compare the results with existing research. The results obtained from this study are also compared with existing state-of-the-art studies that have used the same EEG datasets.

The major contributions of this study are compiled as follows:

1. A noble framework using the DL-based ConvLSTM model is proposed for subject-independent SZ classification.
2. For the first time, the ConvLSTM model is used for SZ classification from EEG data.
3. A web-based system is developed using the proposed classification framework for clinical use.

4. Performance of the proposed framework is validated using both LOSO and a 10-fold CV.
5. Explore the performance on two different datasets of SZ disease.
6. Increase classification performance over existing approaches using the same dataset.
7. Validate the proposed ConvLSTM model using different ablation studies and layer-wise t-SNE feature visualisation.

The rest of the chapter contains the details of the proposed method and the evaluation results, along with a detailed discussion of the developed web system.

## 7.2 Methods and materials

In this research study, we have developed a ConvLSTM-based SZ classification framework using EEG signal data. The proposed framework consists of several steps: first, EEG data is collected from publicly available sources, and then those signals are segmented into small time frames. After that, the proposed ConvLSTM model is trained using those signal segments, and finally, the trained model is used to perform the classification on the test datasets and calculate different evaluation parameter values. An overview of the proposed framework is given in Figure 7.1. A detailed discussion of those steps is given in the below subsections.

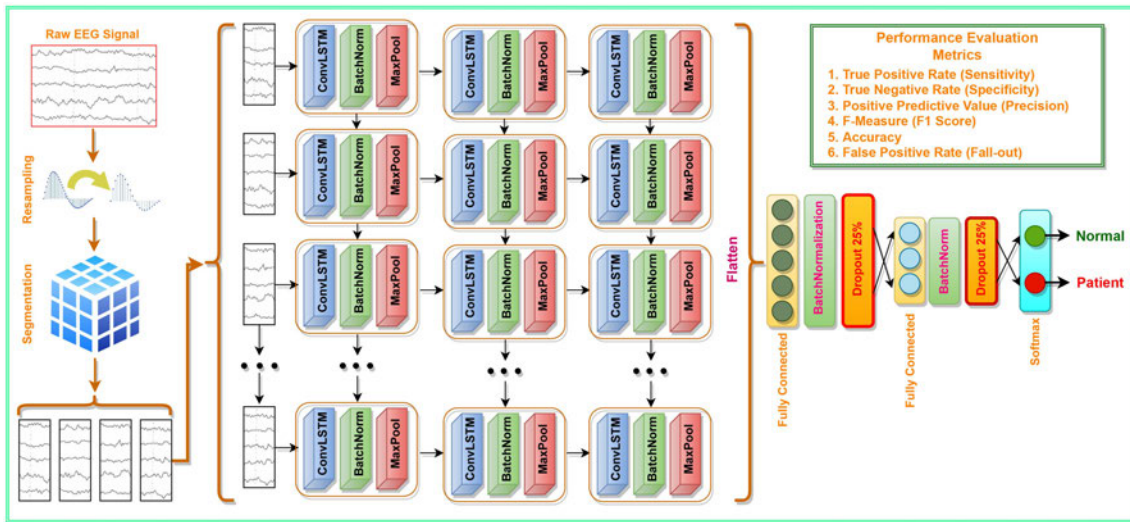


FIGURE 7.1: An overview illustration of the proposed framework and steps involved in the classification process.

### 7.2.1 EEG data collection

Here, we have used two publicly available EEG datasets for SZ disease. A brief description of those datasets is given below:

- The first dataset (hereafter referred to as the Kaggle dataset) is collected from the Kaggle website [239]. There are 81 participants in all; 49 of them are SZ sufferers and 32 are HC. EEG data is recorded from 64 channels at a sampling rate of 1024 Hz during a task of pressing a button.
- Second Schizophrenia Dataset (hereafter referred to as the Warsaw Dataset) is comprised of 28 subjects (14 age- and sex-matched subjects from the SZ and HC groups) that were collected at the Institute of Psychiatry and Neurology in Warsaw, Poland [78]. The signals are recorded in the resting state at a 250 Hz sampling rate from 19 channels of a standard 10–20 EEG electrode system.

Each participant provided their informed consent to the publication of their data at the time the data was gathered, and all of these datasets are openly available online. The confidentiality of the participants was also protected by not posting any personally identifiable information about the respondents; therefore, no ethical approval was required for our study. Table 7.1 summarises the demographic data of the participants for the used datasets. [78], [239] contains more information on those datasets.

TABLE 7.1: Demographic data for the datasets used in this study.

	Datasets	
	Kaggle	Warsaw
Patients (Male/Female)	49 (41/8)	14 (7/7)
Normal (Male/Female)	32 (26/6)	14 (7/7)
Patients Age range	40.02±13.70	28.10±3.70
HCs Age range	38.38±13.70	27.75±3.15
Sampling Frequency	1024	256
Resampled Frequency	256	256
Recorded no of channel	64	19
Used no of channel	64	19
<b>Samples generated after segmentation</b>		
Segments (Patient/Normal)	4728/3108	5146/4235

### 7.2.2 Segmentation of the EEG signals

In the field of EEG signal analysis using deep learning-based algorithms, data shortages are a critical challenge. The segmentation approach is frequently used by researchers to address this problem. This method increases the data sample size while maintaining an equal ratio by segmenting the original EEG data into brief informative segments and giving them the same level as the original one [79], [90], [91], [100], [153], [190], [194]. Similar to the authors of [91], [100], [190], we have divided the signals in this experiment into three-second (3s) time segments. After segmentation, 4728 and 5146 segments were generated from SZ subjects for the Kaggle and Warsaw datasets, respectively, while for normal

subjects, those numbers are 3108 and 4235, respectively. These numbers are reported in the bottom row of Table 7.1.

### 7.2.3 Proposed Subject Independent Schizophrenia Detection neural Network (SISDNet) model

We have used a DL-based ConvLSTM model to extract features from the EEG data and conduct classification. ConvLSTM was designed to deal with precipitation nowcasting by fusing LSTM with CNN [248]. It is appropriate for classifying EEG signals because it can extract spatiotemporal information from time-series data. The ConvLSTM cell was developed by replacing the internal matrix multiplication operation of LSTM with convolution operations, which retain the dimensions of the data flowing through it and also retain the spatial information of the data. ConvLSTM predicts a grid cell's future state based on the inputs and previous states of its nearby neighbours by using a convolution operator in state-to-state and input-to-state transitions [248]. Internal operation of the ConvLSTM cell consists of the following key equation 7.1:

$$\begin{aligned}
 i_t &= \sigma(W_{xi} * \chi_t + W_{hi} * H_{t-1} + W_{ci} \circ C_{t-1} + b_i) \\
 f_t &= \sigma(W_{xf} * \chi_t + W_{hf} * H_{t-1} + W_{cf} \circ C_{t-1} + b_f) \\
 C_t &= f_t \circ C_{t-1} + i_t \circ \tanh(W_{xc} * \chi_t + W_{hc} * H_{t-1} + b_c) \\
 o_t &= \sigma(W_{xo} * \chi_t + W_{ho} * H_{t-1} + W_{co} \circ C_t + b_o) \\
 H_t &= o_t \circ \tanh(C_t)
 \end{aligned} \tag{7.1}$$

Here,  $\chi_1, \chi_2, \dots, \chi_t$  are cell inputs,  $C_1, C_2, \dots, C_t$  are cell outputs,  $H_1, H_2, \dots, H_t$  are hidden states,  $i_t, f_t, o_t$  are the input, forget, and output gates;  $W$  is the weight matrix; and '\*' and  $\circ$  denote the convolution operation and Hadamard product, respectively.

Here, we have developed a ConvLSTM model named SISDNet to perform classification of the raw EEG signal data. The architecture of the proposed ConvLSTM model is given in Figure 7.2.

The proposed model contains three ConvLSTM and two fully connected layers. The first three ConvLSTM layers are followed by a batch normalisation layer and a 3D max-pooling layer, while the last two connected layers are followed by a batch normalisation layer and a dropout layer. The number of filters in the first, second, and third ConvLSTM layers is 32, 16, and 8, respectively, and for the fully connected two layers, those are 256 and 128. The kernel size of all ConvLSTM layers is 7x7, with a tangent hyperbolic (tanh) activation function, a hard sigmoid recurrent activation function, and the same padding. The dropout rates for the first and second dropout layers are 25% and 50%, respectively. The last activation layer employs a softmax activation function to activate one of two outputs: normal or schizophrenia. A categorical cross-entropy loss function and Adam optimiser are utilised to build the model. Table 7.2 lists the details of the configuration of those layers.

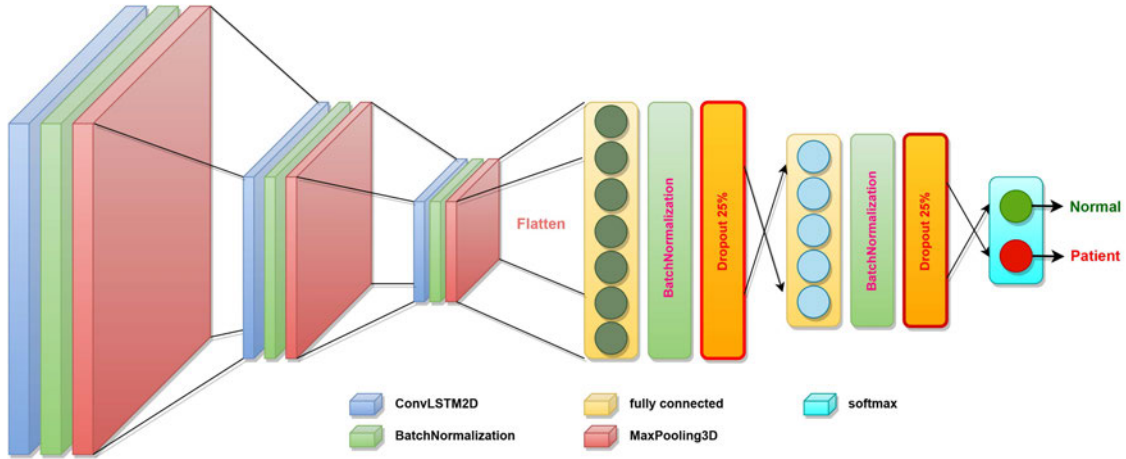


FIGURE 7.2: Proposed ConvLSTM based SISDNet model layout.

TABLE 7.2: SISDNet model’s architectural specifics.

Layers	# Filter	Kernel size	Option
ConvLSTM2D	32	7x7	padding=same
Activation			tanh
BatchNormalisation			
MaxPooling3D		1x4x2	padding=same
ConvLSTM2D	16	7x7	padding=same
Activation			tanh
BatchNormalisation			
MaxPooling3D		1x4x2	padding=same
ConvLSTM2D	8	7x7	padding=same
Activation			tanh
BatchNormalisation			
MaxPooling3D		1x4x2	padding=same
Flatten			
Dense	256		
Activation			relu
BatchNormalisation			
Dropout			25%
Dense	128		
Activation			relu
BatchNormalisation			
Dropout			50%
Dense (classifier)	2		
Total params: 504,258			
Trainable params: 503,378			
Non-trainable params: 880			

### 7.2.4 Classification using proposed SISDNet model

In this step, the proposed model is trained and tested on the used datasets. To do that, we have to split the dataset into train and test subsets so that we can use the training

subset to train the model and the test subset to test the trained model.  $K$ -fold cross validation is a technique used in machine learning to evaluate the performance of a model [90]. The basic idea behind  $k$ -fold cross validation is to split the available data into  $k$  equally sized folds. The model is trained on  $k-1$  folds and tested on the remaining fold. This process is repeated  $k$  times, with each fold serving as the test set once. The performance of the model is then averaged across all  $k$  folds. It is useful because it allows for a more accurate estimate of the performance of a model than simply using a single train/test split. By using multiple folds, we can get a better sense of how the model will perform on unseen data. There are a few different variations of  $k$ -fold cross validation, such as subject independent analysis (known as leave-one-out cross validation (LOOCV)) and subject dependent analysis (known as stratified  $k$ -fold), which are designed to handle specific types of data or modelling scenarios.

In this study, we have used both LOOCV and 10-fold cross-validation to validate the proposed SISDNet model. In the LOOCV process, all the signal segments from one subject are left out of the training subset and trained on the model with all of the other subject's data, and then the trained model is used to classify the left-out subject's data segments. This process is repeated for all the subjects in the dataset. On the other hand, in the 10-fold cross-validation technique, the dataset is divided into 10 subsets of equal or nearly equal size, of which 9 are used for training and the rest are used for testing. This process is repeated 10 times so that each subset belongs to the test set only once.

### 7.2.5 Performance evaluation matrices

We have used six well-known evaluation parameters to evaluate the performance of the proposed SISDNet model, namely: sensitivity (Sen), specificity (Spec), precision (Prec), F1 score (F1), accuracy (Acc), and false positive rate (FPR). Equations ((7.2)) - ((7.7)) are used to calculate those six parameters:

$$Sen = \frac{n_{SZ}}{N_{SZ}} \times 100\% \quad (7.2)$$

$$Spec = \frac{n_{Normal}}{N_{Normal}} \times 100\% \quad (7.3)$$

$$Prec = \frac{n_{SZ}}{n_{Normal-SZ} + n_{SZ}} \times 100\% \quad (7.4)$$

$$F1 = \frac{2 \times Sen \times Prec}{Sen + Prec} \quad (7.5)$$

$$Acc = \frac{n_{SZ} + n_{Normal}}{N_{SZ} + N_{Normal}} \times 100\% \quad (7.6)$$

$$FPR = 100 - Spec \quad (7.7)$$

Here,  $n_{SZ}$  and  $n_{Normal}$  are the correctly identified SZ and normal subjects, respectively;  $N_{SZ}$  and  $N_{Normal}$  are the actual number of patients and normal subjects, respectively.  $n_{SZ-Normal}$  denotes the number of SZ subjects identified as normal, while  $n_{Normal-SZ}$  denotes the number of normal subjects classified as SZ patients. These criteria allow us

to grasp an idea about the classifier's behaviour on the test data [91], [98], [100], [154], [181], [190], [194].

## 7.3 Results and discussion

In this study, an SZ classification framework is developed using a deep learning-based ConvLSTM model. We have used two SZ datasets to test the proposed model. We have used both LOOCV and 10-fold cross-validation techniques to validate the model on the tested datasets. A detailed discussion of the experimental setup and results is given in the next two subsections.

### 7.3.1 Experimental setup

In the proposed system, we have segmented the raw EEG data into three-second (3s) time frames. This segmentation process produced 5146 and 4235 signal segments for SZ and normal subjects, respectively, in the Warsaw dataset, while for the Kaggle dataset, those numbers are 4728 and 3108, respectively. Each of the produced signal segments has a size of  $c \times p$ , where  $p$  is the number of sampling points and  $c$  is the number of channels.  $p$  can be further defined as  $f \times t$ , where  $f$  is the sampling frequency and  $t$  is the segment length. In this study, for the Kaggle dataset,  $f$  is 256 Hz,  $t$  is 3s,  $c$  is 64, and  $p$  is 768 ( $256 \times 3$ ) making a signal segment a matrix of  $64 \times 768$ . On the other hand, for the Warsaw dataset,  $f$  is 256Hz,  $t$  is 3s,  $c$  is 19, and  $p$  is 768 ( $256 \times 3$ ) making a signal segment a matrix of  $19 \times 768$ .

After the segmentation process, we have divided the dataset into train and test subparts based on the validation technique. For the subject-independent analysis, the total number of subparts is equal to the total number of subjects in the dataset, while for the subject-dependent analysis, there are 10 subparts as we have used the 10-fold cross validation. The experiments are carried out on a computer with an AMD Threadripper Pro processor, 256 GB of RAM, and 48 GB of graphics memory. The proposed SISDNet model is trained with 100 epochs for the Kaggle dataset and 50 epochs for the Warsaw dataset, as the model starts overfitting after those epochs. We have used mini-batch mode for batch size selection to speed up the learning process. In this study, we have used three training batch sizes (32, 64, and 128) to train the model.

### 7.3.2 Results

In this research work, we have validated the proposed model using two different validation techniques: subject-independent analysis and subject-dependent analysis. Details of those experimental results are discussed in sections 7.3.2.1 and 7.3.2.2.

#### 7.3.2.1 Subject independent analysis

In this validation technique, all the signal segments of a subject are kept out of the training process and used for testing the system. This process is repeated for the total number of

subjects in the system, and the final result is calculated by averaging those results. Details of the results of the subject independent analysis on the Kaggle and Warsaw datasets with different training batch sizes are given in Table 7.3.

TABLE 7.3: Performance of the proposed SISDNet model in subject independent analysis on the Kaggle and Warsaw datasets with different training batch sizes.

Batch size	Kaggle dataset						Warsaw dataset					
	Sen%	Spec%	Prec%	F1	Acc%	FPR%	Sen%	Spec%	Prec%	F1	Acc%	FPR%
32	97.88	80.37	88.35	0.93	90.94	19.63	<b>96.32</b>	99.17	99.30	<b>0.98</b>	<b>97.61</b>	0.8297
64	97.80	86.94	91.93	0.95	93.49	13.06	91.77	99.93	99.94	0.96	95.45	0.0691
128	<b>98.73</b>	<b>90.25</b>	<b>93.90</b>	<b>0.96</b>	<b>95.37</b>	<b>9.75</b>	92.07	<b>99.98</b>	<b>99.98</b>	0.96	95.64	<b>0.0230</b>

From Table 7.3, we can see that, for the Kaggle dataset, batch size 128 has produced the best result among the three tested batch sizes. It has produced an accuracy of 95.37% with 98.73% sensitivity, 90.25% specificity, 93.90% precision, a 0.96 F1 score, and a 9.75 FPR. On the other hand, batch size 32 produced the lowest accuracy of 90.94% and batch size 64 gave the highest accuracy of 93.49%.

For the Warsaw dataset, batch size 32 has produced the best performance with an accuracy of 97.61%, sensitivity of 96.32%, and an F1 score of 0.98. For specificity, precision, and FPR parameters, batch size 128 has produced the best result with 99.98%, 99.98% and 0.023, respectively.

To further show the proposed model’s performance on the tested datasets in subject-independent analysis, we have plotted the subject-wise accuracy for three different training batch sizes as shown in Figs. 7.3 and 7.4.

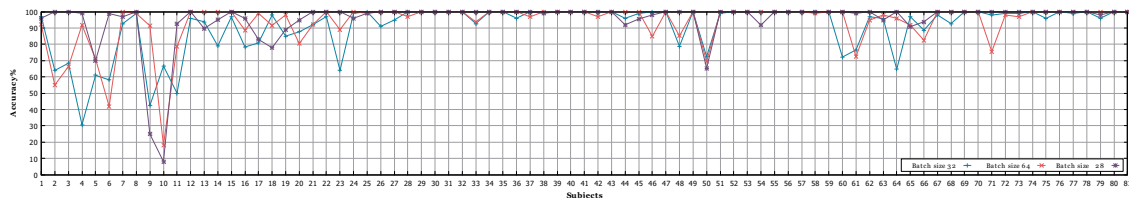


FIGURE 7.3: Subject-wise accuracy comparison of the SISDNet model for the three training batch sizes on the Kaggle dataset.

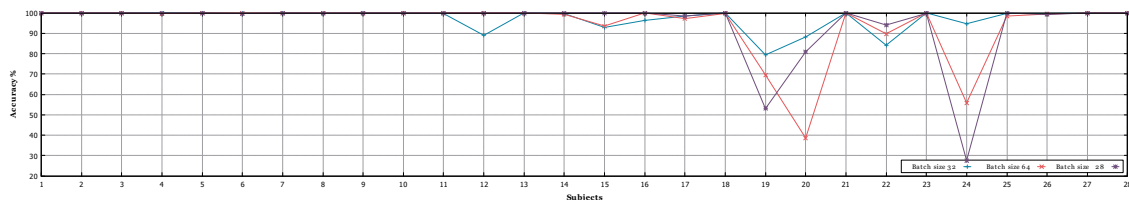


FIGURE 7.4: Subject-wise accuracy comparison of the SISDNet model for the three training batch sizes on the Warsaw dataset.

From the Figure 7.3, we can see that for the Kaggle dataset, among the 81 subjects, we have achieved more than 95% accuracy for 65 subjects for batch size 128, 10 subjects have accuracy between 85% and 95%, 2 subjects have accuracy between 75% and 85%,

and the rest of the 4 subjects have accuracy below 75%. On the other hand, for the Warsaw dataset from Figure 7.4, we can see that among the 28 subjects, 24 subjects have an accuracy over 90% and the rest 4 subjects have an accuracy between 80% and 90% for a training batch size of 32.

### 7.3.2.2 Subject dependent analysis

In this analysis, we performed 10-fold cross-validation on the datasets, where each dataset is randomly divided into 10 subparts, of which 9 are used for training the model and the rest are used for testing the trained model. This process is repeated ten times, so that each subpart belongs to the test set once. Table 7.4 reports the batch size-wise 10-fold average performance result for both the tested datasets.

TABLE 7.4: Ten-fold average performance results of the SISDNet model on multi-class classification.

Batch size	Kaggle dataset						Warsaw dataset					
	Sen%	Spec%	Prec%	F1	Acc%	FPR%	Sen%	Spec%	Prec%	F1	Acc%	FPR%
<b>32</b>	97.47	94.29	96.28	<b>0.97</b>	96.20	<b>4.594</b>	<b>99.27</b>	99.07	99.25	<b>0.99</b>	99.19	0.960
<b>64</b>	97.58	<b>94.44</b>	<b>96.37</b>	<b>0.97</b>	<b>96.31</b>		99.22	99.26	99.39	<b>0.99</b>	<b>99.24</b>	0.739
<b>128</b>	<b>97.64</b>	94.18	96.24	<b>0.97</b>	96.26	5.824	98.80	<b>99.42</b>	<b>99.52</b>	<b>0.99</b>	99.09	<b>0.576</b>

From Table 7.4, we can see that for both datasets, batch size 64 has given the best performance among the tested three batch sizes, with an average accuracy of 96.31% and 99.24% for the Kaggle and Warsaw datasets, respectively. To further assess the fold-wise performance of the proposed model, we have plotted fold and batch size-wise sensitivity, specificity, precision, F1 score, FPR, and accuracy in Figs. 7.5 and 7.6, for the Kaggle and Warsaw datasets, respectively.

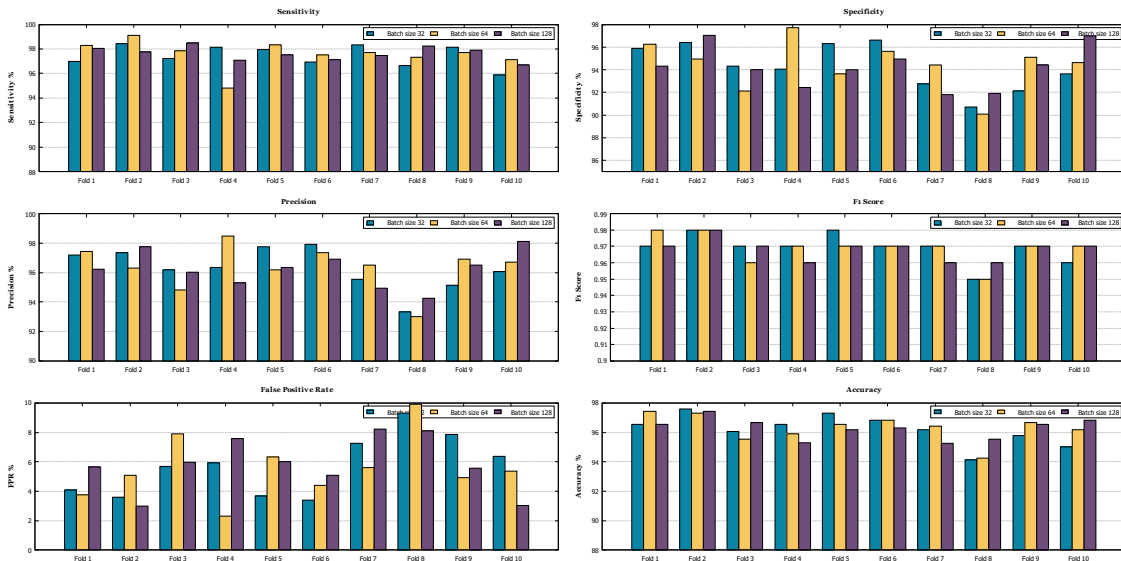


FIGURE 7.5: Fold and batch size-wise comparison of the evaluation parameters for the Kaggle dataset.

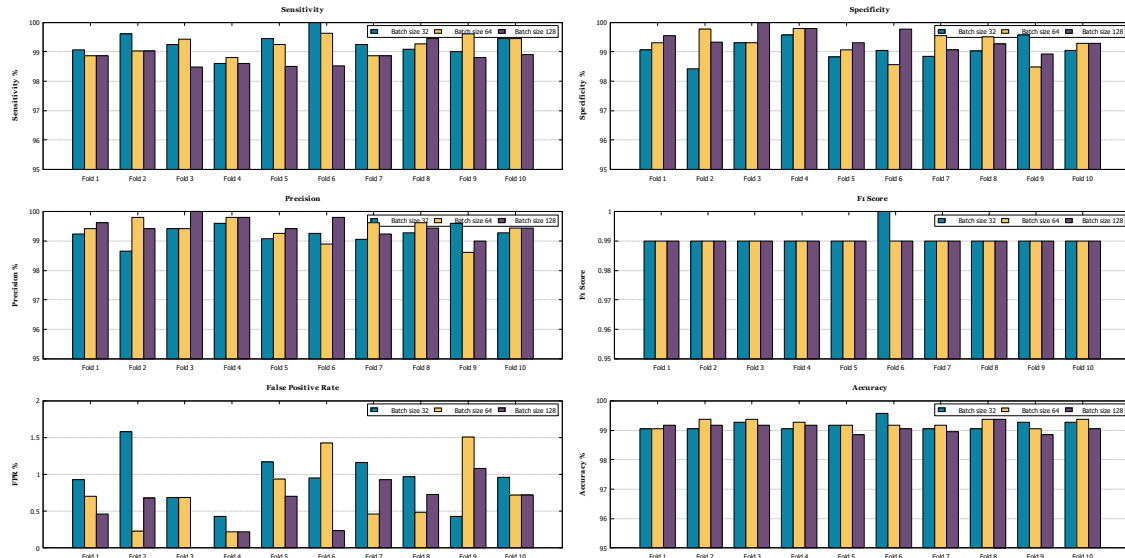


FIGURE 7.6: Fold and batch size-wise comparison of the evaluation parameters for the Warsaw dataset.

From Table 7.4 and Figs. 7.5 and 7.6, we can see that for the Kaggle dataset, a single fold highest sensitivity of 99.11% is achieved for fold 2 with batch size 64, while for the Warsaw dataset, it is 100% for fold 6 with batch size 32. Over the 10-fold, the Kaggle dataset has the highest average sensitivity value of 97.64% for batch size 128, and for the Warsaw dataset, the highest average sensitivity is 99.27% for batch size 32. For the precision parameter, in the Kaggle dataset, a single fold highest value of 98.49% is achieved in fold 4 of batch size 64, and for the Warsaw dataset, it is 100% for fold 3 of batch size 128. Overall, an average of 96.37% and 99.52% precision values are obtained for the Kaggle and Warsaw datasets, respectively, with batch sizes of 64 and 128, respectively.

In cases of specificity, the highest values are obtained 97.69% (fold 4 with batch size 64) and 100% (fold 3 with batch size 128) for datasets Kaggle and Warsaw, respectively. The average 10-fold highest specificity values are 94.44% (batch size 64) and 99.42% (batch size 128) for the Kaggle and Warsaw datasets, respectively. Since FPR is calculated using specificity and is preferred to be minimum, the settings that have obtained the highest specificity have also produced the best FPR, and the best values are 4.594% and 0.576% for the Kaggle and Warsaw datasets, respectively.

The fifth parameter we have used to measure the performance of the proposed model is the F1 score, which is the harmonic mean of precision and recall and whose value ranges from 0 to 1, with 1 indicating perfect precision and recall. For the Kaggle dataset, we achieved the highest 0.98 F1 score for a couple of folds with different training batch sizes. Overall, the 10-fold average F1 score obtained for all three training batch sizes is 0.97. On the other hand, for the Warsaw dataset, we achieved an F1 score of 1 for fold 6 with a training batch size of 32. The 10-fold-foldage F1 score obtained for all three training batch sizes is 0.99.

The final evaluation parameter that we have considered is accuracy. From the Figs. 7.5 and 7.6, we can see that for the Kaggle dataset, a single-fold highest accuracy value

of 97.58% is obtained for batch size 32, and a lowest of 94.13% is also achieved for the same batch size. Over the 10-fold, the highest and lowest average accuracy values of 96.31% and 96.20% are obtained for batch sizes 64 and 32, respectively. Similarly, for the Warsaw dataset, the single-fold highest and lowest accuracy values of 99.58% and 98.86% are achieved using batch sizes of 32 and 128, respectively. Overall, the 10-fold highest and lowest accuracy values obtained are 99.24% and 99.09%, respectively.

### 7.3.3 Discussion

In this study, a subject-independent deep learning-based model named SISDNet is proposed to classify schizophrenia disorder using EEG data. In this section, we have discussed different aspects of the proposed SISDNet model in terms of feature visualisation, model optimisation, developed web applications, and performance comparison with previous studies.

#### 7.3.3.1 Layer-wise feature visualisation using t-SNE

We have generated two-dimensional (2D) representations of the retrieved features from each layer of the proposed SISDNet model using t-distributed stochastic neighbour embedding (t-SNE) [244] visualisation. t-SNE is a dimensionality reduction technique used to visualise high-dimensional data in a lower-dimensional space, usually two or three dimensions. The goal of t-SNE is to preserve the pairwise similarities between each high-dimensional data point and map them to a low-dimensional point. In other words, data points should be similar in low-dimensional space if they are similar in high-dimensional space. We have plotted the layer-wise extracted features for the proposed SISDNet model on the Warsaw dataset for 10-fold cross-validation with batch size 32, which is given in Figure 7.7. For simplicity, we have shown a single fold's classification process for over 800 test subjects. The figure displays a two-dimensional map of the multidimensional feature vectors, with each symbol denoting a distinct sample from the test set.

A t-SNE plot helps to visualise the layer-wise clustering process of the extracted features of a classifier and how separable those features are at the end of the final layer. From Figure 7.7, we can see that in the input layer, extracted feature points from all the test subjects of two classes are randomly mixed up, and as the data passes through the layers of SISDNet, they start forming clusters of two classes. The extracted features started forming clusters after the first dense layer, as shown in Figure 7.7, from which they formed two completely separable clusters in the final dense layer. Finally, the activation layer projects those two clusters into two different groups (healthy vs. patient), which indicates the better performance of the proposed SISDNet model.

#### 7.3.3.2 Ablation study

In the context of machine learning and artificial intelligence, ablation studies are used to identify the key elements that influence a model's performance. In an ablation study, one or more elements of the model are removed or disabled, and the performance of the model

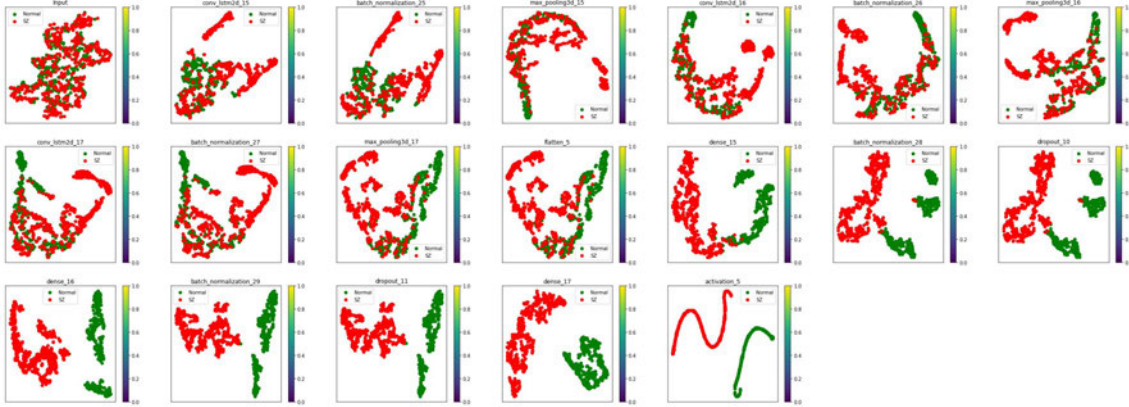


FIGURE 7.7: Visualisation of the layer-wise classification process in the SISDNet model using t-SNE images. Here visualisation is plotted from the input layer to the output layer for the tested Warsaw dataset with batch size 64. At the input layer, there was no clear cluster between two classes (SZ vs. Normal), but as the data progressed from the hidden layers to the output layer, it formed two clearly separable clusters of two classes.

is assessed to determine the effect of the disabled elements. To validate the structure of the proposed SISDNet model, we have conducted eleven different ablation studies using both datasets. Here, we have used the results of the SISDNet model for batch size 32 as the baseline result and performed those ablation studies using the same setup. In the ablation process, we have varied the processing units and filters to check their impact on the proposed model, as shown in Table 7.5. From the Table 7.5, we can see that changing the number of filters, kernel size, and adding or removing different components (ConvLSTM, Maxpooling 3D, Batch Normalisation, Dropout) in different layers reduces the classification performance. The proposed SISDNet model provides better results than the other examined models, as demonstrated by all tested ablation techniques.

TABLE 7.5: Ablation study results on tested Kaggle and Warsaw datasets for 10-fold cross-validation Here, we have conducted the ablation study using a training batch size of 32 for both datasets and compared the results of other tested models with the base model’s results.

Model	Layer 1	Layer 2	Layer 3	Kaggle	Warsaw
base	CL (32)(7,7) + BN + Pool (1,4,2)	CL (16)(7,7) + BN + Pool (1,4,2)	CL (8) (7,7) + BN + Pool (1,4,2)	96.2	99.19
1	CL (8)(7,7) + BN + Pool (1,4,2)	CL (8)(7,7) + BN + Pool (1,4,2)	CL (8) (7,7) + BN + Pool (1,4,2)	95.98	98.18
2	CL (8)(3,3) + Pool (1,2,2) + DO (25%)	CL (8)(3,3) + Pool (1,2,2) + DO (25%)	CL (8)(3,3) + Pool (1,2,2) + DO (25%)	94.82	95.24
3	CL (8)(3,3) + Pool (1,2,2) + DO (25%)	CL (8)(3,3) + Pool (1,2,2) + DO (25%)	no	88.97	96.18
4	CL (8)(3,3) + Pool (1,2,2) + DO (25%)	CL (16)(3,3) + Pool (1,2,2) + DO (25%)	no	88.54	94.64
5	CL (16)(3,3) + Pool (1,2,2) + DO (25%)	CL (8)(3,3) + Pool (1,2,2) + DO (25%)	no	88.08	95.84
6	CL (16)(3,3) + BN + Pool (1,2,2)	CL (16)(3,3) + Pool (1,2,2) + DO (25%)	no	83.87	96.65
7	CL (16)(3,3) + BN + Pool (1,2,2)	CL (16)(3,3) + BN + Pool (1,2,2) + DO (25%)	no	83.22	96.43
8	CL (8)(5,5) + BN + Pool (1,2,2)	CL (8)(5,5) + BN + Pool (1,2,2) + DO (25%)	no	83.92	97.97
9	CL (16)(5,5) + BN + Pool (1,2,2)	CL (16)(5,5) + BN + Pool (1,2,2) + DO (25%)	no	84.55	98.02
10	CL (8)(7,7) + BN + Pool (1,4,2)	CL (8)(7,7) + BN + Pool (1,4,2) + DO (25%)	no	92.48	98.71
11	CL (16)(7,7) + BN + Pool (1,2,2)	CL (16)(7,7) + BN + Pool (1,2,2) + DO (25%)	no	84.11	98.37

\* CL = ConvLSTM, Pool = Maxpooling 3D, BN = Batch Normalisation, DO = Dropout.

### 7.3.3.3 Comparison with existing studies

Finally, to compare the performance of the proposed SISDNet model with existing state-of-the-art (SoA) research work that has used the same datasets as we have used in this

study, we have listed the SoA works with our accuracy in Table 7.6 and 7.7.

From Table 7.6, we can see that, for the Kaggle dataset, our proposed model is the first study that has been evaluated using LOSO. On the other hand, for 10-fold cross-validation, our study achieved better accuracy than all other studies that have used this dataset.

TABLE 7.6: Comparative analysis of the proposed model with Kaggle dataset’s existing research.

Study	Method	Validation	Acc.
[250]	Empirical WT with SVM	10-Fold	88.70%
[154]	EMD-based features with EBT	10-Fold	89.59%
[251]	Statistical features with RF	10-Fold	81.10%
[252]	F-TQWT-based scheme with F-LSSVM	10-Fold	91.39%
[253]	Electrical marker with CNN	NA	92.00%
[254]	RVMD-based OELM method	10-Fold	92.93%
[190]	Topographic image and CNN	10-Fold	89.20%
[155]	SPWVD-based TFR and CNN	10-Fold	93.36%
[249]	GoogLeNet	10-Fold	95.09%
			10-fold CV
Ours	ConvLSTM	10-Fold and LOSO	<b>96.31%</b> LOSO <b>95.37%</b>

For the Warsaw dataset, from Table 7.7, we can see that our proposed method has outperformed all other previous studies in the LOSO validation approach. In the case of 10-fold cross validation, study [159] produced 99.91% accuracy, but their LOSO accuracy was way below (84.33%) than ours (97.61%). Moreover, they have tested their proposed method on one dataset only, which leaves the question of its applicability to other datasets. In summary, the presented ConvLSTM-based SISDNet framework attained the best classification accuracy for LOSO in both the tested datasets, and in 10-fold cross validation, it attained the best accuracy for the Kaggle dataset and close to the best accuracy for the Warsaw dataset.

#### 7.3.3.4 Web-based system for schizophrenia classification

We have developed a web-based system to classify schizophrenia using EEG data. Figure 7.8 shows the workflow of the developed web system. In this web system, users need to create an account to access the service. After creation of the account, the user can upload the recorded EEG data in csv format into the classification service by using the upload

TABLE 7.7: Comparative analysis of the proposed model with Warsaw dataset’s existing research.

Study	Method	Seg.	Validation	Acc.
[152]	Spectral analysis, RF	1min	10-Fold	96.77%
[255]	Multivariate empirical model decomposition, entropy computation, recursive feature elimination, and SVM	2s	10-Fold	93.00%
[101]	Time-domain feature, LSTM	4s	88:12	99.00%
[203]	FFT, spectral feature extraction, CNN, and LSTM	5s	90:10	98.96%
[256]	TQWT, statistical moment, ReliefF, and kNN	25s	10-Fold	99.12%
[158]	Graphical feature extraction, forward selection algorithm, and kNN	-	10-Fold	94.80%
[157]	CNN-LSTM	25s	5-Fold	99.25%
[190]	Topographic image and CNN	3s	10-Fold	97.85%
[150]	Custom CNN design	25s	10-Fold & LOSO	10-Fold CV 98.07% LOSO 81.26%
[257]	L1 Norm, ES-KNN	25s	10-Fold & LOSO	10-fold CV 99.21% LOSO CV 97.20%
[159]	CGP17Pat, MAP, INCA, kNN, and iterative hard majority voting	25s	10-Fold & LOSO	10-fold CV 99.91% LOSO CV 84.33%
Ours	ConvLSTM	3s	10-Fold & LOSO	10-fold CV <b>99.24%</b> LOSO CV <b>97.61%</b>

interface. After completion of the data upload, the web server starts the classification process.

At first, the web server communicates with the data processing service to pre-process the uploaded EEG data. In this step, the pre-processing service checks whether the uploaded data is in the proper format or not and then segments the data into a 3-second time window to make it ready for the classification model. On completion of the segment generation process, this data processing server informs the web server about the availability of data for the classification task.

On receiving this notification, the web server contacts the classification server to perform the categorisation task on the generated segments. After receiving the request, the

classification server conducts the categorisation process on the generated segments of the uploaded EEG data using the pre-trained model of the proposed SISDNet framework. It labels each segment either SZ or normal with the classification probability of being in that category. Finally, the web server counts the number of segments with a high probability of being SZ or normal and shows the ratio of the two numbers as the probability of the uploaded data being SZ or normal.

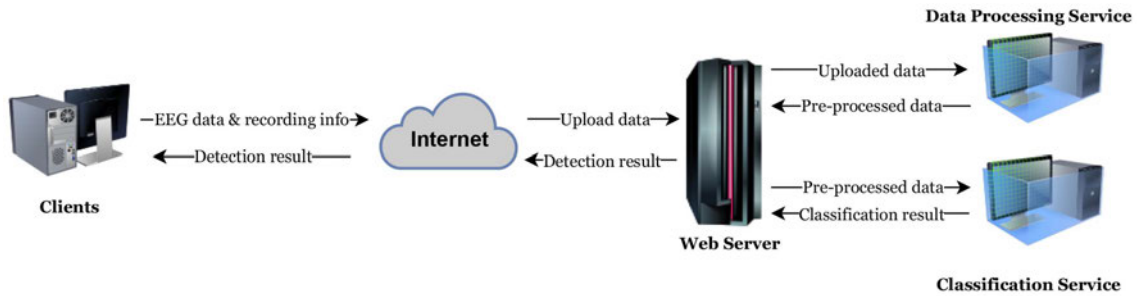


FIGURE 7.8: Workflow of the developed web-based system using the proposed SISDNet framework. The user uploads EEG data to the web server using a computer device. The server uses two services to perform the classification task: 1) the data processing service pre-processes the uploaded data, and 2) the classification service performs the classification on the processed data.

Figure 7.9 - 7.19 shows screen shots of different pages from the developed website. Details of those pages with functionality are discussed below.

Figure 7.9 shows the home page of the website. It contains a menu at the top of the page, and the user can switch to different pages by using that menu. It also shows the three steps involved in using the classification service, which are: i) prepare data; ii) upload data; and iii) check the result. The user can see more details of those steps by clicking the "Learn More" button or by using the "Classification" menu, under which there are three sub-menus for the three steps. This page also contains the project information for this research work.

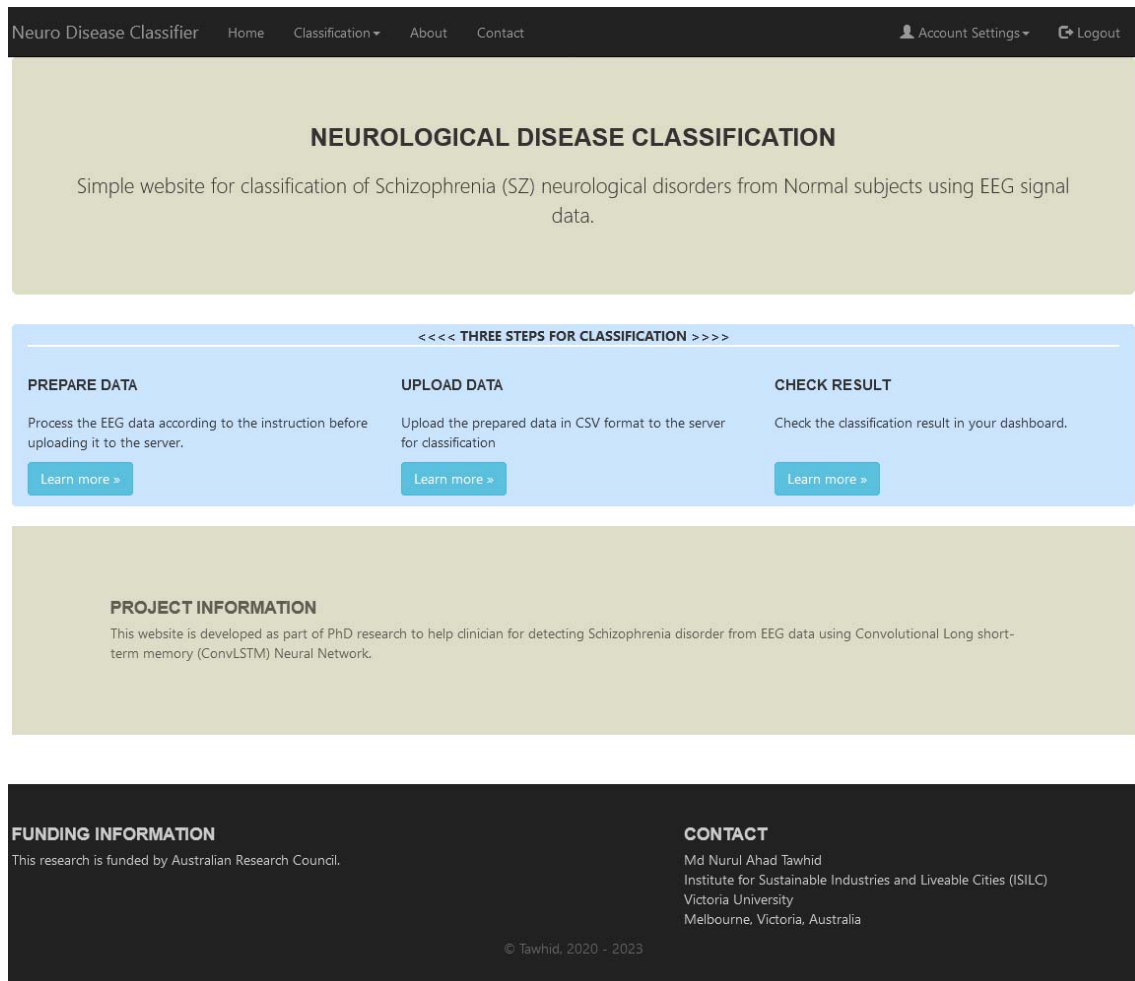


FIGURE 7.9: The Homepage of the developed web-based classification system.

Figure 7.10 shows the project information and the personnel involved in this research work with their different research profile links. Here, we have added the Google Scholar, LinkedIn, and personal profiles of their corresponding institutions if people are interested in seeing any information about any member of the research team.

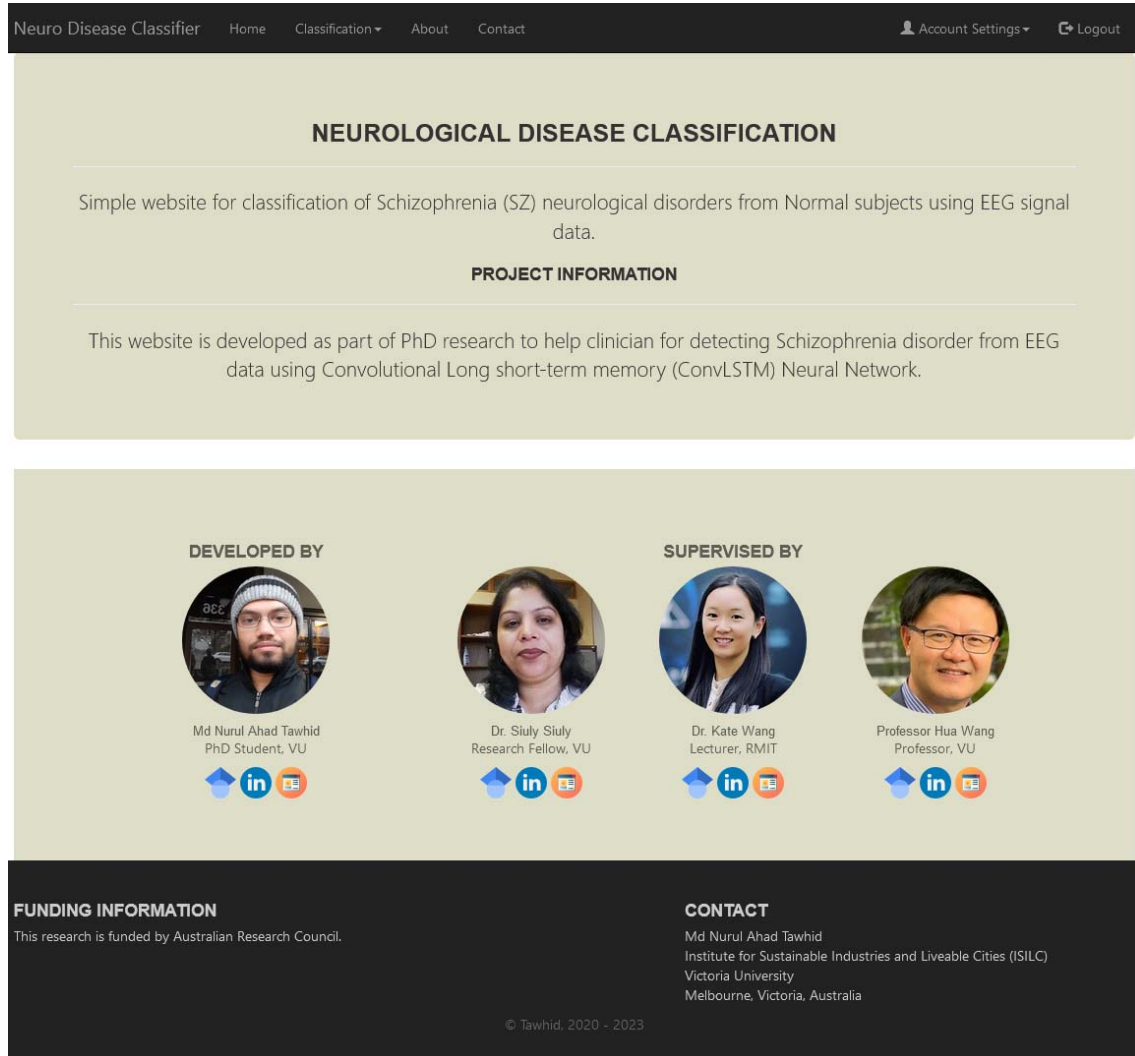


FIGURE 7.10: Information page of the developed web-based classification system. It contains information about the developer and the supervisor panel of the project, as well as links to their profiles on different social and institutional sites.

Figure 7.11 shows the contact page for the user. If any user of the website wants to contact us about any query or issue, they can use this form to do so. Users need to provide their name, email address, subject, query, and any attachment related to the query and send it to us, and we will see if we can solve the issues after receiving the email. To add an attachment, the user needs to click on the "Browse" button, which will open a file selection box from which the user will select the desired file and then click "Open" to attach the chosen file with the query.

The screenshot displays the 'CONTACT US' form on the Neuro Disease Classifier website. The form is set against a light olive-green background. At the top, a dark navigation bar contains the site name and menu items. The form fields are as follows:

- Name:** A single-line text input field.
- Subject:** A single-line text input field.
- Email:** A single-line text input field.
- Message:** A rich text editor with a toolbar containing options for undo, redo, bold, italic, bulleted list, numbered list, link, and unlink. The text area contains a single paragraph 'p'.
- Attachment:** A section with a 'Browse...' button and the text 'No file selected.' Below this is a 'Send' button.

The footer is a dark grey/black bar with white text. It is divided into two columns:

- FUNDING INFORMATION:** This research is funded by Australian Research Council.
- CONTACT:** Md Nurul Ahad Tawhid, Institute for Sustainable Industries and Liveable Cities (ISILC), Victoria University, Melbourne, Victoria, Australia.

© Tawhid, 2020 - 2023

FIGURE 7.11: Contact page of the website. On this page, an user can contact the system support team with any issues or suggestions regarding the website.

To use the classification service, users need to have an account in the system, and they need to login to the system using those credentials. Figure 7.12 shows the authentication page of the system, where users need to provide their email address and password to get authenticated into the developed system. If the user is not yet registered in the system and is a new user, s/he can register by clicking on the "Register" link on the page, which will redirect her/him to the account creation page. On the other hand, if the user forgets her or his password, she or he can retrieve it by clicking on the "Forgot Password?" link.

Neuro Disease Classifier Home Classification About Contact Sign Up Login

### LOGIN

Email

Password

Login

[Register](#) | [Forgot Password?](#)

**FUNDING INFORMATION**  
This research is funded by Australian Research Council.

**CONTACT**  
Md Nurul Ahad Tawhid  
Institute for Sustainable Industries and Liveable Cities (ISILC)  
Victoria University  
Melbourne, Victoria, Australia

© Tawhid, 2020 - 2023

FIGURE 7.12: Login page of the website. Users need to have an account to use the classification service of the system. By using the email and password, they can login to the system.

A new user can create an account on the website to use the web service. Figure 7.13 shows the account creation page of the website. Users can access the page by clicking the "Sign Up" link on the top right menu bar or by clicking the "Register" link on the login page. To create an account, the user needs to provide their name, a valid email address, and the password that they want to use for logging into the system. After filling out all the fields and clicking the "Sign up" button, an account activation email will be sent to the user's email address. The user needs to click on the link to activate her or his account in the system.

Neuro Disease Classifier Home Classification About Contact Sign Up Login

### REGISTER

Name

Email

Password

Confirm Password

Sign up

**FUNDING INFORMATION**  
This research is funded by Australian Research Council.

**CONTACT**  
Md Nurul Ahad Tawhid  
Institute for Sustainable Industries and Liveable Cities (ISILC)  
Victoria University  
Melbourne, Victoria, Australia

© Tawhid, 2020 - 2023

FIGURE 7.13: Login page of the website. Users need to have an account to use the classification service of the system. By using the email and password, they can login to the system.

If an existing user forgets her or his password to login into the system, then s/he can request resetting the password of her or his account using the reset password page. On this page, the user needs to provide the email address that s/he used to open the account and then press the "Reset" button. After that, if the email address is correct and exists in the system, the user will receive an email with a link to reset their password. By clicking the reset link, the user will be redirected to the password reset page, where s/he will provide the new password for her/his existing account.

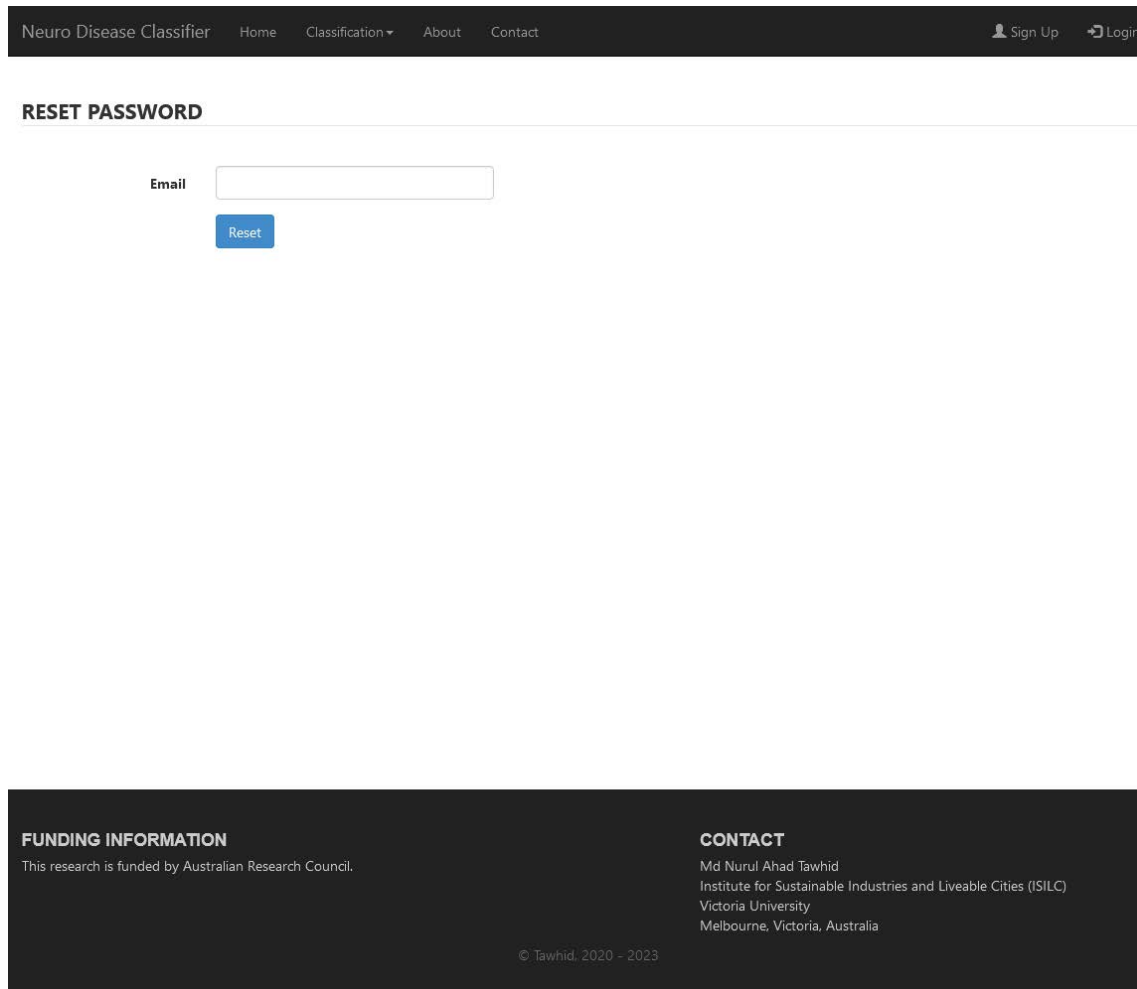


FIGURE 7.14: This page is for resetting the account password. If the user forgets her or his password, then she or he can request to reset it by using this page.

To change the password of an existing account, the user can use the "Change Password" page, which s/he can access by clicking on the "Account Settings" drop-down menu on the top right of the page. The page contains three input fields for inputting the passwords, as shown in Figure 7.15. In the first input field, s/he needs to put the current password that s/he wants to change, and in the following two fields, s/he needs to put the new password that s/he wants to use for next time's login. After that, s/he needs to press the "Change" button to save the changed password in the system.

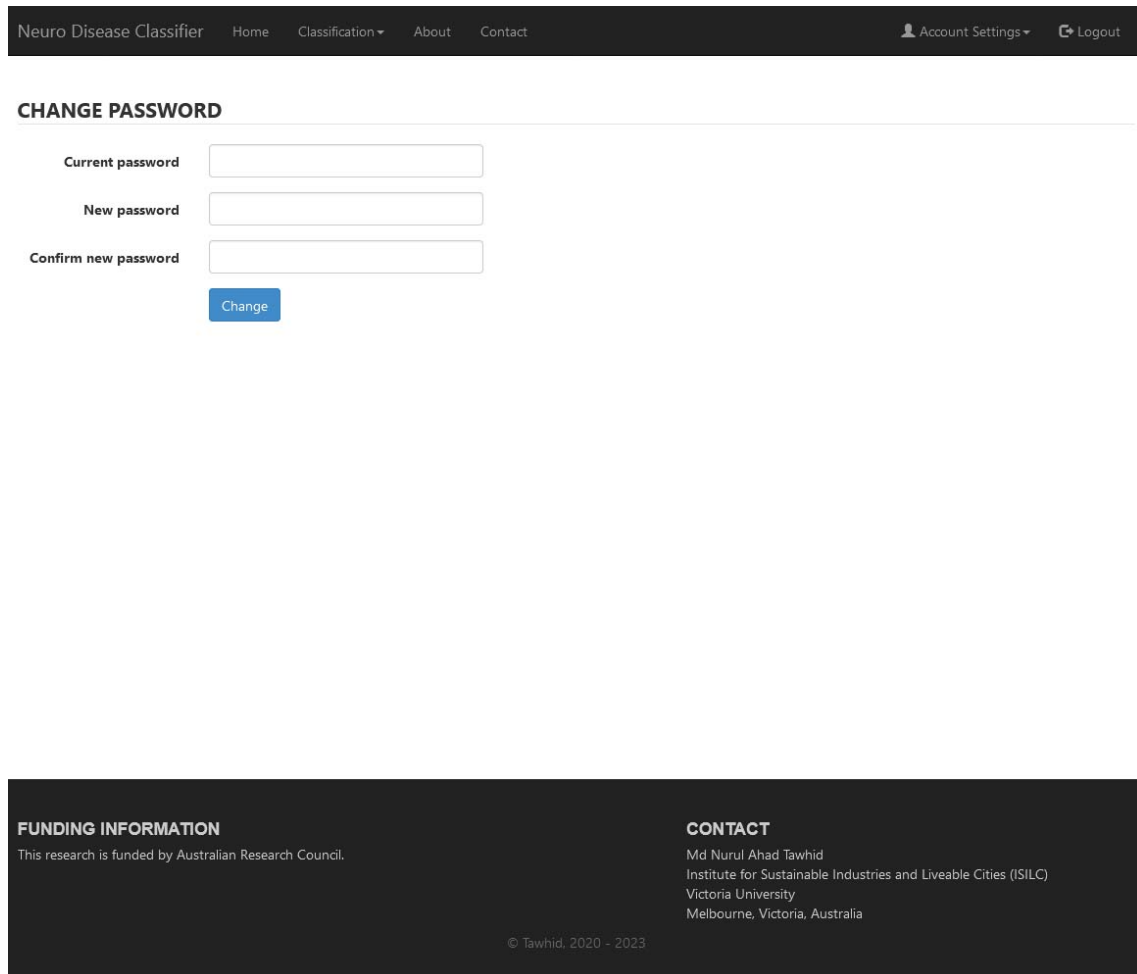


FIGURE 7.15: This page is for changing the account password. The user needs to put the current password and the new password for changing the account password.

To use the classification service of the developed website, users need to do some preparation of their data before uploading it to the website. Figure 7.16 shows the Prepare Data page that contains the instructions about preparing data before uploading to the system. If the user's data meets the preparation instruction, then s/he can upload the data to the system by clicking the "Upload Data" button at the bottom of the instruction or by using the top menu under the "Classification" drop-down menu item.

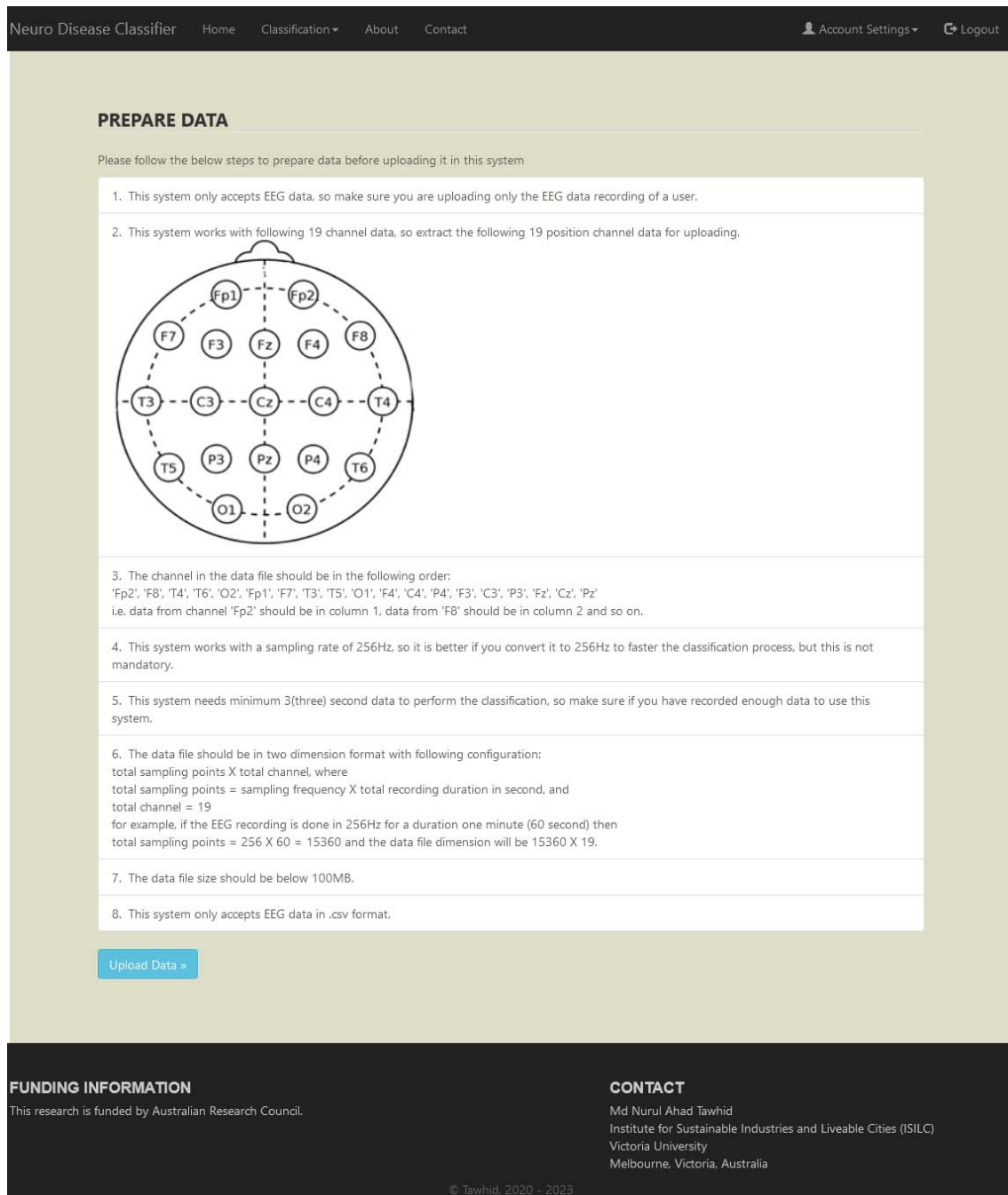


FIGURE 7.16: This page shows the data preparation instruction before uploading to the classification service.

On the upload page, the user will upload the prepared data to the web server for classification purposes. Figure 7.17 shows the screen shot of the upload page. On this page, there are some check boxes to check by the user to ensure that s/he has followed the instructions for preparing the data and s/he has consented to upload the data in the developed system, as the system stores the uploaded data. If the user agrees to all the check lists, then the data upload panel is enabled to upload the data. The system also asks for some basic demographic information about the test subject. After filling out those details and selecting the csv data file, the user needs to click on the "Upload" button to finish the upload task.

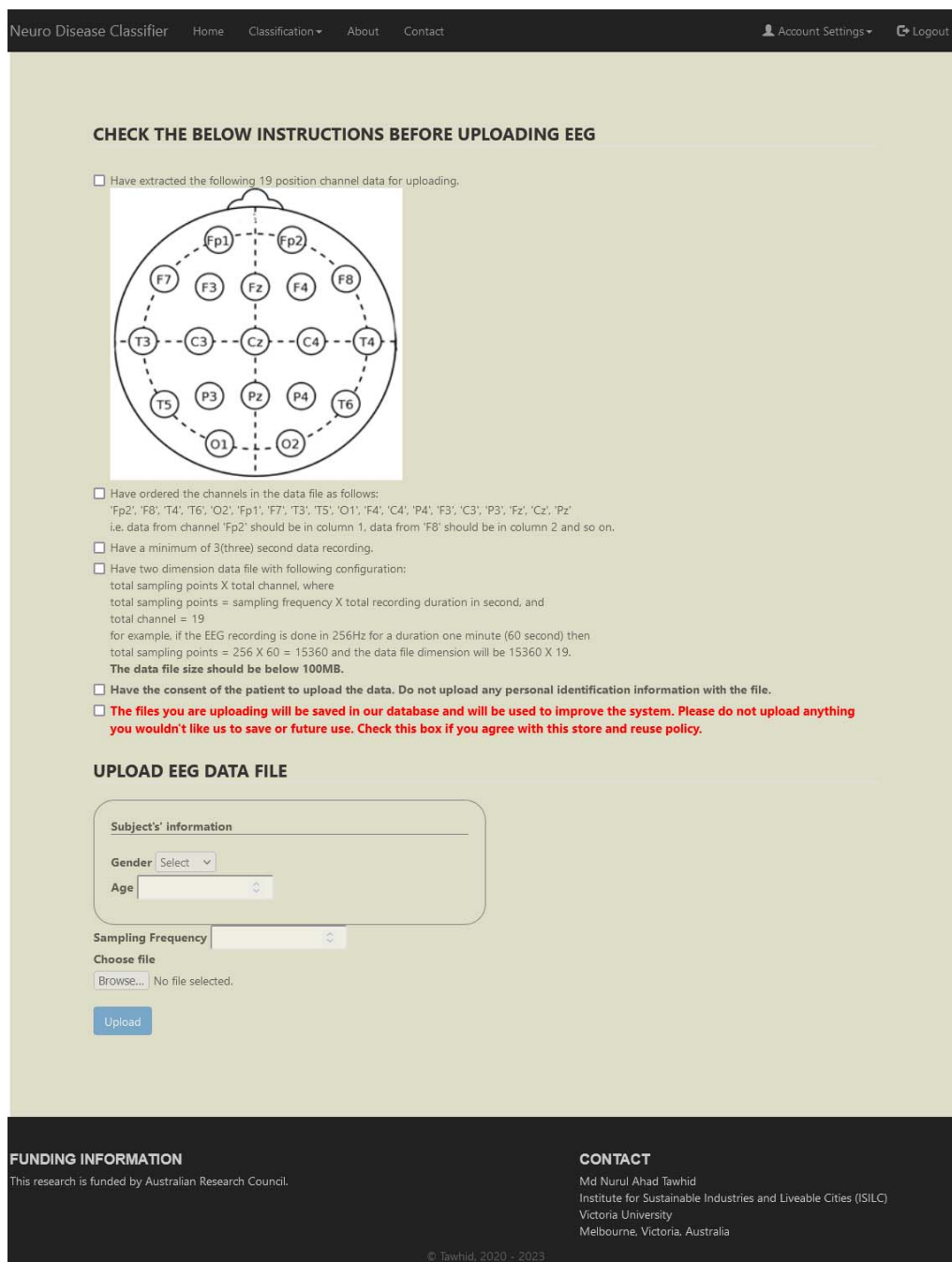


FIGURE 7.17: Web page for uploading the data to the classification server.

After uploading the data to the server, the user can check the classification status and results using the "Classification Results" page. On this page, the user can see the list of classification tasks s/he has uploaded till now, with the latest submission at the top of the list, as shown in Figure 7.18. The page contains a list of requests with the request number, the time when the request was made, the status of the requested task, the uploaded file name, and a link to view the details of the task's result if it was a success. The Status field value varies based on the current task done by the classification system, like pre-processing data, classification, error, completed etc.

**CLASSIFICATION RESULTS**

Refresh Want to check new file? [Upload New](#)

Show  entries Search:

Request Number	Requested Time	Status	FileName	
313202314377709	31/03/2023 2:37:07 PM	Completed	h14.csv	<a href="#">View Details Result</a>
3132023142740308	31/03/2023 2:27:40 PM	Completed	s14.csv	<a href="#">View Details Result</a>
3132023141931288	31/03/2023 2:19:31 PM	Classifying	h04.csv	Details result not available yet
3132023141346198	31/03/2023 2:13:46 PM	Error	h04.csv	Details result not available yet
172202313253871	17/02/2023 1:25:03 PM	Completed	h03.csv	<a href="#">View Details Result</a>
522023112244643	5/02/2023 11:22:44 AM	Completed	h14.csv	<a href="#">View Details Result</a>
522023111032578	5/02/2023 11:10:32 AM	Completed	s14.csv	<a href="#">View Details Result</a>
52202311853119	5/02/2023 11:08:53 AM	Completed	h01.csv	<a href="#">View Details Result</a>
52202311743687	5/02/2023 11:07:43 AM	Completed	h02.csv	<a href="#">View Details Result</a>
522023105437500	5/02/2023 10:54:37 AM	Error	h01.csv	Details result not available yet

Showing 1 to 10 of 118 entries First Previous  2 3 4 5 ... 12 Next Last

**FUNDING INFORMATION**  
This research is funded by Australian Research Council.

**CONTACT**  
Md Nurul Ahad Tawhid  
Institute for Sustainable Industries and Liveable Cities (ISILC)  
Victoria University  
Melbourne, Victoria, Australia

© Tawhid, 2020 - 2023

FIGURE 7.18: This page shows the list of classification request an user have made till now. They can also see the details result of the classification by clicking on the view result button at the end of each row.

DETAILS RESULT

<< BACK TO REQUEST LIST



**Details information of the classification request**

Request Number	313202314377709	Request Time	31/03/2023 2:37:07 PM
Gender	Male	Age	56
Sampling Frequency	250 Hz	Uploaded File	h14.csv
Data Processing Start Time	31/03/2023 2:37:07 PM	Data Processing End Time	31/03/2023 2:37:13 PM
Classification Start Time	31/03/2023 2:37:13 PM	Classification End Time	31/03/2023 2:37:37 PM

SEGMENT WISE RESULT

Show 10 entries Search:

Segment Number	Normal	Schizophrenia	Classification Result
1	99.95%	0.05%	Normal
2	99.96%	0.04%	Normal
3	99.96%	0.04%	Normal
4	97.12%	2.88%	Normal
5	100%	0%	Normal
6	99.92%	0.08%	Normal
7	99.48%	0.52%	Normal
8	44.67%	55.33%	Schizophrenia
9	94.31%	5.69%	Normal
10	100%	0%	Normal

Showing 1 to 10 of 288 entries First Previous 1 2 3 4 5 ... 29 Next Last

FIGURE 7.19: Details result page of a classification request displayed using different charts and tables.

On the classification result page, if the user clicks on the "View Details Result" link of a particular requested task that has a "Success" status field value, then s/he will be redirected to this page where s/he can see the details result of that particular classification request as shown in Figure 7.19. On this page, the user will see the detailed result of the classification task. The page has four sections: On the top section, a summary of the classification result is presented in tabular format. The first row of the table contains the total number of segments generated by the segmentation process of the uploaded data; the second row shows the number of segments identified as normal; the third row contains the number of segments identified as schizophrenia; and the fourth row contains the probability of the uploaded data being normal vs. schizophrenia. In the second section, there are two graphs showing the probability of the two classes and their distribution. The third section contains detailed information about the uploaded data, like demographic information, upload file name, upload time, processing start/end time, classification start/end time, etc. Finally, the fourth segment contains the individual segments probability of being either normal or schizophrenia.

## 7.4 Summary

In this chapter, a subject-independent deep learning-based model named SISDNet is proposed to classify schizophrenia disorder using EEG data. SISDNet is a ConvLSTM-based model that is designed to take input raw EEG signal data and train its internal layers with the significant features of the data to perform classification tasks. Along with the subject-independent analysis, we have also evaluated the proposed model for the 10-fold cross-validation technique. We have tested the model on two different datasets of schizophrenia disorders to validate the obtained results. We have also tested three different training batch sizes to observe the impact on training the model.

In subject-independent analysis, for the Kaggle dataset, we obtained an accuracy of 95.37% with batch size 128, while for Warsaw, it is 96.32% using batch size 32, and both are higher than state-of-the-art works using those datasets. For subject-dependent 10-fold cross-validation, we have achieved 96.31% and 99.24% accuracy for the Kaggle and Warsaw datasets, respectively. We have done several ablation studies to validate the proposed SISDNet model. Additionally, a t-SNE image-based analysis of the extracted features of the proposed model is also performed to check the classification performance of SISDNet. At last, we have developed a web-based schizophrenia classification system to help clinicians in their real-life work.

Finally, the findings show that this method can be used to categorise other neurological disorders and can also be used in other signal processing tasks. Moreover, the developed web-based system can be improved to work and be used in real-world clinics, and it needs to be extended to other neurological disorders.

## Chapter 8

# Conclusions and Future Work

### 8.1 Summary of the dissertation

The EEG is a non-invasive method used to record electrical activity in the brain. It provides valuable insights into brain functioning and has considerable potential in the context of mental and neurodegenerative diseases and abnormalities. EEG enables researchers and medical professionals to observe patterns of brain activity, analyse changes over time, and identify potential irregularities in brain function.

EEG plays a crucial role in the diagnosis and treatment of various mental and brain neurodegenerative disorders. By analysing EEG data, medical practitioners can detect anomalies and patterns associated with specific conditions, aiding in early diagnosis and providing a foundation for effective treatment strategies. This non-invasive technique has become an essential tool in the fields of neuroscience and clinical neurology.

Classifying EEG signals is a significant challenge in biomedical research. The diversity and complexity of brain activity patterns require the analysis of large datasets to identify and differentiate various types of EEG signals accurately. Effective classification methods are necessary for distinguishing normal brain activity from abnormal patterns associated with different diseases.

To classify EEG signals accurately, it is essential to extract representative features from the large datasets. These features act as characteristic markers that help differentiate between different types of brain activity. By identifying and selecting relevant features, researchers can enhance the accuracy and efficiency of EEG signal classification algorithms.

The passage mentions that the dissertation revolves around studying and developing EEG signal processing and classification techniques. The primary aim is to identify and differentiate between various types of EEG signals effectively. The three main objectives of the dissertation are likely to involve refining existing signal processing techniques, developing novel classification algorithms, and applying these methods to real-world EEG data for accurate identification of brain activity patterns.

In this research study, we have developed some EEG signal processing and classification techniques to meet the following goals:

1. Developed methods for the classification of ASD and SZ subjects from HC subjects using EEG signals.

2. Developed a multi-class classification framework for classifying multiple neurological disorders using a single system.
3. Developed a generic EEG signal classification framework independent of dataset and disorder.
4. Developed a web-based system for classification of the SZ disorder using EEG data.

To achieve those goals, we have developed a spectrogram image-based EEG classification framework for ASD signal detection (Chapter 3). This spectrogram image-based classification technique was first used in this study for the ASD classification process from EEG data. In this process, we first filtered the data to remove different noises and then generated spectrogram images from the filtered signals using an STFT-based plotting technique and segmented them into small time-frame segments. After that, those images are used for classification using different ML and DL-based techniques. In ML-based classification, we extracted histogram base features using tCENTRIST, reduced the dimension of the extracted features using PCA, and finally used six different ML-based classifiers (NB, RF, SVM, LDA, LR, and  $k$ NN) are used to classify the reduced features. On the other hand, in DL-based classification, we have developed three different CNN models and used those to classify the spectrogram images. We have evaluated the proposed model using the dataset from King Abdulaziz University (KAU) Hospital, Saudi Arabia, Jeddah [177] and obtained an accuracy of 95.25% for the ML-based approach using the SVM classifier and 99.15% for the DL-based approach. Experimental results show that the proposed system is capable of distinguishing ASD signals from healthy signals.

In our second method, we developed a topographic image with a deep learning-based CNN model to categorise SZ from HC subjects (Chapter 4). This topographic image-based framework is also first used in this study for SZ classification from EEG signals. In this approach, at first the signals were segmented into small time frames, and then the topographic images were generated from the signal segments using topographic plotting of the entropy values calculated by Shannon entropy. After that, the generated images were classified into SZ vs. HC using a newly proposed CNN model. The proposed framework was evaluated using two different open-access EEG datasets of SZ disorders. This framework also shows promising results in the classification of EEG data for SZ detection.

In the third approach, we extended the spectrogram image-based method for designing a novel multi-class neurological disorder classifier for classifying four neurological disorders, namely: ASD, SZ, PD, and EP, from HC subjects (Chapter 5). Similar to the first approach, we filtered the EEG signals and generated the spectrogram images using the STFT-based plotting technique. After that, we used both ML- and DL-based techniques to perform the classification of those images. In the ML-based approach, we used two feature extractors named tCENTRIST and cCENTRIST separately and reduced the extracted feature dimension using PCA. Finally, four ML-based classifiers (RF, SVM, LDA, and  $k$ NN) are used to compare the classification performance on the reduced features. On the DL-based approach, we modified the best proposed model of the first method for multi-class classification among the five classes (ASD vs. SZ vs. PD vs. EP vs. HC). We

also conducted binary classification (disorder vs. HC) of the used datasets for the DL-based approach. The proposed approaches were evaluated using four EEG datasets: ASD, SZ, EP, and EP disorder. The experimental result shows the possibility of developing a common system for the classification of EEG signals for multiple diseases.

A noble generic CNN model is proposed to classify EEG data from different neurological disorders (Chapter 6). This proposed model shows that instead of developing a separate framework for each dataset or disease, a single framework can be developed that will work on different datasets of a single disease as well as different datasets from different diseases. In this approach, we first segmented the raw EEG data into small time frames and then developed a CNN model to perform classification on those segments. To check the generalisability, we tested the proposed framework on seven different datasets from six different diseases. We tested three different segment lengths, four different training batch sizes, and the 10-fold CV technique. We also performed a multi-class classification using four of the tested datasets. The experimental results outperformed all the state-of-the-art results for the datasets used in this study. The findings showed that this method is versatile and may be applied to different disease classification tasks using EEG data and other signal processing tasks.

Finally, we developed a web-based system for SZ detection using a new technique to perform subject-independent classification tasks (Chapter 7). This new approach will reduce classification errors, training time, and the analysis and classification of EEG brain signals. Also, the developed web-based CAD system will help clinicians in their diagnosis process. In this proposed method, the EEG data are first segmented into small time frames, and then a DL-based model is developed using ConvLSTM to perform classification on those signal segments. We evaluated the proposed framework using both LOOCV and 10-fold CV on two different publicly available datasets of SZ disorders and obtained better performance than the existing methods. We have also developed a web-based system using the trained model in the back-end of the website to do the classification task on the uploaded data to the system.

In summary, the main focus of this PhD work was on ASD and SZ detection from EEG signal data, and the research presented here in this dissertation has found some innovative and effective systems for classification of EEG signals in the biomedical signal processing field. These methods will make it possible for neurologists to accurately and efficiently detect brain degenerative disorders. Moreover, the developed web-based system will be helpful for clinicians in the clinical diagnosis process and for brain disorder patients to improve the quality of their lives.

## 8.2 Limitations of this research work

While our study provides valuable insights, it is not without its limitations. Some of the limitations of this work are reported below:

In this study, we've directed our attention towards Autism Spectrum Disorder (ASD) and Schizophrenia (SZ) despite the existence of over six hundred neurological disorders.

This focus was necessitated by time constraints that limited the scope of the research. While numerous neurological disorders warrant investigation, the complexities and depth required for comprehensive analysis within a limited time-frame made focusing on ASD and SZ more feasible.

A significant challenge faced during this research was the availability and size of datasets. Publicly accessible datasets pertaining to these specific neurological conditions are notably scarce. Furthermore, the datasets that do exist are often limited in terms of the number of subjects included. This limitation can potentially impact the depth and robustness of our study's conclusions. The smaller sample size might restrict the generalisability of findings and the ability to draw comprehensive conclusions representative of the entire population affected by ASD and SZ.

An additional constraint we encountered relates to the collection of data. While the ideal approach would involve gathering our own dataset to mitigate limitations found in existing datasets, this was unattainable due to constraints in both time and budget. The process of collecting data can be resource-intensive and time-consuming, and these constraints prevented us from acquiring a more extensive and tailored dataset that might have enriched the study's outcomes.

These limitations acknowledge the boundaries within which the research was conducted and emphasize the challenges faced. Despite these constraints, the study aims to provide valuable insights within the specified scope and dataset limitations, while also highlighting the need for more extensive datasets and additional research efforts in the field of neurological disorders.

### 8.3 Future work

We believe that the approaches described in this dissertation have a positive impact in the field of neurological disorders, particularly ASD and SZ classification from EEG signal data. Future research will focus on examining the viability of applying the techniques to other neurological disorder categorisations from EEG data. Additionally, we have highlighted a few key issues that can be addressed in the future.

Firstly, EEG signals can be prone to contamination by various artefacts that can stem from multiple sources, including the subject's physiological factors and interference from the equipment used to measure the EEG signals. Unfortunately, in the context of this specific dissertation, the proposed methods did not focus on the development of techniques to effectively remove these artefacts from EEG data. However, recognising the significance of artefact-free EEG data for the success of the proposed algorithms, the need for further investigation and study in this area becomes evident. The main objective is to devise robust methodologies that can successfully eliminate artefacts without compromising the integrity and quality of the underlying EEG signals. As the research progresses, future iterations of the algorithms will be fine-tuned and enhanced to accommodate artefact removal effectively. This refinement process is expected to yield substantial improvements in signal classification, ultimately leading to more accurate and reliable results. By ensuring

that the EEG signals are free from contamination, the algorithms' performance will be optimised, and their potential applications in various domains, such as brain-computer interfaces and neurological research, can be fully realised.

Secondly, in most of our proposed methods, we have used the full frequency bands of the EEG signal for analysis and classification, but as we know, EEG signals have different frequency sub-bands like delta, theta, alpha, beta, and gamma. So, in the future, we can focus on finding the frequency sub-bands that have more influence over other sub-bands in the classification process of EEG signals. EEG signals offer important data on the electrical activity of the brain. Researchers and physicians can acquire insights into certain brain functions, such as different sleep stages, cognitive activities, emotional states, or epileptic seizures, by finding important frequency sub-bands. Researchers may examine the dynamics and interconnectedness of the brain since each frequency sub-band corresponds to a certain neural activity. Additionally, certain neurological and psychiatric disorders exhibit characteristic patterns in specific frequency subbands. Identifying these patterns can aid in the diagnosis, monitoring, and understanding of the underlying mechanisms of different neurological disorders.

Thirdly, most of the proposed methods have used all the channel recordings of the EEG data, but in the future, we can focus on finding the important channels for classifying different neurological disorders. EEG signals are measured from different electrodes placed on the scalp, each corresponding to a specific brain region. Identifying important EEG channels provides valuable insights into brain function, localised brain activity, and brain disorders. It contributes to advancements in neuroscience, personalised medicine, brain-computer interfaces, and other brain-related applications. Understanding the significance of specific EEG channels enhances our knowledge of the brain and its complexities, leading to improved diagnosis, treatment, and overall brain health.

Fourthly, we have developed a web-based system that works only for schizophrenia, but it can be extended to other disorders like AD, MCI, PD, ASD, etc. Moreover, the developed system is currently in the initial phase, which can be enhanced based on the clinician's feedback for real-life use.

Finally, it is hoped that the output of this research work will be beneficial to the medical field while at the same time contributing to knowledge enhancement in the academic world.

# Bibliography

- [1] W. H. Organization *et al.*, “Optimizing brain health across the life course: Who position paper,” 2022.
- [2] WHO, *What are neurological disorders?* (Date last accessed February 2022). [Online]. Available: <https://www.who.int/news-room/questions-and-answers/item/mental-health-neurological-disorders>.
- [3] WHO, *Mental health*, (Date last accessed February 2023). [Online]. Available: <https://www.who.int/news-room/facts-in-pictures/detail/mental-health>.
- [4] A. I. of Health and Welfare, “Australian burden of disease study 2022,” 2022.
- [5] W. H. Organization *et al.*, “Global status report on the public health response to dementia,” 2021.
- [6] M. Elsabbagh, G. Divan, Y.-J. Koh, *et al.*, “Global prevalence of autism and other pervasive developmental disorders,” *Autism research*, vol. 5, no. 3, pp. 160–179, 2012.
- [7] WHO, *Autism spectrum disorders*, (Date last accessed June 2023). [Online]. Available: <https://www.who.int/news-room/fact-sheets/detail/autism-spectrum-disorders>.
- [8] J. Zeidan, E. Fombonne, J. Scolah, *et al.*, “Global prevalence of autism: A systematic review update,” *Autism research*, vol. 15, no. 5, pp. 778–790, 2022.
- [9] A. S. A. (Aspect), *Autism prevalence rate up by an estimated 40people*, (Date last accessed August 2020). [Online]. Available: <https://www.autismspectrum.org.au/news/autism-prevalence-rate-up-by-an-estimated-40-to-1-in-70-people-11-07-2018>.
- [10] A. Speaks, *Autism statistics and facts*, (Date last accessed August 2020). [Online]. Available: <https://www.autismspeaks.org/autism-statistics>.
- [11] N. I. of Mental Health, *Schizophrenia*, (Date last accessed February 2023). [Online]. Available: <https://www.nimh.nih.gov/health/topics/schizophrenia>.
- [12] D. of Health and H. S. Australia, *Schizophrenia*, (Date last accessed February 2023). [Online]. Available: <https://www.betterhealth.vic.gov.au/health/conditionsandtreatments/schizophrenia>.
- [13] WHO, *Schizophrenia*, (Date last accessed February 2023). [Online]. Available: <https://www.who.int/news-room/fact-sheets/detail/schizophrenia>.

- [14] M. A. Hofman, "Design principles of the human brain: An evolutionary perspective," *Progress in brain research*, vol. 195, pp. 373–390, 2012.
- [15] N. R. Carlson, *Foundations of physiological psychology*. Pearson Education New Zealand, 2005.
- [16] D. Purves, G. J. Augustine, D. Fitzpatrick, W. Hall, A.-S. LaMantia, and L. White, *Neurosciences*. De Boeck Supérieur, 2019.
- [17] D. K. Ravish, S. S. Devi, S. G. Krishnamoo, and M. R. Karthikeya, "Detection of epileptic seizure in eeg recordings by spectral method and statistical analysis," *Journal of Applied Sciences*, vol. 13, no. 2, pp. 207–219, Feb. 2013. DOI: [10.3923/jas.2013.207.219](https://doi.org/10.3923/jas.2013.207.219).
- [18] B. Blankertz, R. Tomioka, S. Lemm, M. Kawanabe, and K.-R. Muller, "Optimizing spatial filters for robust eeg single-trial analysis," *IEEE Signal processing magazine*, vol. 25, no. 1, pp. 41–56, 2007.
- [19] Ö. F. Alçın, S. Siuly, V. Bajaj, Y. Guo, A. Şengu, and Y. Zhang, "Multi-category eeg signal classification developing time-frequency texture features based fisher vector encoding method," *Neurocomputing*, vol. 218, pp. 251–258, 2016.
- [20] Y. Kutlu, M. Kuntalp, and D. Kuntalp, "Optimizing the performance of an mlp classifier for the automatic detection of epileptic spikes," *Expert Systems with Applications*, vol. 36, no. 4, pp. 7567–7575, 2009.
- [21] A. Subasi and E. Ercelebi, "Classification of eeg signals using neural network and logistic regression," *Computer methods and programs in biomedicine*, vol. 78, no. 2, pp. 87–99, 2005.
- [22] S. Siuly, Y. Li, and Y. Zhang, "Eeg signal analysis and classification," *IEEE Trans Neural Syst Rehabil Eng*, vol. 11, pp. 141–4, 2016.
- [23] F. Gray, *Anatomy for the Medical Clinician: Relating Structure to Function, Symptomatology, Diagnosis and Treatment*. Gray, F J, 2002, ISBN: 9780646411224.
- [24] M. Nedergaard and S. A. Goldman, "Brain drain," *Scientific American*, vol. 314, no. 3, p. 44, 2016.
- [25] K. Miller, *Biomechanics of the Brain*. Springer, 2011.
- [26] J. H. Medicine, *Brain anatomy and how the brain works*, (Date last accessed July 2023). [Online]. Available: <https://www.hopkinsmedicine.org/health/conditions-and-diseases/anatomy-of-the-brain>.
- [27] E. R. Kandel, J. H. Schwartz, T. M. Jessell, S. Siegelbaum, A. J. Hudspeth, S. Mack, *et al.*, *Principles of neural science*. McGraw-hill New York, 2000, vol. 4.
- [28] T. Roostaei, A. Nazeri, M. A. Sahraian, and A. Minagar, "The human cerebellum: A review of physiologic neuroanatomy," *Neurologic clinics*, vol. 32, no. 4, pp. 859–869, 2014.
- [29] S. Herculano-Houzel, "The human brain in numbers: A linearly scaled-up primate brain," *Frontiers in human neuroscience*, p. 31, 2009.

- [30] B. Szymik, *Neuron anatomy*, (Date last accessed August 2023), May 2011. [Online]. Available: <https://askbiologist.asu.edu/neuron-anatomy>.
- [31] S. Luengo-Sanchez, C. Bielza, R. Benavides-Piccione, I. Fernaud-Espinosa, J. De-Felipe, and P. Larrañaga, “A univocal definition of the neuronal soma morphology using gaussian mixture models,” *Frontiers in neuroanatomy*, vol. 9, p. 137, 2015.
- [32] M. A. Miller and J. F. Zachary, “Mechanisms and morphology of cellular injury, adaptation, and death,” *Pathologic basis of veterinary disease*, p. 2, 2017.
- [33] N. I. of Neurological Disorders and Stroke, *Brain basics: Know your brain*, (Date last accessed August 2023), Mar. 2023. [Online]. Available: <https://www.ninds.nih.gov/health-information/public-education/brain-basics/brain-basics-know-your-brain>.
- [34] H. L. Atwood and W. A. MacKay, *Essentials of neurophysiology*. Mosby Inc, 1989.
- [35] J. W. Britton, L. C. Frey, J. L. Hopp, *et al.*, “Electroencephalography (eeg): An introductory text and atlas of normal and abnormal findings in adults, children, and infants,” 2016.
- [36] H. Berger, “Über das elektroenkephalogramm des menschen,” *Archiv für psychiatrie und nervenkrankheiten*, vol. 87, no. 1, pp. 527–570, 1929.
- [37] S. Sanei and J. A. Chambers, *EEG signal processing*. John Wiley & Sons, 2013.
- [38] Alchetron, *Hans berger*, (Date last accessed August 2023), Oct. 2022. [Online]. Available: <https://alchetron.com/Hans-Berger>.
- [39] J. S. Ebersole, “Cortical generators and eeg voltage fields,” *Current practice of clinical electroencephalography*, pp. 12–31, 2003.
- [40] A. Ahani, H. Wahbeh, H. Nezamfar, M. Miller, D. Erdogmus, and B. Oken, “Quantitative change of eeg and respiration signals during mindfulness meditation,” *Journal of neuroengineering and rehabilitation*, vol. 11, no. 1, pp. 1–11, 2014.
- [41] H. H. Jasper, “Ten-twenty electrode system of the international federation,” *Electroencephalogr Clin Neurophysiol*, vol. 10, pp. 371–375, 1958.
- [42] V. Jurcak, D. Tsuzuki, and I. Dan, “10/20, 10/10, and 10/5 systems revisited: Their validity as relative head-surface-based positioning systems,” *Neuroimage*, vol. 34, no. 4, pp. 1600–1611, 2007.
- [43] W. R. Martins, L. R. Diniz, J. C. Blasczyk, *et al.*, “Immediate changes in electroencephalography activity in individuals with nonspecific chronic low back pain after cranial osteopathic manipulative treatment: Study protocol of a randomized, controlled crossover trial,” *BMC complementary and alternative medicine*, vol. 15, no. 1, pp. 1–7, 2015.
- [44] E. Niedermeyer and F. L. da Silva, *Electroencephalography: basic principles, clinical applications, and related fields*. Lippincott Williams & Wilkins, 2005.
- [45] B. J. Fisch and R. Spehlmann, “Eeg primer: Basic principles of digital and analog eeg,” *Elsevier Health Sciences*, pp. 23–27, 1999.

- [46] P. A. Abhang, B. W. Gawali, and S. C. Mehrotra, *Introduction to EEG-and speech-based emotion recognition*. Academic Press, 2016.
- [47] M. Corsi-Cabrera, M. A. Guevara, C Arce, Y Villanueva-Hernández, *et al.*, “Eeg bands during wakefulness, slow-wave and paradoxical sleep as a result of principal component analysis in man.,” *Sleep*, vol. 23, no. 6, pp. 738–744, 2000.
- [48] G. Adelman, “Encyclopedia of,” *Neuroscience. Boston, Birkhauser*, 1987.
- [49] M. Abo-Zahhad, S. M. Ahmed, and S. N. Abbas, “A new eeg acquisition protocol for biometric identification using eye blinking signals,” *International Journal of Intelligent Systems and Applications*, vol. 7, no. 6, p. 48, 2015.
- [50] F. A. Gibbs and E. L. Gibbs, “Atlas of electroencephalography.,” 1941.
- [51] D. American Psychiatric Association, A. P. Association, *et al.*, *Diagnostic and statistical manual of mental disorders: DSM-5*. American psychiatric association Washington, DC, 2013, vol. 5.
- [52] J. Baio, L. Wiggins, D. L. Christensen, *et al.*, “Prevalence of autism spectrum disorder among children aged 8 years—autism and developmental disabilities monitoring network, 11 sites, united states, 2014,” *MMWR Surveillance Summaries*, vol. 67, no. 6, p. 1, 2018.
- [53] C. for Disease Control and Prevention, *Data and statistics on autism spectrum disorder*, (Date last accessed August 2023), Apr. 2023. [Online]. Available: <https://www.cdc.gov/ncbddd/autism/data.html>.
- [54] R. Coben, A. R. Clarke, W. Hudspeth, and R. J. Barry, “Eeg power and coherence in autistic spectrum disorder,” *Clinical neurophysiology*, vol. 119, no. 5, pp. 1002–1009, 2008.
- [55] S. Schwartz, R. Kessler, T. Gaughan, and A. W. Buckley, “Electroencephalogram coherence patterns in autism: An updated review,” *Pediatric neurology*, vol. 67, pp. 7–22, 2017.
- [56] T. A. Stroganova, G. Nygren, M. M. Tsetlin, *et al.*, “Abnormal eeg lateralization in boys with autism,” *Clinical Neurophysiology*, vol. 118, no. 8, pp. 1842–1854, 2007.
- [57] A. Lefebvre, R. Delorme, C. Delanoë, *et al.*, “Alpha waves as a neuromarker of autism spectrum disorder: The challenge of reproducibility and heterogeneity,” *Frontiers in neuroscience*, vol. 12, p. 662, 2018.
- [58] G. Shou, M. W. Mosconi, L. E. Ethridge, J. A. Sweeney, and L. Ding, “Resting-state gamma-band eeg abnormalities in autism,” in *2018 40th Annual International Conference of the IEEE Engineering in Medicine and Biology Society (EMBC)*, IEEE, 2018, pp. 1915–1918.
- [59] L. A. De Stefano, L. M. Schmitt, S. P. White, M. W. Mosconi, J. A. Sweeney, and L. E. Ethridge, “Developmental effects on auditory neural oscillatory synchronization abnormalities in autism spectrum disorder,” *Frontiers in integrative neuroscience*, vol. 13, p. 34, 2019.

- [60] J. M. Peters, M. Taquet, C. Vega, *et al.*, “Brain functional networks in syndromic and non-syndromic autism: A graph theoretical study of eeg connectivity,” *BMC medicine*, vol. 11, no. 1, pp. 1–16, 2013.
- [61] C. O’Reilly, J. D. Lewis, and M. Elsabbagh, “Is functional brain connectivity atypical in autism? a systematic review of eeg and meg studies,” *PloS one*, vol. 12, no. 5, e0175870, 2017.
- [62] E. J. Marco, L. B. Hinkley, S. S. Hill, and S. S. Nagarajan, “Sensory processing in autism: A review of neurophysiologic findings,” *Pediatric research*, vol. 69, no. 8, pp. 48–54, 2011.
- [63] E. V. Orekhova, T. A. Stroganova, A. O. Prokofyev, G. Nygren, C. Gillberg, and M. Elam, “Sensory gating in young children with autism: Relation to age, iq, and eeg gamma oscillations,” *Neuroscience letters*, vol. 434, no. 2, pp. 218–223, 2008.
- [64] I. of health Metrics and E. (IHME), *Global health data exchange (ghdx)*, (Date last accessed February 2023). [Online]. Available: [https://ghdx.healthdata.org/ihme\\_data](https://ghdx.healthdata.org/ihme_data).
- [65] A.-M. Hanga and J. S. D. Völker, “Hidden strains: Understanding schizophrenia’s impact on families and communities,” 2023.
- [66] N. C. Venables, E. M. Bernat, and S. R. Sponheim, “Genetic and disorder-specific aspects of resting state eeg abnormalities in schizophrenia,” *Schizophrenia bulletin*, vol. 35, no. 4, pp. 826–839, 2009.
- [67] S. Williams and P. Boksa, “Gamma oscillations and schizophrenia,” *Journal of psychiatry & neuroscience: JPN*, vol. 35, no. 2, p. 75, 2010.
- [68] Y. Sun, F. Farzan, M. S. Barr, *et al.*, “Gamma oscillations in schizophrenia: Mechanisms and clinical significance,” *Brain research*, vol. 1413, pp. 98–114, 2011.
- [69] C. Basar-Eroglu, A. Brand, H. Hildebrandt, K. K. Kedzior, B. Mathes, and C. Schmiedt, “Working memory related gamma oscillations in schizophrenia patients,” *International journal of psychophysiology*, vol. 64, no. 1, pp. 39–45, 2007.
- [70] M. J. Magnée, B. Oranje, H. van Engeland, R. S. Kahn, and C. Kemner, “Cross-sensory gating in schizophrenia and autism spectrum disorder: Eeg evidence for impaired brain connectivity?” *Neuropsychologia*, vol. 47, no. 7, pp. 1728–1732, 2009.
- [71] P. Danjou, G Viardot, D Maurice, *et al.*, “Electrophysiological assessment methodology of sensory processing dysfunction in schizophrenia and dementia of the alzheimer type,” *Neuroscience & Biobehavioral Reviews*, vol. 97, pp. 70–84, 2019.
- [72] A. L. Bailliard and S. C. Whigham, “Linking neuroscience, function, and intervention: A scoping review of sensory processing and mental illness,” *The American Journal of Occupational Therapy*, vol. 71, no. 5, 7105100040p1–7105100040p18, 2017.
- [73] D. Umbricht and S. Krljes, “Mismatch negativity in schizophrenia: A meta-analysis,” *Schizophrenia research*, vol. 76, no. 1, pp. 1–23, 2005.

- [74] M. A. Erickson, A. Ruffle, and J. M. Gold, "A meta-analysis of mismatch negativity in schizophrenia: From clinical risk to disease specificity and progression," *Biological psychiatry*, vol. 79, no. 12, pp. 980–987, 2016.
- [75] A. M. A. Mahmoud, M. A.-E. Eissa, E. A. Kolkaila, R. A. R. Amer, and M. A. Kotait, "Mismatch negativity as an early biomarker of cognitive impairment in schizophrenia," *The Egyptian Journal of Neurology, Psychiatry and Neurosurgery*, vol. 59, no. 1, pp. 1–13, 2023.
- [76] A. Peled, A. B. Geva, W. S. Kremen, H. M. Blankfeld, R. Esfandiari, and T. E. Nordahl, "Functional connectivity and working memory in schizophrenia: An eeg study," *International Journal of Neuroscience*, vol. 106, no. 1-2, pp. 47–61, 2001.
- [77] S. Micheloyannis, E. Pachou, C. J. Stam, *et al.*, "Small-world networks and disturbed functional connectivity in schizophrenia," *Schizophrenia research*, vol. 87, no. 1-3, pp. 60–66, 2006.
- [78] E. Olejarczyk and W. Jernajczyk, "Graph-based analysis of brain connectivity in schizophrenia," *PLoS One*, vol. 12, no. 11, e0188629, 2017.
- [79] M. N. A. Tawhid, S. Siuly, and H. Wang, "Diagnosis of autism spectrum disorder from eeg using a time–frequency spectrogram image-based approach," *Electronics Letters*, 2020.
- [80] S. Siuly and Y. Zhang, "Medical big data: Neurological diseases diagnosis through medical data analysis," *Data Science and Engineering*, vol. 1, no. 2, pp. 54–64, 2016.
- [81] B. Hjorth, "Eeg analysis based on time domain properties," *Electroencephalography and clinical neurophysiology*, vol. 29, no. 3, pp. 306–310, 1970.
- [82] N. Kane, J. Acharya, S. Beniczky, *et al.*, "A revised glossary of terms most commonly used by clinical electroencephalographers and updated proposal for the report format of the eeg findings. revision 2017," *Clinical neurophysiology practice*, vol. 2, p. 170, 2017.
- [83] V. K. Harpale and V. K. Bairagi, "Time and frequency domain analysis of eeg signals for seizure detection: A review," in *2016 International Conference on Microelectronics, Computing and Communications (MicroCom)*, IEEE, 2016, pp. 1–6.
- [84] D. P. Subha, P. K. Joseph, R. Acharya U, and C. M. Lim, "Eeg signal analysis: A survey," *Journal of medical systems*, vol. 34, pp. 195–212, 2010.
- [85] A. S. Al-Fahoum and A. A. Al-Fraihat, "Methods of eeg signal features extraction using linear analysis in frequency and time-frequency domains," *International Scholarly Research Notices*, vol. 2014, 2014.
- [86] R. O. Duda, P. E. Hart, *et al.*, *Pattern classification and scene analysis*. Wiley New York, 1973, vol. 3.

- [87] R. Brunelli, *Template matching techniques in computer vision: theory and practice*. John Wiley & Sons, 2009.
- [88] S Siuly, Y. Li, and P. P. Wen, “Clustering technique-based least square support vector machine for eeg signal classification,” *Computer Methods and Programs in Biomedicine*, vol. 104, no. 3, pp. 358–372, 2011.
- [89] P. D. Velu and V. R. de Sa, “Single-trial classification of gait and point movement preparation from human eeg,” *Frontiers in neuroscience*, vol. 7, p. 84, 2013.
- [90] M. N. A. Tawhid, S. Siuly, H. Wang, F. Whittaker, K. Wang, and Y. Zhang, “A spectrogram image based intelligent technique for automatic detection of autism spectrum disorder from eeg,” *Plos one*, vol. 16, no. 6, e0253094, 2021.
- [91] M. N. A. Tawhid, S. Siuly, K. Wang, and H. Wang, “Textural feature based intelligent approach for neurological abnormality detection from brain signal data,” *Plos one*, vol. 17, no. 11, e0277555, 2022.
- [92] M. N. A. Tawhid, S. Siuly, K. Wang, and H. Wang, “Automatic and efficient framework for identifying multiple neurological disorders from eeg signals,” *IEEE Transactions on Technology and Society*, vol. 4, no. 1, pp. 76–86, 2023. DOI: [10.1109/TTS.2023.3239526](https://doi.org/10.1109/TTS.2023.3239526).
- [93] S. Siuly and Y. Li, “Designing a robust feature extraction method based on optimum allocation and principal component analysis for epileptic eeg signal classification,” *Computer methods and programs in biomedicine*, vol. 119, no. 1, pp. 29–42, 2015.
- [94] A. Subasi and M. I. Gursoy, “Eeg signal classification using pca, ica, lda and support vector machines,” *Expert systems with applications*, vol. 37, no. 12, pp. 8659–8666, 2010.
- [95] K. Lee, D. Liu, L. Perroud, R. Chavarriaga, and J. d. R. Millán, “A brain-controlled exoskeleton with cascaded event-related desynchronization classifiers,” *Robotics and Autonomous Systems*, vol. 90, pp. 15–23, 2017.
- [96] H. Wang, Y. Zhang, *et al.*, “Detection of motor imagery eeg signals employing naïve bayes based learning process,” *Measurement*, vol. 86, pp. 148–158, 2016.
- [97] E. Kabir, Y. Zhang, *et al.*, “Epileptic seizure detection from eeg signals using logistic model trees,” *Brain informatics*, vol. 3, no. 2, pp. 93–100, 2016.
- [98] S. Siuly, Ö. F. Alçin, E. Kabir, *et al.*, “A new framework for automatic detection of patients with mild cognitive impairment using resting-state eeg signals,” *IEEE Transactions on Neural Systems and Rehabilitation Engineering*, vol. 28, no. 9, pp. 1966–1976, 2020.
- [99] A. Craik, Y. He, and J. L. Contreras-Vidal, “Deep learning for electroencephalogram (eeg) classification tasks: A review,” *Journal of neural engineering*, vol. 16, no. 3, p. 031001, 2019.

- [100] M. N. A. Tawhid, S. Siuly, and T. Li, "A convolutional long short-term memory based neural network for epilepsy detection from eeg," *IEEE Transactions on Instrumentation and Measurement*, vol. 71, pp. 1–11, 2022. DOI: [10.1109/TIM.2022.3217515](https://doi.org/10.1109/TIM.2022.3217515).
- [101] A Nikhil Chandran, K. Sreekumar, and D. Subha, "Eeg-based automated detection of schizophrenia using long short-term memory (lstm) network," in *Advances in Machine Learning and Computational Intelligence*, Springer, 2021, pp. 229–236.
- [102] P. Wang, A. Jiang, X. Liu, J. Shang, and L. Zhang, "Lstm-based eeg classification in motor imagery tasks," *IEEE transactions on neural systems and rehabilitation engineering*, vol. 26, no. 11, pp. 2086–2095, 2018.
- [103] R. Djemal, K. AlSharabi, S. Ibrahim, and A. Alsuwailem, "Eeg-based computer aided diagnosis of autism spectrum disorder using wavelet, entropy, and ann," *BioMed Research International*, vol. 2017, 2017.
- [104] M. Ahmadlou, H. Adeli, and A. Adeli, "Improved visibility graph fractality with application for the diagnosis of autism spectrum disorder," *Physica A: Statistical Mechanics and its Applications*, vol. 391, no. 20, pp. 4720–4726, 2012.
- [105] F. A. Alturki, K. AlSharabi, A. M. Abdurraqueeb, and M. Aljalal, "Eeg signal analysis for diagnosing neurological disorders using discrete wavelet transform and intelligent techniques," *Sensors*, vol. 20, no. 9, p. 2505, 2020.
- [106] A. Shalhaf, S. Bagherzadeh, and A. Maghsoudi, "Transfer learning with deep convolutional neural network for automated detection of schizophrenia from eeg signals," *Physical and Engineering Sciences in Medicine*, vol. 43, pp. 1229–1239, 2020.
- [107] S. Supriya, S. Siuly, H. Wang, J. Cao, and Y. Zhang, "Weighted visibility graph with complex network features in the detection of epilepsy," *IEEE access*, vol. 4, pp. 6554–6566, 2016.
- [108] R. Singh, S. Subramani, J. Du, *et al.*, "Antisocial behavior identification from twitter feeds using traditional machine learning algorithms and deep learning.," *EAI Endorsed Transactions on Scalable Information Systems*, e17, 2023. [Online]. Available: <https://api.semanticscholar.org/CorpusID:258671645>.
- [109] R. Sarki, K. Ahmed, H. Wang, Y. Zhang, and K. N. Wang, "Convolutional neural network for multi-class classification of diabetic eye disease," *EAI Endorsed Trans. Scalable Inf. Syst.*, vol. 9, p. 5, 2022. [Online]. Available: <https://api.semanticscholar.org/CorpusID:245295045>.
- [110] P. S. Akash, M. E. Kadir, A. A. Ali, M. N. A. Tawhid, and M. Shoyaib, "Introducing confidence as a weight in random forest," in *2019 International Conference on Robotics, Electrical and Signal Processing Techniques (ICREST)*, IEEE, 2019, pp. 611–616.

- [111] M. N. U. Laskar, M. N. A. Tawhid, and T. Chung, "Extended kalman filter (ekf) and k-means clustering approach for state space decomposition of autonomous mobile robots," in *2012 7th International Conference on Electrical and Computer Engineering*, IEEE, 2012, pp. 113–116.
- [112] K. M. Sabrin, T. Zhang, S. Chen, *et al.*, "An intensity and size invariant real time face recognition approach," in *International Conference Image Analysis and Recognition*, Springer, 2009, pp. 502–511. DOI: [https://doi.org/10.1007/978-3-642-02611-9\\_50](https://doi.org/10.1007/978-3-642-02611-9_50).
- [113] S. Ahmed, M. N. A. Tawhid, K. Sakib, and M. M. Rahman, "A multi-objective evolutionary approach to reconstruct gene regulatory network using recurrent neural network model," *Biojournal of Science and Technology*, vol. 2, pp. 1–11, 2015.
- [114] F. Osisanwo, J. Akinsola, O Awodele, J. Hinmikaiye, O Olakanmi, J Akinjobi, *et al.*, "Supervised machine learning algorithms: Classification and comparison," *International Journal of Computer Trends and Technology (IJCTT)*, vol. 48, no. 3, pp. 128–138, 2017.
- [115] M. A. Rahman, M. A. Haque, M. N. A. Tawhid, and M. S. Siddik, "Classifying non-functional requirements using rnn variants for quality software development," in *Proceedings of the 3rd ACM SIGSOFT International Workshop on Machine Learning Techniques for Software Quality Evaluation*, 2019, pp. 25–30.
- [116] S. S. Islam, E. K. Dey, M. N. A. Tawhid, and B. M. Hossain, "A cnn based approach for garments texture design classification," *Advances in Technology Innovation*, vol. 2, no. 4, p. 119, 2017.
- [117] M. Asad, R. M. Yasir, S. Shahriar, N. Nahar, and M. N. A. Tawhid, "Analyzing program comprehensibility of go projects," in *The 33rd International Conference on Software Engineering and Knowledge Engineering*, 2021, pp. 255–260.
- [118] A. Tahmid, M. N. A. Tawhid, S. Ahmed, and K. Sakib, "Code sniffer: A risk based smell detection framework to enhance code quality using static code analysis," *International Journal of Software Engineering, Technology and Applications*, vol. 2, no. 1, pp. 41–63, 2017.
- [119] S. Siuly and Y. Li, "Improving the separability of motor imagery eeg signals using a cross correlation-based least square support vector machine for brain-computer interface," *IEEE Transactions on Neural Systems and Rehabilitation Engineering*, vol. 20, no. 4, pp. 526–538, 2012.
- [120] N. Nahar, S. Ali, and M. N. A. Tawhid, "An improved code clone tracking approach in evolving software.," *International Journal of Advanced Research in Computer Science*, vol. 7, no. 7, 2016.
- [121] R. Domingues, M. Filippone, P. Michiardi, and J. Zouaoui, "A comparative evaluation of outlier detection algorithms: Experiments and analyses," *Pattern recognition*, vol. 74, pp. 406–421, 2018.

- [122] Q. Lin, C.-H. Wu, W.-C. Gu, *et al.*, “A novel approach for epileptic eeg signals classification based on biclustering technique,” in *2016 international conference on machine learning and cybernetics (ICMLC)*, IEEE, vol. 2, 2016, pp. 756–760.
- [123] A. Sheikhan, H. Behnam, M. R. Mohammadi, M. Noroozian, and P. Golabi, “Connectivity analysis of quantitative electroencephalogram background activity in autism disorders with short time fourier transform and coherence values,” in *2008 Congress on Image and Signal Processing*, IEEE, vol. 1, 2008, pp. 207–212.
- [124] A. Sheikhan, H. Behnam, M. R. Mohammadi, M. Noroozian, and M. Mohammadi, “Detection of abnormalities for diagnosing of children with autism disorders using of quantitative electroencephalography analysis,” *Journal of medical systems*, vol. 36, no. 2, pp. 957–963, 2012.
- [125] W. K. Shams and A. W. A. Rahman, “Characterizing autistic disorder based on principle component analysis,” in *2011 IEEE Symposium on Industrial Electronics and Applications*, IEEE, 2011, pp. 653–657.
- [126] W. Bosl, A. Tierney, H. Tager-Flusberg, and C. Nelson, “Eeg complexity as a biomarker for autism spectrum disorder risk,” *BMC medicine*, vol. 9, no. 1, p. 18, 2011.
- [127] W. J. Bosl, H. Tager-Flusberg, and C. A. Nelson, “Eeg analytics for early detection of autism spectrum disorder: A data-driven approach,” *Scientific reports*, vol. 8, no. 1, pp. 1–20, 2018.
- [128] M. Ahmadlou, H. Adeli, and A. Adeli, “Fractality and a wavelet-chaos-neural network methodology for eeg-based diagnosis of autistic spectrum disorder,” *Journal of Clinical Neurophysiology*, vol. 27, no. 5, pp. 328–333, 2010.
- [129] M. Ahmadlou, H. Adeli, and A. Adeli, “Fuzzy synchronization likelihood-wavelet methodology for diagnosis of autism spectrum disorder,” *Journal of neuroscience methods*, vol. 211, no. 2, pp. 203–209, 2012.
- [130] W. Jamal, S. Das, I.-A. Oprescu, K. Maharatna, F. Apicella, and F. Sicca, “Classification of autism spectrum disorder using supervised learning of brain connectivity measures extracted from synchrostates,” *Journal of neural engineering*, vol. 11, no. 4, p. 046 019, 2014.
- [131] J. Eldridge, A. E. Lane, M. Belkin, and S. Dennis, “Robust features for the automatic identification of autism spectrum disorder in children,” *Journal of neurodevelopmental disorders*, vol. 6, no. 1, p. 12, 2014.
- [132] E. Grossi, C. Olivieri, and M. Buscema, “Diagnosis of autism through eeg processed by advanced computational algorithms: A pilot study,” *Computer methods and programs in biomedicine*, vol. 142, pp. 73–79, 2017.
- [133] E. Grossi, M. Buscema, F. Della Torre, and R. J. Swatzyna, “The “ms-rom/ifast” model, a novel parallel nonlinear eeg analysis technique, distinguishes asd subjects from children affected with other neuropsychiatric disorders with high degree of accuracy,” *Clinical EEG and neuroscience*, vol. 50, no. 5, pp. 319–331, 2019.

- [134] E. Grossi, G. Valbusa, and M. Buscema, "Detection of an autism eeg signature from only two eeg channels through features extraction and advanced machine learning analysis," *Clinical EEG and Neuroscience*, vol. 52, no. 5, pp. 330–337, 2021.
- [135] E. Abdulhay, M. Alafeef, H. Hadoush, N. Alomari, and M. Bashayreh, "Frequency 3d mapping and inter-channel stability of eeg intrinsic function pulsation: Indicators towards autism spectrum diagnosis," in *2017 10th Jordanian International Electrical and Electronics Engineering Conference (JIEEEEC)*, IEEE, 2017, pp. 1–6.
- [136] A. Dejman, A. Khadem, and A. Khorrami, "Exploring the disorders of brain effective connectivity network in asd: A case study using eeg, transfer entropy, and graph theory," in *2017 Iranian Conference on Electrical Engineering (ICEE)*, IEEE, 2017, pp. 8–13.
- [137] T Heunis, C. Aldrich, J. Peters, *et al.*, "Recurrence quantification analysis of resting state eeg signals in autism spectrum disorder—a systematic methodological exploration of technical and demographic confounders in the search for biomarkers," *BMC medicine*, vol. 16, no. 1, pp. 1–17, 2018.
- [138] N. Alotaibi and K. Maharatna, "Classification of autism spectrum disorder from eeg-based functional brain connectivity analysis," *Neural Computation*, vol. 33, no. 7, pp. 1914–1941, 2021.
- [139] D. Bakheet and K. Maharatna, "Linear and nonlinear analysis of intrinsic mode function after facial stimuli presentation in children with autism spectrum disorder," *Computers in Biology and Medicine*, vol. 133, p. 104376, 2021.
- [140] J. Kang, Y. Jin, G. Liang, and X. Li, "Accurate assessment of low-function autistic children based on eeg feature fusion," *Journal of Clinical Neuroscience*, vol. 90, pp. 351–358, 2021.
- [141] B. Ari, N. Sobahi, Ö. F. Alçin, A. Sengur, and U. R. Acharya, "Accurate detection of autism using douglas-peucker algorithm, sparse coding based feature mapping and convolutional neural network techniques with eeg signals," *Computers in Biology and Medicine*, vol. 143, p. 105311, 2022.
- [142] A. R. Aslam, N. Hafeez, H. Heidari, and M. A. B. Altaf, "Channels and features identification: A review and a machine-learning based model with large scale feature extraction for emotions and asd classification," *Frontiers in Neuroscience*, vol. 16, p. 844851, 2022.
- [143] P. Chawla, S. B. Rana, H. Kaur, and K. Singh, "Computer-aided diagnosis of autism spectrum disorder from eeg signals using deep learning with fawt and multiscale permutation entropy features," *Proceedings of the Institution of Mechanical Engineers, Part H: Journal of Engineering in Medicine*, vol. 237, no. 2, pp. 282–294, 2023.
- [144] M. Sabeti, S. Katebi, and R. Boostani, "Entropy and complexity measures for eeg signal classification of schizophrenic and control participants," *Artificial intelligence in medicine*, vol. 47, no. 3, pp. 263–274, 2009.

- [145] M. Sabeti, R. Behroozi, and E. Moradi, "Analysing complexity, variability and spectral measures of schizophrenic eeg signal," *International Journal of Biomedical Engineering and Technology*, vol. 21, no. 2, pp. 109–127, 2016.
- [146] L. Santos-Mayo, L. M. San-José-Revuelta, and J. I. Arribas, "A computer-aided diagnosis system with eeg based on the p3b wave during an auditory odd-ball task in schizophrenia," *IEEE transactions on biomedical engineering*, vol. 64, no. 2, pp. 395–407, 2016.
- [147] A. Piryatinska, B. Darkhovsky, and A. Kaplan, "Binary classification of multichannel-eeg records based on the  $\epsilon$ -complexity of continuous vector functions," *Computer methods and programs in biomedicine*, vol. 152, pp. 131–139, 2017.
- [148] T. B, S. D. S, B. K, and M. M, "Eeg signal complexity analysis for schizophrenia during rest and mental activity," *Biomedical Research*, vol. 28, no. 1, pp. 1–9, 2017.
- [149] V Jahmunah, S. L. Oh, V Rajinikanth, *et al.*, "Automated detection of schizophrenia using nonlinear signal processing methods," *Artificial intelligence in medicine*, vol. 100, p. 101 698, 2019.
- [150] S. L. Oh, J. Vicnesh, E. J. Ciaccio, R. Yuvaraj, and U. R. Acharya, "Deep convolutional neural network model for automated diagnosis of schizophrenia using eeg signals," *Applied Sciences*, vol. 9, no. 14, p. 2870, 2019.
- [151] C. A. T. Naira, C. Jos, *et al.*, "Classification of people who suffer schizophrenia and healthy people by eeg signals using deep learning," *International Journal of Advanced Computer Science and Applications*, vol. 10, no. 10, 2019.
- [152] R. Buettner, D. Beil, S. Scholtz, and A. Djemai, "Development of a machine learning based algorithm to accurately detect schizophrenia based on one-minute eeg recordings," in *Proceedings of the 53rd Hawaii International Conference on System Sciences*, 2020.
- [153] Z. Aslan and M. Akin, "Automatic detection of schizophrenia by applying deep learning over spectrogram images of eeg signals.," *Traitement du Signal*, vol. 37, no. 2, pp. 235–244, 2020.
- [154] S. Siuly, S. K. Khare, V. Bajaj, H. Wang, and Y. Zhang, "A computerized method for automatic detection of schizophrenia using eeg signals," *IEEE Transactions on Neural Systems and Rehabilitation Engineering*, vol. 28, no. 11, pp. 2390–2400, 2020.
- [155] S. K. Khare, V. Bajaj, and U. R. Acharya, "Spwvd-cnn for automated detection of schizophrenia patients using eeg signals," *IEEE Transactions on Instrumentation and Measurement*, vol. 70, pp. 1–9, 2021.
- [156] J. Sun, R. Cao, M. Zhou, *et al.*, "A hybrid deep neural network for classification of schizophrenia using eeg data," *Scientific Reports*, vol. 11, no. 1, p. 4706, 2021.
- [157] A. Shoeibi, D. Sadeghi, P. Moridian, *et al.*, "Automatic diagnosis of schizophrenia in eeg signals using cnn-lstm models," *Frontiers in Neuroinformatics*, vol. 15, 2021.

- [158] H. Akbari, S. Ghofrani, P. Zakalvand, and M. T. Sadiq, "Schizophrenia recognition based on the phase space dynamic of eeg signals and graphical features," *Biomedical Signal Processing and Control*, vol. 69, p. 102 917, 2021.
- [159] E. Aydemir, S. Dogan, M. Baygin, *et al.*, "Cgp17pat: Automated schizophrenia detection based on a cyclic group of prime order patterns using eeg signals," in *Healthcare*, MDPI, vol. 10, 2022, p. 643.
- [160] J. E. WeiKoh, V. Rajinikanth, J. Vicnesh, *et al.*, "Application of local configuration pattern for automated detection of schizophrenia with electroencephalogram signals," *Expert Systems*, e12957, 2022.
- [161] T. S. Kumar, K. N. Rajesh, S. Maheswari, V. Kanhangad, and U. R. Acharya, "Automated schizophrenia detection using local descriptors with eeg signals," *Engineering Applications of Artificial Intelligence*, vol. 117, p. 105 602, 2023.
- [162] S. Siuly, O. F. Alcin, V. Bajaj, A. Sengur, and Y. Zhang, "Exploring hermite transformation in brain signal analysis for the detection of epileptic seizure," *IET Science, Measurement & Technology*, vol. 13, no. 1, pp. 35–41, 2018.
- [163] J. Yin, J. Cao, S. Siuly, and H. Wang, "An integrated mci detection framework based on spectral-temporal analysis," *International Journal of Automation and Computing*, vol. 16, no. 6, pp. 786–799, 2019.
- [164] D. Haputhanthri, G. Brihadiswaran, S. Gunathilaka, *et al.*, "An eeg based channel optimized classification approach for autism spectrum disorder," in *2019 Moratuwa Engineering Research Conference (MERCCon)*, IEEE, 2019, pp. 123–128. DOI: <https://doi.org/10.1109/MERCCon.2019.8818814>.
- [165] D. Haputhanthri, G. Brihadiswaran, S. Gunathilaka, *et al.*, "Integration of facial thermography in eeg-based classification of asd," *International Journal of Automation and Computing*, vol. 17, no. 6, pp. 837–854, 2020. DOI: <https://doi.org/10.1007/s11633-020-1231-6>.
- [166] D. Abdolzadegan, M. H. Moattar, and M. Ghoshuni, "A robust method for early diagnosis of autism spectrum disorder from eeg signals based on feature selection and dbscan method," *Biocybernetics and Biomedical Engineering*, vol. 40, no. 1, pp. 482–493, 2020. DOI: <https://doi.org/10.1016/j.bbe.2020.01.008>.
- [167] B. Rim, N.-J. Sung, S. Min, and M. Hong, "Deep learning in physiological signal data: A survey," *Sensors*, vol. 20, no. 4, p. 969, 2020.
- [168] L. Yuan and J. Cao, "Patients' eeg data analysis via spectrogram image with a convolution neural network," in *International Conference on Intelligent Decision Technologies*, Springer, 2017, pp. 13–21.
- [169] M. Li, X. Sun, W. Chen, Y. Jiang, and T. Zhang, "Classification epileptic seizures in eeg using time-frequency image and block texture features," *IEEE Access*, vol. 8, pp. 9770–9781, 2019.

- [170] P. Jadhav, G. Rajguru, D. Datta, and S. Mukhopadhyay, "Automatic sleep stage classification using time–frequency images of cwt and transfer learning using convolution neural network," *Biocybernetics and Biomedical Engineering*, vol. 40, no. 1, pp. 494–504, 2020.
- [171] E. K. Dey, M. Tawhid, N. Ahad, and M. Shoyaib, "An automated system for garment texture design class identification," *Computers*, vol. 4, no. 3, pp. 265–282, 2015.
- [172] J. Wu and J. M. Rehg, "Centrist: A visual descriptor for scene categorization," *IEEE transactions on pattern analysis and machine intelligence*, vol. 33, no. 8, pp. 1489–1501, 2010.
- [173] M. N. A. Tawhid and E. K. Dey, "A gender recognition system from facial image," *International Journal of Computer Applications*, vol. 180, no. 23, pp. 5–14, 2018.
- [174] C.-C. Chang and C.-J. Lin, "Libsvm: A library for support vector machines," *ACM transactions on intelligent systems and technology (TIST)*, vol. 2, no. 3, pp. 1–27, 2011.
- [175] H.-C. Shin, H. R. Roth, M. Gao, *et al.*, "Deep convolutional neural networks for computer-aided detection: Cnn architectures, dataset characteristics and transfer learning," *IEEE transactions on medical imaging*, vol. 35, no. 5, pp. 1285–1298, 2016.
- [176] L. Deng and D. Yu, "Deep learning: Methods and applications," *Foundations and trends in signal processing*, vol. 7, no. 3–4, pp. 197–387, 2014.
- [177] M. J. Alhaddad, M. I. Kamel, H. M. Malibary, *et al.*, "Diagnosis autism by fisher linear discriminant analysis flda via eeg," *International Journal of Bio-Science and Bio-Technology*, vol. 4, no. 2, pp. 45–54, 2012.
- [178] Google, *Welcome to colab*, (Date last accessed January 2021). [Online]. Available: <https://colab.research.google.com/notebooks/intro.ipynb>.
- [179] S. Siuly, E. Kabir, H. Wang, and Y. Zhang, "Exploring sampling in the detection of multicategory eeg signals," *Computational and mathematical methods in medicine*, vol. 2015, 2015.
- [180] A. R. Hassan, S. Siuly, and Y. Zhang, "Epileptic seizure detection in eeg signals using tunable-q factor wavelet transform and bootstrap aggregating," *Computer methods and programs in biomedicine*, vol. 137, pp. 247–259, 2016.
- [181] S. Siuly, X. Yin, S Hadjiloucas, and Y. Zhang, "Classification of thz pulse signals using two-dimensional cross-correlation feature extraction and non-linear classifiers," *Computer Methods and Programs in Biomedicine*, vol. 127, pp. 64–82, 2016.
- [182] J. He, J. Rong, L. Sun, H. Wang, Y. Zhang, and J. Ma, "A framework for cardiac arrhythmia detection from iot-based ecgs," *World Wide Web*, pp. 1–16, 2020.

- [183] A. M. Alvi, S. Siuly, H. Wang, L. Sun, and J. Cao, "An adaptive image smoothing technique based on localization," pp. 866–873, 2020. DOI: [https://doi.org/10.1142/9789811223334\\_0104](https://doi.org/10.1142/9789811223334_0104).
- [184] S. Supriya, S. Siuly, H. Wang, and Y. Zhang, "Automated epilepsy detection techniques from electroencephalogram signals: A review study," *Health Information Science and Systems*, vol. 8, no. 1, pp. 1–15, 2020.
- [185] T. Fawcett, "An introduction to roc analysis," *Pattern recognition letters*, vol. 27, no. 8, pp. 861–874, 2006.
- [186] E. A. Alsaggaf and M. I. Kamel, "Using eegs to diagnose autism disorder by classification algorithm," *Life Science Journal*, vol. 11, no. 6, pp. 305–308, 2014.
- [187] M. I. Kamel, M. J. Alhaddad, H. M. Malibary, *et al.*, "Eeg based autism diagnosis using regularized fisher linear discriminant analysis," *International Journal of Image, Graphics and Signal Processing*, vol. 4, no. 3, p. 35, 2012.
- [188] A. A. Nur, "Autism spectrum disorder classification on electroencephalogram signal using deep learning algorithm," *IAES International Journal of Artificial Intelligence*, vol. 9, no. 1, p. 91, 2020.
- [189] S. Jayarathna, Y. Jayawardana, M. Jaime, and S. Thapaliya, "Electroencephalogram (eeg) for delineating objective measure of autism spectrum disorder," in *Computational Models for Biomedical Reasoning and Problem Solving*, IGI Global, 2019, pp. 34–65. DOI: <https://doi.org/10.4018/978-1-5225-7467-5.ch002>.
- [190] M. Tawhid, N. Ahad, S. Siuly, K. Wang, and H. Wang, "Brain data mining framework involving entropy topography and deep learning," in *Australasian Database Conference*, Springer, 2022, pp. 161–168. DOI: [https://doi.org/10.1007/978-3-031-15512-3\\_13](https://doi.org/10.1007/978-3-031-15512-3_13).
- [191] S. Siuly and Y. Li, "Discriminating the brain activities for brain–computer interface applications through the optimal allocation-based approach," *Neural Computing and Applications*, vol. 26, no. 4, pp. 799–811, 2015.
- [192] S. Supriya, S. Siuly, H. Wang, and Y. Zhang, "Eeg sleep stages analysis and classification based on weighed complex network features," *IEEE Transactions on Emerging Topics in Computational Intelligence*, vol. 5, no. 2, pp. 236–246, 2018.
- [193] F. Demir, N. Sobahi, S. Siuly, and A. Sengur, "Exploring deep learning features for automatic classification of human emotion using eeg rhythms," *IEEE Sensors Journal*, 2021.
- [194] M. Tawhid, N. Ahad, S. Siuly, K. Wang, and H. Wang, "Data mining based artificial intelligent technique for identifying abnormalities from brain signal data," in *International Conference on Web Information Systems Engineering*, Springer, 2021, pp. 198–206.
- [195] M. Dash and H. Liu, "Feature selection for classification," *Intelligent data analysis*, vol. 1, no. 1-4, pp. 131–156, 1997.

- [196] H. R. Al Ghayab, Y. Li, S. Siuly, and S. Abdulla, "Epileptic eeg signal classification using optimum allocation based power spectral density estimation," *IET Signal Processing*, vol. 12, no. 6, pp. 738–747, 2018.
- [197] M. F. Anjum, S. Dasgupta, R. Mudumbai, A. Singh, J. F. Cavanagh, and N. S. Narayanan, "Linear predictive coding distinguishes spectral eeg features of parkinson's disease," *Parkinsonism & Related Disorders*, vol. 79, pp. 79–85, 2020.
- [198] S. L. Oh, Y. Hagiwara, U Raghavendra, *et al.*, "A deep learning approach for parkinson's disease diagnosis from eeg signals," *Neural Computing and Applications*, vol. 32, no. 15, pp. 10 927–10 933, 2020.
- [199] W. Skrandies, "Electroencephalogram (eeg) topography," *Encyclopedia of Imaging Science and Technology*, 2002.
- [200] M. J. Rivera, M. A. Teruel, A. Maté, and J. Trujillo, "Diagnosis and prognosis of mental disorders by means of eeg and deep learning: A systematic mapping study," *Artificial Intelligence Review*, pp. 1–43, 2021.
- [201] R. M. Sabbatini, *Mapping the brain*, 1997. [Online]. Available: <https://cerebromente.org.br/n03/tecnologia/eeg.htm>.
- [202] B. Roach, *Eeg data from sensory task in schizophrenia*, 2019. [Online]. Available: <https://www.kaggle.com/datasets/broach/button-tone-sz>.
- [203] K. Singh, S. Singh, and J. Malhotra, "Spectral features based convolutional neural network for accurate and prompt identification of schizophrenic patients," *Proceedings of the Institution of Mechanical Engineers, Part H: Journal of Engineering in Medicine*, vol. 235, no. 2, pp. 167–184, 2021.
- [204] W. H. Organization, *Neurological disorders: public health challenges*. World Health Organization, 2006.
- [205] M. neuroscience network, "Review of the burden of disease for neurological, mental health and substance use disorders in australia," 2019.
- [206] J. Wang, R. Peng, Q. Liu, and H. Peng, "A hybrid classification to detect abstinent heroin-addicted individuals using eeg microstates," *IEEE Transactions on Computational Social Systems*, vol. 9, no. 3, pp. 700–709, 2022.
- [207] M. I. Vanegas, M. F. Ghilardi, S. P. Kelly, and A. Blangero, "Machine learning for eeg-based biomarkers in parkinson's disease," in *2018 IEEE International Conference on Bioinformatics and Biomedicine (BIBM)*, IEEE, 2018, pp. 2661–2665.
- [208] A. Keihani, A. M. Mohammadi, H. Marzbani, S. Nafissi, M. R. Haidari, and A. H. Jafari, "Sparse representation of brain signals offers effective computation of cortico-muscular coupling value to predict the task-related and non-task semg channels: A joint hdeeg-semg study," *Plos one*, vol. 17, no. 7, e0270757, 2022. DOI: <https://doi.org/10.1371/journal.pone.0270757>.

- [209] M. N. A. Tawhid, S. Siuly, E. Kabir, and Y. Li, "Exploring frequency band-based biomarkers of eeg signals for mild cognitive impairment detection," *IEEE Transactions on Neural Systems and Rehabilitation Engineering*, vol. 32, pp. 189–199, 2023.
- [210] K. Akrofi, M. C. Baker, M. W. O'Boyle, and R. B. Schiffer, "Clustering and modeling of eeg coherence features of alzheimer's and mild cognitive impairment patients," in *2008 30th Annual International Conference of the IEEE Engineering in Medicine and Biology Society*, IEEE, 2008, pp. 1092–1095.
- [211] J. C. McBride, X. Zhao, N. B. Munro, *et al.*, "Sugihara causality analysis of scalp eeg for detection of early alzheimer's disease," *NeuroImage: Clinical*, vol. 7, pp. 258–265, 2015.
- [212] C. Ieracitano, N. Mammone, A. Hussain, and F. C. Morabito, "A novel multi-modal machine learning based approach for automatic classification of eeg recordings in dementia," *Neural Networks*, vol. 123, pp. 176–190, 2020.
- [213] B. Oltu, M. F. Akşahin, and S. Kibaroglu, "A novel electroencephalography based approach for alzheimer's disease and mild cognitive impairment detection," *Biomedical Signal Processing and Control*, vol. 63, p. 102223, 2021.
- [214] S. Ibrahim, R. Djemal, and A. Alsuwailam, "Electroencephalography (eeg) signal processing for epilepsy and autism spectrum disorder diagnosis," *Biocybernetics and Biomedical Engineering*, vol. 38, no. 1, pp. 16–26, 2018.
- [215] A. Pereira and J. Fiel, *Resting-state interictal eeg recordings of refractory epilepsy patients*, 2019. DOI: [10.17632/6HX2SMC7NW.1](https://doi.org/10.17632/6HX2SMC7NW.1). [Online]. Available: <https://data.mendeley.com/datasets/6hx2smc7nw/1>.
- [216] X. Jiang, G.-B. Bian, and Z. Tian, "Removal of artifacts from eeg signals: A review," *Sensors*, vol. 19, no. 5, p. 987, 2019.
- [217] P. N. Srinivasu, G. JayaLakshmi, R. H. Jhaveri, and S. P. Praveen, "Ambient assistive living for monitoring the physical activity of diabetic adults through body area networks," *Mobile Information Systems*, vol. 2022, 2022. DOI: <https://doi.org/10.1155/2022/3169927>.
- [218] R. Zabih and J. Woodfill, "Non-parametric local transforms for computing visual correspondence," in *European conference on computer vision*, Springer, 1994, pp. 151–158. DOI: <https://doi.org/10.1007/BFb0028345>.
- [219] T. Cover and P. Hart, "Nearest neighbor pattern classification," *IEEE transactions on information theory*, vol. 13, no. 1, pp. 21–27, 1967.
- [220] L. Breiman, "Random forests," *Machine learning*, vol. 45, no. 1, pp. 5–32, 2001.
- [221] E. Zorarpacı, "A hybrid dimension reduction based linear discriminant analysis for classification of high-dimensional data," in *2021 IEEE Congress on Evolutionary Computation (CEC)*, IEEE, 2021, pp. 1028–1036.

- [222] W. Hussain, M. T. Sadiq, S. Siuly, and A. U. Rehman, "Epileptic seizure detection using 1 d-convolutional long short-term memory neural networks," *Applied Acoustics*, vol. 177, p. 107941, 2021.
- [223] A. Krizhevsky, I. Sutskever, and G. E. Hinton, "Imagenet classification with deep convolutional neural networks," *Advances in neural information processing systems*, vol. 25, pp. 1097–1105, 2012.
- [224] K. He, X. Zhang, S. Ren, and J. Sun, "Deep residual learning for image recognition," in *Proceedings of the IEEE conference on computer vision and pattern recognition*, 2016, pp. 770–778.
- [225] F. Zhang, Y. Wang, S. Liu, and H. Wang, "Decision-based evasion attacks on tree ensemble classifiers," *World Wide Web*, vol. 23, no. 5, pp. 2957–2977, 2020.
- [226] M. You, J. Yin, H. Wang, J. Cao, and Y. Miao, "A minority class boosted framework for adaptive access control decision-making," in *International Conference on Web Information Systems Engineering*, Springer, 2021, pp. 143–157.
- [227] R. Sarki, K. Ahmed, H. Wang, and Y. Zhang, "Automated detection of mild and multi-class diabetic eye diseases using deep learning," *Health Information Science and Systems*, vol. 8, no. 1, pp. 1–9, 2020.
- [228] N. A. Tawhid, N. U. Laskar, and H. Ali, "A vision-based facial expression recognition and adaptation system from video stream," *International Journal of Machine Learning and Computing*, vol. 2, no. 5, p. 535, 2012. DOI: <https://doi.org/10.7763/IJMLC.2012.V2.183>.
- [229] N. Anjum, Z. Latif, C. Lee, I. A. Shoukat, and U. Iqbal, "Mind: A multi-source data fusion scheme for intrusion detection in networks," *Sensors*, vol. 21, no. 14, p. 4941, 2021. DOI: <https://doi.org/10.3390/s21144941>.
- [230] L. Qiu, J. Li, and J. Pan, "Parkinson's disease detection based on multi-pattern analysis and multi-scale convolutional neural networks," *Frontiers in Neuroscience*, vol. 16, 2022.
- [231] A. Zülfikar and A. Mehmet, "Empirical mode decomposition and convolutional neural network-based approach for diagnosing psychotic disorders from eeg signals," *Applied Intelligence*, pp. 1–13, 2022.
- [232] V. Geraedts, M Koch, M. Contarino, *et al.*, "Machine learning for automated eeg-based biomarkers of cognitive impairment during deep brain stimulation screening in patients with parkinson's disease," *Clinical Neurophysiology*, vol. 132, no. 5, pp. 1041–1048, 2021.
- [233] R. Jana and I. Mukherjee, "Deep learning based efficient epileptic seizure prediction with eeg channel optimization," *Biomedical Signal Processing and Control*, vol. 68, p. 102767, 2021.

- [234] S. K. Khare, V. Bajaj, and U. R. Acharya, "Pdcnnet: An automatic framework for the detection of parkinson's disease using eeg signals," *IEEE Sensors Journal*, vol. 21, no. 15, pp. 17 017–17 024, 2021.
- [235] C. Ieracitano, N. Mammone, A. Bramanti, A. Hussain, and F. C. Morabito, "A convolutional neural network approach for classification of dementia stages based on 2d-spectral representation of eeg recordings," *Neurocomputing*, vol. 323, pp. 96–107, 2019.
- [236] H. Chen, Y. Song, and X. Li, "A deep learning framework for identifying children with adhd using an eeg-based brain network," *Neurocomputing*, vol. 356, pp. 83–96, 2019.
- [237] A. E. Alchalabi, S. Shirmohammadi, A. N. Eddin, and M. Elsharnouby, "Focus: Detecting adhd patients by an eeg-based serious game," *IEEE Transactions on Instrumentation and Measurement*, vol. 67, no. 7, pp. 1512–1520, 2018.
- [238] O. Mecarelli, "Electrode placement systems and montages," in *Clinical Electroencephalography*, Springer, 2019, pp. 35–52.
- [239] B. Roach, *Eeg data from basic sensory task in schizophrenia*, (Date last accessed February 2021). [Online]. Available: <https://www.kaggle.com/broach/button-tone-sz>.
- [240] M. Kashefpoor, H. Rabbani, and M. Barekatin, "Automatic diagnosis of mild cognitive impairment using electroencephalogram spectral features," *Journal of medical signals and sensors*, vol. 6, no. 1, p. 25, 2016.
- [241] A. Motie Nasrabadi, A. Allahverdy, M. Samavati, and M. R. Mohammadi, "Eeg data for adhd / control children," 2020. DOI: [10 . 21227 / rzfh - zn36](https://doi.org/10.21227/rzfh-zn36). [Online]. Available: <https://dx.doi.org/10.21227/rzfh-zn36>.
- [242] I. Goodfellow, Y. Bengio, and A. Courville, *Deep Learning*. MIT Press, 2016, <http://www.deeplearningbook.org>.
- [243] A. Lavatelli and E. Zappa, "A displacement uncertainty model for 2-d dic measurement under motion blur conditions," *IEEE Transactions on Instrumentation and Measurement*, vol. 66, no. 3, pp. 451–459, 2017.
- [244] L. Van der Maaten and G. Hinton, "Visualizing data using t-sne.," *Journal of machine learning research*, vol. 9, no. 11, 2008.
- [245] X. Yu, M. Z. Aziz, M. T. Sadiq, K. Jia, Z. Fan, and G. Xiao, "Computerized multidomain eeg classification system: A new paradigm," *IEEE Journal of Biomedical and Health Informatics*, 2022.
- [246] M. Baygin, O. Yaman, T. Tuncer, S. Dogan, P. D. Barua, and U. R. Acharya, "Automated accurate schizophrenia detection system using collatz pattern technique with eeg signals," *Biomedical Signal Processing and Control*, vol. 70, p. 102 936, 2021.

- [247] A. Ekhiasi, A. M. Nasrabadi, and M. Mohammadi, "Classification of the children with adhd and healthy children based on the directed phase transfer entropy of eeg signals," *Frontiers in Biomedical Technologies*, vol. 8, no. 2, pp. 115–122, 2021.
- [248] S. Xingjian, Z. Chen, H. Wang, D.-Y. Yeung, W.-K. Wong, and W.-c. Woo, "Convolutional lstm network: A machine learning approach for precipitation nowcasting," in *Advances in neural information processing systems*, 2015, pp. 802–810.
- [249] S. Siuly, Y. Li, P. Wen, and O. F. Alcin, "Schizogoolnet: The googlenet-based deep feature extraction design for automatic detection of schizophrenia.," *Computational Intelligence & Neuroscience*, 2022.
- [250] S. K. Khare, V. Bajaj, S. Siuly, and G. Sinha, "Classification of schizophrenia patients through empirical wavelet transformation using electroencephalogram signals," *Modelling and Analysis of Active Biopotential Signals in Healthcare*, vol. 1, pp. 1–26, 2020.
- [251] L. Zhang, "Eeg signals classification using machine learning for the identification and diagnosis of schizophrenia," in *2019 41st Annual International Conference of the IEEE Engineering in Medicine and Biology Society (EMBC)*, IEEE, 2019, pp. 4521–4524.
- [252] S. K. Khare and V. Bajaj, "A self-learned decomposition and classification model for schizophrenia diagnosis," *Computer Methods and Programs in Biomedicine*, vol. 211, p. 106 450, 2021.
- [253] Z. Guo, L. Wu, Y. Li, and B. Li, "Deep neural network classification of eeg data in schizophrenia," in *2021 IEEE 10th Data Driven Control and Learning Systems Conference (DDCLS)*, IEEE, 2021, pp. 1322–1327.
- [254] S. K. Khare and V. Bajaj, "A hybrid decision support system for automatic detection of schizophrenia using eeg signals," *Computers in Biology and Medicine*, vol. 141, p. 105 028, 2022.
- [255] P. T. Krishnan, A. N. J. Raj, P. Balasubramanian, and Y. Chen, "Schizophrenia detection using multivariate empirical mode decomposition and entropy measures from multichannel eeg signal," *Biocybernetics and Biomedical Engineering*, vol. 40, no. 3, pp. 1124–1139, 2020.
- [256] M. Baygin, "An accurate automated schizophrenia detection using tqwt and statistical moment based feature extraction," *Biomedical Signal Processing and Control*, vol. 68, p. 102 777, 2021.
- [257] M. Sharma and U. R. Acharya, "Automated detection of schizophrenia using optimal wavelet-based  $l_1$  norm features extracted from single-channel eeg," *Cognitive Neurodynamics*, vol. 15, no. 4, pp. 661–674, 2021.
- [258] Y. Kwak, K. Kong, W.-J. Song, and S.-E. Kim, "Subject-invariant deep neural networks based on baseline correction for eeg motor imagery bci," *IEEE Journal of Biomedical and Health Informatics*, 2023.